Volcanic Aerosols in the Upper Troposphere and Stratosphere – Aircraft- and Satellite-Based Observations

Andersson, Sandra

2015

Volcanic Aerosols in the Upper Troposphere and Stratosphere

Aircraft- and Satellite-Based Observations

Sandra M. Andersson

LUNDS
UNIVERSITET

DOCTORAL DISSERTATION
by due permission of the Faculty of Engineering, Lund University, Sweden.

To be defended on Friday 6th of March at 9.15, 2015, in the Rydberg Hall at the Department of Physics, Sölvegatan 14, Lund.

Faculty opponent

Dr. Radovan Krejci, Department of Applied Environmental Science,
Stockholm University, Sweden

Organization

LUND UNIVERSITY

Division of Nuclear Physics
Box 118, SE-22100, Lund

Author(s): Sandra M. Andersson

Document name

DOCTORAL DISSERTATION

Date of issue

Sponsoring organization

Title: Volcanic Aerosols in the Upper Troposphere and Stratosphere – Aircraft- and Satellite-Based Observations

Abstract

Volcanic eruptions are the largest source of variability in the stratospheric particle concentration as they inject SO_2 that is subsequently converted into sulphate particles. No major perturbation of the stratospheric aerosol load has been observed since the large eruption of Pinatubo in 1991, but several moderate eruptions after 2000 have caused deviations from stratospheric background conditions. Atmospheric particles are of concern with regard to climate because they scatter and absorb radiation. This thesis presents results from observations of the aerosol in the upper troposphere and stratosphere during the period 1999-2013.

Measurements of aerosol particles and trace gases were performed with the CARIBIC flying observatory, where instrumentation is installed on a Lufthansa passenger aircraft during monthly intercontinental flights at altitudes of 9-12 km. The elemental composition of particles in the diameter range 0.08-2 µm was obtained from sampling and subsequent ion beam analysis (PIXE and PESA). Size distributions of particles with diameters of 0.12-1 µm were measured during flight by an optical particle counter. Lidar observations from the satellite CALIPSO were used to reveal the vertical distribution and global effect of three volcanic eruptions from 2008 to 2011. These observations were used to determine stratospheric aerosol optical depth and radiative forcing, in order to estimate the climate impact received from the lowermost stratosphere (LMS).

It was found that the LMS particle concentrations were on average higher in the years 2005-2008 than 1999-2002. While the latter period is considered to represent background conditions, the increase in 2005-2008 was attributed to three tropical eruptions with subsequent transport of the aerosol into the LMS by the shallow and deep branches of the Brewer–Dobson circulation. In 2008-2012, volcanism had considerable impact during due to both extra-tropical and tropical eruptions. Three main components were identified in volcanic particles sampled one week to more than 18 weeks after the eruptions: sulphate, ash and a carbonaceous fraction. The residence time of SO_2 in the stratosphere was estimated to be 45±22 days.

The stratosphere below 15 km altitude was found to contribute 55% to the total stratospheric aerosol optical depth and 42% to the total aerosol radiative forcing from the Kasatochi (2008), Sarychev (2009) and Nabro (2011) eruptions. Thus, currently used estimates of the impact of volcanic eruptions on climate based on data obtained above 15 km or the 380 K isentrope should be updated to include the effect of volcanism on the LMS. Furthermore, higher concentrations of sulphate particles were observed in the upper troposphere during volcanically influenced periods, with a positive trend in 2001-2011. The opposite trend was observed in cirrus cloud reflectance in the same period. This suggests that the volcanic aerosol has a significant indirect effect on climate, which requires further investigation.

Key words: Stratospheric aerosol, volcanism, lowermost stratosphere, upper troposphere, volcanic particles, ash, sulphate, carbonaceous aerosol, aerosol optical depth, radiative forcing

Classification system and/or index terms (if any)

Supplementary bibliographical information

Language: English

ISSN and key title

ISBN 978-91-7623-245-3

Recipient's notes

Number of pages: 162

Price

Security classification

Signature Sandra Andersson Date 2015-01-27

Volcanic Aerosols in the Upper Troposphere and Stratosphere

Aircraft- and Satellite-Based Observations

Sandra M. Andersson

LUNDS
UNIVERSITET

Faculty of Engineering
Division of Nuclear Physics
LUTFD2/(TFKF-1043)/1 - 71 (2015)
ISBN 978-91-7623-245-3 (print)
ISBN 978-91-7623-246-0 (pdf)

Tryckt i Sverige av Media-Tryck, Lunds universitet
Lund 2015

Populärvetenskaplig sammanfattning

Den här avhandlingen handlar om partiklar i den delen av atmosfären som kallas stratosfären. Stratosfären börjar på ungefär 8-15 km höjd, framförallt beroende på latitud, och sträcker sig till ungefär 50 km över marken. I stratosfären finns nästan inga moln, och därmed ingen nederbörd som kan ta med sig partiklarna till marken. Eftersom de är små, med diameter av ungefär en tiotusendels millimeter, har de en nästan försumbar fallhastighet. Därför har de en lång livstid i stratosfären, ungefär ett år, vilket kan jämföras med ungefär en vecka för partiklar i den underliggande troposfären där nederbörd renar luften. Trots detta är koncentrationen av partiklar i stratosfären oftast väldigt låg jämfört med nära marken, eftersom det endast är ett fåtal källor till partiklar som når hit. En viktig, men sporadisk källa är vulkanutbrott, som med stor kraft kan injicera betydande mängder partiklar och gaser tiotals kilometer upp i luften. Framförallt viktig är gasen svaveldioxid (SO_2), som omvandlas till svavelpartiklar i stratosfären.

Varför behöver man forska på stratosfäriska partiklar? En viktig anledning är att de påverkar jordens klimat genom att de har förmågan att sprida solljus, som då hindras från att nå jordytan och värma jorden. År 1815 var det ett enormt utbrott i vulkanen Tambora i Indonesien, som nådde en höjd på mer än 30 km och skapade över 100 miljoner ton svavelpartiklar. Partiklarna spreds över jordklotet och bidrog till en global temperatursänkning och vad som kallats ”året utan sommar”, med bl.a. dåliga skördar, svält och ekonomisk kris som följd.

Idag är problemet av motsatt karaktär, genom den globala uppvärmningen som våra utsläpp av växthusgaser med stor sannorlikhet orsakar. För att förstå hur vi människor har påverkat och kommer att påverka klimatet, måste vi förstå samtliga delar av klimatsystemet, och kunna skilja på naturliga och antropogena (av människan skapade) förändringar. Den här avhandlingen fokuserar på perioden 1999-2013, som helt saknar utbrott i storleksordning av Tamborra. Istället har stratosfären påverkats av en rad mindre utbrott, som visats bidra mer till mängden stratosfäriska partiklar än vad man från början trodde.

I de studier som ingår i avhandlingen har framförallt två mätmetoder använts. Partiklar i den lägsta delen av stratosfären har regelbundet samlats in från ett passagerarflygplan inom forskningskonsortiet CARIBIC. För att ta fram partiklarnas kemiska sammansättning och massa har de analyserats i laboratorium genom kärnfysikaliska metoder, där de bestrålats med protoner från en accelerator. Från flygplanet har också storleken på partiklarna mätts. Den kemiska sammansättningen ger information om varifrån partiklarna kommer. Partiklarnas sammansättning och storlek bestämmer dess förmåga att sprida ljus och hur de påverkar molnegenskaper. Detta är viktig information som kan användas i klimatmodeller, men också behövs för noggranna optiska mätmetoder som bygger på att mäta partiklarnas ljusspridning.

Den andra observationsmetoden är mätningar från satelliten CALIPSO. Ombord finns en lidar som genom att skicka ut laserpulser och mäta mängden ljus som sprids tillbaka, ger en vertikalt högupplöst bild av mängden moln och partiklar i atmosfären. Mätningar från satelliter ger en global bild av mängden och fördelningen av partiklar över jorden, och kan därmed användas för att uppskatta den totala inverkan från stratosfäriska partiklar.

Med hjälp av dessa metoder har betydelsen av vulkanutbrott för mängden partiklar i lägsta stratosfären studerats. Vulkaniska partiklars sammansättning av aska, svavel och kol har undersökts, varav vi fortfarande vet lite om ursprunget och formen av kolkomponenten som inte är en självklar del av utsläppen från vulkaner. Ett viktigt resultat som presenteras i avhandlingen är att dagens uppskattningar av vulkaners klimatpåverkan troligen är kraftigt underskattade. Klimatberäkningarna använder satellitmätningar av stratosfärisk aerosol som är begränsade till över 15 km höjd. Därmed har den lägsta delen av stratosfären, som innehåller ungefär 40 % av dess totala luftmassa, förbisetts. Denna del av atmosfären påverkades kraftigt av vulkanism under delar av den studerade tidsperioden (1999-2013). Dessutom visas att vulkaniska partiklar som transporteras ner i troposfären kan påverka de reflekterande egenskaperna hos högt liggande moln. Detta innebär också att de absorberar mindre värmestrålning från jorden, vilket betyder en kylande effekt på klimatet. På så vi har vulkaniska partiklar bidragit till att motverka den globala uppvärmningen, både genom att direkt sprida solljus i stratosfären, och genom att ändra molnens egenskaper. Detta kan vara en viktig del i att förklara avvikelser som finns mellan klimatmodeller och den verkliga temperaturutvecklingen under de senaste 15 åren.

List of papers and the author's contributions

Paper I

Andersson, S. M., Martinsson, B. G., Friberg, J., Brenninkmeijer, C. A. M., Rauthe-Schöch, A., Hermann, M., van Velthoven, P. F. J., and Zahn, A.: *Composition and evolution of volcanic aerosol from eruptions of Kasatochi, Sarychev and Eyjafjallajökull in 2008–2010 based on CARIBIC observations*, Atmospheric Chemistry and Physics, 13, 1781-1796, 2013.

I contributed to the sample analysis, performed most of the data evaluation and wrote the paper.

Paper II

Friberg, J., Martinsson, B. G., Andersson, S. M., Brenninkmeijer, C. A. M., Hermann, M., van Velthoven, P. F. J, and Zahn, A.: *Sources of increase in lowermost stratospheric sulphurous and carbonaceous aerosol background concentrations during 1999-2008 derived from CARIBIC flights*, Tellus B, 66, 23428, 2014.

I contributed to the sample analysis, assisted in data evaluation and contributed to discussions of the manuscript.

Paper III

Martinsson, B. G., Friberg, J., Andersson, S. M., Weigelt, A., Hermann, M., Assmann, D., Voigtländer, J., Brenninkmeijer, C. A. M., van Velthoven, P. F. J, and Zahn, A.: *Comparison between CARIBIC aerosol samples analysed by accelerator-based methods and optical particle counter measurements*, Atmospheric Measurement Techniques. , 7, 2581-2596, 10.5194/amt-7-2581-2014, 2014.

I contributed to the sample analysis, assisted in data evaluation and contributed to discussions of the manuscript.

Paper IV

Andersson, S. M., Martinsson, B. G., Vernier, J. P., Friberg, J., Brenninkmeijer, C. A. M., Hermann, M., van Velthoven, P. F. J., and Zahn, A.: *Significant radiative impact of volcanic aerosol in the lowermost stratosphere,* submitted manuscript

I contributed to the sample analysis. I developed tools for using CALIPSO satellite data, performed the data evaluation and wrote the paper.

Paper V

Friberg, J., Martinsson, B. G., Sporre, M. K., Andersson, S. M., Brenninkmeijer, C. A. M., Hermann, M., Velthoven, P. F. J. v., and Zahn, A.: *Variability in LMS volcanic sulfurous aerosol and consequences for the UT aerosol and midlatitude cirrus clouds,* submitted manuscript

I contributed to the sample analysis, assisted in data evaluation and contributed to discussions of the manuscript.

Contents

1 Scope of this thesis

Volcanic eruptions sometimes emit large amounts of gases and particles high into the atmosphere. If they reach the stratosphere, small volcanic particles have long residence times since there are few removal processes in this part of the atmosphere. Volcanic eruptions are the largest source of variability in the amount of aerosol particles in the stratosphere. They are of concern as particles take part in chemical processes, such as the depletion of stratospheric ozone. At lower altitudes, especially ash particles are hazardous to air traffic. Above all, atmospheric particles affect the climate by scattering and absorption of radiation. To understand the climate system and our influence on it through the emission of greenhouse gases and particles, the natural variability must be carefully quantified. Volcanic eruptions constitute a sporadic, and sometimes large, natural source of variability in the Earth's climate.

The aim of the studies presented in this thesis was to improve our knowledge on the amount, characteristics, lifetime and radiative effect of aerosol particles in the upper troposphere and stratosphere resulting from volcanic eruptions.

The experimental studies were based on regular sampling and measurements of aerosol particles and trace gases using the CARIBIC observatory, which is mounted on a passenger aircraft, and lidar measurements from the satellite CALIPSO. Detailed information on aerosol composition, mass and size is obtained from the CARIBIC data, which facilitates investigations of the amount, sources and transport patterns of the sampled aerosol. The satellite, on the other hand, provides global observations of the distribution of the aerosol with both latitude and altitude, and its interaction with radiation. Together, these instruments provide a useful means of quantifying the impact of volcanism on the atmosphere and the climate, which is the ultimate goal of the studies presented.

2 Background

2.1 Aerosol properties

An aerosol is defined as a collection of solid and liquid particles suspended in a gas, which is stable long enough to be observed or measured (Kulkarni et al., 2011). However, in atmospheric science, the particles (not the air) are generally of greatest interest. Important parameters used to describe aerosol particles are their size, shape, composition and aerodynamic or light scattering properties. This section describes some of the elementary concepts of particle characteristics and behaviour, intended as a basis for later descriptions and discussions on particle measurements, their characteristics and their effects on climate.

2.1.1 Particle size and shape

Particle size is perhaps the most basic characteristic of a particle and is of relevance for many physical and chemical processes. The size (together with the composition and shape) affects how fast the particles settle under gravitation, their ability to scatter light, and to act as nuclei for the condensation of water vapour to form clouds. Aerosol particles in the atmosphere have a wide range of sizes, from few nm up to about 100 µm. The upper size limit results from the quick sedimentation velocity of larger particles. Aerosol particles can have many different shapes, from long fibres to cubic salt grains and spherical droplets, although many atmospheric particles tend to be more or less spherical as a consequence of growth by the condensation of gases into liquids (Kulkarni et al., 2011). There is no simple way of describing the size of an irregular particle. To solve this, an equivalent diameter is often used, which is the diameter of a sphere with a particular physical property equal to that of the irregular particle. The choice of equivalent diameter usually depends on the measurement technique used or a particular property of interest.

The aerodynamic diameter is used when sampling particles with impactors, as is the case with the CARIBIC observatory (described in the Methods Sec.). It is defined as the diameter of a sphere with a density of 1000 kg/m^3 (standard particle density, equal to that of a water droplet) and the same settling velocity (i.e. aerodynamic behaviour) as the irregular particle. Using a standard density solves the problems encountered when sampling particles with unknown composition and

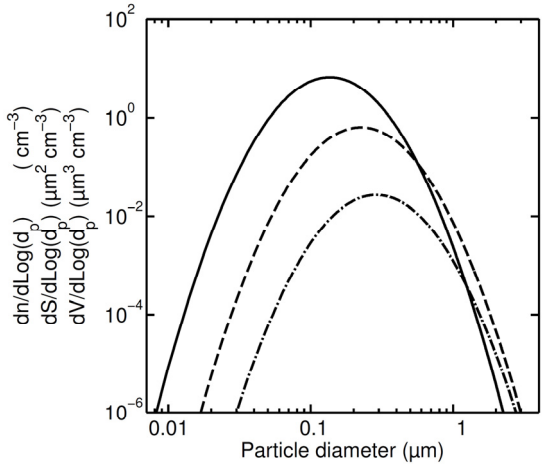

Figure 2.1 Number (solid line), surface area (dashed line) and volume (dash dotted line) particle size distributions for stratospheric aerosol in 1999 derived from balloon measurements at 20 km altitude. Adapted from Jäger and Deshler, (2002).

porosity. However, it means that two particles with the same aerodynamic diameter can have very different sizes in the reality, if their density and shape differ.

An aerosol that consists of particles with the same size (or that has a very narrow range of diameters) is called monodispersed. Such an aerosol can be carefully produced in the laboratory. However, most natural aerosols consist of particles with a wide range of diameters, often hundredfold, and these are referred to as polydispersed (Kulkarni et al., 2011). A common way of describing the particles in an aerosol is by the size distribution of the particles with a specific aerosol property, usually the number, surface area or volume (Fig. 2.1). Aerosol size distributions are often lognormal (i.e. a skewed normal distribution). Such a distribution appears normally distributed when plotted using a logarithmic x-scale, and this is usually done to include the smallest particles. The lognormal number distribution can be expressed as:

$$dn(\mathrm{d}_p) = \frac{N_t}{\sqrt{2\pi}\,\log(\sigma_g)} exp\left(-\frac{(\log(\mathrm{d}_p)-\log(CMD))^2}{2\log(\sigma_g)^2}\right) dlog\mathrm{d}_p \qquad (3.1)$$

where N_t is the total number concentration of particles, σ_g the geometric standard deviation and *CMD* is the count median diameter. To obtain the surface area and mass distributions, *CMD* is replaced by the corresponding median diameters and N_t by the total surface area or mass, respectively.

To express the particle sizes in a distribution, the (geometric) mean, median or mode (the size of the largest number of particles) diameter is often used (Hinds, 1999). Another commonly used description of the size of particles in an aerosol is

the effective radius, which is the area-weighted mean radius of the particle distribution.

$$r_e = \frac{\int_0^\infty r^3 n(r) dr}{\int_0^\infty r^2 n(r) dr} \tag{3.2}$$

The effective radius is used as an approximation of the mean radius for light scattering (Hansen and Travis, 1974) commonly used in optical measurements and calculations.

2.1.2 Light scattering of aerosol particles

The interaction of aerosol particles with light is an important property, as it is used in optical measurement techniques, and is of concern for the Earth's climate. All particles scatter radiation, and many adsorb light to varying degrees (Seinfeld and Pandis, 2006). Light scattering by particles is dependent on the refractive index of the particle and the relation between particle diameter (d) and the wavelength of the light (λ), expressed by the size parameter, $\alpha = \pi d/\lambda$. Very small particles and molecules in the atmosphere, for which $\alpha << 1$, belong to the Rayleigh scattering regime. They scatter light symmetrically in the forward and backward directions relative to the incoming light (Fig. 2.2a). Larger particles, of approximately the same size as the wavelength of light ($\alpha \approx 1$) belong to the Mie scattering regime, where the angular distribution of scattered light depends strongly on particle size. The fraction of light scattered in the forward direction increases with increasing particle diameter (Fig. 2.2b-c) (Hinds, 1999). Therefore, small particles have a greater effect on climate, as their backscattering is larger. Geometric scattering by large particles ($\alpha >> 1$), such as cloud particles, is further complicated by the strong dependence on particle shape and orientation (Seinfeld and Pandis, 2006).

For climate considerations, only the fraction scattered upwards back into space, called the upscatter fraction, is relevant. The dependence of the upscatter fraction on particle size and solar zenith angle for stratospheric sulphuric acid particles is

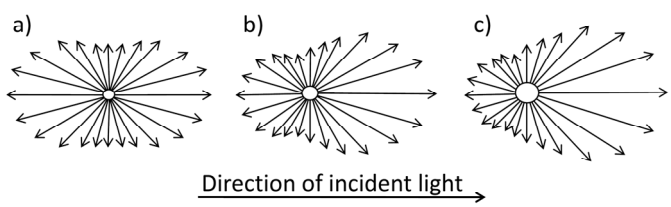

Figure 2.2 Illustration of light scattering by sulphate particles. a) Rayleigh scattering for particle diameters < 0.05 µm, b) Mie scattering for a particle diameter of 0.12 µm and c) Mie scattering for a particle diameter of 0.16 µm. Adapted from Schwartz (2011).

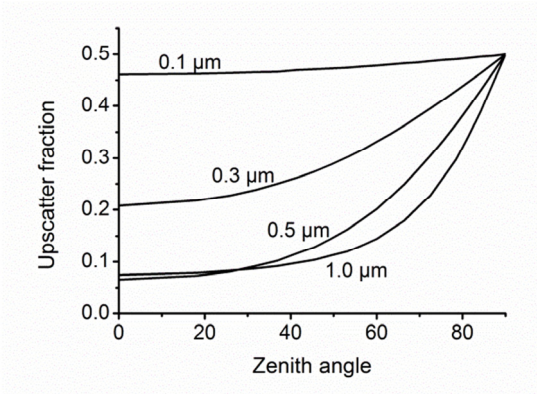

Figure 2.3 Upscatter fraction as a function of solar zenith angle for stratospheric sulphuric acid particles of different diameters. Adapted from Schwartz (2011).

shown in Fig. 2.3. Since light scattering is symmetric for small particles, the upscatter fraction becomes increasingly dependent on the solar zenith angle for increasing particle diameters. This leads to a strong dependence of the effect of aerosol particles on the climate on latitude, time of day and time of year (Nemesure et al., 1995).

The scattering and absorption of light by particles causes attenuation. The fractional depletion of radiance per unit path length is called the extinction coefficient (m^{-1}). Integration over the extinction coefficient in the atmospheric column gives the total fractional depletion of light, referred to as the aerosol optical depth or thickness (AOD or τ). This is a commonly used optical measure of the "amount" of aerosol and the light extinction in the atmospheric column.

2.2 Aerosols and climate

To understand anthropogenic climate change, all components of the climate system must be quantified, both natural and anthropogenic. Climate forcing is the term used to describe an imposed change in the planetary energy balance (Hansen et al., 2005). It is usually expressed as the difference in ingoing and outgoing radiative flux (W/m^2) at the tropopause or at the top of the atmosphere. There are many definitions of radiative forcing depending on the adjustment of the climate system that is allowed to take place before the change in energy balance is calculated. An overview is given by Hansen et al. (2005). Atmospheric aerosols play an important role in the climate system. Their effect can be divided into two categories: radiative forcing resulting from aerosol–radiation interactions (the direct effect) and radiative forcing arising from aerosol–cloud interactions (the indirect effect) (Forster et al., 2007; Boucher et al., 2013).

The indirect effect of aerosol particles refers to changes in cloud microphysics such as the number and size of cloud droplets, thereby affecting the amount of clouds, and their radiative properties and lifetime (Boucher et al., 2013; Forster et al., 2007). Clouds play a vital role in the Earth's radiative balance. They are mainly affected by tropospheric aerosols on which water condenses to form cloud droplets. This thesis is manly focused on stratospheric aerosols, for which the effects of direct scattering and absorption of radiation are most established. However, as discussed in Paper V, aerosol particles transported from the stratosphere into the upper troposphere may have an effect on the reflectivity of cirrus clouds.

The direct effect is greatest in the short-wave (solar) radiation spectrum, but large particles can also absorb and scatter long wave (terrestrial) radiation (Myhre et al., 2013). For stratospheric sulphate particles, a particle effective diameter of 4 μm has been found to be the limit between net surface cooling and heating (Lacis et al., 1992). The background (non-volcanic) stratospheric aerosol has an effective diameter of about 0.44 μm, but following the large eruption in Pinatubo in 1991, the effective diameter was found to increase to 1 μm or larger (Bauman et al., 2003). Stratospheric aerosols are thus unlikely to cause an increase in surface temperature unless the circumstances are extreme. However, the effect of long-wave forcing reduces the cooling (Lacis et al., 1992).

The magnitude of stratospheric aerosol forcing depends on the particle load, size and composition, which varies over time. Radiative forcing from the stratospheric aerosol has been estimated to be -0.06 W/m^2 over the period 1999-2002 (when there was no significant volcanic influence), and -0.11 W/m^2 from 2008 to 2011 (when there was moderate volcanic activity) (Myhre et al., 2013). In comparison, the net effective radiative forcing from the tropospheric aerosol (including their effects on clouds and rapid adjustments) was estimated to be -0.9 W/m^2 (range -1.9 to -0.1 with a 5 to 95% uncertainty), largely as a result of positive forcing from black carbon particles and negative forcing from sulphate particles (Myhre et al., 2013). Large volcanic eruptions can, however, cause substantially larger effects. The Pinatubo eruption in 1991 caused a net radiative forcing of 4.3W/m^2 between 40^{o}S and 40^{o}N, and a net cooling of the global climate (-0.5 ^{o}C) strong enough to exceed greenhouse warming in 1991-1992 (McCormick et al., 1995).

Global mean temperature shows an increasing trend since the late 19th century (Hartmann et al., 2013); more than half of this increase is very likely a consequence of anthropogenic emissions of greenhouse gases (Bindoff et al., 2013). However, during the past 15 years (1998-present) the trend in global warming has been slower than in the previous 30-60 years (Fig. 2.4), in particular in the Northern Hemisphere (Flato et al., 2013). This reduction occurs despite steadily increasing greenhouse gas concentrations (Hartmann et al., 2013), and is not predicted by most CMIP5 (coupled model intercomparison project) models (Fyfe et al., 2013b; Flato et al., 2013). It has been suggested that the discrepancy between model predictions and the actual trend in temperature increase is caused

by a combination of internal climate variability not captured by the models, missing or incorrect radiative forcing and model climate response error (Flato et al., 2013). One possible reason for the lack of radiative forcing currently being investigated is that cooling induced by moderate volcanic eruptions after 2000 was not taken into account in these models. Recent results suggest that volcanic forcing may account for 15% (Santer et al., 2014), or as much as 30% (Schmidt et al., 2014), of the discrepancy.

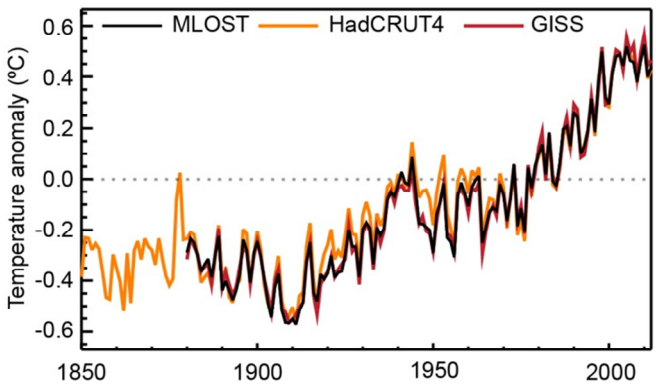

Figure 2.4 Annual global mean surface temperature anomalies relative to 1961-1990 climatology from three datasets. Reproduced from fig. 2.20 in IPCC, Hartmann et al., 2013.

2.3 The structure and dynamics of the upper troposphere and stratosphere

Before describing the stratospheric aerosol in detail, it is relevant to discuss the structure and transport patterns of the upper troposphere (UT) and stratosphere. Fig. 2.5 shows a simple illustration of the UT and stratosphere and the meridional circulation. The stratosphere and troposphere are separated by the tropopause, a region of strong stability that acts as a transport barrier (Gettelman et al., 2011). The tropopause is traditionally defined as the thermal tropopause, which is the lowest altitude at which the temperature lapse rate (i.e. the rate at which the atmospheric temperature decreases with increasing altitude) is less than 2 K m^{-1} continuously for 2 km or more. In addition, the dynamic tropopause (based on potential vorticity) and the chemical tropopause (based on trace gas gradients) are frequently used (Gettelman et al., 2011). The lowermost stratosphere (LMS, the shaded region in Fig. 2.5), is found mainly in the extra-tropics and is bounded downwards by the tropopause and upwards by the 380 K potential temperature surface (the 380 K isentrope) (Dessler et al., 1995; Holton et al., 1995). Although

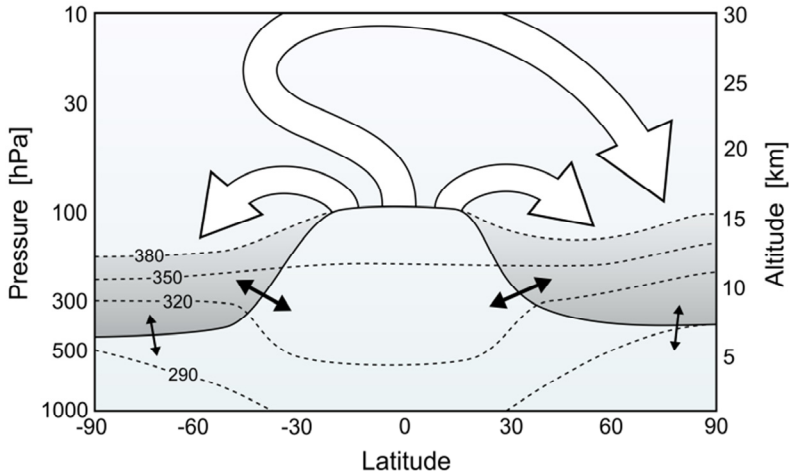

Figure 2.5 Illustration of the structure and transport in the upper troposphere and stratosphere during the Northern Hemisphere winter. The solid black line indicates the tropopause, dotted lines potential temperature surfaces ≤ 380K, and the shaded grey area the lowermost stratosphere. The Brewer-Dobson circulation is illustrated by the large white arrows and mixing across the tropopause by small black arrows (based on Holton et al., 1995 and Birner and Bönisch, 2011).

the LMS occupies a relatively small altitude span in the extra-tropics, approximately 10 to 15 km, it accounts for about 40% of the total stratospheric mass (Appenzeller et al., 1996). The LMS differs from the stratosphere above the 380K isentrope in that isentropes in the LMS cross the tropopause, along which adiabatic exchange between the stratosphere and troposphere can occur (Hoskins, 1991; Dessler et al., 1995).

The stratosphere is characterised by increasing temperature with altitude, which counteracts vertical transport. However, high zonal wind speeds in the extra-tropical stratosphere transport air rapidly along the latitude bands. The stratospheric zonal circulation is characterised by easterly winds in the summer hemisphere and westerly winds in the winter hemisphere, with maximum wind speeds of 70 m/s or more at altitudes of about 60 km (Holton, 2004). Meridional and vertical transport occur mainly in an overturning circulation referred to as the Brewer–Dobson circulation (large white arrows in Fig. 2.5). The Brewer–Dobson circulation is induced by the wave driven transport of air from the tropics to the poles, causing upwelling of air in the tropics and downwelling in the extra-tropics (Holton et al., 1995). This transport can be considered to take place in two branches: a shallow branch that transports air from the tropics to the extra-tropics just above the tropopause on a timescale of a few months, and a deep branch reaching up to the mesosphere, where transport to the extra-tropical LMS takes place on the timescale of years (Birner and Bönisch, 2011).

The LMS contains a mixture of air transported from the stratosphere above the 380 K isentrope via the Brewer–Dobson circulation, and air transported across the

tropopause (Dessler et al., 1995). Two-way cross-tropopause transport mainly occurs along crossing isentropes in the subtropics, but also in association with tropopause folds (Sprenger and Wernli, 2003) and convection (Fischer et al., 2003; Tang et al., 2011). Mixing across the tropopause results in what is referred to as the extra-tropical transition layer, characterised by strong gradients in trace gases such as ozone and carbon monoxide, extending from the tropopause and 2 km upwards (Gettelman et al., 2011; Hoor et al., 2002). Much of the exchange is transient in nature, and the exchanged air remain in the stratosphere/troposphere for only a few hours (Stohl et al., 2003). The mass of the LMS and the strength of the transport paths vary over the year (Appenzeller et al., 1996). The Brewer–Dobson circulation is strongest in the winter hemisphere. The largest seasonal dependence is observed for the deep branch being almost insignificant during summer (Birner and Bönisch, 2011). This leads to a change in the mean age of the air (i.e. its time in the stratosphere) in the LMS, with minimum mean age in fall and maximum in late spring (Bönisch et al., 2009).

2.4 Sources and characteristics of the stratospheric aerosol

The stratospheric aerosol load shows substantial variation over time, mainly as a consequence of particles produced from large volcanic eruptions (Sato et al., 1993; Ammann et al., 2003). The first measurements of the stratospheric aerosol were, however, performed in volcanically quiescent times, in the late 1950s by Junge et al. (1961). They used balloon-borne impactors and revealed a layer of sulphate aerosol at approximately 20 km altitude, thereafter referred to as the "Junge layer". Later measurements by Rosen (1971), indicated that the composition was approximately 75% sulphuric acid and 25% water.

The main source of the "background" aerosol was attributed to the transport of carbonyl sulphide (OCS) from the troposphere (Crutzen, 1976). OCS originates from both natural and anthropogenic sources, emitted directly or from the conversion of other sulphur-containing gases. The ocean is the largest natural source of OCS (Seinfeld and Pandis, 2006). OCS is relatively inert and can therefore be transported into the stratosphere by tropical upwelling (Brühl et al., 2012). In the stratosphere, OCS is photodissociated into SO_2, and subsequently oxidized to from a sulphate aerosol (Crutzen, 1976). However, it is unclear whether OCS alone can explain the abundance of the stratospheric sulphate aerosol (Chin and Davis, 1995). Direct transport of SO_2 or sulphate aerosol into the stratosphere can also be important (Pitari et al., 2002; Myhre et al., 2004). More recent research suggests, however, that OSC from natural and anthropogenic sources can explain the observed aerosol load (Brühl et al., 2012).

The sulphate aerosol layer at an altitude of 20 km is the result of tropical upwelling of sulphurous precursor gases, followed by nucleation and growth by condensation and coagulation and, finally, removal by transport to the troposphere (Deshler, 2008). The size distribution of the background stratospheric aerosol is mono-modal with a particle median diameter of approximately 0.16 μm (Fig. 2.1) (Jäger and Deshler, 2002). Due to the small size of the particles, gravitational sedimentation is slow, compared to transport of air across the extra-tropical tropopause (Martinsson et al., 2005; Deshler, 2008).

Apart from sulphate, the stratospheric aerosol contains a large carbonaceous fraction (Nguyen et al., 2008; Murphy et al., 2007). A study of the morphology of the sulphurous and carbonaceous aerosol sampled in the LMS has shown separated fractions of these compounds in complicated branched structures within the particles (Nguyen et al., 2008). The nature and origin of the carbonaceous aerosol in the stratosphere is, as yet, poorly understood. It has been suggested that the carbonaceous aerosol is transported from the UT, and it shows a decrease in abundance in the stratosphere with distance from the tropopause (Murphy et al., 2013). In addition, results presented in Paper II show that in the period 2005-2008 the LMS carbonaceous aerosol was associated with tropical volcanism. This aerosol contained a carbonaceous fraction that was approximately 22% of the sulphurous mass, and probably of organic nature.

Murphy et al. (2007) identified three main categories of stratospheric particles during "background conditions" over the southern parts of North America: 1) almost pure sulphuric acid with associated water, 2) organic sulphate particles originating from the troposphere, and 3) sulphuric acid with metals from the ablation of meteoroids. Ablated meteoritic material was found in about half of the 0.2-3 μm diameter particles, and increased with altitude (Cziczo et al., 2001). Meteoritic iron constitutes a small fraction (0.5-1%) of the particle mass.

Other minor sources of the stratospheric aerosol are material from the Earth's crust particles produced by air traffic exhaust and particles from large forest fires. Dust particles are frequently found in the LMS with higher than average concentrations during spring (on average 18% crustal iron of the sulphur mass) (Martinsson et al., 2005). Aircraft emissions are estimated to have a minor effect on UT/LMS sulphate mass (< 1%), but can be important regarding the number concentration of small particles (< 0.05 μm diameter) (Kjellström et al., 1999; Ferry et al., 1999).

Particles from forest fires can be transported into the stratosphere by pyro-convection during specific meteorological conditions that enhance the strong convection caused by heat from the fire (Fromm and Servranckx, 2003). Such events have been reported from satellite observations (Fromm and Servranckx, 2003) and *in situ* observations (Jost et al., 2004). One large event in 2001 was estimated to have contributed more than 5% to the background aerosol mass in the lower stratosphere. However, the global importance of pyro-convection is not yet fully understood (Fromm et al., 2008; Fromm et al., 2010). It has been estimated

that, on average, six such events per year lead to the injection of particles to altitudes above 8 km, with the potential to reach the LMS (Guan et al., 2010). Although the effects of pyro-convection are not comparable to those of large volcanic eruptions, there is some evidence that this phenomenon can explain some of the stratospheric variability previously assigned to volcanic eruptions, based on poor evidence (Fromm et al., 2010).

2.5 Volcanic influence on the stratospheric aerosol

Volcanic eruptions inject large amounts of ash and gases into the atmosphere. The main compounds emitted are, in descending order with respect to mass: water vapour, CO_2, SO_2, H_2S, HCl, HF, H_2, CO and HBr. The amounts of these components differ greatly between eruptions, and with time (von Glasow et al., 2009). SO_2 is relevance for the atmospheric aerosol load, as large amounts are emitted and is converted into sulphate particles in the atmosphere.

Ash particles are the smallest fragments of magma and wall rock, and are defined as being less than 2 mm in size (Heiken and Wohletz, 1985). In the field of aerosol science, 2 mm is a very large size, and these particles will settle quickly. Fine ash particles in the μm size range, on the other hand, can be transported long distances (Rose and Durant, 2009), and have been observed in the atmosphere several months after eruptions (Pueschel et al., 1994; Andersson et al., 2013; Griessbach et al., 2014). In addition, aerosols sampled during periods of volcanic influence have been found to contain a large organic component that is still not fully understood (Martinsson et al., 2009; Schmale et al., 2010). However, it was hypothesized Paper I that carbonaceous particles could be transported from the boundary layer with the volcanic plume.

Three main factors control the impact of a volcanic eruption on the atmospheric aerosol: the injection altitude, the amount of SO_2 (and ash) emitted, and the geographical location. To cause a lasting influence, an eruption must be explosive enough to reach into the stratosphere, where the residence time of aerosol particles is longer than in the troposphere. The location of an eruption is important as this determines the spread and lifetime of the aerosol produced. Eruptions in the tropics that reaches into the stratosphere at about 17 km altitude (Gettelman et al., 2011), can be spread globally or hemispherically by the pole-ward Brewer–Dobson circulation, and have a global effect. Extra-tropical eruptions enter the stratosphere at lower altitudes, on average 10 km (Gettelman et al., 2011). As a result of the extra-tropical decent of stratospheric air, the aerosol in these regions is expected to have a shorter residence time.

Historically, a number of strong volcanic eruptions have dramatically perturbed the stratospheric aerosol load (Fig. 2.6)(Sato et al., 1993). In the 19th century large perturbations were caused by the eruption of Anung (1963), El Chicon (1982) and

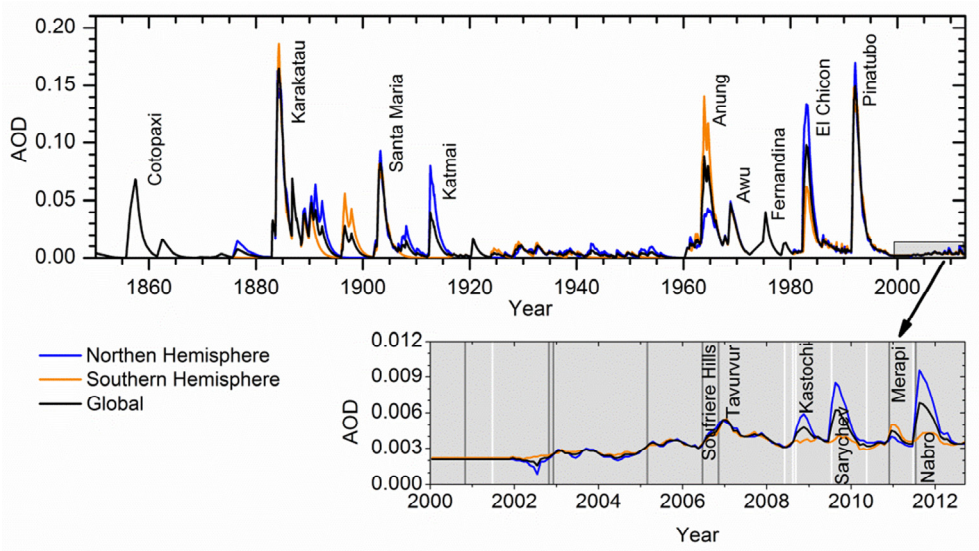

Figure 2.6 Time series of stratospheric aerosol optical depth (AOD) used in several climate modelling studies (data taken from Sato et al., 1993, http://data.giss.nasa.gov/modelforce/strataer/). The grey area in the upper graph is shown enlarged, where the dates of extra-tropical and tropical eruptions are indicated by vertical white and grey lines, respectively.

Pinatubo (1991). Since the Pinatubo eruption no major perturbation of the stratospheric aerosol load has occurred. Due to the lack of large eruptions, the stratospheric AOD has been assumed to be at the background state since 2000 until recently. However, an increasing trend in AOD of 4-7% per year from 2000 to 2008 has been reported, initially suggested to be the result of increased coal burning (Hofmann et al., 2009). Vernier et al. (2011b) subsequently showed that this increase could be attributed to moderate tropical volcanism, previously not considered sufficient to significantly affect the stratosphere (Table 2.1 and Fig. 2.6). In particular, the tropical volcanoes Soufrière Hills (2006), Tavurvur (2006), Merapi (2010) and Nabro (2011) were significant sources of stratospheric aerosols (Vernier et al., 2011b; Bourassa et al., 2012). A number of extra-tropical eruptions also occurred in this time period; the greatest effect being from the eruptions of Kasatochi (2008) and Sarychev (2009) (Paper IV).

The Pinatubo eruption in 1991 is the largest eruption in modern time, and has been thoroughly investigated using a broad range of measurement methods and models. Pinatubo injected about 20 Tg of SO_2 into the atmosphere, which was converted into a sulphate aerosol layer initially located at an altitude of 20-27 km (McCormick et al., 1995). The residence time of SO_2 was estimated to be about 30 days (e.g. Bluth et al., 1992; Read et al., 1993; Guo et al., 2004). The aerosol spread globally and had pronounced effects on both tropospheric and stratospheric temperatures. Initially, the stratosphere became warmer than average due to the absorption of radiation by the particles produced. However, since the stratospheric

Table 2.1 Volcanic eruptions post year 2000 with a Volcanic Explosivity Index ≥ 4.

Tropical volcanoes	Eruption date	Extra-tropical volcanoes	Eruption date
Ruang	25/9/2002	Shiveluch	22/5/2001
Reventador	3/11/2002	Chaitèn	2/5/2008
Manam	27/1/2005	Okmok	12/7/2008
Soufrière Hills	20/5/2006	Kasatochi	7/8/2008
Tavurvur	7/10/2006	Sarychev	12/6/2009
Merapi	20/10/2010	Eyjafjallajökull	14/4/2010
Nabro	13/6/2011	Grímsvötn	21/5/2011

aerosol acts as a surface for reactions releasing reactive chlorine, which depletes ozone, lower than average stratospheric temperatures were subsequently observed (McCormick et al., 1995). Not only the amount, but the size of the aerosol particles increased, from a median count diameter of 0.16 μm to a bimodal distribution, with modes peaking at diameters of 0.3 and 0.9 μm six months after the eruption (Jäger and Deshler, 2002). The aerosol produced by Pinatubo decayed with an e-folding time of about 1 year, similar to estimates of the residence time of the aerosol from the eruption of El-Chicon, of 10 months (Jäger, 2005).

Much of what is known about volcanic aerosols has been established from studies of the Pinatubo eruption. The SO_2 emissions from subsequent eruptions were factors of 10-100 smaller. Volcanic clouds from the extra-tropical eruptions of Kasatochi (2008) and Sarychev (2009) have been studied using satellite remote sensing (Heard et al., 2012) and *in situ* observations (Schmale et al., 2010; Andersson et al., 2013), and induced modelling of the development and radiative effects of these volcanic clouds (Haywood et al., 2010; Kravitz et al., 2010; Kravitz et al., 2011; Heard et al., 2012). However, difficulties in estimating the size and effects of the eruptions were reported, related to detection limits of SO_2 (Heard et al., 2012) and mixing with stratospheric air (Krotkov et al., 2010), as well as a mismatch between the observed and modelled AOD (Kravitz et al., 2010). The last mentioned is probably linked to limitations of the stratospheric AOD to altitudes above the 380 K isentrope (excluding the LMS), as discussed in Sec. 4.3 and Paper IV. Because of the altitude restrictions of currently existing stratospheric AOD datasets based on satellite observations (Sato et al., 1993; Vernier et al., 2009; Bourassa et al., 2012), the effects of tropical and, in particular, extra-tropical eruptions on the stratospheric aerosol burden and climate have not been fully represented.

Although modelling showed no significant cooling of surface temperatures as a result of the Kasatochi (Kravitz et al., 2010) and Sarychev (Haywood et al., 2010) eruptions, subsequent studies suggest that stratospheric variability induced by volcanism after 2000 must be considered in climate modelling (Solomon et al., 2011), otherwise surface temperatures may be overestimated by approximately 0.02-0.07 degrees (Solomon et al., 2011; Fyfe et al., 2013a; Haywood et al., 2014).

Furthermore, these eruptions may help explain the present global temperature hiatus (Schmidt et al., 2014; Santer et al., 2014). To understand the importance of volcanic eruptions after 2000, quantification of their impact on the stratospheric aerosol load, in terms of mass and aerosol microphysics, as well as cloud effects, is required.

3 Measurements and Methods

Studies of aerosols in the stratosphere and UT can be performed by *in situ* measurements from aircraft or balloons, or by remote sensing using ground-based or satellite-borne platforms. Satellite- and aircraft-based platforms have the advantage of not observing a fixed location; especially satellites have near global coverage. However, remote sensors cannot provide the same detail as *in situ* observations. The papers included in this thesis are mainly based on aerosol sampling using the CARIBIC (Civil Aircraft for the Regular Investigation of the atmosphere Based on an Instrument Container) flying observatory, and lidar measurements from the CALIPSO (Cloud-Aerosol Lidar and Infrared Pathfinder Satellite Observations) satellite. While CARIBIC observations were used in all the papers, CALIPSO observations were the primary method used in the study presented in Paper IV. Furthermore, cirrus reflectance from the MODIS instruments on the Terra and Aqua satellites were used in the study described in Paper V.

3.1 CARIBIC

The CARIBIC scientific collaboration started to perform regular atmospheric measurements in 1997 using an instrument container on board a Boeing 767-300 ER operated by LTU International Airways. The first phase of the project (1997-2002) was carried out using this passenger aircraft by performing *in situ* measurements of O_3, CO and particle number concentrations, as well as sampling of air and particles for laboratory analysis (Brenninkmeijer et al., 1999). In late 2004 the second (present) phase of the project was started, with an extended scientific payload, now mounted in the cargo bay of an Airbus A340-600 operated by Lufthansa (Brenninkmeijer et al., 2007).

The CARIBIC instrument container is installed in the aircraft during 4-6 intercontinental flights per month from Frankfurt Airport (Germany) and back. Flight destinations in Southeast Asia, East Asia, Southern Africa, and North and South America offer good cover of the Northern Hemisphere. Measurements at flight altitudes of 9-12 km provide data for the study of the free troposphere in tropical regions and the UT/LMS in the extra-tropics. In addition, three special flights were carried out in April and May 2010 to study the fresh volcanic cloud

from the Eyjafjallajökull eruption (Iceland) at altitudes of 4-12 km. Measurements take place through a shrouded inlet mounted underneath the aircraft. The inlet has three separate probes for sampling of total water (gas, liquid and ice), trace gases and aerosols. The present instrument container weighs about 1.6 tonnes, and contains instruments for *in situ* measurements of total and gaseous H_2O, NO and NO_y, CO, CO_2, O_3 and Hg as well as the collection of air samples that are analysed in the laboratory for greenhouse gases, hydro- and halocarbons (Brenninkmeijer et al., 2007). The inlet system is equipped with a spectrometer for remote sensing of total column measurements of trace gases, such as SO_2 from volcanic eruptions (Heue et al., 2010), and a video camera to observe the environment during flight.

Aerosol characteristics are measured using three different instruments in the container. Particle number concentrations and size distributions are provided by three condensation particle counters, and an optical particle counter (OPC), respectively (Martinsson et al., 2014; Hermann et al., 2003). Sampling of aerosol particles followed by laboratory analyses provides the aerosol mass and elemental concentration (Nguyen et al., 2006; Nguyen and Martinsson, 2007; Martinsson et al., 2014). Previously, the morphology of the collected particles was also studied (Nguyen et al., 2008). The chemical characterisation of the collected aerosol is performed at Lund University, and is the main methodology used for the studies presented in this thesis. Aerosol sampling and analysis are described below.

3.1.1 Aerosol sampling

Aerosol sampling of particles in the size range 0.08-2 μm diameter is performed by impaction technique onto 0.2 μm thick polyimide films (Nguyen et al., 2006). This technique is based on the acceleration of an airstream in a small nozzle towards the film. Particles that have too high inertia to follow the airstream when it bends at the surface of the film, impact on to the film and are deposited. The cut-off diameter of the sampler (at which 50% of the particles impact) defines the lower size limit (0.08 μm). This is determined by the flow rate of the air and the diameter of the orifice (Hinds, 1999). The upper size limit of 2 μm is obtained by placing a cyclone before the sampler to remove larger particles (Nguyen et al., 2006). A cyclone removes particles above a certain aerodynamic diameter by rotating the air, which causes large particles to be deposited on the walls of the instrument due to the centrifugal force (Hinds, 1999).

The CARIBIC aerosol sampler consists of 16 separate impactor samplers, all but two of these channels are used for sequential sampling during flight with a sampling time of typically 100 minutes, corresponding to a sampling volume of 0.25 m^3 of air at STP (standard temperature (273.15 K) and pressure (1013.25 hPa)). Each of these channels has a nozzle with four orifices, 0.5 mm diameter. The two remaining impactor channels are used to collect integral samples, and are open during the entire sampling time, when travelling from or back to Frankfurt

Airport. They consist of only one orifice with the same diameter as the others. The integral samples are used for contamination control, by comparing the concentrations in the integral samples to the sum of the sequential samples (Nguyen et al., 2006).

In the first phase of CARIBIC (1999-2002), a different sampler was used, which consisted of 12 channels for sequential sampling with a longer typical sampling time of 150 minutes (~0.09 m^3 air STP), and two channels for integral sampling. Each of these impactor nozzles consisted of only one orifice with similar upper and lower cut-off diameters to the present sampler. Also, two different sampling inlets have been used, however, both have an estimated collection efficiency for particles of 0.1-1 µm diameter of 90%, or more in phase 2 (Hermann et al., 2001; Martinsson et al., 2014).

3.1.2 Aerosol analysis

The elemental concentrations of the sampled particles are determined by irradiating the samples with a 2.55 MeV proton beam. Two methods are employed: proton-induced X-ray emission (PIXE) and, since 2005, particle elastic scattering analysis (PESA). The uncertainty of both methods is estimated to be 10% (Papaspiropoulos et al., 2002; Nguyen and Martinsson, 2007). The analyses are performed in high vacuum, approximately 10^{-5} hPa, and evaporative losses of elements with high vapour pressure at room temperature can occur (Martinsson et al., 2014).

The PIXE method takes advantage of the interaction between atomic electrons and the protons, which can lead to the ejection of inner shell electrons. This gives rise to electromagnetic radiation when the vacancies created are filled with outer shell electrons. The radiation that is emitted is in the keV energy range and is referred to as characteristic X-rays, because the energy is specific to the element and excitation state of the atom (Johansson and Campbell, 1988). The spectra obtained show X-ray peaks positioned on a background from bremsstrahlung and gamma rays. Analysis of the size of the peaks yields absolute concentrations in the sample.

PIXE is a very sensitive technique, which makes it suitable for aerosol analysis where the collected mass is often low. It is optimal for proton energies of few MeV (Johansson and Campbell, 1988). PIXE is used for the detection of elements with atomic numbers ≥14 (Si) in the aerosol samples, although Si can only be determined if this component is large enough, due to interference from the often dominating S peak (Andersson et al., 2013). Typical detection limits in units of ng m^{-3} at STP are 2, 0.2 and 0.1 for S, K and Fe, respectively.

For elements with lower atomic number, the sensitivity decreases and thus a complementary method is needed. Therefore, the PESA technique is applied to determine the concentrations of important elements with low atomic numbers, H,

C, N and O. In this method the energy of protons elastically scattered from the atomic nuclei of the target is measured. This energy is determined by the energy of the proton beam, the mass of the scattering nucleus and the scattering angle. Concentrations of C, N and O are obtained by measuring the proton backscattering, while the amount of H is obtained from forward scattering. Typical detection limits are 1, 15, 3 and 7 ng m^{-3} at STP for H, C, N and O, respectivley.

Analysis by PIXE and PESA is carried out in two steps, using proton beams with different sizes. A 5.5 mm diameter beam is used to cover all four aerosol deposit spots to obtain total elemental concentrations with PIXE technique. In order to determine the amounts of the light elements (H, C, N and O), additional analysis is performed by both PIXE and PESA using a smaller beam 1 mm in diameter, sequentially positioned at one of the aerosol spots and at two positions on the blank film on both sides of the deposits. The two irradiations of the blank film provide the background concentrations of H, C, N and O in the film, which are subsequently subtracted from the concentrations obtained in the deposit spot. Analysis over only one aerosol deposit spot provides better aerosol-to-backing ratios, needed to obtain sufficiently low detection limits for PESA. The degree of variability between the two blank spots determines the detection limit. The relative concentrations obtained from analysing one of the aerosol deposit spots can be related to the total concentrations in all the deposited material obtained from analysis with the larger beam using PIXE. Although only one of the four aerosol

Table 3.1 Classification of aerosol deposit patterns and the expected effect on the results of analysis, where QI= 0,1or 2 indicates no significant losses, discernible and serious analytical losses, respectively. (From table 1 in Paper III.)

Category, Explanation	No. samples	QI
Type 1 – The expected pattern		
1.1 medium–high-loaded samples	30	0
1.2 low-loaded samples	3	0
Type 2 – Wetting of sampling substrate by liquid		
2.1 wetting only within beam area	29	0
2.2 minor wetting outside beam area	5	0
2.3 considerable wetting outside beam area	1	2
Type 3 – Secondary deposition pattern		
3.1 central spot visible	21	1
3.2 cross visible	7	2
3.3 cross clearly visible	3	2
Type 4 – Large number of particles outside main deposit	7	2
Qualitative Indicator (QI)		
0 types 1.1, 1.2, 2.1, 2.2	67	0
1 type 3.1	21	1
2 types 2.3, 3.2, 3.3, 4	18	2
All QI all types	106	All

deposit spots is analysed, the large number of particles in one spot ensures that it is representative of the sampled aerosol and the air mass encountered (Nguyen 2007).

3.1.3 Effects due to sampling artefacts

Non-ideal sampling of the aerosol can affect the measured concentrations. If the aerosol is deposited outside the area covered by the 5.5 mm beam used for PIXE analysis, the measured concentrations will be underestimated. In Paper III, the deposition patterns of aerosol samples collected in the 1-year period from April 2011 to March 2012 were investigated. Four different kinds of deposition patterns (Fig. 3.1) could be identified:

1. Samples with good sampling characteristics indicated by four distinct spots.
2. Samples of liquid particles that caused wetting of the sampling substrate forming filaments of deposits outside the four impaction spots.
3. Samples with secondary deposition of aerosol in the centre between the four original deposition spots, and sometimes in a cross between them, caused by particle bounce-off.
4. Samples with a large number (>15) of particles outside the main spots, probably caused by particle bouncing or imperfections in the film.

These categories were further divided into sub-types, as listed in Table 3.1, together with the number of samples of each kind. A qualitative indicator (QI) describing how these sample types are expected to affect the analysis is also included, where QI = 0 corresponds to no significant analytical losses, QI = 1 discernible losses and QI = 2 more serious losses. It can be seen from Table 3.1 that although most of the samples analysed show sampling characteristics that are not expected to lead to significant underestimation (83%, QI = 0 or 1), 18 out of 106 analysed samples had significant deposition outside the beam area.

In particular, sampling in ice clouds or sampling of aerosols with a high crustal component caused problems. When ice particles hit the inlet at cruising speed, they were found to break off Ni particles from the coating of the inlet. These Ni particles seem to be affected by bounce-off to a higher degree (type 3 or 4) and, most importantly, contribute with artificial particle mass. Crustal particles also show a higher tendency to bounce. Stratospheric samples were most affected by wetting, because they are often most heavily loaded, although only one out of 35 samples was affected by wetting to such a degree that it caused serious problems in the analyses.

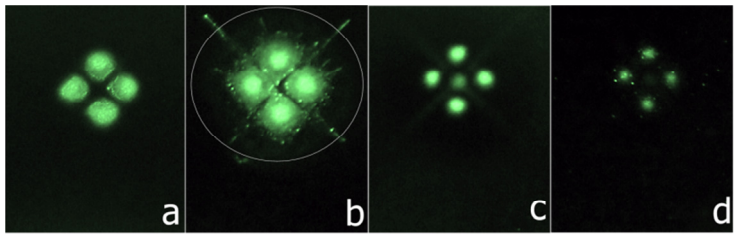

Figure 3.1 Typical aerosol deposit patterns for the four types of samples identified. a) Type 1: the expected pattern, b) Type 2: wetting of sampling substrate by liquid particles, c) Type 3: secondary deposition pattern, d) Type 4: large number of particles outside the main deposit. The size of the irradiated area is illustrated by the ellipse in b).

3.1.4 Particle size distributions and volume-to-mass comparisons

Aerosol size distributions in the CARIBIC set-up are obtained from the 16-channel OPC by the detection of scattered light from a diode laser at a wavelength of 830 nm. The lower detection limit for size distributions is 0.12 µm diameter, and the upper limit is 1-1.3 µm, depending on the particle refractive index and the calibration curves. Larger particles are counted, but the size cannot be accurately determined. The particle refractive index is set to 1.479 - 0.0143*i* based on the composition of UT particles from the literature, composing 44% H_2SO_4, 44% $(NH_4)_2SO_4$, 10% organic carbon and 2% soot. The refractive index and the sampling air flow determine the measurement uncertainties: 10% in particle size and 19% in particle number concentration, resulting in a 50% uncertainty in the particle volume.

A comparison of the aerosol mass obtained from accelerator analysis and from the integrated volume distributions from the OPC (Paper III), averaged over the aerosol sampling time, showed that most analysed samples have a volume-to-mass ratio (C_v/C_m) within a relatively narrow interval of 0.55-1.55 (Fig. 3.2). Outliers from this interval were associated with uncertain size determination of particles with a refractive index different from that assumed in the calibration, non-ideal aerosol deposition (see previous Sec.), and/or mismatch in the size range of sampled particles for the OPC (optical diameter) and aerosol sampler (aerodynamic diameter). Sampling in ice clouds in particular caused deviating C_v/C_m ratios (> 1.55) due to Ni particles released from the inlet when hit by ice. These probably caused problems because of their large diameter, their deviating refractive index and bounce-off at deposition. Large C_v/C_m ratios were also found for samples containing crustal particles, due to similar problems as the artificial Ni particles. Values of C_v/C_m lower than 0.55 were found for particles with a large carbonaceous component, which were found to be small particles not fully captured by the OPC, and probably due to problems associated with the refractive index. Outliers with $C_v/C_m > 1.55$ were related to uncertain size determination of

the particles with large volume mean diameter, associated with the shape of the calibration curve used for the OPC.

The relation between the total mass and volume of the aerosol yields a particle density of 1.15 g/cm^3, when samples with C_v/C_m outside the 0.55-1.55 range and those with defective deposition patterns were excluded. This is lower than values given in the literature based on measurements in remote and urban locations, which indicate a density of ~1.5 g/cm^3. However, the 30% lower density obtained from the CARIBIC measurements lies within the uncertainty of 50% in the particle density from the combined uncertainties in the particle volume and mass. The conditions under which aerosol measurements and sampling were carried out varied considerably, over a factor 50 in aerosol concentration (see Fig. 3.2), and over a factor 100 in the mass ratio of the two main components sampled, S and C. The comparison of volume and mass confirms that consistent results can be obtained despite the large variations in sampling conditions and the vastly different measurement principles of the techniques.

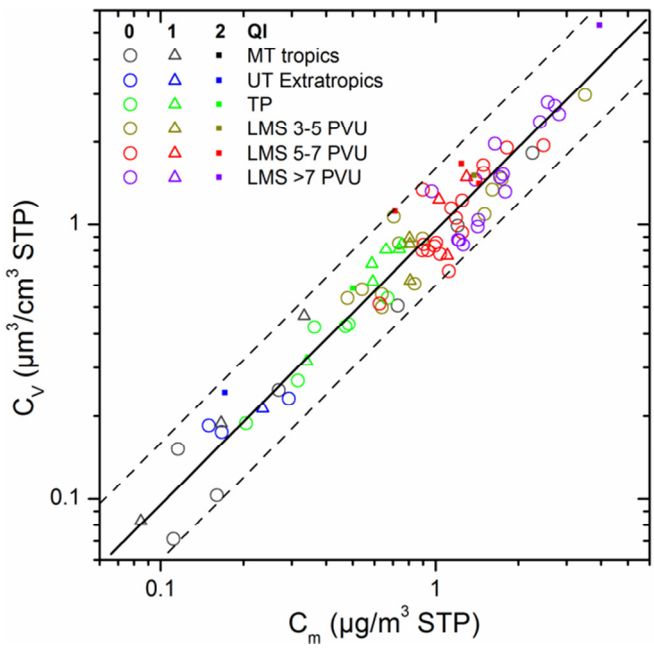

Figure 3.2 Particle volume concentrations (Cv) from the OPC vs. particle mass concentrations (Cm) from aerosol samples within a C_v/C_m interval of 0.55-1.55 (17 outliers excluded). The colour of the symbols indicates the sampling location: Middle Troposphere (MT), Upper Troposphere (UT), Tropopause Region (TP) and Lowermost Stratosphere (LMS). The symbols indicate the qualitative indicator (QI) of the expected analytical result (see text for explanation).

3.1.5 Stratospheric tracers

In the analysis of the collected aerosol, potential vorticity (PV) and ozone (O_3) are used as tracers for the sampling depth in the LMS and the degree of influence of the deep stratosphere, respectively. PV is defined by:

$$PV = g(\zeta_\theta + f)\frac{d\theta}{dP} \tag{3.1}$$

which is the product of the gravitational constant (g), and the sum of the relative (ζ) and planetary (f) vorticity and the static stability ($d\theta/dP$) of the air mass, θ denotes potential temperature and P pressure. The unit of PV is 10^{-6} m^2 s^{-1} K kg^{-1} = 1 PV unit or 1 PVU (Bluestein, 1993). PV increases rapidly above the tropopause, and is used to define the dynamical tropopause, usually in the region 1.5-3.5 PVU. The PV along the CARIBIC flight paths is obtained from the European Centre for Medium Range Weather Forecasts (ECMWF) archived analyses, linearly interpolated to the aircraft's position from the original resolution of 1x1 degree horizontal and 91 vertical hybrid sigma pressure model levels. Figure 3.3 illustrates average potential vorticity (PV) during flights in 1999-2013.

Ozone mixing ratios along the flight path are measured by two instruments on board the CARIBIC platform. A UV photometer accurately measure the ozone concentration by the absorption of UV light, and serves as a standard for a chemiluminescence detector with high temporal resolution (10 Hz), which at cruise speed yields an effective spatial resolution of 30-40 m. The accuracy in CARIBIC phase 2 was estimated to be 2% (4% or 4 ppb in phase 1)(Zahn et al., 2002; Zahn et al., 2012). For use in the analysis of sampled aerosols, O_3 and PV are averaged to the sampling resolution of the aerosol sampler (100 minutes).

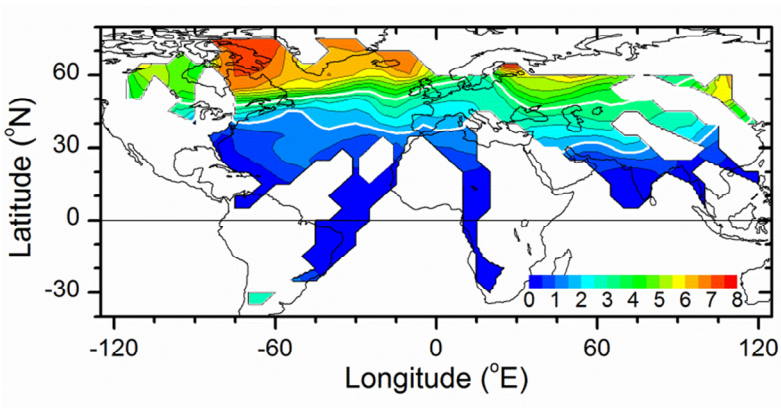

Figure 3.3 Geographical distribution of PV at CARIBIC flight altitudes of 9-12 km, based on conditions during aerosol sampling in 1999-2013. The white lines show PV isopleths of 1.5 and 3.5 PVU, within which the dynamical tropopause is often defined.

3.2 CALIPSO

CALIPSO was launched in April 2006, and is part of the NASA A-Train consisting of 5 satellites (Aqua, CloudSat, CALIPSO, PARASOL and Aura) currently orbiting the Earth with the mission to improve our understanding of the atmosphere and its interaction with climate. CALIPSO covers the globe between 82^{o} N and 82^{o} S, and has a 16-day repeat cycle. The main instrument aboard CALIPSO for atmospheric observations is the Cloud-Aerosol LIdar with Orthogonal Polarization (CALIOP) instrument. In addition the Imaging Infrared Radiometer (IIR) measures infrared radiation at three different wavelengths providing information on cloud particle type, size and radiative properties. The Wide Field Camera, a high-resolution digital camera, provides information on the horizontal extension of features detected by the lidar (Winker et al., 2009).

3.2.1 The CALIOP instrument

CALIOP is the first satellite lidar instrument optimized for aerosol and cloud measurements. The instrumentation and signal processing have been documented in several papers (e.g. Hostetler et al., 2006; Hunt et al., 2009; Winker et al., 2009). CALIOP sends out laser pulses towards the Earth's surface from two Nd:YAG lasers operating at 1064 nm and 532 nm, with a pulse repetition rate of 20.16 Hz and a pulse length of 20 ns. The beam diameter is approximately 70 m at the surface. The laser beams are scattered by clouds, aerosols and molecules in the atmosphere. The backscattered radiation is collected by a one meter diameter telescope, providing information on the vertical structure (height and thickness) of clouds and aerosols. Each satellite swath provides information on a slice of the atmosphere, and a three-dimensional picture can be obtained by combining several orbits.

The laser light is linearly polarized (99%), i.e. the light waves are oriented in the same direction. The 532 nm return signal is separated into its parallel and perpendicular components by a polarization beam splitter, and thus the degree of depolarization of the light during scattering is obtained. This gives information on the type of particles, since some particles, such as ice or dust depolarize the light, while spherical aerosol particles or cloud droplets do not. In addition, information on particle size can be obtained by combining the 532 and 1064 nm signals, as large particles scatter the 1064 nm laser beam more than small particles.

The recorded backscatter signal is processed in several ways before it is downlinked, including altitude determination, background subtraction, analogue-to-digital signal conversion and averaging. The background illumination is estimated from the region between 112 and 97 km altitude where the backscattering of the laser light is small and can be neglected. CALIOP has a

sampling resolution of 30 m in the vertical direction and 333 m in the horizontal direction. The scattering by the atmosphere at high altitudes is weaker and more uniform than at low altitudes, therefore, altitude-dependent averaging is performed to reduce the amount of data. Full resolution is used at low altitudes and lower resolution at higher altitudes, see Table 3.2.

Table 3.2 Horizontal and vertical resolution of the 532 nm signal. *The lowest land elevations is below sea level. Adapted from (Hostetler et al., 2006).

Altitude range (km)	Horizontal resolution (km)	Vertical resolution (m)
-0.5* to 8.2	0.33	30
8.2 to 20.2	1.0	60
20.2 to 30.1	1.67	180
30.1 to 40.0	5.0	300

The processing for Level 1 data provided by the NASA Langley Research Center (and used in Paper IV) further includes geolocation and calibration of the 532 nm parallel and perpendicular signals and the 1064 nm backscatter signal. Calibration is performed against modelled molecular backscattering using the 532 nm parallel signal at 30-34 km to represent pure molecular scattering. The altitude range 30-34 km was chosen as an aerosol-free reference altitude since it contains low amounts of particles while the molecular scattering is still sufficient. The resulting product, the total attenuated backscatter coefficient (β') at the wavelength λ = 532 or λ =1064 nm and altitude z can be expressed as:

$$\beta'_{\lambda}(z) = \left(\beta_{\lambda,m}(z) + \beta_{\lambda,p}(z)\right) T^2_{\lambda,m}(z) T^2_{\lambda,03}(z) T^2_{\lambda,p}(z) \tag{3.1}$$

where $\beta_{\lambda,m}$ is the backscatter coefficient and T^2 is the two-way transmittance due to scattering and absorption from molecules (m), particles (p) and ozone (O_3).

3.2.2 Data processing

To study the global distribution of the stratospheric aerosol (Paper IV), CLAIPSO Level 1, night-time 532 nm total (β'_{532}) and perpendicular ($\beta'_{532\perp}$) attenuated backscatter coefficients were used. The data were processed using the methodology described by Vernier et al. (2009). To obtain the signal from aerosol particles only, the signals from clouds and atmospheric molecules were removed. To calculate the molecular backscatter needed for the latter, total air and ozone number density are needed. Both these parameters are obtained from the Global Modelling and Assimilation Office (GMAO) and are included in the CAIPSO Level 1 data file. However, an error has been found in the GMAO temperature data (Vernier et al., 2011a), and the number density was therefore calculated from

temperature and pressure data from the ECMWF ERA interim reanalysis data. The lidar backscatter coefficients and meteorological data along each satellite swath were processed using the following steps:

1. averaging horizontally to 1^{o} latitude resolution,
2. removal of clouds,
3. setting of vertical resolution to 180 m,
4. removal of noisy regions,
5. calculation of the scattering ratios (SR), and
6. recalibration of SR.

To remove clouds from the lidar data, the depolarization ratio ($\delta = \beta'_{532\perp} / \beta'_{532}$) was used. This ratio is useful to distinguish spherical aerosol particles from ice particles in high-level clouds, as ice particles depolarize the light, and thus increase $\beta'_{532\perp}$. A cloud mask was created for pixels with $\delta > 5\%$ and $\beta'_{532} > 2.5 \times 10^{-4}$; the latter limit is needed since the depolarization ratio becomes noisy for small backscatter values in thin air at high altitudes. Noise was further handled by removing features smaller than 2x2 latitude-altitude pixels. The cloud mask was expanded upwards 2 pixels (360 m) to avoid misclassification of the upper cloud edge, and downwards all the way to the minimum level used (4 km) to remove the attenuated signal below the clouds.

The vertical resolution of the data was set to 180 m. Due to the variable vertical resolution of β'_{532} and $\beta'_{532\perp}$, this requires averaging below 20.2 km altitude and linear interpolation above 30.1 km, according to Table 3.2.

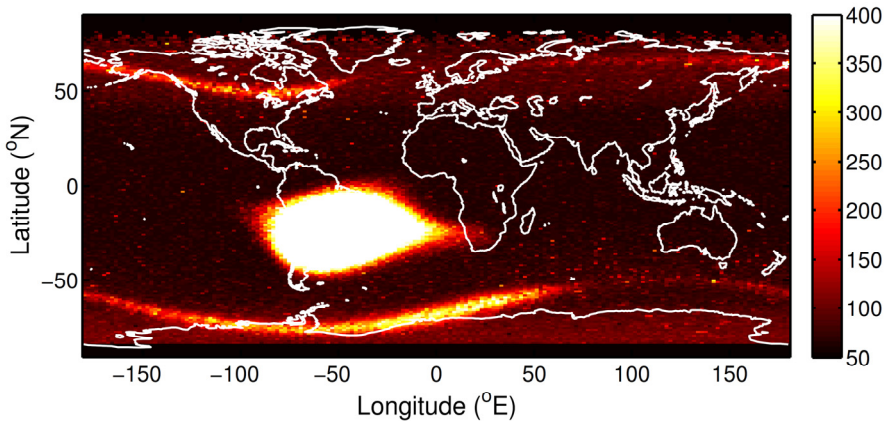

Figure 3.4 Average RMS noise signal form two months of CALIPSO data. High values indicate regions where large standard deviations in the data occur. The Southern Atlantic Anomaly is clearly visible. The curved lines in the Polar Regions results from the auroral ovals.

Peaks in the data that are as large as two orders of magnitude larger than pulses from single photoelectrons are the result of high-energy protons or cosmic rays. These are especially frequent in the South Atlantic anomaly (SAA), where charged particles from the solar winds trapped by the Earth's magnetic field in the inner Van Allen radiation belt are closest to the Earth, at altitudes reaching down to the satellite orbit. Regions near the poles along the auroral ovals (where the Northern and Southern Lights occur) also have a higher frequency of noise peaks (Hunt et al., 2009). These regions are visible in Fig. 3.4, which shows the root mean square (RMS) noise signal that was used to remove noisy regions by a threshold of 140 (J.-P. Vernier, personal communication). The RMS noise is obtained for each laser shot by taking the standard deviation of 1000 samples (15 m vertical resolution) obtained from the altitude region 60.3-75.3 km, and includes the detector dark current and noise from background radiation (Hostetler et al., 2006).

For recalibration of the backscatter data, and further use, the aerosol scattering ratio was calculated.

$$SR = \beta'_{532}/(T^2_{m,O_3}\beta_m) \tag{3.2}$$

The two-way transmission is needed to correct β'_{532} for the attenuation of the signal by scattering and absorption of atmospheric molecules:

$$T^2_{m,O_3}(z) = \exp(-2\int_{z=k}^{40}(\sigma_m(z) + \sigma_{O_3}(z))dz), \tag{3.3}$$

where σ_m and σ_{O3} are the extinction coefficients for Rayleigh scattering by molecules and the absorption by ozone, respectively. The extinction coefficients are obtained by multiplying the total number of air or ozone molecules by the corresponding scattering cross section per molecule for ozone (Q_{O3}) or standard air (Q_m), where Q_{O3} = 2.2x10^{-25} m^2 (Sica et al., 2001) and Q_m = 5.167x10^{-31} m^2 (Hostetler et al., 2006). T^2 for each altitude is obtained by integration from 40 km altitude; the contribution from higher altitudes being negligible.

The molecular backscatter used in Eq. 3.2 is given by:

$$\beta_m = \frac{\sigma_m(z,\lambda)}{S_m(\lambda)} \tag{3.4}$$

where $S_m = (8\pi/3)k_{bw}$ is the extinction to backscatter ratio for molecular scattering, and the King factor of air, k_{bw}, is estimated to be 1.0313 (Hostetler et al., 2006).

As previously described, CALIPSO backscatter data are calibrated using 30-34 km altitude as an aerosol-free reference altitude. However, it has been shown that there is significant scattering from aerosols at this altitude in tropical regions, which leads to underestimation of the scattering coefficients (Thomason et al., 2007; Vernier et al., 2009). Therefore, SR was recalibrated using 36-39 km as the

new reference altitude. This is done by normalising SR with an average SR at 36-39 km, to shift the altitude of pure molecular scattering (SR=1), as described by Vernier et al. (2009), who also provided recalibration coefficients ($C_{ad} = 1/\overline{SR}_{36-39}$). This shift increases SR in the tropics by 2-12% over the time period 2006-2008 (Vernier et al., 2009).

After this initial processing, the data were further averaged to different degrees over several satellite swaths to study the distribution of the volcanic aerosol (Paper IV). In addition to SR aerosol scattering (AS) and AOD were calculated.

$$AS = \frac{\beta'_{532}}{T^2_{m,O_3}} - \beta_m = (SR - 1)\beta_m \tag{3.5}$$

To obtain the AOD, AS was converted into extinction coefficients by multiplying it by a conversion factor of 50 (Jäger and Deshler, 2003) and integrating over the stratospheric depth. The conversion factor is dependent on the particle size distribution, here represented by the background stratospheric aerosol in 1999 (Jäger and Deshler, 2002). The volcanic eruptions considered in this thesis probably had little influence on the size distribution of the stratospheric aerosol. Number size distributions from the Nabro and Grimsvötn eruptions measured with the CARIBIC OPC (see Sec. 4.1.2 and Fig. 4.5) are similar to distributions measured before the eruptions and to the stratospheric aerosol size distribution in 1999 (Jäger and Deshler, 2002).

4 Results

The results from observations of volcanic aerosols presented in the 5 papers included in this thesis are presented in this chapter. These papers describe observations made at periods with varying degrees of volcanic influenc on the stratospheric aerosol load. Fig. 4.1 shows the ratio of particulate S/O_3 found when sampling in the stratosphere (PV>2 PVU) during the entire period of CARIBIC data collection from 1999 until 2013. Non-volcanic sulphate particles and O_3 are mainly produced deep in the stratosphere, where the actinic flux is high, and are then transported into the LMS. The S/O_3 ratio is thus stable when there is no extra source of sulphate, e.g. that from volcanic activity. This ratio therefore provides a good indicator of volcanic influence. The CARIBIC data can thus be categorized according to the degree of volcanic influence using the S/O_3 ratio.

In the years 1999-2002, during the first phase of the CARIBIC project, stable S/O_3 ratios indicate no significant volcanic influence. This is in agreement with satellite estimates of stratospheric AOD (Vernier et al., 2011b). This period therefore represents LMS background conditions, and has been used to normalise the values in Fig. 4.1. The period following this, from 2005 to mid-2008 was characterised by somewhat elevated S/O_3 ratios, following the eruptions of the volcanoes Manam, Soufrière Hills and Rabaul in the tropics. From mid-2008 to mid-2012 a clear volcanic influence can be seen following the eruptions of the extra-tropical volcanoes Kasatochi, Sarychev, Grimsvötn and the tropical volcano Nabro, causing increases in S/O_3 by up to a factor 10. The Nabro eruption ends this period of high volcanic influence, after which S/O_3 ratios approach background levels.

4.1 Characteristics of volcanic aerosols from eruptions in 2008-2011

Samples clearly influenced by volcanism in the years 2008-2011 provide the opportunity to study the volcanic aerosol in detail. Paper I deals with the composition and ageing of samples from the tropopause region and the LMS clearly influenced by the Kasatochi and Sarychev eruptions. In addition, special flights were performed following the Eyjafjallajökull eruption in 2010 to investigate its volcanic effluents. These samples were collected in the troposphere and are not included in Fig. 4.1, which only shows stratospheric samples. Paper III

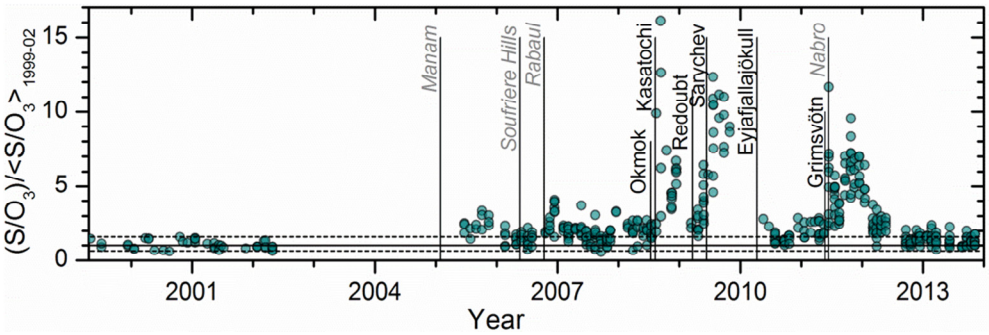

Figure 4.1 Time series of S/O_3 ratios for stratospheric samples (PV>2 PVU), normalized to the average S/O_3 value over the years 1999-2002 (solid horizontal line) representing stratospheric background conditions. The maximum and minimum for the period 1999-2002 are given by the broken line. The dates of tropical (grey italics) and extra-tropical (black roman) eruptions that affected the LMS of the Northern Hemisphere are indicated by vertical lines.

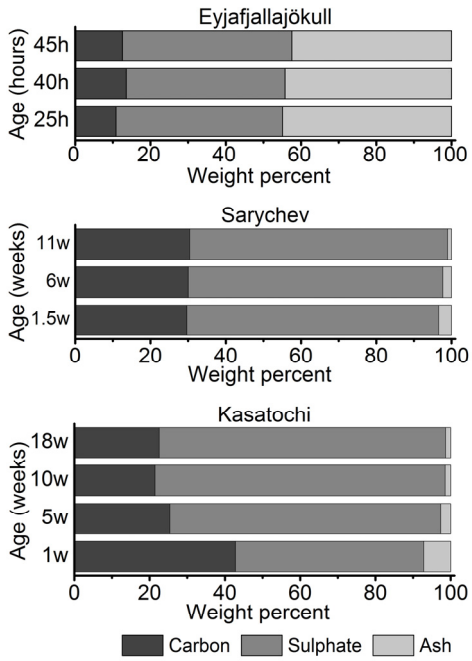

Figure 4.2 Main components of volcanic aerosol from the Eyjafjallajökull, Sarychev and Kasatochi eruptions. Samples collected close in time, approximately 1.5, 6 and 11 weeks (3, 6 and 2 samples, respectively) after the Sarychev eruption and 18 weeks (3 samples) after the Kasatochi eruption are shown as averages. The Sarychev carbonaceous component is an average of all samples, since it showed a dependence on latitude obstructing the time dependence presented in this figure.

presents a comparison between mass concentrations obtained from the aerosol sampler and particle volume distributions obtained from the OPC in the period April 2011 to March 2012. It thus covers the time of the Grimsvötn and Nabro eruptions, for which aerosol size distributions are presented, and will be discussed in somewhat more detail here. The following sections thus present in situ observations of volcanic aerosols with ages ranging from only a few days (Eyjafjallajökull) up to several months (Kasatochi, Sarychev and Nabro), which is rare in the literature.

4.1.1 Composition of volcanic aerosol

The volcanic aerosol from Kasatochi and Sarychev was identified by an elevated S/O_3 ratio and that their composition of crustal elements (Fe, K, Ti, Ca, Si, Mn, Zr and Sr) was similar to that of ash. Samples taken in the volcanic cloud from Eyjafjallajökull were recognised by high concentrations of S, and in particular, by very high concentrations of elements indicating ash. Connections to the specific eruptions were verified using air mass trajectories for the first samples collected. The samples from the volcanic cloud from Eyjafjallajökull were sampled within two days from the eruption and had a crustal composition very similar to that of a sample of ash fall-out. Aerosol samples following the Kasatochi and Sarychev eruptions also had a similar but more variable ash composition, probably as the result of mixing in the atmosphere, as these samples were collected one to 18 weeks after the eruptions.

The main components, calculated from the elemental composition of these samples, are illustrated in Fig. 4.2. The Kasatochi and Sarychev samples were relatively similar in composition, the main fractions being sulphate (on average 50-77%) and carbon (21-43%), and a small ash component (<10%). The samples collected following the eruption of Eyjafjallajökull composed of approximately equally large components of ash and sulphate (on average ~45 %) and a relatively small fraction of carbon (~10%). The sulphate and carbon contents were of the same magnitude or somewhat smaller than in the Kasatochi and Sarychev samples.

Ash particles are injected directly into the atmosphere by volcanic eruptions, and sulphate particles are produced from emitted SO_2. The origin of the carbonaceous component is, however, less clear. Carbonaceous aerosols are often associated with combustion. However only pyro-convection is expected to be strong enough to transport large amounts of carbonaceous aerosols into the stratosphere. The collected aerosol was not sampled close in time to any identified pyro-convection event. Furthermore, the relation between K and Fe in the aerosol samples did not correspond to that of biomass burning. Instead, it was suggested that entrainment of carbonaceous particles and/or precursor gases in the volcanic plume is the most likely source. Tropospheric boundary layer air contains large concentrations of organic aerosol, at both urban and rural locations. Organic material from the

oceans can be an important source of entrained particles for the aerosol studied, since the volcanoes are surrounded by oceans and erupted during the biologically active part of the year. Analysis of carbonaceous aerosols from tropical volcanism (Paper II) indicates that the carbonaceous fraction is of organic nature.

4.1.2 Residence time of volcanic SO_2

It is interesting to compare the composition of aerosols sampled at different times after the volcanic eruptions studied (Fig. 4.2). In samples associated with Kasatochi and Sarychev, the ash and carbonaceous components (for Kasatochi, see figure text for explanation) decreased, while the sulphate component increased, mainly as a consequence of the transformation of SO_2 into sulphate particles. The conversion rate of SO_2 was estimated using the Fe/S ratio (Fig. 4.3), by assuming that the decrease in Fe/S was due only to the production of particulate S from SO_2, and that the removal of ash and sulphate by coagulation and sedimentation was negligible. Using this ratio is a means of normalising for dilution of the volcanic cloud and for different aerosol density at the sampling sites. Only samples influenced by the Kasatochi and Sarychev eruptions were included in this analysis, since their compositions were similar, and collection one week or more after the eruptions minimizes the effects of initial coagulation and sedimentation processes (Rose et al., 2001). The number concentration of SO_2 molecules decays exponentially due to the reaction with OH, which mainly controls the conversion into sulphate. From this decay an expression of Fe/S as function of time were derived:

$$\frac{C_{Fe}^{m}}{C_{S}^{m}(t)} = \frac{A}{1-e^{-kt}}, \tag{4.1}$$

where C^m denotes mass concentrations, the constant A is the mass concentration ratio of Fe from ash and S from initial SO_2, and k is the loss rate constant for SO_2 conversion. Fitting the Fe/S ratios to this equation resulted in a residence time (1/k) for SO_2 of 45±22 days.

Comparing this result to previous estimates revealed some interesting aspects. While estimated residence times associated with the Pinatubo eruption show consistency, 23-35 days (Bluth et al., 1992; Read et al., 1993; Guo et al., 2004), estimates of the SO_2 conversion rates after the Kasatochi and Sarychev eruptions showed a greater spread, ranging from 9 to 62 days (Krotkov et al., 2010; Karagulian et al., 2010; Jurkat et al., 2010; Haywood et al., 2010). These results were based on both satellite and *in situ* observations of SO_2 or sulphate aerosols.

Possible explanations of these deviating results are the smaller amounts of SO_2 emitted, and the lower altitude of the volcanic clouds produced by Kasatochi and Sarychev compared with the Pinatubo eruption. Both these factors make

observations more challenging, as instrument detection limits are reached faster and the proximity to the extra-topical dynamic tropopause makes it difficult to separate stratospheric air from tropospheric, where residence times are significantly shorter (McGonigle et al., 2004; Carn et al., 2011). Aircraft observations suffer less from these problems than satellite observations, but the former have limited spatial coverage and are more affected by inhomogeneity in the volcanic cloud. Thus, it is valuable to compare different types of observations to obtain reliable results.

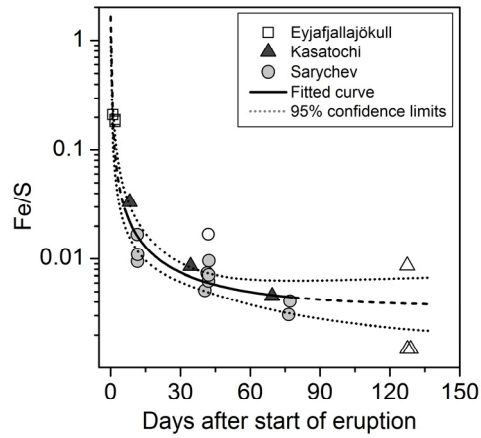

Figure 4.3 Evolution of the ratio of Fe (representing ash) to S (representing sulphate) in volcanic aerosol over time since the start of the eruptions. The solid line is fitted to the Fe/S mass ratios using Eq. 4.1. Open symbols were not used in the fitting procedure.

4.1.3 Size distributions of volcanic aerosols

Number size distributions of aerosols at 10-12 km altitude influenced by the Grimsvötn and Nabro eruptions are presented in Fig. 4.4, together with number size distributions of the stratospheric aerosol sampled before the Grimsvötn eruption, where the S/O_3 ratio (Fig. 4.1) indicated only a weak volcanic influence. The particle size distribution under stratospheric background conditions in 1999 at 20 km altitude, obtained from balloon measurements (Jäger and Deshler, 2002), is also shown. The first samples of aerosol from Grimsvötn were collected 26-27 days after the eruption, while samples from Nabro were collected 4.5 months after the eruption. The size distributions, especially following the Grimsvötn eruption, are very similar to distributions of stratospheric aerosols sampled before the eruptions, and to the distribution in 1999. The CARIBIC OPC does not cover all particle sizes of the particle mode. Based on calculations of the extinction efficiency for the particle distribution in 1999 given by Jäger and Deshler (2002),

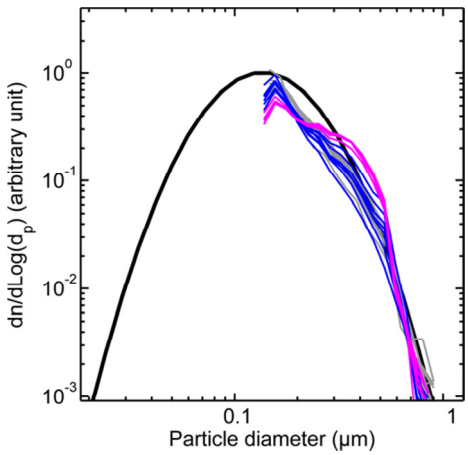

Figure 4.4 Number size distributions from OPC measurements during a period of low volcanic influence in April-May 2011 (grey lines) and following the Grimsvötn (blue lines) and Nabro (magenta lines) eruptions. Background stratospheric conditions in 1999 (Jäger and Deshler, 2002) are shown by the black line. All distributions are normalized to the number of particles in the OPC sampling region (0.12-1 µm).

the OPC can, however, be considered to cover the optically important part of the distribution that is relevant for climate. In contrast to the Pinatubo eruption in 1991, which led to a significant increase in the particle size of the stratospheric aerosol (Deshler et al., 2003; Bauman et al., 2003), eruptions of smaller magnitude seem to have little influence on the particle size. This finding is important for the conversion of optical measurements of particle backscattering into particle extinction, which relies on particle size (Jäger and Deshler, 2003) and are needed for climate calculations.

4.2 Identification of tropical volcanism 2005-2008

On average, the S/O_3 ratios were higher during the period 2005-2008 than during 1999-2002. The greatest increase was seen in 2008, where the S/O_3 ratio was twice that in 1999-2002. Increased concentrations in the period 2005-2008 were also observed, both for particulate S and C, resulting in increases in the S/O_3 and C/O_3 ratios from 2006 to 2008 of 23% and 70%, respectively (Paper II). In comparison, stratospheric aerosol backscatter obtained from lidar measurements in the tropics was observed to increase by 73% in 2000-2009 (Hofmann et al., 2009), subsequently associated with tropical volcanic eruptions (Vernier et al., 2011b) (Fig. 2.6 and Sec. 2.5). The source of the increase in particulate S and C in the extra-tropical LMS observed in the CARIBIC measurements was investigated based on analyses of transport patterns into the LMS (Paper II).

4.2.1 Transport and origin of particulate S and C

A model describing the seasonal variation of the influence of stratospheric air by the deep branch of the Brewer–Dobson circulation was created by fitting a sine function to the O_3/PV ratio (Fig. 4.5). Ozone is a reliable tracer of the influence of the deep branch of the Brewer–Dobson circulation, while PV can be used to normalise for the depth into the stratosphere at which the aerosol samples were collected. A maximum in O_3/PV is observed in June and a minimum in November. This model of seasonal variation was applied to the S/PV and C/PV ratios.

The background stratospheric aerosol is to a large extent formed from OCS, by conversion into SO_2 and subsequently sulphate aerosol in the deep Brewer–Dobson branch (Crutzen, 1976; Chin and Davis, 1995; Brühl et al., 2012). In the shallow branch the actinic flux is insufficient for photolysis of OCS. The S/PV ratio therefore follows the model reasonably well. The seasonal oscillation showed a higher amplitude in the period 2005-2008, suggesting that additional sulphur was transported mainly by the deep Brewer–Dobson branch during these years. Clear deviations from the model were found in late 2006 and late in 2007, which is the time of year when the influence from the deep branch is low. Thus, these deviations indicate transport of additional sulphur from the shallow branch, where high S and low O_3 lead to large S/O_3 ratios.

The measured values of C/PV showed no clear resemblance to the model, which suggests that the formation of particulate C within the deep branch is not as important as for particulate S. However, elevations in C are often identified simultaneously with elevated S, especially at the end of 2006 and the end of 2007 and throughout the whole of 2008. These components therefore appear to be connected.

The seasonal transport patterns of particulate S was further corroborated by comparing monthly averages of S/O_3 (where the statistics were sufficient) in the periods 1999-2002 and 2005-2008 (Fig. 4.6). Normalisation with O_3 removes the seasonal cycle from the deep branch. In 1999-2002, the S/O_3 ratio was relatively constant, suggesting that transport by the deep branch is the main source of sulphate particles. A small increase in S/O_3 was observed in November and December. In general, higher values of S/O_3 were observed in 2005-2008, with a clear seasonal pattern. A steep increase was seen from October to December, indicating the production of sulphate aerosol from SO_2 in the shallow branch, being transported down to flight altitudes in the LMS during this time of year.

In 2005-2008, eruptions of the tropical volcanoes Manam, Soufrière Hills and Rabaul perturbed stratospheric aerosol concentrations. CARIBIC data in 2005 following the eruption of Manam are scarce and difficult to analyse. The eruptions of Soufrière Hills and Rabaul occurred within a relatively narrow timespan. Satellite observations of the aerosol produced within 50^{o}N/S revealed that the aerosol from Soufrière Hills was located deeper into the stratosphere (>20 km)

than that from Rabaul (≤ 18 km) (Vernier et al., 2011b; Vernier et al., 2009). Based on the transport patterns described above, both Soufrière Hills and Rabaul could have contributed to the deviation in S/PV (and S/O_3, Fig. 4.1) in late 2006, by transport in the shallow Brewer–Dobson branch, and mainly Soufrière Hills in late 2007 and throughout 2008 by transport in the deep branch (transport time 1-2 years). Tropical volcanism in this period thus not only affected aerosol concentrations in the tropical stratosphere, but also the concentrations of particulate C and S in the extra-tropics.

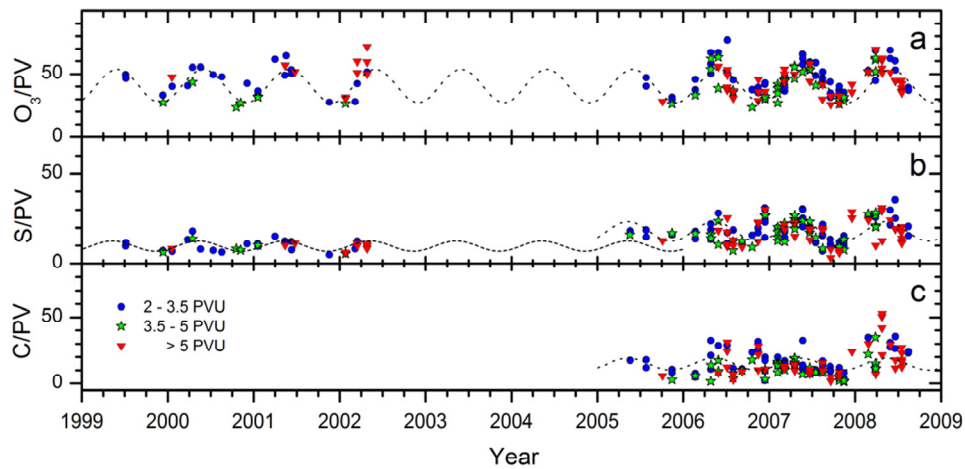

Figure 4.5 Time series of the ratios: a) O_3/PV (ppbv PVU $^{-1}$), b) S/PV (ng m^{-3} STP PVU^{-1}) and c) C/PV (ng m^{-3} STP PVU^{-1}). A sine function was fitted to the seasonal variation observed in a) and applied to b) and c) by changing the relative amplitude of the sine curves.

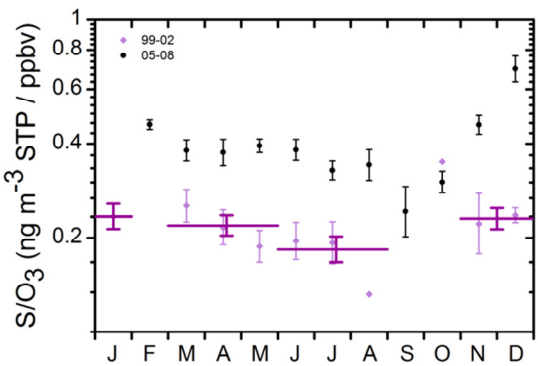

Figure 4.6 Monthly geometric averages of S/O_3 in the periods 1999-2002 (light purple symbols) and 2005-2008 (black symbols). In 1999-2002 averaging was performed over January, March-May, June-August and November-December (dark purple lines) to obtain sufficient statistics . Error bars represent standard errors.

4.3 Volcanic radiative impact from an overlooked part of the stratosphere

Perhaps the most important reason for studying volcanic aerosols is their effect on climate. Their potential role in the discrepancy between the modelled and observed surface temperature trend is a question that has attracted much attention recently. Several studies have been carried out to investigate the effect of volcanism on the climate since 2000 (Kravitz et al., 2010; Haywood et al., 2010; Solomon et al., 2011; Fyfe et al., 2013a), and its role in the climate hiatus (Schmidt et al., 2014; Santer et al., 2014; Haywood et al., 2014). These studies were based on or compared to AOD observations of the stratosphere above the 380 K isentrope or an altitude of 15 km (Sato et al., 1993; Vernier et al., 2011b; Bourassa et al., 2012). However, the results decribed in previous sections clearly demonstrate that the LMS, situated below 380K (~15 km), was affected to various degrees by both tropical and extra-tropical volcanism in the period 2005-2013. The importance of including the LMS in global stratospheric AOD and radiative forcing calculations was therefore investigated (Paper IV).

4.3.1 The distribution of aerosol from the eruption of Kasatochi

The eruption of the extra-tropical volcano Kasatochi had the greatest impact on S/O_3 in the LMS (Fig. 4.1). The distribution of the volcanic cloud was investigated using CALIPSO lidar data. It can be seen from Figure 4.7 that the eruption produced 2 separate layers of aerosol, one located above 15 km, which spread rapidly over the entire Northern Hemisphere, and one located below 15 km in the UT/LMS. Figure 4.7 also clearly demonstrates that the lower cloud contained the main part of the aerosol produced in the eruption. This aerosol remained for approximately 10 weeks before being transported into the troposphere. The S/O_3 ratios in Fig. 4.1 decreased during this time, but were elevated again in December, when the upper cloud reached the LMS. Thus, neglecting the aerosol at altitudes below 15 km would have significantly underestimated the impact of the Kasatochi eruption, in terms of both the magnitude and the duration of the influence.

4.3.2 Volcanic impact on the lowermost stratosphere

The global effect of the Kasatochi, Sarychev and Nabro eruptions on stratospheric AOD and aerosol radiative forcing is illustrated in Fig. 4.8. For Kasatochi calculations were done down to 2 km below the tropopause, since part of the volcanic cloud resided in the UT. The impact of an eruption is determined by the magnitude of the perturbation and by the residence time of the aerosol. Thus, to

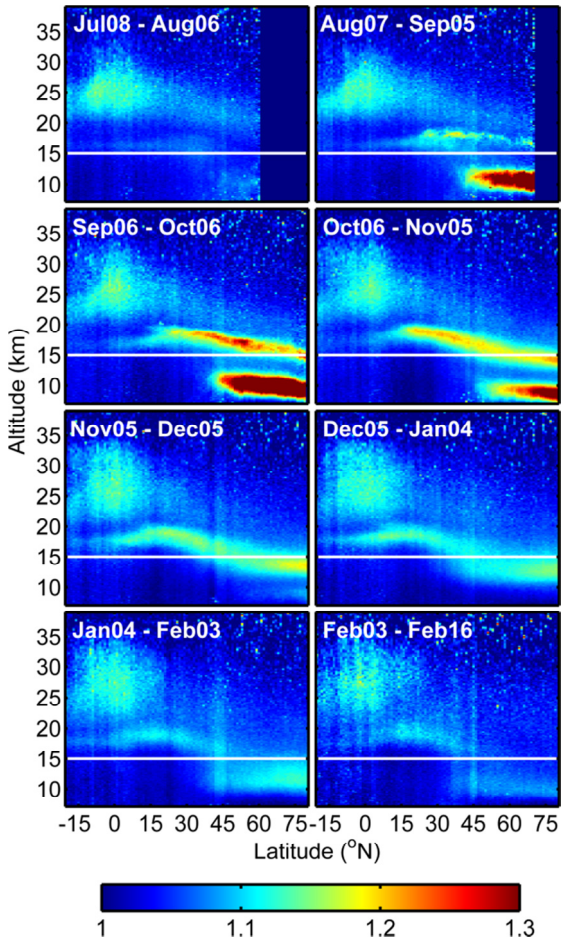

Figure 4.7 Distributions of Kasatochi volcanic aerosol with latitude and altitude, shown as monthly (2 weeks in Feb.) and zonally averaged scattering ratios (total backscatter from CALIPSO/molecular backscatter) from July 2008 - Feb 2009. The horizontal white line indicates an altitude of 15 km, used as the lower limit in many previous studies. Note that the feature in the tropics at 25 km is present already before the Kasatochi eruption.

obtain an estimate of the impact of Kasatochi, Sarychev and Nabro, the number of "AOD days" and "RF days" were calculated (Table 4.1) by integrating over the perturbations from the eruptions (shaded areas in Fig. 4.8a and b). The "background" was set to the values of AOD and radiative forcing between the respective eruptions. The importance of including the LMS in estimates of stratospheric AOD and aerosol can be seen from the fraction observed above 15 km altitude (Table 4.1), and depends on the amount of aerosol placed in/transported to the LMS and for the radiative forcing also strongly on season. On average, 45% of the AOD and 58% of the radiative forcing originates above 15 km altitude, and the effect resulting from the UT/LMS is thus somewhat larger on the AOD than on radiative forcing.

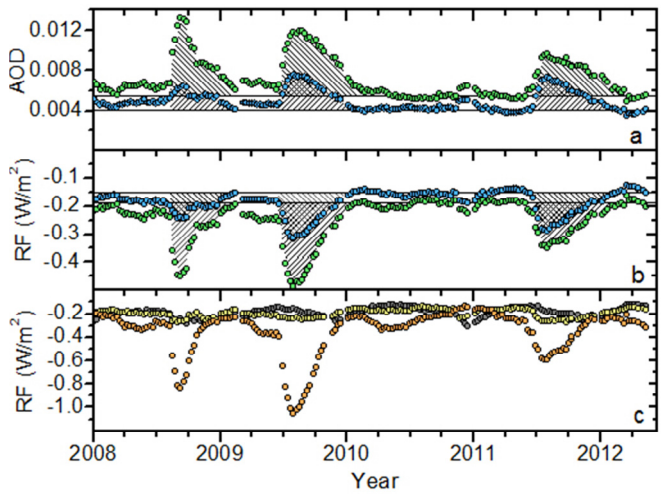

Figure 4.8 Globally averaged a) aerosol optical depth (AOD) and b) aerosol radiative forcing derived from CALIPSO aerosol scattering data. Two altitude ranges were studied: 15-35 km (blue symbols) and the tropopause - 35 km (-2 km in Aug-Nov 2008 to include the influence of Kasatochi on the UT) (green symbols). The solid lines in a) and b) represent concentrations between the volcanic perturbations. c) The latitude distribution of the stratospheric radiative forcing in three regions equal in surface area: 90^{o}S to 20^{o}S (grey symbols), -20^o S to 20^{o}N (yellow symbols) and 20^{o}N to 90^{o}N (orange symbols).

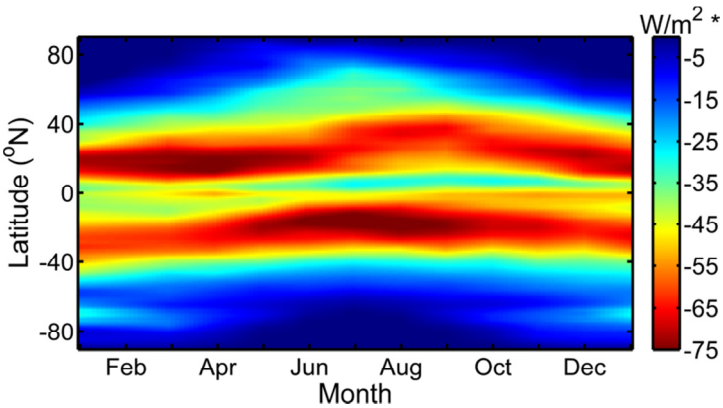

Figure 4.9 Average net radiative forcing in 2008-2011 for AOD = 1, normalized to relative latitude area(*). The seasonal and latitudinal dependence are caused by differences in day length, cloudiness, surface albedo and solar zenith angle. The solar zenith angle affects the upscatter fraction, insolation, path length through the aerosol layer and atmospheric transmission down to the aerosol layer.

Simultaneous research by Ridley et al. (2014), based on sun photometers and ground-based lidar, suggests that the stratosphere below 15 km contributes 30-70% of the total stratospheric AOD during the years 2000-2014. In comparison, the results presented in Paper IV indicate a contribution of, on average, 30% in the more volcanically influenced period 2008-2011; the maximum contribution being 55% from the Kasatochi eruption. Ridley et al. (2014) thus seem to overestimate the effect of volcanism, and the size, shape and timing of their peaks in AOD are very different from the CALIPSO observations. The results presented in Paper IV are the first high-resolution global estimates of the influence of volcanism arising from the LMS.

Table 4.1. Volcanic impact on total stratospheric aerosol optical depth (AOD) and net aerosol radiative forcing (RF), and the influence from altitudes above 15 km, derived from Fig. 4.8.

	Kasatochi	**Sarychev**	**Nabro**
AOD days	0.69	0.87	0.60
RF days	-20	-31	-19
Fraction AOD >15 km	32%	46%	59%
Fraction RF > 15 km	44%	56%	77%

4.3.3 Seasonal dependence

Seasonal variation of the aerosol radiative forcing (Fig. 4.9) from the extra-tropically oriented LMS (mainly polewards of 40^{o}) is caused by the variation in the number of sunlight hours and the solar zenith angle, as lower zenith angles are accompanied by a higher upscatter fraction of aerosol particles (Fig. 2.3, Sec. 2.2). Low zenith angles are also accompanied by lower solar insolation, but this effect is cancelled out as the path length through the aerosol layer increases by the same factor. There are also (small) variations in zonal average cloudiness and surface albedo with season. In particular, the variation in daylight hours causes the radiative forcing from the extra-tropics and polar regions to be strong in the summer and weak in the winter. However, it should be noted that the Polar Regions, which are most strongly affected by this seasonal dependence, contribute little to the global radiative forcing due to their small surface area (7% beyond 60^{o}). The eruptions studied mainly affected the Northern Hemisphere AOD (Fig. 4.8c). The smallest effect from the LMS on the radiative forcing was from the Nabro eruption due to its tropical location, with maximum transport into the LMS in late autumn and winter. To account for the seasonal and latitudinal dependence of the RF, detailed information on the latitudinal distribution of the stratospheric aerosol is critical, but often not adequately considered.

4.4 Volcanic influence on the upper troposphere

CARIBIC aerosol sampling at flight altitudes of 10-12 km takes place in the UT/LMS at high latitudes, and in the middle troposphere in tropical regions. Martinsson et al. (2005) showed that particulate S in the LMS during volcanically quiescent periods exhibits a positive gradient with increasing distance from the tropopause, demonstrating that downward transport from the stratosphere above is the major source of particulate S in the LMS. The extra-tropical downwelling of the stratospheric aerosol and its transport out of the stratosphere may have an effect on aerosol concentrations in the UT and on high-altitude clouds before removal of the aerosol. The effect of volcanism on UT aerosol concentrations and cirrus clouds was therefore investigated (Paper V).

4.4.1 Aerosol concentrations in the upper troposphere

Sulphate aerosol collected in the UT during spring (March-July) shows an increase with latitude (Fig. 4.10). A greater increase was seen north of 30°N, in the years 2005-2008 and 2013 than in samples collected in 1999-2002. The years 2009-2011 were excluded due to the direct influence of eruptions of extra-tropical volcanoes and the strong influence of the 2011 tropical Nabro eruption. Increasing particulate S concentrations were found in the LMS in the years 2005-2008 as a consequence of tropical volcanism (Sec. 4.2, Paper II). The simultaneous increase in S in the extra-tropical UT clearly indicates that volcanism during this period also affected the UT.

The Brewer–Dobson circulation is strongest during the winter, causing maximum stratospheric influence of the LMS in the spring and summer, while transport in the shallow branch during the summer leads to larger fractions of air of recent

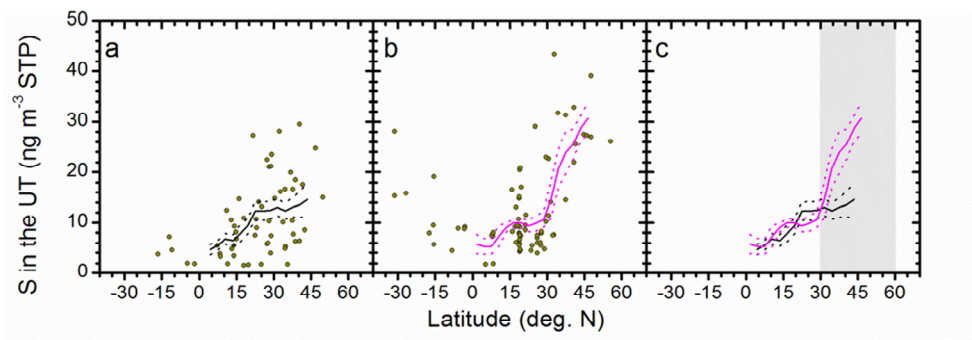

Fig 4.10 Latitude dependence of S in the UT during March-July in a) 1999-2002 and b) 2005-2008 and 2013, and c) a direct comparison of running averages (solid lines) of these periods. The dashed lines indicate the 95% prediction interval. The northern mid-latitudes are indicated by the shaded area.

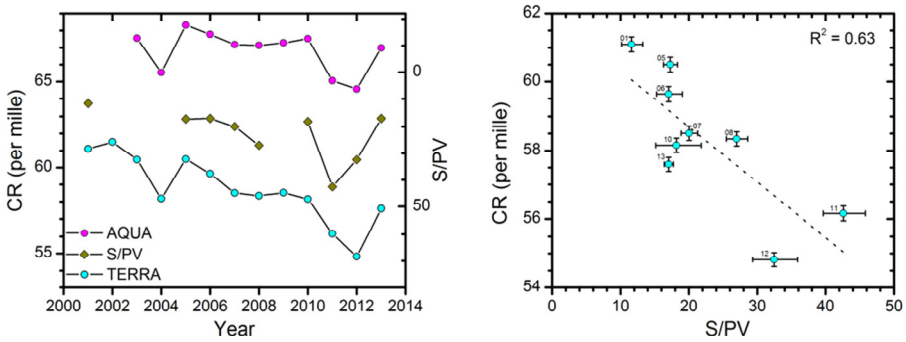

Fig 4.11 a) Time series of yearly averaged spring (March-July) cirrus cloud reflectance (CR) from the satellites Terra and Aqua, and S/PV obtained from CARIBIC? (note reversed S/PV scale). The generally higher values from the Aqua satellite could be due to its later overpass time, which implies more convective activity, leading to cirrus anvils. b) Scatter plot of Terra cloud reflectance vs. CARIBIC S/PV. The dotted line shows the fit using linear regression.

tropospheric origin during the autumn (Bönisch et al., 2009). The seasonal variation in particulate S in the LMS was described in Sec. 4.2 (Fig. 4.5), using the S/PV ratio. A very similar seasonal pattern was observed in total S concentration in the UT (using samples collected north of 30^o during 2005-2008 and 2013, shaded area in Fig. 4.10c), supporting a coupling between concentrations of particulate S in the LMS and UT. Furthermore, correlations between S in the UT and S/PV in the LMS were found between yearly averages over the spring (March-July, R^2=0.73) and autumn (August-November, R^2=0.95). A steeper gradient was seen in spring (4 times larger than in the autumn), which was attributed to greater transport across the tropopause in this period (Sprenger and Wernli, 2003).

4.4.2 Volcanic effects on cirrus clouds

After establishing the effect of the LMS on concentrations of particulate S in the UT, the potential effect on cirrus clouds in the UT was investigated using cirrus reflectance from the MODIS instrument on the Terra and Aqua satellites (limited to 30^o - 60^{o}N). To compare to the increase in particulate S, values of the S/PV ratio in the LMS (limited to values below 5 PVU and north of 30^{o}N) from March to July were used, as the LMS data have better statistics than the UT data (already demonstrated to be coupled to the LMS). While the S/PV ratio increased from 2001-2011, the MODIS cloud reflectance from Terra and Aqua showed a decreasing trend (Fig. 4.11). When using the cirrus reflectance from Terra an anti-correlation was obtained (R^2=0.63) showing a decrease in cloud reflectance of 8±2% simultaneously with an increase in sulphur concentration in the LMS of a factor 3-4.

The indirect effect from volcanism on cirrus clouds may thus have an important effect on climate in addition to the direct effect of volcanic particles. The decrease in reflectance implies a decrease in cloud optical depth, and thus that the clouds both scatter less sunlight and absorb less radiation; the latter effect being dominant (Storelvmo et al., 2013). The net effect is thus expected to be negative, and was estimated to be -2 W/m^2, inducing cooling of the Earth's surface temperature. This indirect effect of volcanic aerosols has not been taken into account in the current debate on the temperature hiatus since 2000, and could be an important piece of the puzzle.

5 Conclusions and Outlook

Using satellite- and aircraft-based aerosol observations, the results presented here show that the LMS of the Northern Hemisphere was affected by volcanism to varying degrees during the period 2005-2012. During the period 2005-2008, transport of aerosols from the tropics following eruptions of Manam, Soufrière Hills and Rabaul caused most of the observed elevations in particle concentrations. In the period following that, 2008-2012, particle concentrations were occasionally strongly enhanced as a consequence of direct injection of SO_2 and particles by eruptions of the extra-tropical volcanoes Kasatochi, Sarychev and Grimsvötn, and by rapid transport of aerosol from the tropical Nabro eruption.

Volcanic aerosols were sampled in the less than two-day-old volcanic plume from Eyjafjallajökull (2010) and 1-18 weeks after the Kasatochi (2008) and Sarychev (2009) eruptions. The aerosol from Eyjafjallajökull consisted mainly of ash and sulphate (~45% each) and a small carbonaceous component, while the largest components following the eruptions of Sarychev and Kasatochi were sulphate (50-77%) and carbon (21-43%). Despite the fact that the carbonaceous component is generally not associated with volcanic particles, large carbonaceous fractions were found in samples following the eruptions of both extra-tropical and tropical volcanoes. It is instead suggested that the carbonaceous aerosol was transported into the stratosphere from the boundary layer with the volcanic plume.

The fraction of sulphate was observed to increase with the age of the volcanic aerosol. The stratospheric residence time of SO_2 was estimated to be 45±22 days. Comparison with the findings in previous studies revealed a large spread in estimated SO_2 residence times following the Kasatochi and Sarychev eruptions, indicating that estimating the residence time after moderate extra-tropical eruptions is difficult. The proximity to the tropopause is probably a considerable source of error, since total column estimates of SO_2 do not differentiate between tropospheric and stratospheric air, where conversion and deposition rates differ significantly.

Using stratospheric observations from CALIPSO it was show that the stratosphere below 15 km contributed significantly to the total effect of the eruptions of Kasatochi, Sarychev and Nabro in 2008-2011. Existing datasets for the stratospheric AOD used in several climate studies do not include the aerosol in the LMS, and the volcanic influence on the stratosphere is thus underestimated. Including the effect from the LMS to that from the stratosphere above an altitude of 15 km increases the AOD and radiative forcing from the Kasatochi, Sarychev

and Nabro eruptions by factors of 2.2 and 1.7, respectively. On average, inclusion of the LMS gives rise to 30% higher stratospheric radiative forcing in 2008-2011.

Elevated aerosol concentrations in the LMS were observed to affect upper tropospheric aerosol concentrations. An increase in particulate sulphur concentrations of a factor 3.5 was observed from 2001-2011. Cirrus reflectance observed from the MODIS instruments on the Terra and Aqua satellites showed the opposite trend, with an 8±2% decrease in the same period. This suggests that the effect of volcanic aerosols is to lower the optical depth of cirrus clouds, resulting in less light scattering and, more importantly, lower absorption of longwave radiation, and thus a cooling effect on climate.

Outlook

During the past 15 years, global warming has slowed down, despite steadily increasing emissions of greenhouse gases. Most CIMP5 climate models used in the IPCC report fail to reflect this decreasing trend in the surface temperature, thus leading to overestimation of global warming. Volcanic eruptions since 2000 have been suggested to be the missing factor in these climate models, since they assume stratospheric aerosol background conditions since the late 1990s, after the decay of the influence of the Pinatubo eruption in 1991. Recent studies suggest that cooling resulting from subsequent moderately sized volcanic eruptions explains 15-30% of the differences between models and observations. However, the influence of volcanic aerosols in the LMS, constituting 40% of the total stratospheric mass, has not yet been properly taken into account.

Results presented in this thesis show that the LMS was affected by volcanism most of the time from 2005-2013, and strongly so by eruptions of the extra-tropical volcanoes Kasatochi and Sarychev and the tropical volcano Nabro, with substantial contributions to global AOD and aerosol radiative forcing. The extra-tropical location of the LMS further emphasizes the importance of accurate representation of the latitude distribution of volcanic aerosols and the related seasonal variation in the radiative forcing to fingerprint hemispheric or global climate anomalies, instead of using the globally averaged AOD and corresponding average aerosol radiative forcing, as has been done in several previous studies. The identified effects on upper tropospheric aerosol concentrations and cirrus cloud reflectance suggest additional cooling. More investigation is needed, but this indirect effect of volcanic aerosols can further reduce the discrepancies between modelled and actual global surface temperatures.

Estimates of the impact on climate of volcanism also rely on the accuracy of stratospheric measurements. Discrepancies have been observed between established data of stratospheric AOD at 532 nm. These arise from the conversion of scattering coefficients or between AOD at different wavelengths, which

depends on accurate knowledge of aerosol size and composition. Thus, further research is needed to fully quantify the amount and distribution of volcanic aerosols and the interaction between volcanism and global climate.

Acknowledgements

There are several people that in some way have contributed to this thesis and shaped my life as a PhD student. Therefore I would like to thank …

…my supervisor Bengt Martinsson, for always being open for discussions and sharing of knowledge and for always welcome my opinions and being encouraging. I am very grateful that I have got the chance to work with the fantastic datasets from CARIBIC and CALIPSO.

…my fellow PhD student within CARIBIC, Johan Friberg, for great company and for always having time for a chat. Thank you for getting us to the right places when we travel and keeping me in a happy mode.

…Carl Brenninkmeijer, Markus Hermann, Armin Rauthe-Schöch, Peter van Velthoven, Andreas Zahn and the rest of the CARIBIC team, for providing a friendly research atmosphere, for careful commenting on manuscripts and for encouraging words.

…Jean-Paul Vernier, for great supervision during my work with the CALIPSO lidar data.

…friends and colleagues at the Division of Nuclear Physics, for discussions and laughs about both physics and common life, and for help with various things when needed.

…André Ahlgren, for being both my boyfriend and my computer expert. Thank you for the many hours you have spent helping me with MATLAB programming and with images for this thesis. Thank you for being my best friend and greatest support and for inspiring me to become a PhD student.

…my family for being loving and supporting during these years, and for providing relaxing brakes from life at the university.

References

Ammann, C. M., Meehl, G. A., Washington, W. M., and Zender, C. S.: A monthly and latitudinally varying volcanic forcing dataset in simulations of 20th century climate, Geophys. Res. Lett., 30, 1657-1661, 2003.

Andersson, S. M., Martinsson, B. G., Friberg, J., Brenninkmeijer, C. A. M., Rauthe-Schöch, A., Hermann, M., van Velthoven, P. F. J., and Zahn, A.: Composition and evolution of volcanic aerosol from eruptions of Kasatochi, Sarychev and Eyjafjallajökull in 2008–2010 based on CARIBIC observations, Atm. Chem. Phys., 13, 1781-1796, 2013.

Appenzeller, C., Holton, J. R., and Rosenlof, K. H.: Seasonal variation of mass transport across the tropopause, J. Geophys. Res., 101, 15071-15078, 1996.

Bauman, J. J., Russell, P. B., Geller, M. A., and Patrick, H.: A stratospheric aerosol climatology from SAGE II and CLAES measurements: 2. Results and comparisons, 1984–1999, J. Geophys. Res., 108, D13, 4383, 2003.

Bindoff, N. L., Stott, P. A., AchutaRao, K. M., Allen, M. R., Gillett, N., Gutzler, D., Hansingo, K., Hegerl, G., Hu, Y., Jain, S., Mokhov, I. I., Overland, J., Perlwitz, J., Sebbari, R., and Zhang, X.: Detection and Attribution of Climate Change: from Global to Regional. In: Climate Change 2013: The Physical Science Basis. Contribution of Working Group I to the Fifth Assessment Report of the Intergovernmental Panel on Climate Change, Cambridge University Press, Cambridge, United Kingdom and New York, NY, USA., 2013.

Birner, T., and Bönisch, H.: Residual circulation trajectories and transit times into the extratropical lowermost stratosphere, Atmos. Chem. Phys., 11, 817-827, 2011.

Bluestein, H. B.: Synoptic-dynamic Meteorology in Midlatitudes: Observations and theory of weather systems, Oxford university press, Inc., New York, 1993.

Bluth, G. J. S., Doiron, S. D., Schnetzler, C. C., Krueger, A. J., and Walter, L. S.: Global tracking of the SO2 clouds from the june, 1991 Mount-Pinatubo eruptions, Geophys. Res. Lett., 19, 151-154, 1992.

Boucher, O., Randall, D., Artaxo, P., Bretherton, C., Feingold, G., Forster, P., Kerminen, V.-M., Kondo, Y., Liao, H., Lohmann, U., Rasch, P., Satheesh, S. K., Sherwood, S., Stevens, B., and Zhang, X. Y.: Clouds and Aerosols. In: Climate Change 2013: The Physical Science Basis. Contribution of Working Group I to the Fifth Assessment Report of the Intergovernmental Panel on Climate Change Cambridge University Press, Cambridge, United Kingdom and New York, NY, USA., 2013.

Bourassa, A. E., Robock, A., Randel, W. J., Deshler, T., Rieger, L. A., Lloyd, N. D., Llewellyn, E. T., and Degenstein, D. A.: Large volcanic aerosol load in the stratosphere linked to Asian monsoon transport, Science, 337, 78-81, 2012.

Brenninkmeijer, C., Crutzen, P., Fischer, H., Güsten, H., Hans, W., Heinrich, G., Heintzenberg, J., Hermann, M., Immelmann, T., and Kersting, D.: CARIBIC-Civil aircraft for global measurement of trace gases and aerosols in the tropopause region, J. Atmos. Ocean. Tech., 16, 1373-1383, 1999.

Brenninkmeijer, C. A. M., Crutzen, P., Boumard, F., Dauer, T., Dix, B., Ebinghaus, R., Filippi, D., Fischer, H., Franke, H., Friess, U., Heintzenberg, J., Helleis, F., Hermann, M., Kock, H. H., Koeppel, C., Lelieveld, J., Leuenberger, M., Martinsson, B. G., Miemczyk, S., Moret, H. P., Nguyen, H. N., Nyfeler, P., Oram, D., O'Sullivan, D., Penkett, S., Platt, U., Pupek, M., Ramonet, M., Randa, B., Reichelt, M., Rhee, T. S., Rohwer, J., Rosenfeld, K., Scharffe, D., Schlager, H., Schumann, U., Slemr, F., Sprung, D., Stock, P., Thaler, R., Valentino, F., van Velthoven, P., Waibel, A., Wandel, A., Waschitschek, K., Wiedensohler, A., Xueref-Remy, I., Zahn, A., Zech, U., and Ziereis, H.: Civil Aircraft for the regular investigation of the atmosphere based on an instrumented container: The new CARIBIC system, Atmos. Chem. Phys, 7, 4953-4976, 2007.

Brühl, C., Lelieveld, J., Crutzen, P. J., and Tost, H.: The role of carbonyl sulphide as a source of stratospheric sulphate aerosol and its impact on climate, Atmos. Chem. Phys., 12, 1239-1253, 2012.

Bönisch, H., Engel, A., Curtius, J., Birner, T., and Hoor, P.: Quantifying transport into the lowermost stratosphere using simultaneous in-situ measurements of SF 6 and CO2, Atm. Chem. Phys., 9, 5905-5919, 2009.

Carn, S. A., Froyd, K. D., Anderson, B. E., Wennberg, P., Crounse, J., Spencer, K., Dibb, J. E., Krotkov, N. A., Browell, E. V., Hair, J. W., Diskin, G., Sachse, G., and Vay, S. A.: In situ measurements of tropospheric volcanic plumes in Ecuador and Colombia during TC4, J. Geophys. Res., 116, D00J24, 2011.

Chin, M., and Davis, D. D.: A reanalysis of carbonyl sulfide as a source of stratospheric background sulfur aerosol, J Geophys. Res., 100, 8993-9005, 1995.

Crutzen, P. J.: The possible importance of CSO for the sulfate layer of the stratosphere, Geophys. Res. Lett., 3, 73-76, 1976.

Cziczo, D. J., Thomson, D. S., and Murphy, D. M.: Ablation, Flux, and Atmospheric Implications of Meteors Inferred from Stratospheric Aerosol, Science, 291, 1772-1775, 2001.

Deshler, T., Hervig, M., Hofmann, D., Rosen, J., and Liley, J.: Thirty years of in situ stratospheric aerosol size distribution measurements from Laramie, Wyoming (41°N), using balloon-borne instruments, J. Geophys. Res., 108, 4167, 2003.

Deshler, T.: A review of global stratospheric aerosol: Measurements, importance, life cycle, and local stratospheric aerosol, Atmos. Res., 90, 223-232, 2008.

Dessler, A. E., Hintsa, E. J., Weinstock, E. M., Anderson, J. G., and Chan, K. R.: Mechanisms controlling water vapor in the lower stratosphere:“A tale of two stratospheres”, J. Geophys Res., 100, 23167-23172, 1995.

Ferry, G. V., Pueschel, R. F., Strawa, A. W., Kondo, Y., Howard, S. D., Verma, S., Mahoney, M. J., Bui, T. P., Hannan, J. R., and Fuelberg, H. E.: Effects of aircraft on aerosol abundance in the upper troposphere, Geophys. Res. Lett., 26, 2399–2402, 1999.

Fischer, H., Reus, M. d., Traub, M., Williams, J., Lelieveld, J., Gouw, J. d., C.Warneke, Schlager, H., A.Minikin, Scheele, R., and Siegmund, P.: Deep convective injection of boundary layer air into the lowermost stratosphere at midlatitudes, 3, 739–745, 2003.

Flato, G., Marotzke, J., Abiodun, B., Braconnot, P., Chou, S. C., Collins, W., Cox, P., Driouech, F., Emori, S., Eyring, V., Forest, C., Gleckler, P., Guilyardi, E., Jakob, C., Kattsov, V., and, C. R., and Rummukainen, M.: Evaluation of Climate Models. In: Climate Change 2013: The Physical Science Basis. Contribution of Working Group I to the Fifth Assessment Report of the Intergovernmental Panel on Climate Change Cambridge University Press, Cambridge, United Kingdom and New York, NY, USA, 2013.

Forster, P., Ramaswamy, V., Artaxo, P., Berntsen, T., Betts, R., Fahey, D. W., Haywood, J., Lean, J., Lowe, D. C., Myhre, G., Nganga, J., Prinn, R., Raga, G., Schulz, M., and Dorland, R. V.: Changes in Atmospheric Constituents and in Radiative Forcing. In: Climate Change 2007: The Physical Science Basis. Contribution of Working Group I to the Fourth Assessment Report of the Intergovernmental Panel on Climate Change Cambridge University Press, Cambridge, United Kingdom and New York, NY, USA., 2007.

Fromm, M., Shettle, E. P., Fricke, K. H., Ritter, C., Trickl, T., Giehl, H., Gerding, M., Barnes, J. E., Neill, M. O., Massie, S. T., Blum, U., McDermid, I. S., Leblanc, T., and Deshler, T.: Stratospheric impact of the Chisholm pyrocumulonimbus eruption: 2. Vertical profile perspective, J Geophys. Res., 113, D08203, 2008.

Fromm, M., Lindsey, D. T., Servranckx, R., Yue, G., Trickl, T., Sica, R., Doucet, P., and Godin-Beekmann, S.: The untold story of pyrocumulonimbus, B. Am. Meteorol. Soc., 91, 1193-1209, 2010.

Fromm, M. D., and Servranckx, R.: Transport of forest fire smoke above the tropopause by supercell convection, Geophys. Res. Lett., 30, 2003.

Fyfe, J., Salzen, K., Cole, J., Gillett, N., and Vernier, J. P.: Surface response to stratospheric aerosol changes in a coupled atmosphere–ocean model, Geophys. Res. Lett., 40, 584-588, 2013a.

Fyfe, J. C., Gillett, N. P., and Zwiers, F. W.: Overestimated global warming over the past 20 years, Nature Clim. Change, 3, 767-769, 2013b.

Gettelman, A., Hoor, P., Pan, L. L., Randel, W. J., Hegglin, M. I., and Birner, T.: The Extratropical Upper Troposphere and Lower Stratosphere, Rev. Geophys., 49, 2011.

Griessbach, S., Hoffmann, L., Spang, R., and Riese, M.: Volcanic ash detection with infrared limb sounding: MIPAS observations and radiative transfer simulations, Atmos. Meas. Tech., 7, 1487-1507, 2014.

Guan, H., Esswein, R., Lopez, J., Bergstrom, R., Warnock, A., Follette-Cook, M., Fromm, M., and Iraci, L. T.: A multi-decadal history of biomass burning plume heights identified using aerosol index measurements, Atm. Chem. Phys., 10, 6461-6469, 2010.

Guo, S., Bluth, G., J. S., Rose, W. I., Watson, I. M., and Prata, A. J.: Re-evaluation of SO2 release of the 15 June 1991 Pinatubo eruption using ultraviolet and infrared satellite sensors, Geochem. Geophy. Geosy., 5, Q04001, 2004.

Hansen, J., Sato, M., Ruedy, R., Nazarenko, L., Lacis, A., Schmidt, G., Russell, G., Aleinov, I., Bauer, M., and Bauer, S.: Efficacy of climate forcings, J. Geophys Res., 110, D18104, 2005.

Hansen, J. E., and Travis, L. D.: Light scattering in planetary atmospheres, Space Sci. Rev., 16, 527-610, 1974.

Hartmann, D. L., Tank, A. M. G. K., Rusticucci, M., Alexander, L. V., Brönnimann, S., Charabi, Y., Dentener, F. J., Dlugokencky, E. J., Easterling, D. R., Kaplan, A., Soden, B. J., Thorne, P. W., Wild, M., and Zhai, P. M.: Observations:Atmosphere and Surface. In:Climate Change 2013: The Physical Science Basis. Contribution of Working Group I to the Fifth Assessment Report of the Intergovernmental Panel on Climate Change, Cambridge University Press, Cambridge, United Kingdom and New York, NY, USA., 2013.

Haywood, J. M., Clerbaux, C., Coheur, P., Degenstein, D., Braesicke, P., Jones, A., Clarisse, L., Bourassa, A., Barnes, J., Telford, P., Bellouin, N., Boucher, O., and Agnew, P.: Observations of the eruption of the Sarychev volcano and simulations using the HadGEM2 climate model, J. Geophys. Res. , 115, D21212, 2010.

Haywood, J. M., Jones, A., and Jones, G. S.: The impact of volcanic eruptions in the period 2000–2013 on global mean temperature trends evaluated in the HadGEM2-ES climate model, Atmos. Sci. Lett., 15, 92-96, 2014.

Heard, I. P. C., Manning, A. J., Haywood, J. M., Witham, C., Redington, A., Jones, A., Clarisse, L., and Bourassa, A.: A comparison of atmospheric dispersion model predictions with observations of SO2 and sulphate aerosol from volcanic eruptions, J. Geophys. Res., 117, 2012.

Heiken, G., and Wohletz, K.: Volcanic ash, edited by: Sharp, D. H., and Simmons, L. M., University of California Press, Berkeley, 1985.

Hermann, M., Stratmann, F., Wilck, M., and Wiedensohler, A.: Sampling characteristics of an aircraft-borne aerosol inlet system, J. Atmos. Ocean. Tech., 18, 7-19, 2001.

Hermann, M., Heintzenberg, J., Wiedensohler, A., Zahn, A., Heinrich, G., and Brenninkmeijer, C.: Meridional distributions of aerosol particle number concentrations in the upper troposphere and lower stratosphere obtained by Civil Aircraft for Regular Investigation of the Atmosphere Based on an Instrument Container (CARIBIC) flights, J. Geophys Res., 108, 2003.

Heue, K. P., Brenninkmeijer, C. A. M., Wagner, T., Mies, K., Dix, B., Frieß, U., Martinsson, B. G., Slemr, F., and van Velthoven, P. F. J.: Observations of the 2008 Kasatochi volcanic SO2 plume by CARIBIC aircraft DOAS and the GOME-2 satellite, Atm. Chem. Phys., 10, 4699-4713, 2010.

Hinds, W. C.: Aerosol technology: properties, behavior, and measurement of airborne particles, Book, John Wiley & Sons, New York, 1999.

Hofmann, D., Barnes, J., O'Neill, M., Trudeau, M., and Neely, R.: Increase in background stratospheric aerosol observed with lidar at Mauna Loa Observatory and Boulder, Colorado, Geophys. Res. Lett., 36, L15808, 2009.

Holton, J. R., Haynes, P. H., McIntyre, M. E., Douglass, A. R., Rood, R. B., and Pfister, L.: Stratosphere-troposphere exchange, Rev. Geophys., 33, 403-439, 1995.

Holton, J. R.: An introduction to dynamic meteorology, 4 ed., International Geophysics series, Amsterdam, 2004.

Hoor, P., Fischer, H., Lange, L., Lelieveld, J., and Brunner, D.: Seasonal variations of a mixing layer in the lowermost stratosphere as identified by the CO-O3 correlation from in situ measurements, J. Geophys. Res, 107, ACL 1-1-ACL 1-11, 2002.

Hoskins, B. J.: Towards a PV-θ view of the general circulation, Tellus A, 43, 27-35, 1991.

Hostetler, C. A., Liu, Z., Regan, J., Vaughan, M., Winker, D., Osborn, M., Hunt, W. H., Powell, K. A., and Trepte, C.: CALIOP AlgorithmTheoretical Basis Document (ATBD): Calibration and level 1 data pro-ducts, Doc. PC-SCI-201, 2006.

Hunt, W. H., Winker, D. M., Vaughan, M. A., Powell, K. A., Lucker, P. L., and Weimer, C.: CALIPSO Lidar Description and Performance Assessment, J. Atmos. Ocean. Tech., 26, 1214-1228, 2009.

Jost, H. J., Drdla, K., Stohl, A., Pfister, L., Loewenstein, M., Lopez, J. P., Hudson, P. K., Murphy, D. M., Cziczo, D. J., and Fromm, M.: In-situ observations of mid-latitude forest fire plumes deep in the stratosphere, Geophys. Res. Lett., 31, 2004.

Junge, C. E., Chagnon, C. W., and Manson, J. E.: A World-wide Stratospheric Aerosol Layer, Science, 133, 1478-1479, 1961.

Jurkat, T., Voigt, C., Arnold, F., Schlager, H., Aufmhoff, H., Schmale, J., Schneider, J., Lichtenstern, M., and Dornbrack, A.: Airborne stratospheric ITCIMS measurements of SO2, HCl, and HNO3 in the aged plume of volcano Kasatochi, J. Geophys. Res., 115, D00L17, 2010.

Jäger, H., and Deshler, T.: Lidar backscatter to extinction, mass and area conversions for stratospheric aerosols based on midlatitude balloonborne size distribution measurements, Geophys. Res. Lett., 29, 19, 1929, 2002.

Jäger, H., and Deshler, T.: Correction to "Lidar backscatter to extinction, mass and area conversions for stratospheric aerosols based on midlatitude balloonborne size distribution measurements", Geophys. Res. Lett., 30, 1382, 2003.

Jäger, H.: Long-term record of lidar observations of the stratospheric aerosol layer at Garmisch-Partenkirchen, J Geophys. Res., 110, D08106, 2005.

Karagulian, F., Clarisse, L., Clerbaux, C., Prata, A. J., Hurtmans, D., and Coheur, P. F.: Detection of volcanic SO2, ash, and H2SO4 using the Infrared Atmospheric Sounding Interferometer (IASI), J. Geophys. Res., 115, D00L02, 2010.

Kjellström, E., Feichter, J., Sausen, R., and Hein, R.: The contribution of aircraft emissions to the atmospheric sulfur budget, Atmos. Environ., 33, 3455-3465, 1999.

Kravitz, B., Robock, A., and Bourassa, A.: Negligible climatic effects from the 2008 Okmok and Kasatochi volcanic eruptions, J. Geophys Res., 115, D00L05, 2010.

Kravitz, B., Robock, A., Bourassa, A., Deshler, T., Wu, D., Mattis, I., Finger, F., Hoffmann, A., Ritter, C., Bitar, L., Duck, T. J., and Barnes, J. E.: Simulation and observations of stratospheric aerosols from the 2009 Sarychev volcanic eruption, J. Geophys. Res., 116, D18211, 2011.

Krotkov, N. A., Schoeberl, M. R., Morris, G. A., Carn, S., and Yang, K.: Dispersion and lifetime of the SO2 cloud from the August 2008 Kasatochi eruption, J. Geophys. Res., 115, D00L20, 2010.

Kulkarni, P., Baron, P. A., Willeke, K.: Introduction to Aerosol Characterization, in Aerosol Measurement: Principles, Techniques, and Applications, Book, John Wiley & Sons, Inc., Hoboken, N.J., 2011

Lacis, A., Hansen, J., and Sato, M.: Climate forcing by stratospheric aerosols, Geophys. Res. Lett., 19, 1607-1610, 1992.

Martinsson, B. G., Nguyen, H. N., Brenninkmeijer, C. A., Zahn, A., Heintzenberg, J., Hermann, M., and Van Velthoven, P. F.: Characteristics and origin of lowermost stratospheric aerosol at northern midlatitudes under volcanically quiescent conditions based on CARIBIC observations, J. Geophys Res., 110, D12201, 2005.

Martinsson, B. G., Brenninkmeijer, C. A. M., Carn, S. A., Hermann, M., Heue, K. P., van Velthoven, P. F. J., and Zahn, A.: Influence of the 2008 Kasatochi volcanic eruption on sulfurous and carbonaceous aerosol constituents in the lower stratosphere, Geophys. Res. Lett., 36, L12813, 2009.

Martinsson, B. G., Friberg, J., Andersson, S. M., Weigelt, A., Hermann, M., Assmann, D., Voigtländer, J., Brenninkmeijer, C. A. M., Velthoven, P. J. F. v., and Zahn, A.: Comparison between CARIBIC aerosol samples analysed by accelerator-based methods and optical particle counter measurements, Atmos. Meas. Tech. , 7, 2581-2596, 2014.

McCormick, M. P., Thomason, L. W., and Trepte, C. R.: Atmospheric effects of the Mt Pinatubo eruption, Nature, 373, 399-404, 1995.

McGonigle, A. J. S., Delmelle, P., Oppenheimer, C., Tsanev, V. I., Delfosse, T., Williams-Jones, G., Horton, K., and Mather, T. A.: SO2 depletion in tropospheric volcanic plumes, Geophys. Res. Lett., 31, L13201, 2004.

Murphy, D. M., Cziczo, D. J., Hudson, P. K., and Thomson, D. S.: Carbonaceous material in aerosol particles in the lower stratosphere and tropopause region, J. Geophys. Res., 112, D04203, 2007.

Murphy, D. M., Froyd, K. D., Schwarz, J. P., and Wilson, J. C.: Observations of the chemical composition of stratospheric aerosol particles, Q. J. Roy. Meteor. Soc., 140, 1269–1278, 2013.

Myhre, G., Berglen, T. F., Myhre, C. E. L., and Isaksen, I. S. A.: The radiative effect of the anthropogenic influence on the stratospheric sulfate aerosol layer, Tellus B, 56, 294-299, 2004.

Myhre, G., Shindell, D., Bréon, F.-M., Collins, W., Fuglestvedt, J., Huang, J., Koch, D., Lamarque, J.-F., Lee, D., Mendoza, B., Nakajima, T., Robock, A., Stephens, G., Takemura, T., and Zhang, H.: Anthropogenic and Natural Radiative Forcing. In: Climate Change 2013: The Physical Science Basis. Contribution of Working Group I to the Fifth Assessment Report of the Intergovernmental Panel on Climate Change, Cambridge University Press, Cambridge, United Kingdom and New York, NY, USA, 2013.

Nemesure, S., Wagener, R., and Schwartz, S. E.: Direct shortwave forcing of climate by the anthropogenic sulfate aerosol: Sensitivity to particle size, composition, and relative humidity, J. Geophys Res., 100, 26105-26116, 1995.

Nguyen, H. N., and Martinsson, B. G.: Analysis of C, N and O in aerosol collected on an organic backing using internal blank measurements and variable beam size, Nucl. Instrum. Methods, 264, 96–102, 2007.

Nguyen, H. N., Martinsson, B. G., Wagner, J. B., Carlemalm, E., Ebert, M., Weinbruch, S., Brenninkmeijer, C. A. M., Heintzenberg, J., Hermann, M., Schuck, T., Velthoven, P. F. J. v., and Zahn, A.: Chemical composition and morphology of individual

aerosol particles from a CARIBIC flight at 10 km altitude between 50 N and 30 S, J. Geophys. Res., 113, D2320, 2008.

Nguyen, N. H., Gudmundsson, A., and Martinsson, B.: Design and calibration of a multi-channel aerosol sampler for tropopause region studies from the CARIBIC platform, Aerosol Sci. Tech. , 40, 649-655, 2006.

Papaspiropoulos, G., Martinsson, B. G., Zahn, A., Brenninkmeijer, C. A. M., Hermann, M., Heintzenberg, J., Fischer, H., and Velthoven, P. F. J. v.: Aerosol elemental concentrations in the tropopause region from intercontinental flights with the Civil Aircraft for Regular Investigation of the Atmosphere Based on an Instrument Container (CARIBIC) platform, J. Geophys. Res., 107, D23, 4671, 2002.

Pitari, G., Mancini, E., Rizi, V., and Shindell, D. T.: Impact of Future Climate and Emission Changes on Stratospheric Aerosols and Ozone, J. Atmos. Sci. , 59, 414-440, 2002.

Pueschel, R. F., Russell, P. B., Allen, D. A., Ferry, G. V., Snetsinger, K. G., Livingston, J. M., and Verma, S.: Physical and optical properties of the Pinatubo volcanic aerosol: Aircraft observations with impactors and a Sun-tracking photometer, J. Geophys. Res., 99, 12915-12922, 1994.

Read, W. G., Froidevaux, L., and Waters, J. W.: Microwave Limb Sounder measurement of stratospheric SO2 from the Mt. Pinatubo volcano, Geophys. Res. Lett., 20, 1299-1302, 1993.

Ridley, D., Solomon, S., Barnes, J., Burlakov, V., Deshler, T., Dolgii, S., Herber, A., Nagai, T., Neely, R., and Nevzorov, A.: Total volcanic stratospheric aerosol optical depths and implications for global climate change, Geophys. Res. Lett., 41, 7763 - 7769, 2014.

Rose, W. I., Bluth, G. J. S., Schneider, D. J., Ernst, G. G. J., Riley, C. M., Henderson, L. J., and McGimsey, R. G.: Observations of Volcanic Clouds in Their First Few Days of Atmospheric Residence: The 1992 Eruptions of Crater Peak, Mount Spurr Volcano, Alaska, J. Geol., 109, 677-694, 2001.

Rose, W. I., and Durant, A. J.: Fine ash content of explosive eruptions, J. Volcanol. Geoth. Res., 186, 32-39, 2009.

Rosen, J. M.: The boiling point of stratospheric aerosols, Journal of Applied Meteorology, 10, 1044-1046, 1971.

Santer, B. D., Bonfils, C., Painter, J. F., Zelinka, M. D., Mears, C., Solomon, S., Schmidt, G. A., Fyfe, J. C., Cole, J. N. S., Nazarenko, L., Taylor, K. E., and Wentz, F. J.: Volcanic contribution to decadal changes in tropospheric temperature, Nat. Geosci., 7, 185-189, 2014.

Sato, M., Hansen, J. E., McCormick, M. P., and Pollack, J. B.: Stratospheric aerosol optical depths, 1850–1990, J. Geophys Res., 98, 22987-22994, 1993.

Schmale, J., Schneider, J., Voigt, T. J., Kalesse, H., Rautenhaus, M., Lichtenstern, M., Schlager, H., Ancellet, G., Arnold, F., Gerding, M., Mattis, I., Wendisch, M., and Borrmann, S.: Aerosol layers from the 2008 eruptions of Mount Okmok and Mount Kasatochi: In situ upper troposphere and lower stratosphere measurements of sulfate and organics over Europe J. Geophys. Res., 115, D00L07, 2010.

Schmidt, G. A., Shindell, D. T., and Tsigaridis, K.: Reconciling warming trends, Nat.Geosci., 7, 158-160, 2014.

Schwartz, S. E. in Aerosol Metrology for Climate Workshop,Gaithersburg, MD (http://www.ecd.bnl.gov/steve/pres/NIST_aerosol_pptiesW.pdf, 2011).

Seinfeld, J. H., and Pandis, S. N.: Atmospheric chemistry and physics: from air pollution to climate change, 2nd ed., Book, John Wiley &Sons, Inc., Hoboken, N.J, 2006.

Sica, R. J., Zylawy, Z. A., and Argall, P. S.: Ozone corrections for Rayleigh-scatter temperature determinations in the middle atmosphere, J. Atmos. Ocean.Tech., 18, 1223-1228, 2001.

Solomon, S., Daniel, J. S., NeelyIII, R. R., 3rd, Vernier, J. P., Dutton, E. G., and Thomason, L. W.: The persistently variable "background" stratospheric aerosol layer and global climate change, Science, 333, 866-870, 2011.

Sprenger, M., and Wernli, H.: A northern hemispheric climatology of cross-tropopause exchange for the ERA15 time period (1979–1993), J. Geophys. Res, 108(D12), 8521, 2003.

Stohl, A., Meloen, J., and Siegmund, P.: Stratosphere-troposphere exchange: A review, and what we have learned for STACCATO, J. Geophys. Res., 108(D12), 8516, 2003.

Storelvmo, T., Kristjansson, J., Muri, H., Pfeffer, M., Barahona, D., and Nenes, A.: Cirrus cloud seeding has potential to cool climate, Geophys. Res. Lett., 40, 178-182, 2013.

Tang, Q., Prather, M. J., and Hsu, J.: Stratosphere-troposphere exchange ozone flux related to deep convection, Geophys. Res. Lett., 38, L03806, 2011.

Thomason, L. W., Pitts, M. C., and Winker, D. M.: CALIPSO observations of stratospheric aerosols: a preliminary assessment, Atm. Chem. Phys., 7, 5283-5290, 2007.

Walter, J.: Size distribution characteristics of aerosols, Aerosol Measurement: Principles, Techniques and Applications, 2010.

Vernier, J.-P., Pommereau, J.-P., Thomason, L., Pelon, J., Garnier, A., Deshler, T., Jumelet, J., and Nielsen, J.: Overshooting of clean tropospheric air in the tropical lower stratosphere as seen by the CALIPSO lidar, Atmos. Chem. Phys, 9683–9696, 2011a.

Vernier, J.-P., Thomason, L. W., Pommereau, J.-P., Bourassa, A., Pelon, J., Garnier, A., Hauchecorne, A., Blanot, L., Trepte, C., Degenstein, D., and Vargas, F.: Major influence of tropical volcanic eruptions on the stratospheric aerosol layer during the last decade, Geophys. Res. Lett., 38, L12807, 2011b.

Vernier, J. P., Pommereau, J. P., Garnier, A., Pelon, J., Larsen, N., Nielsen, J., Christensen, T., Cairo, F., Thomason, L. W., Leblanc, T., and McDermid, I. S.: Tropical stratospheric aerosol layer from CALIPSO lidar observations, J. Geophys Res., 114, D00H10, 2009.

Winker, D. M., Vaughan, M. A., Omar, A., Hu, Y. X., Powell, K. A., Liu, Z. Y., Hunt, W. H., and Young, S. A.: Overview of the CALIPSO Mission and CALIOP Data Processing Algorithms, J. Atmos. Ocean. Tech., 26, 2310-2323, 2009.

von Glasow, R., Bobrowski, N., and Kern, C.: The effects of volcanic eruptions on atmospheric chemistry, Chem. Geol., 263, 131-142, 2009.

Zahn, A., Brenninkmeijer, C., Asman, W., Crutzen, P., Heinrich, G., Fischer, H., Cuijpers, J., and Van Velthoven, P.: Budgets of O3 and CO in the upper troposphere: CARIBIC passenger aircraft results 1997–2001, J. Geophys Res., 107, ACH 6-1-ACH 6-20, 2002.

Zahn, A., Weppner, J., Widmann, H., Schlote-Holubek, K., Burger, B., Kuhner, T., and Franke, H.: A fast and precise chemiluminescence ozone detector for eddy flux and airborne application, Atmos. Meas. Tech., 5, 363-375, 2012.

Paper I

Atmos. Chem. Phys., 13, 1781–1796, 2013
www.atmos-chem-phys.net/13/1781/2013/
doi:10.5194/acp-13-1781-2013

Atmospheric Chemistry and Physics Open Access

Composition and evolution of volcanic aerosol from eruptions of Kasatochi, Sarychev and Eyjafjallajökull in 2008–2010 based on CARIBIC observations

S. M. Andersson[1], B. G. Martinsson[1], J. Friberg[1], C. A. M. Brenninkmeijer[2], A. Rauthe-Schöch[2], M. Hermann[3], P. F. J. van Velthoven[4], and A. Zahn[5]

[1]Division of Nuclear Physics, Lund University, Lund, Sweden
[2]Max Planck Institute for Chemistry, Atmospheric Chemistry, Mainz, Germany
[3]Leibniz Institute for Tropospheric Research, Leipzig, Germany
[4]Royal Netherlands Meteorological Institute, de Bilt, The Netherlands
[5]Institute for Meteorology and Climate Research, Karlsruhe Institute of Technology (KIT), Germany

Correspondence to: S. M. Andersson (sandra.andersson@nuclear.lu.se)

Received: 12 April 2012 – Published in Atmos. Chem. Phys. Discuss.: 22 August 2012
Revised: 7 January 2013 – Accepted: 5 February 2013 – Published: 18 February 2013

Abstract. Large volcanic eruptions impact significantly on climate and lead to ozone depletion due to injection of particles and gases into the stratosphere where their residence times are long. In this the composition of volcanic aerosol is an important but inadequately studied factor. Samples of volcanically influenced aerosol were collected following the Kasatochi (Alaska), Sarychev (Russia) and also during the Eyjafjallajökull (Iceland) eruptions in the period 2008–2010. Sampling was conducted by the CARIBIC platform during regular flights at an altitude of 10–12 km as well as during dedicated flights through the volcanic clouds from the eruption of Eyjafjallajökull in spring 2010. Elemental concentrations of the collected aerosol were obtained by accelerator-based analysis. Aerosol from the Eyjafjallajökull volcanic clouds was identified by high concentrations of sulphur and elements pointing to crustal origin, and confirmed by trajectory analysis. Signatures of volcanic influence were also used to detect volcanic aerosol in stratospheric samples collected following the Sarychev and Kasatochi eruptions. In total it was possible to identify 17 relevant samples collected between 1 and more than 100 days following the eruptions studied. The volcanically influenced aerosol mainly consisted of ash, sulphate and included a carbonaceous component. Samples collected in the volcanic cloud from Eyjafjallajökull were dominated by the ash and sulphate component (∼45 % each) while samples collected in the tropopause region and LMS mainly consisted of sulphate (50–77 %) and carbon (21–43 %). These fractions were increasing/decreasing with the age of the aerosol. Because of the long observation period, it was possible to analyze the evolution of the relationship between the ash and sulphate components of the volcanic aerosol. From this analysis the residence time (1/e) of sulphur dioxide in the studied volcanic cloud was estimated to be 45 ± 22 days.

1 Introduction

Despite its modest size, the eruption of Eyjafjallajökull volcano in the spring of 2010 caused considerable disruption of European air traffic due to the ash and sulphate aerosol it produced. In particular ash particles are hazardous, since they can damage jet engines and disrupt avionics and navigation systems (Casadevall, 1994), whereas sulphate aerosol have been reported to cause crazing of aircraft windows (Carn et al., 2009). Above all the complex effects of volcanoes on atmospheric chemistry and physics are also of concern for climate (Ammann et al., 2003). Not only the amount of ejected material, the location of the volcano and the force of the eruption, but also the properties of volcanic aerosol play a considerable role in these contexts. Unfortunately, our present understanding of the composition of volcanically influenced

atmospheric aerosol is limited since quantitative measurements in the free troposphere and in the stratosphere are scarce. To improve this situation, we report here on the investigation of the elemental composition of volcanic aerosol sampled directly in the volcanic cloud from the Eyjafjallajökull eruption in 2010, and moreover sampled in the upper troposphere/lowermost stratosphere (UT/LMS) following eruptions of the volcanoes Kasatochi (Alaska, 2008) and Sarychev (Russia, 2009).

The scattering and absorbing properties of volcanic aerosol affect the Earth's radiation budget and thus result in temperature gradients that perturb circulation patterns and impact climate (IPCC, 2007). After the eruption of Mount Pinatubo in 1991, with a large Volcanic Explosivity Index (VEI) (Newhall and Self, 1982) of 6, the global, tropospheric temperature was estimated to have been 0.5 °C lower than the climatological average temperature. Another large eruption in Tambora (1815, VEI 7) caused an estimated drop in global mean temperature of 0.4 to 0.7 °C (McCormick et al., 1995). Stratospheric aerosols also act as surfaces for heterogeneous reactions that affect the distribution of ozone and other trace gases (IPCC, 2007). Not only massive eruptions such as those mentioned above are of importance to the stratospheric aerosol load. A study by Vernier et al. (2011) based on satellite observations shows that eruptions of lower explosivity are also an important source of stratospheric aerosol. Their effect is visible in the increase of the stratospheric aerosol layer that has occurred since 2002 after a period with little volcanic influence. This increase in the stratospheric aerosol load has also been observed in other data sets, however, anthropogenic influence cannot be ruled out (Hofmann et al., 2009; Solomon et al., 2011).

In the absence of volcanic eruptions, stratospheric aerosol is mainly found at altitudes of 20–30 km (Junge et al., 1961). This aerosol layer, referred to as the Junge layer, mainly consists of sulphate aerosol that is chiefly formed by sulphur dioxide (SO_2) produced from photo-dissociation of carbonyl sulphide (OCS) transported from the troposphere (Crutzen, 1976). However studies indicate that OCS is not enough to explain the observed aerosol load (Chin and Davis, 1995), and direct transport of SO_2 or sulphate aerosol have been suggested as important contributions to stratospheric aerosol (Pitari et al., 2002; Myhre et al., 2004). Volcanic injections however makes it difficult to determine the background state of the stratospheric aerosol layer (Solomon et al., 2011), and thereby the importance of different sources for its production. A carbonaceous component of the UT/LMS aerosol was identified by Murphy et al. (1998), which was subsequently found to be a large fraction of the aerosol (Nguyen et al., 2008; Murphy et al., 2007). Martinsson et al. (2009) found that volcanic aerosol contains a large carbonaceous component. Additional sources contributing to the aerosol load in the UT/LMS, include air traffic (Ferry et al., 1999; Kjellström et al., 1999), meteorites (Cziczo et al., 2001) and boundary layer aerosol and precursor gases transported across the tropopause (Papaspiropoulos et al., 2002; Köppe et al., 2009). Especially aerosol from forest fires can be brought to high altitudes by extreme convection, however, the frequency and global contribution of such events is poorly understood (Fromm et al., 2004, 2008). Guan et al. (2010) estimated that on average about six such events per year lead to injection of particles to altitudes above 8 km. With a frequency of one or a few events per year, volcanic eruptions contribute to stratospheric aerosol mass of similar magnitude as OCS does (Vernier et al., 2011), and in a few events per century volcanism is by far the strongest source of stratospheric aerosol (Ammann et al., 2003).

Volcanic eruptions inject large quantities of ash and gases into the atmosphere. Sulphur dioxide is the third most abundant gas in volcanic emissions, after water vapor and carbon dioxide (von Glasow et al., 2009). It is oxidized in the atmosphere thus leading to sulphate aerosol. Enhanced concentrations of stratospheric aerosol following the eruptions of El Chichón (1982) and Pinatubo (1991) had a residence time (1/e) of 10.3 and 12.0 months respectively (Jäger, 2005; Deshler, 2008). Especially the number concentration of particles larger than 1 µm in diameter was observed to increase substantially following the Pinatubo eruption (Deshler, 2008). The directly emitted ash particles exhibit a size of 2 mm or less (by definition) (Heiken and Wohletz, 1985), and show a large span in size with particle diameters down to less than 1 µm (Rose and Durant, 2009; Mather et al., 2003). Large particles sediment quickly while very fine ash particles ($<$15 µm) have been found to have a residence time of days to weeks in the UT/LMS (Rose and Durant, 2009; Niemeier et al., 2009). During the first 24 h after an eruption a rapid decrease of the fine ash ($<$25 µm) content of the volcanic cloud have been observed, likely caused by aggregation into larger particles with higher settling velocities (Rose et al., 2001). After this initial phase, ash concentrations decrease more slowly together with concentrations of SO_2. Ash and SO_2 clouds can either be travelling collocated or separated in the atmosphere. Vertical separation occurs due to the eruption style or by different sedimentation velocity of ash and SO_2, and horizontal separation due to wind shear (Thomas and Prata, 2011). Although research has shown that fine ash particles are spread and deposited over large areas (Rose and Durant, 2009), we know little about the atmospheric fate (change in composition, lifetime) of volcanic particles in the micrometer size range.

Most research into atmospheric influence of volcanic eruptions is based on remote sensing from the surface or from satellite to follow the dispersal of volcanic SO_2 clouds or to investigate the influence of eruptions on the stratospheric aerosol load. The actual composition of volcanic aerosol has been investigated by aircraft-based measurements by Martinsson et al. (2009) and Schmale et al. (2010) following the Kasatochi eruption in 2008 and recently by Schumann et al. (2011) in the volcanic cloud from Eyjafjallajökull. However these studies only consider aerosol composition from

single eruptive events and do not address evolution of the composition of volcanic aerosol in the atmosphere. In the study by Martinsson et al. (2009) a subset of the data presented in this study was used to investigate the development of the sulphurous and carbonaceous components of the volcanically influenced aerosol.

Here we present and discuss the multi elemental composition of aerosol from three eruptions with VEI 4. The volcanic aerosol was collected between one and over 100 days after the eruptions, which provides a unique opportunity to investigate the evolution of the aerosol. Aerosol sampling and measurements of trace gases were performed by the CARIBIC (Civil Aircraft for Regular Investigation of the atmosphere Based on an Instrument Container) platform operating on a passenger aircraft (Brenninkmeijer et al., 2007; www.caribic-atmospheric.com).

2 Experimental methods

Samples of volcanic aerosol particles were obtained from the CARIBIC platform during regular long-distance passenger flights in the UT/LMS following large eruptions of the Kasatochi (2008) and Sarychev (2009) volcanoes, as well as during special flights at 4–12 km altitudes on 16 May and 19 May 2010, which were conducted to investigate the composition of the volcanic clouds produced by the Eyjafjallajökull eruption (Rauthe-Schöch et al., 2012). The CARIBIC measurement container is mounted in the forward cargo bay of a Lufthansa Airbus 340–600 during four sequential flights (Brenninkmeijer et al., 2007) on a monthly basis. From Frankfurt (Germany) destinations in North and South America, South Africa and South and East Asia are reached, thus covering a large geographical area mainly in the Northern Hemisphere. Instruments in the container automatically measure concentrations of many trace gases, aerosol number concentrations and the aerosol size distribution. In addition sampling of air and aerosol particles for laboratory analysis takes place. This study concentrates on volcanically influenced aerosol samples collected between 2008 and 2010, but also uses measurements of the background aerosol collected from 1999 to 2002 (Martinsson et al., 2005) and somewhat volcanically influenced samples from 2005 to 2008.

Aerosol particles of 0.08–2 µm aerodynamic diameter were collected in a multi-channel aerosol sampler on 0.2 µm thick polyimide foils (Nguyen et al., 2006) by impaction. The upper size limit is determined by a cyclone separator placed between the aerosol inlet and the sampler, and the lower limit by the cutoff diameter of the aerosol sampler. The sampler has 16 sampling channels with 14 for sequential collection and 2 for integral samples used to monitor contamination by comparing the integral samples to the sum of the sequential samples. The sampling time for each sequential sample is typically 100 min, corresponding to a flight distance of approximately 1500 km at cruising speed, and a sampling volume of approximately 0.25 m^3 STP (Standard Temperature (273 K) and Pressure (1013 hPa)). Sampling is suspended when the outside pressure is above 350 hPa. However, during the special flights through the Eyjafjallajökull volcanic cloud, collection of aerosol at lower altitudes was allowed and the sampling time was reduced to 50 min.

Aerosol samples were analyzed by accelerator-based techniques at the Lund ion beam analysis facility using two methods to obtain elemental concentrations: PIXE (Particle-Induced X-ray Emission) and PESA (Particle Elastic Scattering Analysis). In both methods the samples were mounted in a high vacuum chamber and irradiated with a beam of 2.55 MeV protons. Concentrations of elements with atomic numbers of 16 (*S*) or more were obtained by PIXE (Johansson and Campbell, 1988), and concentrations of hydrogen, carbon, nitrogen and oxygen by PESA (Nguyen and Martinsson, 2007). PESA was implemented for analysis of samples collected after 2005. Detection limits reached from several down to 0.1 ng m^{-3} STP, depending on element. The accuracy for elemental determination by both methods is estimated to be 10 % (Nguyen and Martinsson, 2007). The PIXE technique can also detect silicon (Si) when the concentrations are high, such as in aerosol samples which are dominated by aerosol particles from volcanic eruptions. In samples with low concentrations of Si problems arise due to interference with sulphur, which is often dominant. In samples with a S/Si ratio below a critical value, these effects have been corrected for, but for larger S/Si ratios corrections were not possible and the measured Si concentrations were excluded from the results. Elements that usually are below the detection limit (Sr, Zr) were detectable in samples collected in the Eyjafjallajökull volcanic clouds, using longer than usual analysis times.

We further use data from ozone measurements performed by two instruments on the CARIBIC platform. A UV-photometer is used for accurate determination of the ozone concentration by absorption of UV light and also serves as a standard for a fast chemiluminescence detector which enables ozone detection with high temporal resolution. The accuracy is estimated to be 0.3–1 % at typical mixing ratios at a measurement frequency of 10 Hz (Zahn et al., 2012).

Also measurements of SO_2 concentrations and particle size distributions during the flights in the volcanic cloud from Eyjafjallajökull were used in this study. Concentrations of SO_2 are obtained from the CARIBIC DOAS (Differential Optical Absorption Spectroscopy) instrument (Dix et al., 2009), detecting NO_2, HCHO, HONO, BrO, OClO, O_3, SO_2 and O_4 simultaneously by measuring scattered or reflected sunlight, collected with three telescopes pointing to $-82°$, $-10°$ and $+10°$ relative to the horizon, with a temporal resolution of 8 s. During the volcanic flights the instrument was only functioning properly on May 16, measuring in the $-82°$ and $-10°$ directions (Heue et al., 2011). Particle size distributions are measured with an integrated OPC (Optical Particle Counter), which measures particles with a diameter in the

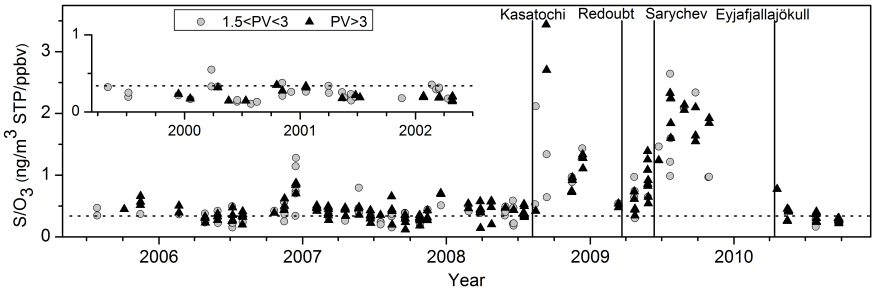

Fig. 1. Ratio of particulate sulphur to ozone concentration in aerosol samples collected in the tropopause region (grey circles) and the lowermost stratosphere (black triangles). The dotted line indicates the geometrical mean of samples collected before the eruption of Kasatochi in August 2008. The occasions of major eruptions are marked by vertical lines.

range of approximately 0.1–1µm. OPC measurements from the volcanic flight on 19 May were used in this study (Heue et al., 2011; Rauthe-Schöch et al., 2012). A time resolution of 3 min was used to calculate the OPC size distributions during this flight.

Potential vorticity (PV) at the location of the aircraft was used to determine whether collected particles were of tropospheric or stratospheric origin, the tropopause region was defined as the region between 1.5–3 PVU (Potential Vorticity Unit; $1\,\mathrm{PVU} = 10^{-6}\,\mathrm{K\,m^2\,kg^{-1}\,s^{-1}}$). PV was derived from archived ECMWF (European Centre for Medium-range Weather Forecast) analyses with a resolution of 1×1 degree in the horizontal direction and 91 vertical hybrid sigma-pressure model levels. To obtain PV at the aircraft position the PV values was interpolated linearly in latitude, longitude, log pressure and time for each sample.

The recent history of probed air was investigated by means of 5-days backward air mass trajectories, calculated every third minute along the flight route using the trajectory model TRAJKS (Scheele et al., 1996) and the horizontal and vertical wind fields provided by ECMWF.

Complementary to trajectory analysis, lidar measurements from the CALIPSO (Cloud-Aerosol Lidar and Infrared Pathfinder Satellite Observations) satellite were used. The lidar is equipped with a Nd:YAG laser producing highly polarized co-aligned beams with wavelengths of 532 and 1064 nm. Clouds and different types of aerosol particles can be identified since the shape and size of particles and droplets cause different scattering properties at these wavelengths (Winker et al., 2009).

3 Results

3.1 Identification of volcanic aerosol

A first indication of volcanic influence on CARIBIC UT/LMS aerosol samples is high concentrations of sulphur. These concentrations correspond to sulphate aerosol produced from SO_2 emitted during eruptions. Such influence is mainly seen in stratospheric samples, where the residence time of aerosol particles is long compared to the troposphere. In Fig. 1 the ratio of S/O_3 is used as an indicator of volcanic influence on stratospheric aerosol. Concentrations of S and O_3 show a correlation in absence of volcanic influence, since both sulphate and ozone are produced in the stratosphere with the aid of shortwave radiation. Consequently, high concentrations of sulphur are usually observed in association with downward transport in the stratosphere, together with elevated O_3 levels (Martinsson et al., 2009). Explosive volcanic eruptions disturb this ratio by injecting large amounts of additional sulphur. In Fig. 1, volcanic influence is indicated by elevated S/O_3 ratios following major eruptions (VEI 4) of the Kasatochi (52.18° N, 175.51° W, August, 2008), Redoubt (60.49° N, 152.74° W, March/April, 2009) and Sarychev (48.09° N, 153.20° E, June, 2009) volcanoes. The sulphurous and carbonaceous components of the aerosol related to the Kasatochi eruption were discussed in detail in the study by Martinsson et al. (2009). Fig. 1 shows that elevated S/O_3 ratios prevailed for at least four months after the Kasatochi eruption and were just reaching background levels when elevated concentrations of sulphur again were observed after the Redoubt and Sarychev eruptions in 2008. The small effects of the Eyjafjallajökull (63.63° N, 19.62° W) eruption in April/May 2010 can be explained by the fact that the emissions were poor in SO_2 and that only a small fraction of the plume reached the stratosphere (BGVN, 2010; Thomas and Prata, 2011). However,

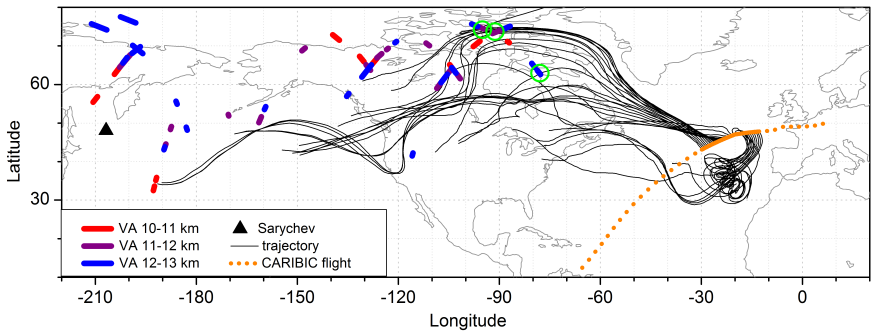

Fig. 2. Air-mass back-trajectories (thin black lines) calculated for one sample collected during the first CARIBIC flight from Frankfurt to Caracas at 23 June 2009 (orange dotted line) following the eruption of Sarychev, combined with volcanic aerosol (VA) layers at 10–13 km altitude (colored lines) obtained from CALIPSO lidar measurements at 21 June 2009. Green circles indicate where trajectories and aerosol layers intersect horizontally and vertically.

very high concentrations of crustal elements were found in three aerosol samples collected during the special flights on 16 May and 19 May 2010, strongly indicating volcanic influence. These samples were collected in the troposphere and are thus not included in Fig. 1, which only shows samples collected in the stratosphere or the tropopause region.

Further connection to the eruptions was established by using 5-days, and in one case 8-days, backward trajectory analysis for samples following the Kasatochi (Martinsson et al., 2009), Sarychev and Eyjafjallajökull eruptions. The first samples following the eruption of Redoubt were collected more than a month after the first explosion; hence trajectory analysis could not be used to verify volcanic origin. In addition, these samples show less elevation in their S/O_3 ratio than the samples following Sarychev and Kasatochi. The eruptions of Sarychev and Kasatochi emitted approximately 1.2 Tg (Haywood et al., 2010) and 2 Tg (Yang et al., 2010) of SO_2, respectively, into the atmosphere which can be compared to only 0.08 Tg by the eruption of Redoubt (Lopez et al., 2009). It is thus unlikely that the sulphate aerosol produced by the Redoubt eruption had large enough influence for a clear identification in sampled aerosol. It is possible that the elevated concentrations in the samples instead are due to downward transport of an upper branch of the aerosol produced in the preceding eruption of Kasatochi. The volcanically influenced aerosol also contains a crustal component, which will be further discussed in Sect. 3.2. Stratospheric concentrations of crustal elements such as potassium (K) and iron (Fe) show a seasonal dependence with high concentrations in spring (March to June) that seem to be connected with transport across the tropopause from the troposphere (Martinsson et al., 2005). The samples collected following the Redoubt eruption were collected at this time of the year; therefore it cannot be excluded that the crustal component of the aerosol has been transported from the boundary layer rather than been injected by the eruption. Due to the uncertainty of the source of the aerosol following the Redoubt eruption, these samples are excluded from further consideration.

Trajectory analysis performed for each of the three samples with large crustal components from the Eyjafjallajökull volcanic clouds showed that the sampled air had passed over the volcano. The transport time from the volcano to the aircraft position, and thus the age of the aerosol, was estimated to have been about 40 and 45 h for the samples collected May 16 and about 25 h for the sample collected May 19. The time for sampling within the volcanic cloud, and thereby the most likely transport path, was determined from peaks in the SO_2 and particle mass concentrations obtained from the CARIBIC DOAS and OPC instruments (Heue et al., 2011; Rauthe-Schöch et al., 2012).

Trajectory analysis conducted for samples following the Sarychev eruption was combined with lidar measurements from CALIPSO (Fig. 2). The large amount of sulphate produced during this eruption made it possible to follow the volcanic aerosol in the lidar measurements up to more than a month after the eruption. Aerosol layers detected by CALIPSO at an altitude between 10 and 13 km were identified, and this information was put together with the path of calculated air mass trajectories. By this method aerosol produced in the eruption earlier than the 5 days backward time span of the trajectories could be linked to the eruption, by investigating if the trajectories intersected these aerosol layers. Three samples collected during the first flight after the Sarychev eruption, taking place 12 days after the start of the eruption, had trajectories that clearly traversed aerosol layers.

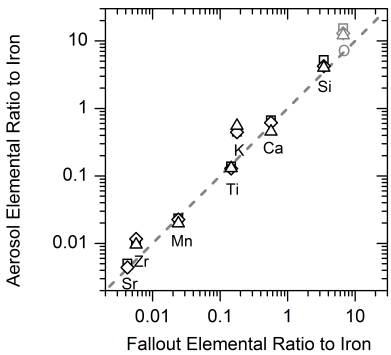

Fig. 3. Elemental ratio to iron in three aerosol samples (shown by different symbols) collected by the CARIBIC platform vs. fall out sample (SRG 5a, Sigmundsson et al., 2010). The dashed line indicates equal ratio. The oxygen content in the fallout sample is not measured and therefore indicated by grey symbols (see text for futher details).

Also samples collected during the next flight, 6 weeks after the eruption, could be connected to the aerosol produced in the eruption by this method, because the volcanic cloud could still be identified in the CALIPSO measurements.

3.2 Ash composition

The high concentrations of crustal elements in three of the samples collected during the Eyjafjallajökull eruption are important indications of volcanic origin. To further investigate this component of the aerosol it was compared to the composition of a fall-out sample of volcanic ash from the eruption site (Sigmundsson et al., 2010). The composition of erupted material can change over time and also with distance from the source due to fractionation and sedimentation (Carey and Sigurdsson, 1982). Thus it is not obvious that the fall out sample should be representative of the ash composition in the aerosol sample. Interestingly the composition for the three CARIBIC samples shows good agreement with the fallout sample for crustal elements (Fig. 3). Only the concentrations of potassium (K) and Zirconium (Zr) show some larger deviations. One explanation to the higher aerosol potassium (K) content in the CARIBIC samples could be fractioning in concentration between different sizes of ash particles in the samples analyzed, due to a larger surface area to mass ratio of small particles. Small ash particles remain in the plume longer than larger particles, and cool faster, which favors condensation of volatiles onto the smaller particles (Witham et al., 2005). Among the elements presented in Fig. 3, K happens to be the most volatile species found enriched in volcanic gases, due to degassing from the magma (Hinkley et al., 1994; Rubin, 1997). Also Zr was found in enhanced concentrations in deposits from a volcanic plume compared to the magma (Moune et al., 2005), indicating that also this element could have been abundant in the gas phase and condensed onto the ash particles.

The oxygen content (corrected for the amount of oxygen assumed bound to sulphurous aerosol in the form of sulphate) is also high compared to that of the fallout sample. The amount of oxygen in the fallout sample was not measured (indicated by grey symbols in Fig. 3), but are expressed as generalized oxygen proportions to the corresponding elements. It should however represent the approximate oxygen content, indicating that there is more oxygen in the aerosol samples. A likely explanation for the extra oxygen is that part of it is bound to the carbonaceous fraction of the aerosol (see Sect. 3.3).

The ash component of the Eyjafjallajökull aerosol is also similar to Earth's crustal composition (Rudnic and Fountain, 1995). Although analysis of rare elements such as the chalcophile metals (Bi, Cd, Cu, In, Pb and Tl), found in volcanic plumes from degassing of silicate melts (Hinkley et al., 1994), would be necessary to distinguish volcanic ash from this type of source, the high concentrations of crustal elements together with elevated sulphur concentrations in the aerosol samples are strong evidence of volcanic origin. On a final note, all of the elements, except manganese (Mn), in these three samples have the highest concentrations noted in the entire CARIBIC data set taken over a 10 years period. Therefore the composition of crustal elements in the Eyjafjallajökull aerosol samples (Fig. 3) is used here to define the ash component of volcanic aerosol.

The ash component of the sampled aerosol caused by the Kasatochi and Sarychev eruptions was identified by comparing it to the ash composition of the Eyjafjallajökull samples, as no fallout samples were available from these eruptions. Since this composition cannot be clearly distinguished from Earth's crustal composition, it was used as an indicator of volcanic ash in those samples with elevated S/O_3 levels, and for early collected samples, where trajectory analysis indicate volcanic origin. In addition the identified samples from the Kasatochi and Sarychev eruptions were collected in the summer to winter period when little influence of crustal particles in the LMS is seen (Martinsson et al., 2005). Only the three first samples following the Sarychev eruption were collected in spring when concentrations are usually elevated. For these samples however there is strong evidence of volcanic influence from the trajectory analysis and aerosol composition. Also meteoritic material can contribute to elements indicative of crustal material. Samples which are mainly influenced by meteorites can be identified by their Fe/Ni ratio (Kopp, 1997), which was used to exclude them from this study.

In Fig. 4 we include all samples having a crustal component classified to be of volcanic origin. These samples have a geometric residual sum of squares (RSS) in their elemental to iron ratios of less than two compared to the geometric mean

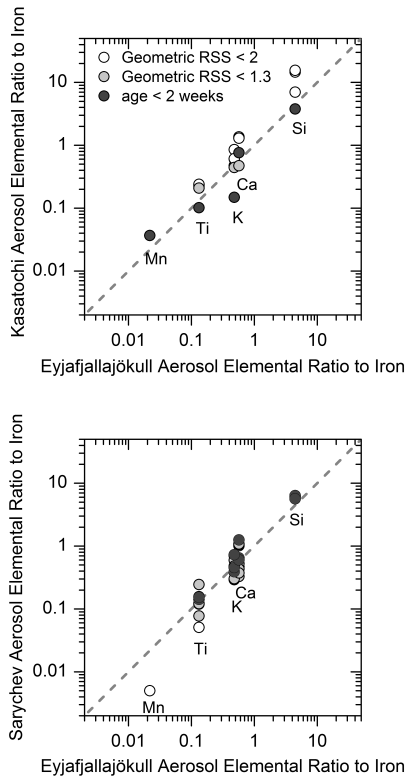

Fig. 4. Elemental ratio to iron in aerosol samples collected following eruptions of Sarychev and Kasatochi vs. geometric mean of volcanic aerosol collected in the volcanic cloud from Eyjafjallajökull. The dashed line indicates equal ratio. Samples with a Residual Sum of Squares (RSS) of less than two are included in the figures. Samples collected less than two weeks after the start of the eruptions are marked by dark circles.

of the Eyjafjallajökull aerosol samples (shown in Fig. 3). A minimum limit of at least three detected elements was applied to be able to examine the composition. Also the detection limit of undetected elements in relation to the iron content was taken into account. Samples were excluded if more than one of the elements K, Ca, Ti or Mn were missing even though they were expected to have had a concentration above the detection limit in relation to the content of Fe in the samples. One missing element was accepted to account for the risk of contamination due to mixing in the atmosphere and since it is likely that the composition of ash from different eruptions is not exactly the same. The ash composition depends on the magma type as well as on the absorption of volatiles onto the ash particles which is controlled by a number of factors such as eruption type, concentration of gases and particles and particle size (Witham et al., 2005). As can be seen from Fig. 4, Si is only represented in a few samples which is due to problems with interference with S as described in Sect. 2. Also Mn is represented only in a few samples since its concentrations in ash is low hence falling below the detection limit in samples of low ash content.

The composition of samples collected 8 days after the Kasatochi eruption and 12 days after the Sarychev eruption (indicated by dark circles in Fig. 4) show good agreement with the composition of the Eyjafjallajökull sample, except for lower concentrations of K in the sample from the Kasatochi eruption. Also samples collected one month or more after the eruptions are similar in their composition but ratios show more scatter. The larger deviations in composition in these samples indicate that the aerosols are more mixed and influenced by other sources. In addition changed emissions during the eruptions can cause variations in the composition of ash. The identified samples, classified as volcanic aerosol both by elevated S/O_3 ratios and composition of the crustal (ash) component, range in age between 8 to 128 days and 12 to 77 days from the start of the explosive phase of the Kasatochi and Sarychev eruptions, respectively. The length of these eruptions adds an uncertainty to these age estimates (1 and 5 days of explosive eruptions in the case of Kasatochi and Sarychev, respectively, BGVN, 2009; Waythomas et al., 2010).

3.3 Carbonaceous aerosol in volcanic clouds

The aerosol in volcanic clouds studied here contains a large fraction of carbonaceous aerosol. This has earlier been observed following the eruption of Kasatochi (Martinsson et al., 2009; Schmale et al., 2010) and in fresh volcanic clouds (Carn et al., 2011). A carbonaceous aerosol component has been observed in volcanic clouds from several volcanoes despite the fact that only for few volcanos lava can interact with carbonates in the crust prior to eruption. The volcanoes considered here do not belong to this category. This is corroborated by the measurements because the stoichiometric relations between carbon, oxygen, sulphur and ash elements in the sampled aerosol do not permit such an oxygen-rich form of carbon. Therefore explanations other than direct volcanic emissions need to be considered. One common source of carbonaceous material is combustion. Pyro-convection during forest fires can inject particles into the UT/LMS. However such events are not frequent and none one of the events identified in Guan et al. (2010) coincides with the eruptions studied here. Also no clearly elevated concentrations of K in excess of the ash concentration are seen in the samples, which would be expected from fires (Andreae et al., 1998). One

alternative explanation is the carbon content of the air that is entrained into the volcanic jet and lifted with the volcanic effluents. Mixing with air creates the buoyancy needed for the formation of a volcanic plume that can reach the stratosphere (Suzuki and Koyaguchi, 2010).

To obtain an estimate on the organic aerosol concentration in the region of the volcanoes studied, we consider the conditions in the boundary layer, where large numbers of observations are available. Boundary layer air contains high concentrations of carbonaceous aerosol from anthropogenic and from natural sources. Jimenez et al. (2009) report average urban organic aerosol concentrations up to 30 000 ng m^{-3} (Beijing, China) and, even at remote sites like Hyytiala, Finland the organic concentration exceeds one thousand ng m^{-3}. In a study focusing on the USA, urban regions average concentrations of several thousand ng m^{-3} were found and in rural areas the organic concentration was of the order 1000 ng m^{-3} (Hand et al., 2012). Interestingly, the Alaskan rural average organic aerosol concentration peaks in August, the month of the Kasatochi eruption, at approximately 3000 ng m^{-3}. Organic aerosol sources extend also to the oceans. Regional and seasonal variation in oceanic biological activity can be derived from SeaWiFS sensor on the OrbView2 satellite. The activity shows strong geographical and seasonal variations (Stramska, 2009). Measurements in Maze Head (Ireland) show organic aerosol concentration of several hundred ng m^{-3} connected with biologic activity in the ocean during spring to autumn (O'Dowd et al., 2004; Yoon et al., 2007). All three volcanoes studied here erupted in the biologically active part of the year. Modelling of the global distribution of yearly average organic aerosol with the ocean source included indicate high, to a large degree ocean-derived, organic aerosol concentration over the ocean surrounding island volcanoes Sarychev, Kasatochi and Eyjafjallajökull. For Sarychev a concentration of approximately 1000 ng m^{-3} was obtained, the same or somewhat lower for Kasatochi and a few hundred ng m^{-3} for Eyjafjallajökull (Spracklen et al., 2008). Additional organic material can be derived from gaseous precursors. Influence of volcanic halogen emissions on organic chemistry is important in the often OH poor volcanic clouds (von Glasow et al., 2009). In the volcanic cloud of Eyjafjalljökull chlorine radicals rapidly depleted organic trace gases to levels well below background concentrations (Baker et al., 2011). Such processes can further add particulate carbon to the volcanic cloud. The LMS particulate carbon concentration measured by CARIBIC outside directly injected volcanic clouds is approximately 100 ng m^{-3} at STP. In volcanic clouds the concentration typically is a few hundred ng m^{-3} STP, reaching more than one thousand ng m^{-3} STP in three observations of the volcanic cloud from Sarychev. The regional average particulate carbon concentrations in the boundary layer around the volcanoes studied here are thus comparable to the observations at high altitude (free troposphere, UT and LMS) in this study. Although sources in direct connection to the volcano, such as burning vegetation and sedimentary layers, also could contribute to carbonaceous aerosol, we hypothesize that organic material in entrained air constitutes a significant fraction of the particulate carbon observed in volcanic clouds.

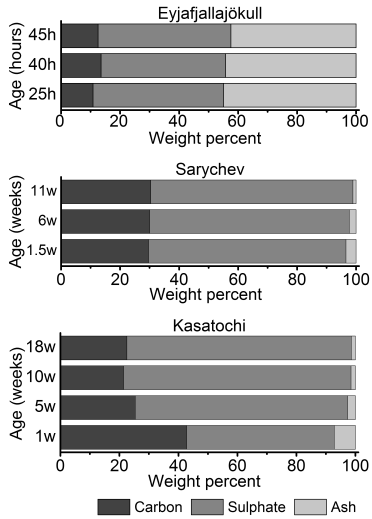

Fig. 5. Major components of aerosol samples collected following eruptions in Eyjafjallajökull, Sarychev and Kasatochi. Aerosol collected 1.5, 6 and 11 weeks after the eruption in Sarychev are shown as averages of 3, 6 and 2 samples respectivley. The composition of aerosol collected 18 weeks after the Kasatochi eruption are an average of 3 samples. The remaining aerosol compositions are each represented by only one sample. The carbonaceous fraction is averaged over all samples of the aerosol from Sarychev, see text for further details.

3.4 Major components

The main components of the samples classified as volcanic aerosol are carbon, sulphate and ash (Fig. 5). Samples influenced by Kasatochi and Sarychev are grouped with respect to age, where the compositions of aerosol collected at approximately the same time from the eruptions (i.e. from the same CARIBIC flight sequence) are presented as mean values. The carbonaceous component is presented as the mass of the measured carbon concentrations, since the stoichiometry of the carbon aerosol is unknown. The mass of sulphate (SO_4) was calculated by adding the amount of oxygen corresponding to the measured mass of sulphur, assuming that all sulphur is in the form of SO_4. In a similar manner the mass of the ash components in the Eyjafjallajökull samples were obtained by adding the mass of oxygen according to the fallout

sample presented in the table by Sigmundsson et al. (2010). Elements found in ash that could not be detected, primarily sodium (Na), magnesium (Mg), aluminum (Al) and phosphorus (P), were calculated according to the composition of the fallout sample using the relation to the iron content. The entire ash components of samples influenced by the Sarychev and Kasatochi eruptions were estimated based on their Fe content since many of the elements were below their detection limits. In these samples the mass of Fe, S and C was corrected for stratospheric background concentrations calculated as averages of samples with concentrations below the 95 percentile collected during the period from 1999 to the eruption of Kasatochi in August 2008. For S and C this correction was done with respect to the O_3 mixing ratios measured during the sampling time since they show a correlation with O_3. For Fe, the background correction was done with respect to season, divided into December–February, June–August and September–November (no samples were obtained in the period March–May). Since the samples from the Eyjafjallajökull eruption originate in lower altitudes than the CARIBIC platform usually measures, no such correction was made for them. Therefore C and S components should be considered to represent maximum estimates. However the concentrations were very high so the background influence most likely was small.

Figure 5 reveals that the samples collected following Eyjafjallajökull's eruption show little variation in their compositions, they mainly consist of ash and sulphate in about equal amounts. In contrast samples influenced by the eruptions of Kasatochi and Sarychev to a large extent consist of sulphate and carbon, while the ash component is well below 10 %. Even though the carbon and sulphate components comprise a smaller part of the mass in the Eyjafjallajökull samples compared to them influenced by the other two volcanoes, the respective concentrations are of similar magnitude as in the Kasatochi and Sarychev samples, while the ash component is approximately a factor of 10 higher in the Eyjafjallajökull samples.

The aerosol from Sarychev shows a strong dependence of the carbon-to-sulphur ratio on latitude, with increasing C/S ratio with increasing latitude, while the iron-to-sulphur ratio shows no such dependence (not shown). Possibly changing properties of the eruptions that persisted for several days and/or differences in carbonaceous aerosol precursor gases combined with transport patterns from the source could explain this latitudinal dependence. The time evolution of C can thus not be given. Instead the average C/S over the volcanically influenced samples taken from June to October 2009 was used to obtain the C component for Sarychev in Fig. 5. A decreasing fraction of ash with time is observed from Sarychev. The aerosol from the Kasatochi eruption has a simpler C-to-S relation. The sulphurous fraction shows an increase with time, whereas the ash and carbonaceous fractions decline.

3.5 Effects of sedimentation and coagulation on the composition evolution

Figure 5 shows that there is a change in the relations of the components of the Kasatochi and Sarychev volcanic aerosol with its age. The relative increase of SO_4 is likely caused by the transformation of SO_2 into SO_4 particles. Also higher rates of removal of ash (and C) might contribute to the observed pattern. Since all samples older than two weeks were taken in the stratosphere or the tropopause region, where little wet scavenging occurs, the solubility of the particles had no or only a small influence on the rate of deposition. The impact of different sedimentation rates of ash and SO_4 particles was investigated by estimating their settling velocity. In the computations the particle diameters that carry most of the mass according to the particle mass distributions were applied. For the sulphate particles, spherical droplets of sulphuric acid solution with a diameter of 0.6 µm (Martinsson et al., 2005) (corresponding to 0.76 µm aerodynamic diameter) and a density of 1600 kg m^{-3} (Yue et al., 1994) were used in the calculations. The diameter of the sulphate aerosol estimated by Martinsson et al. (2005) was obtained from the effective radius of stratospheric aerosol from lidar observations (Bauman et al., 2003) during a period with low volcanic activity. Thus the radius is underestimated for volcanic aerosol which usually exhibit larger diameters (Bauman et al., 2003; Deshler et al., 2003). Ash particles usually have substantially larger diameters (Schumann et al., 2011). The 2 µm aerodynamic diameter upper size limit of the aerosol sampler was thus used to estimate the upper limit in settling velocity of the ash. The thickness of the volcanic aerosol layers from the Sarychev and Kasatochi eruptions, through which the volcanic aerosol has to settle, was estimated by locating the altitude of volcanic aerosol during the first week after the eruptions using CALIPSO lidar measurements. After some time the identified volcanic aerosol layers are assumed to have been horizontally mixed and contributed to a more or less homogeneous aerosol layer. Therefore a cumulative altitude distribution of the volcanically influenced air from 10 km altitude and upwards was calculated, by summing all events when volcanic aerosol was observed at a certain altitude, see Fig. 6. According to the above method about 85 % of the identified aerosol following the Sarychev eruption was injected to a height between 10 and 15 km. Therefore a 5 km thick layer was assumed to have been produced. The aerosol layer formed by the Kasatochi eruption was less homogenous with 75 % of the aerosol located between 10–13 km and the remaining aerosol extending up to ∼20 km. During the 2 months we followed these volcanic clouds, the 2 µm ash particles fall a distance of about 10 % of the thickness of the volcanic aerosol layer produced by Sarychev and about 17 % of the lowest 3 km of the volcanic aerosol produced by Kasatochi. Since the aerosol samples were collected in the lower part of these layers, at 10–11.3 km, there should thus still be large amounts of 2 µm ash particles, originating in the

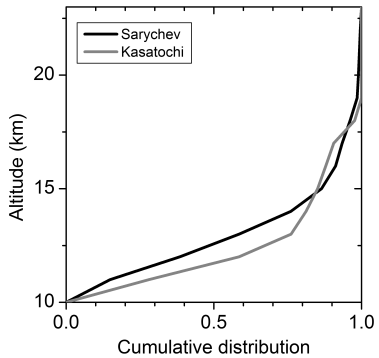

Fig. 6. Cumulative altitude distributions of volcanic injections above 10 km the first week after the Sarychev and Kasatochi eruptions. The distributions was deduced from the number of observations of volcanic aerosol layers in CALIPSO lidar measurements as a function of altitude, see the text for further details.

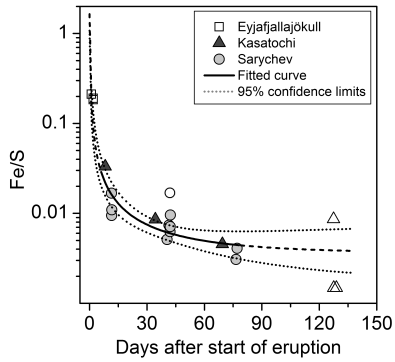

Fig. 7. Mass ratio of iron to sulphur in aerosol samples influenced by three volcanoes (marked by different symbols) vs. time since the start of the eruptions. The line shows a fit to the Fe/S ratio for the samples influenced by the Sarychev and Kasatochi eruptions. Samples shown with open symbols have been excluded from the fit.

upper part of the volcanic aerosol layers. Bearing in mind that the sulphate sedimentation was underestimated and that of ash was overestimated, this simple estimation suggests that the difference in deposition velocity between ash and sulphate particles only has minor importance for the relation between the measured ash and sulphate concentrations on the timescale considered here.

In addition, coagulation of particles needs to be considered as it can enhance the sedimentation velocity and can grow particles to diameters outside the collection range of the sampler. However the paticle concentrations in samples collected more than one week after the Kasatochi and Sarychev eruptions are low, $\sim$22 ng m^{-3} ash and $\sim$156 ng m^{-3} SO_4 in the first sample collected following the Kasatochi eruption. Calculations based on thermal coagulation (Hinds, 1999), points to that the effects of particle coagulation is very small in the concentrations encountered in these volcanic clouds. In order to simplify the estimates of coagulation, the case of monodispersed ash and sulphate particles of the same properties as described for the sedimentation calculations were used. The resulting change in the number concentration both from coagulation of ash and of sulphate particles is less than 1 % during the 2 months considered. Coagulation thus is estimated to be of minor importance because the aerosol concentrations in the observed clouds are too low for that process to be efficient.

3.6 Sulphur dioxide conversion rate in volcanic clouds

To further evaluate the evolution of the volcanic aerosol the sulphate and ash components were studied more in detail. In Fig. 7 the ratio of Fe/S shows the relation between the ash and sulphate components as a function of time after the eruptions. As the difference in sedimentation velocity of ash and sulphate particles in the 0.08–2 µm size range were estimated to be of small importance, the decreaseing trend of Fe/S is likely explained by the conversion rate of SO_2 into sulphate aerosol. The residence time of SO_2 can thus be estimated from the decrease in the Fe/S ratios. From the reaction of SO_2 with OH, which mainly controls the conversion into sulphate aerosol (Weisenstein et al., 1997), an exponential decay rate of the number concentrations of SO_2 can be derived (Seinfeld and Pandis, 2006);

$$C^n_{SO_2}(t) = C^n_{SO_2}(0) \cdot e^{-kt}, \quad (1)$$

where k is the loss rate constant. Since the depletion rate $C^n_{SO_2}(t)/dt$ of SO_2 molecules equals the production rate of SO_4, the mass concentration ratio of Fe and S can be expressed as;

$$\frac{C^n_{Fe}}{C^n_{SO_4}(t)} \propto \frac{C^m_{Fe}}{C^m_S(t)} = \frac{A}{1-e^{-kt}}, \quad (2)$$

where C^n and C^m denotes number respective mass concentrations. The constant A is the mass concentration ratio of Fe from ash and total S from SO_2 that is eventually converted to sulphate. Since the composition of volcanic aerosol depends on the eruption characteristics (magma composition, explosivity, temperature, gas release etc., Mather et al., 2003) aerosol from different eruptive events cannot be expected to have similar Fe/S ratios. Still most samples collected following the Sarychev and Kasatochi eruptions show large similarities in their Fe/S ratio with respect to age. Thus Eq. (2) was fitted to the Fe/S ratio in Sarychev and Kasatochi

samples, assuming similar emission ratio of Fe/S in the eruptions. The logarithm of the Fe/S ratios was used in the fitting to avoid over representing the large ratios appearing the first two weeks after the eruptions. Changed emissions during the eruptions as well as atmospheric conditions that affect mixing and transport also influence the composition of the aerosol. As stated earlier, the ash component was rather simple to recognize within two weeks after the eruption, and thereafter it was more influenced by other sources. Such influences could explain some of the deviations from the decreasing trend in Fig. 7. Also deviations from the average background concentrations used in the corrections have to be considered. Samples taken more than 100 days after the eruptions show large deviations from the general tendency, probably as the result of dilution of the volcanic cloud and mixing, and are excluded from the fit. One younger Sarychev sample shows large deviation compared to other samples collected at approximately the same time, and has therefore also been excluded.

Samples from the Eyjafjallajökull volcanic cloud was not included in this fit. As was seen in Fig. 5, the relative concentration of sulphate is low in samples from the Eyjafjallajökull eruption compared to the samples following Sarychev and Kasatochi, likely due to the large emissions of fine grained ash in the Eyjafjallajökull eruption (BGVN, 2010). In addition these samples were collected close to the eruption which implicates short time for conversion of SO_2 into sulphate aerosol. However the residence time of SO_2 in the troposphere where these samples were collected are considerably shorter than in the stratosphere, only hours to few days (McGonigle et al., 2004; Carn et al., 2011), leading to rapid conversion into sulphate aerosol. These samples should therefore not follow the same decay as those collected at higher altitudes. Also no background correction was made for the Eyjafjallajökull samples as mentioned earlier. An additional important aspect is initial processes in the volcanic cloud that lead to growth by aggregation and rapid sedimentation of fine ash particles (Rose et al., 2001). Such processes could be of importance during sampling in the Eyjafjallajökull volcanic clouds because they were only 1–2 days old.

The residence time of SO_2 (1/k) in the tropopause region and LMS after the eruptions of Kasatochi and Sarychev was from the fitted curve estimated to be 45 ± 22 days (mean $\pm$ standard error). The value of A, representing the ratio of total Fe and S was estimated to 0.0036 corresponding to a final ash/SO_4 mass ratio of approximately 0.016 for particles in the 0.08–2 µm size range considered here.

4 Discussion

Previous estimates of residence time of SO_2 for the volcanic cloud of Kasatochi span from 9 days (Krotkov et al., 2010), to 18 days (Karagulian et al., 2010) and up to 62 days (Jurkat et al., 2010). The residence time of SO_2 following the Sarychev eruption has been estimated to 11 days (Haywood et al., 2010). Thus there is a large spread in estimated residence times. Estimations of the conversion rate of SO_2 following the Pinatubo eruption are less dispersed; 35 days (Bluth and Doiron, 1992), 33 days (Read et al., 1993) and 25 ± 5 as well as 23 ± 5 days (Guo et al., 2004). Except in the work by Guo et al. (2004), uncertainty of the estimated residence time has not been given. Thus it is difficult to compare the validity of our estimate to others. While earlier estimates obtained for the Pinatubo eruption (satellite based) and by aircraft observations for Kasatochi (Jurkat et al., 2010) lie within our uncertainty limits, the results based on satellite observations of the Kasatochi and Sarychev volcanic clouds are considerably lower. The spread in estimated residence time, both between similar and dissimilar methods, underscore that it is valuable to perform calculations of SO_2 residence time in different volcanic clouds and by different methods, and not only rely on the more consistent results from the Pinatubo eruption.

For the Kasatochi and Sarychev eruptions, it seems like the aircraft observations of volcanic clouds (Jurkat et al., 2010; this study) result in longer residence times than the satellite based measurements (see above). Haywood et al. (2010) argue that the detection limit of the IASI satellite measurements could lead to somewhat underestimated residence time (up to 50 %). Measurements following the Kasatochi eruption based on particle detection by OSIRIS on board the satellite Odin corresponded to a SO_2 residence time of approximately 30 days (Bourassa et al., 2010). This points to that the difference between the Kasatochi measurements is connected to whether the measurements are based on detection of SO_2 or particles rather than satellite or in situ. Heard et al. (2012) modelled SO_2 and aerosol optical depth (AOD). Their results were compared with satellite observations from IASI and OSIRIS for the eruption of Sarychev. In their model SO_2 remained longer and the particle concentration rose faster than in the observations. The detection limit of the satellite SO_2 retrieval was suggested as a possible cause for the faster decrease of SO_2 in observed data, while for the AOD the inadequately modelling of nucleation were proposed as the main reason for the earlier peak of the AOD in the model as particle reached the optically active accumulation mode to fast.

Aircraft measurements suffer from the difficulties to follow a volcanic cloud as it ages, and the sampling of volcanically influenced air at one position cannot be guaranteed to be representative for the whole volcanic cloud. The methodology used in this study demands that the ratio of ash and SO_2 injected into the UT/LMS by the volcanoes were constant and that influence from coagulation has declined before the first measurement used in the estimate of the residence time. These assumptions are likely simplifications, where the former causes scatter in the data whereas coagulation would tend to cause a shorter estimate of residence time than the actual one. One important difference between

the aircraft and satellite observations is that while the in-situ measurements are constrained to a well-defined altitude, the remote sensing SO_2 instruments observes the whole atmospheric column. The altitude of the Kasatochi plume is estimated to 12.5 ± 4 km by Karagulian et al. (2010) and 10–12 km by Krotkov et al. (2010). Mixing with tropospheric air, where residence times are shorter, cannot be excluded and would have affected the satellite based estimates. Krotkov et al. (2010) suggest the rather low altitude of the Kasatochi plume and the dynamic UT/LMS in the extra tropics as an explanation for why they derive a shorter SO_2 residence time (9 days) compared to the one observed after the Pinatubo eruption, that injected material well into the stratosphere.

Finally differences in the actual residence times following the eruptions of Sarychev and Kasatochi compared to that following Pinatubo may well be caused by differences in the abundance of OH. The latitudinal dependence could thereby be of significance as Pinatubo is located in the tropics (15.13° N, 120.35° E) where OH concentrations are higher than at the mid-latitudes (Gross and Khalil, 2000), where the Kasatochi and Sarychev volcanoes are located, leading to longer residence times. Since the eruptions occurred in June (Pinatubo and Sarychev) and August (Kasatochi), there should be negligible differences in the OH concentration due to seasonal variation in the UV flux. An important factor is likely to be the altitude for which these estimates were made, since OH concentrations increase strongly above ∼20 km (Gross and Khalil, 2000). The results obtined in this study and by Jurkat et al. (2010) are based on aircraft measurements at altitudes of 7–12 km, which is just below the center of the volcanic cloud as observed by sattelites. The volcanic cloud that was observed by satellite following the Pinatubo eruption was injected well into the stratosphere to altitudes of ∼25 km (Guo et al., 2004). Thus the longer residence times meassured by aircraft might be typical for the altitude and latitude considered.

5 Conclusions

Volcanic aerosol have been collected in the tropopause region and lowermost stratosphere following major eruptions of the Kasatochi and Sarychev volcanoes, and in the troposphere in the volcanic cloud from the Eyjafjallajökull eruption in 2010. The main components of the volcanic aerosol were found to be sulphate, ash and carbonaceous material, where the source of the latter is proposed to be low-altitude tropospheric air that is entrained into the volcanic jet and plume. In samples collected in the volcanic cloud from Eyjafjallajökull ash and sulphate contributed approximately equal amounts to the total aerosol mass (∼45 %). In samples collected following Sarychev and Kasatochi ash was a minor part of the aerosol (1–7 %) while sulphate (50–77 %) and carbon (21–43 %) were dominating. These fractions changed with the age of the aerosol. In this study we could follow the evolution of volcanic aerosol during more than twice the residence time of SO_2 in a volcanic cloud. The first samples collected 1 and 1.5 weeks after the eruption of Kasatochi and Sarychev consisted of 14 % and 5 % ash relative to the mass of sulphate, respectively. After 10 and 11 weeks the ash component was still identifiable, but had decreased to about 2 % relative to the sulphate mass for both eruptions. The ash/sulphate ratio of aerosol collected following the Kasatochi and Sarychev eruptions showed a decreasing trend. From this decay the residence time of SO_2 in the tropopause region and lowermost stratosphere was estimated to be 45 ± 22 days. Previous estimates of SO_2 residence time following the Kasatochi and Sarychev eruptions by different methods based on SO_2 or sulphate detection as well as in situ or remote sensing from satellites, are of the same magnitude although distributed over a rather wide range from 9 to 62 days. In contrast more consistent residence times was observed from satellite measurements following the large eruption of Pinatubo in 1991. This emphasizes that it is more difficult to measure the conversion rates of SO_2 after intermediate eruptions. The difficulties could be connected with variability in composition, detection problem and/or the altitude distribution of SO_2 after the eruptions.

Acknowledgements. We thank all members of the CARIBIC team, especially C. Koeppel, D. S. Scharffe and S. Weber. The collaboration with Lufthansa and Lufthansa Technik is gratefully acknowledged. Aerosol measurements from CALIPSO were produced by NASA Langley Research Center. Financial support from the Swedish Research Council and the Swedish Research Council for Environments, Agricultural Sciences and Spatial Planning under grants 621-2007-4639 and 214-2009-613 is gratefully acknowledged.

Edited by: W. Birmili

References

Ammann, C. M., Meehl, G. A., Washington, W. M., and Zender, C. S.: A monthly and latitudinally varying volcanic forcing dataset in simulations of 20th century climate, Geophys. Res. Lett., 30, 1657–1661, doi:10.1029/2003GL016875, 2003.

Andreae, M. O., Wienhold, F. G., Zenker, T., Andreae, T. W., Annegarn, H., Beer, J., Cachier, H., le Canut, P., Elbert, W., Maenhaut, W., and Salma, I.: Airborne studies of aerosol emissions from savanna fires in southern Africa: 2. Aerosol chemical composition, J. Geophys Res., 103, 32119–32128, doi:10.1029/98JD02280, 1998.

Baker, A. K., Rauthe-Schöch, A., Schuck, T. J., Brenninkmeijer, C. A. M., van Velthoven, P. F. J., Wisher, A., and Oram, D. E.: Investigation of chlorine radical chemistry in the Eyjafjallajökull volcanic plume using observed depletions in non-methane hydrocarbons, Geophys. Res. Lett., 38, L13801, doi:10.1029/2011GL047571, 2011.

Bauman, J. J., Russell, P. B., Geller, M. A., and Patrick, H.: A stratospheric aerosol climatology from SAGE II and CLAES measurements: 2. Results and comparisons, 1984–1999, J. Geophys. Res., 108, 4383, doi:10.1029/2002jd002993, 2003.

BGVN, B. o. t. G. V. N.: Widespread plumes from large 11–16 June 2009 eruption34:06, 2009.

BGVN, B. o. t. G. V. N.: Large explosions from the summit crater; ash plumes close airspace in Europe, 35:04, 2010.

Bluth, G. J. S. and Doiron, S. D.: Global tracking of the SO2 clouds from the june, 1991 mount pinatubo eruptions, Geophys. Res. Lett., 19, 51–154, 1992.

Bourassa, A. E., Degenstein, D. A., Elash, B. J., and Llewellyn, E. J.: Evolution of the stratospheric aerosol enhancement following the eruptions of Okmok and Kasatochi: Odin-OSIRIS measurements, J. Geophys. Res., 115, D00L03, doi:10.1029/2009jd013274, 2010.

Brenninkmeijer, C. A. M., Crutzen, P., Boumard, F., Dauer, T., Dix, B., Ebinghaus, R., Filippi, D., Fischer, H., Franke, H., Friess, U., Heintzenberg, J., Helleis, F., Hermann, M., Kock, H. H., Koeppel, C., Lelieveld, J., Leuenberger, M., Martinsson, B. G., Miemczyk, S., Moret, H. P., Nguyen, H. N., Nyfeler, P., Oram, D., O'Sullivan, D., Penkett, S., Platt, U., Pupek, M., Ramonet, M., Randa, B., Reichelt, M., Rhee, T. S., Rohwer, J., Rosenfeld, K., Scharffe, D., Schlager, H., Schumann, U., Slemr, F., Sprung, D., Stock, P., Thaler, R., Valentino, F., van Velthoven, P., Waibel, A., Wandel, A., Waschitschek, K., Wiedensohler, A., Xueref-Remy, I., Zahn, A., Zech, U., and Ziereis, H.: Civil Aircraft for the regular investigation of the atmosphere based on an instrumented container: The new CARIBIC system, Atmos. Chem. Phys, 7, 4953–4976, doi:10.5194/acp-7-4953-2007, 2007.

Carey, S. N. and Sigurdsson, H.: Influence of particle aggregation on deposition of distal tephra from the may 18, 1980, eruption of Mount St. Helens volcano, J. Geophys. Res., 87, 7061–7072, 1982.

Carn, S. A., Krueger, A. J., Krotkov, N. A., Yang, K., and Evans, K.: Tracking volcanic sulfur dioxide clouds for aviation hazard mitigation, Nat. Hazards, 51, 325–343, doi:10.1007/s11069-008-9228-4, 2009.

Carn, S. A., Froyd, K. D., Anderson, B. E., Wennberg, P., Crounse, J., Spencer, K., Dibb, J. E., Krotkov, N. A., Browell, E. V., Hair, J. W., Diskin, G., Sachse, G., and Vay, S. A.: In situ measurements of tropospheric volcanic plumes in Ecuador and Colombia during TC4, J. Geophys. Res., 116, D00J24, doi:10.1029/2010jd014718, 2011.

Casadevall, T. J.: The 1989–1990 eruption of Redoubt Volcano, Alaska: impacts on aircraft operations, J. Volcanol. Geoth. Res., 62, 301–316, doi:10.1016/0377-0273(94)90038-8, 1994.

Chin, M. and Davis, D. D.: A reanalysis of carbonyl sulfide as a source of stratospheric background sulfur aerosol, J Geophys. Res., 100, 8993–9005, 1995.

Crutzen, P. J.: The possible importance of CSO for the sulfate layer of the stratosphere, Geophys. Res. Lett., 3, 73–76, doi:10.1029/GL003i002p00073, 1976.

Cziczo, D. J., Thomson, D. S., and Murphy, D. M.: Ablation, Flux, and Atmospheric Implications of Meteors Inferred from Stratospheric Aerosol, Science, 291, 1772–1775, 2001.

Deshler, T.: A review of global stratospheric aerosol: Measurements, importance, life cycle, and local stratospheric aerosol, Atmos. Res., 90, 223–232, doi:10.1016/j.atmosres.2008.03.016, 2008.

Deshler, T., Hervig, M., Hofmann, D., Rosen, J., and Liley, J.: Thirty years of in situ stratospheric aerosol size distribution measurements from Laramie, Wyoming (41° N), using balloon-borne instruments, J. Geophys. Res., 108, 4167, doi:10.1029/2002JD002514, 2003.

Dix, B., Brenninkmeijer, C. A. M., Frieß, U., Wagner, T., and Platt, U.: Airborne multi-axis DOAS measurements of atmospheric trace gases on CARIBIC long-distance flights, Atmos. Meas. Tech., 2, 639–652, doi:10.5194/amt-2-639-2009, 2009.

Ferry, G. V., Pueschel, R. F., Strawa, A. W., Kondo, Y., Howard, S. D., Verma, S., Mahoney, M. J., Bui, T. P., Hannan, J. R., and Fuelberg, H. E.: Effects of aircraft on aerosol abundance in the upper troposphere, Geophys. Res. Lett., 26, 2399–2402, doi:10.1029/1999GL900445, 1999.

Fromm, M., Bevilacqua, R., Stocks, B., and Servranckx, R.: New Directions: Eruptive Transport to the Stratosphere: Add Fire-Convection to Volcanoes, Atmos. Environ., 38, 163–165, doi:10.1016/j.atmosenv.2003.10.001, 2004.

Fromm, M., Shettle, E. P., Fricke, K. H., Ritter, C., Trickl, T., Giehl, H., Gerding, M., Barnes, J. E., Neill, M. O., Massie, S. T., Blum, U., McDermid, I. S., Leblanc, T., and Deshler, T.: Stratospheric impact of the Chisholm pyrocumulonimbus eruption: 2. Vertical profile perspective, J. Geophys. Res., 113, D08203, doi:10.1029/2007jd009147, 2008.

Gross, G. W. and Khalil, M. A. K.: OH concentrations from a general circulation model coupled with a tropospheric chemistry model, Chemosphere – Global Change Science, 2, 191–206, doi:10.1016/s1465-9972(99)00054-9, 2000.

Guan, H., Esswein, R., Lopez, J., Bergstrom, R., Warnock, A., Follette-Cook, M., Fromm, M., and Iraci, L. T.: A multi-decadal history of biomass burning plume heights identified using aerosol index measurements, Atm. Chem. Phys., 10, 6461–6469, doi:10.5194/acp-10-6461-2010, 2010.

Guo, S., Bluth, G., J. S., Rose, W. I., Watson, I. M., and Prata, A. J.: Re-evaluation of SO2 release of the 15 June 1991 Pinatubo eruption using ultraviolet and infrared satellite sensors, Geochem. Geophy. Geosy., 5, Q04001, doi:10.1029/2003GC000654, 2004.

Hand, J. L., Schichtel, B. A., Pitchford, M., Malm, W. C., and Frank, N. H.: Seasonal composition of remote and urban fine particulate matter in the United States, J. Geophys. Res., 117, D05209, doi:10.1029/2011JD017122, 2012.

Haywood, J. M., Clerbaux, C., Coheur, P., Degenstein, D., Braesicke, P., Jones, A., Clarisse, L., Bourassa, A., Barnes, J., Telford, P., Bellouin, N., Boucher, O., and Agnew, P.: Observations of the eruption of the Sarychev volcano and simulations using the HadGEM2 climate model, J. Geophys. Res., 115, D21212, doi:10.1029/2010JD014447, 2010.

Heard, I. P. C., Manning, A. J., Haywood, J. M., Witham, C., Redington, A., Jones, A., Clarisse, L., and Bourassa, A.: A comparison of atmospheric dispersion model predictions with observations of SO_2 and sulphate aerosol from volcanic eruptions, J. Geophys. Res., 117, D00U22, doi:10.1029/2011JD016791, 2012.

Heiken, G. and Wohletz, K.: Volcanic ash, University of California Press, Berkeley, 1985.

Heue, K. P., Brenninkmeijer, C. A. M., Baker, A. K., Rauthe-Schoch, A., Walter, D., Wagner, T., Hormann, C., Sihler, H., Dix, B., Friess, U., Platt, U., Martinsson, B. G., van Velthoven, P.

F. J., Zahn, A., and Ebinghaus, R.: SO2 and BrO observation in the plume of the Eyjafjallajokull volcano 2010: CARIBIC and GOME-2 retrievals, Atmos. Chem. Phys, 11, 2973-2989, doi:10.5194/acp-11-2973-2011, 2011.

Hinds, W. C.: Aerosol technology: properties, behavior, and measurement of airborne particles, Book, John Wiley & Sons, New York, USA, 1999.

Hinkley, T. K., Le Cloarec, M. F., and Lambert, G.: Fractionation of families of major, minor, and trace metals across the melt-vapor interface in volcanic exhalations, Geochim. Cosmochim. Ac., 58, 3255–3263, doi:10.1016/0016-7037(94)90053-1, 1994.

Hofmann, D., Barnes, J., O'Neill, M., Trudeau, M., and Neely, R.: Increase in background stratospheric aerosol observed with lidar at Mauna Loa Observatory and Boulder, Colorado, Geophys. Res. Lett., 36, L15808, doi:10.1029/2009GL039008, 2009.

IPCC: Climate Change 2007: The Physical Science Basis. Contribution of Working Group I to the Fourth Assessment Report of the Intergovernmental Panel on Climate Change, edited by: Solomon, S., Qin, D., Manning, M., Chen, Z., Marquis, M., Averyt, K. B., Tignor, M., and Miller, H. L., Cambridge University Press, Cambridge, United Kingdom and New York, NY, USA, 2007.

Jimenez, J. L., Canagaratna, M. R., Donahue, N. M., Prevot, A. S., Zhang, Q., Kroll, J. H., DeCarlo, P. F., Allan, J. D., Coe, H., Ng, N. L., Aiken, A. C., Docherty, K. S., Ulbrich, I. M., Grieshop, A. P., Robinson, A. L., Duplissy, J., Smith, J. D., Wilson, K. R., Lanz, V. A., Hueglin, C., Sun, Y. L., Tian, J., Laaksonen, A., Raatikainen, T., Rautiainen, J., Vaattovaara, P., Ehn, M., Kulmala, M., Tomlinson, J. M., Collins, D. R., Cubison, M. J., Dunlea, E. J., Huffman, J. A., Onasch, T. B., Alfarra, M. R., Williams, P. I., Bower, K., Kondo, Y., Schneider, J., Drewnick, F., Borrmann, S., Weimer, S., Demerjian, K., Salcedo, D., Cottrell, L., Griffin, R., Takami, A., Miyoshi, T., Hatakeyama, S., Shimono, A., Sun, J. Y., Zhang, Y. M., Dzepina, K., Kimmel, J. R., Sueper, D., Jayne, J. T., Herndon, S. C., Trimborn, A. M., Williams, L. R., Wood, E. C., Middlebrook, A. M., Kolb, C. E., Baltensperger, U., and Worsnop, D. R.: Evolution of organic aerosols in the atmosphere, Science, 326, 1525–1529, doi:10.1126/science.1180353, 2009.

Johansson, S. A. E. and Campbell, J. L.: PIXE: A novel technique for elemental analysis, John Wiley & Sons, New York, 1988.

Junge, C. E., Chagnon, C. W., and Manson, J. E.: A Worldwide Stratospheric Aerosol Layer, Science, 133, 1478–1479, doi:10.1126/science.133.3463.1478-a, 1961.

Jurkat, T., Voigt, C., Arnold, F., Schlager, H., Aufmhoff, H., Schmale, J., Schneider, J., Lichtenstern, M., and Dornbrack, A.: Airborne stratospheric ITCIMS measurements of SO_2, HCl, and HNO_3 in the aged plume of volcano Kasatochi, J. Geophys. Res., 115, D00L17, doi:10.1029/2010JD013890, 2010.

Jäger, H.: Long-term record of lidar observations of the stratospheric aerosol layer at Garmisch-Partenkirchen, J. Geophys. Res., 110, D08106, doi:10.1029/2004jd005506, 2005.

Karagulian, F., Clarisse, L., Clerbaux, C., Prata, A. J., Hurtmans, D., and Coheur, P. F.: Detection of volcanic SO2, ash, and H2SO4 using the Infrared Atmospheric Sounding Interferometer (IASI), J. Geophys. Res., 115, D00L02, doi:10.1029/2009JD012786, 2010.

Kjellström, E., Feichter, J., Sausenc, R., and Hein, R.: The contribution of aircraft emissions to the atmospheric sulfur budget, Atmos. Environ., 33, 3455–3465, 1999.

Kopp, E.: On the abundance of metal ions in the lower ionosphere, J. Geophys. Res., 102, 9667–9674, doi:10.1029/97ja00384, 1997.

Krotkov, N. A., Schoeberl, M. R., Morris, G. A., Carn, S., and Yang, K.: Dispersion and lifetime of the SO_2 cloud from the August 2008 Kasatochi eruption, J. Geophys. Res., 115, D00L20, doi:10.1029/2010JD013984, 2010.

Köppe, M., Hermann, M., Brenninkmeijer, C. A. M., Heintzenberg, J., Schlager, H., Schuck, T., Slemr, F., Sprung, D., Velthoven, P. F. J. v., Wiedensohler, A., Zahn, A., and Ziereis, H.: Origin of aerosol particles in the mid-latitude and subtropical upper troposphere and lowermost stratosphere from cluster analysis of CARIBIC data, Atmos. Chem. Phys., 9, 8413–8430, doi:10.5194/acp-9-8413-2009, 2009.

Lopez, T. M., Carn, S. A., Webley, P., and Pfeffer, M. A.: Evaluation of satellite derived sulfur dioxide measurements for volcano monitoring during the 2009 Redoubt eruption American Geophysical Union, Fall Meeting 2009, abstract #V51F-03, 2009.

Martinsson, B. G., Nguyen, H. N., Brenninkmeijer, C. A. M., Zahn, A., Heintzenberg, J., Hermann, M., and Velthoven, P. F. J. v.: Characteristics and origin of lowermost stratospheric aerosol at northern midlatitudes under volcanically quiescent conditions based on CARIBIC observations, J. Geophys. Res., 110, D12201, doi:10.1029/2004JD005644, 2005.

Martinsson, B. G., Brenninkmeijer, C. A. M., Carn, S. A., Hermann, M., Heue, K. P., Velthoven, P. F. J. v., and Zahn, A.: Influence of the 2008 Kasatochi volcanic eruption on sulfurous and carbonaceous aerosol constituents in the lower stratosphere, Geophys. Res. Lett., 36, L12813, doi:10.1029/2009gl038735, 2009.

Mather, T. A., Pyle, D. M., and Oppenheimer, C.: Tropospheric Volcanic Aerosol, Geophys. Monogr., 139, 189–212, doi:10.1029/139GM12, 2003.

McCormick, M. P., Thomason, L. W., and Trepte, C. R.: Atmospheric effects of the Mt Pinatubo eruption, Nature, 373, 399–404, doi:10.1038/373399a0, 1995.

McGonigle, A. J. S., Delmelle, P., Oppenheimer, C., Tsanev, V. I., Delfosse, T., Williams-Jones, G., Horton, K., and Mather, T. A.: SO_2 depletion in tropospheric volcanic plumes, Geophys. Res. Lett., 31, L13201, doi:10.1029/2004gl019990, 2004.

Moune, S., Gauthier, P.-J., Gislason, S. R., and Sigmarsson, O.: Trace element degassing and enrichment in the eruptive plume of the 2000 eruption of Hekla volcano, Iceland, Geochim. Cosmochim. Ac., 70, 461–479, doi:10.1016/j.gca.2005.09.011, 2005.

Murphy, D. M., Thomson, D. S., and Mahoney, M. J.: In situ measurements of organics, meteoritic matierial, mercury, and other elements in aerosols at 5 to 19 kilometers, Science, 282, 1664–1669, 1998.

Murphy, D. M., Cziczo, D. J., Hudson, P. K., and Thomson, D. S.: Carbonaceous material in aerosol particles in the lower stratosphere and tropopause region, J. Geophys. Res., 112, D04203, doi:10.1029/2006JD007297, 2007.

Myhre, G., Berglen, T. F., Myhre, C. E. L., and Isaksen, I. S. A.: The radiative effect of the anthropogenic influence on the stratospheric sulfate aerosol layer, Tellus B, 56, 294–299, doi:10.1111/j.1600-0889.2004.00106.x, 2004.

Newhall, C. G. and Self, S.: The Volcanic Explosivity Index (VEI): An Estimate of Explosive Magnitude for Historical Volcanism, J. Geophys. Res., 87, 1231–1238, doi:10.1029/JC087iC02p01231,

1982.
Nguyen, H. N. and Martinsson, B. G.: Analysis of C, N and O in aerosol collected on an organic backing using internal blank measurements and variable beam size, Nucl. Instrum. Methods, 264, 96–102, 10.1016/j.nimb.2007.08.001, 2007.
Nguyen, N. H., Gudmundsson, A., and Martinsson, B.: Design and calibration of a multi-channel aerosol sampler for tropopause region studies from the CARIBIC platform, Aerosol Sci. Tech., 40, 649–655, doi:10.1080/02786820600767807, 2006.
Nguyen, H. N., Martinsson, B. G., Wagner, J. B., Carlemalm, E., Ebert, M., Weinbruch, S., Brenninkmeijer, C. A. M., Heintzenberg, J., Hermann, M., Schuck, T., Velthoven, P. F. J. v., and Zahn, A.: Chemical composition and morphology of individual aerosol particles from a CARIBIC flight at 10 km altitude between 50° N and 30° S, J. Geophys. Res., 113, D23209, doi:10.1029/2008JD009956, 2008.
Niemeier, U., Timmreck, C., Graf, H.-F., Kinne, S., Rast, S., and Self, S.: Initial fate of fine ash and sulfur from large volcanic eruptions, Atmos. Chem. Phys., 9, 9043–9057, doi:10.5194/acp-9-9043-2009, 2009.
O'Dowd, C. D., Facchini, M. C., Cavalli, F., Ceburnis, D., Mircea, M., Decesari, S., Fuzzi, S., Yoon, Y. J., and Putaud, J.-P.: Biogenically driven organic contribution to marine aerosol, Nature, 431, 676–680, doi:10.1038/nature02959, 2004.
Papaspiropoulos, G., Martinsson, B. G., Zahn, A., Brenninkmeijer, C. A. M., Hermann, M., Heintzenberg, J., Fischer, H., and Velthoven, P. F. J. v.: Aerosol elemental concentrations in the tropopause region from intercontinental flights with the Civil Aircraft for Regular Investigation of the Atmosphere Based on an Instrument Container (CARIBIC) platform, J. Geophys. Res., 107, 4671, doi:10.1029/2002jd002344, 2002.
Pitari, G., Mancini, E., Rizi, V., and Shindell, D. T.: Impact of Future Climate and Emission Changes on Stratospheric Aerosols and Ozone, J. Atmos. Sci., 59, 414–440, doi:10.1175/1520-0469(2002)059<0414:iofcae>2.0.co; 2, 2002.
Rauthe-Schöch, A., Weigelt, A., Hermann, M., Martinsson, B. G., Baker, A. K., Heue, K.-P., Brenninkmeijer, C. A. M., Zahn, A., Scharffe, D., Eckhardt, S., Stohl, A., and Velthoven, P. F. J. v.: CARIBIC aircraft measurements of Eyjafjallajökull volcanic plumes in April/May 2010, Atmos. Chem. Phys., 12, 879–902, doi:10.5194/acp-12-879-2012, 2012.
Read, W. G., Froidevaux, L., and Waters, J. W.: Microwave Limb Sounder measurement of stratospheric SO2 from the Mt. Pinatubo volcano, Geophys. Res. Lett., 20, 1299–1302, 1993.
Rose, W. I. and Durant, A. J.: Fine ash content of explosive eruptions, J. Volcanol. Geoth. Res., 186, 32-39, doi:10.1016/j.jvolgeores.2009.01.010, 2009.
Rose, W. I., Bluth, G. J. S., Schneider, D. J., Ernst, G. G. J., Riley, C. M., Henderson, L. J., and McGimsey, R. G.: Observations of Volcanic Clouds in Their First Few Days of Atmospheric Residence: The 1992 Eruptions of Crater Peak, Mount Spurr Volcano, Alaska, J. Geol., 109, 677–694, 10.1086/323189, 2001.
Rubin, K.: Degassing of metals and metalloids from erupting seamount and mid-ocean ridge volcanoes: Observations and predictions, Geochim. Cosmochim. Ac., 61, 3525–3542, doi:10.1016/s0016-7037(97)00179-8, 1997.
Rudnic, L. R. and Fountain, M. D.: Nature and composition of the continental crust: a lower crustal perspective, Rev. Geophys., 33, 267–309, doi:10.1029/95RG01302, 1995.
Scheele, M. P., Siegmund, P. C., and Velthoven, P. F. J. V.: Sensitivity of trajectories to data resolution and its dependence on the starting point: In or outside a tropopause fold, Meteorol. Appl., 3, 267–273, doi:10.1002/met.5060030308, 1996.
Schmale, J., Schneider, J., Voigt, T. J., Kalesse, H., Rautenhaus, M., Lichtenstern, M., Schlager, H., Ancellet, G., Arnold, F., Gerding, M., Mattis, I., Wendisch, M., and Borrmann, S.: Aerosol layers from the 2008 eruptions of Mount Okmok and Mount Kasatochi: In situ upper troposphere and lower stratosphere measurements of sulfate and organics over Europe, J. Geophys. Res., 115, D00L07, doi:10.1029/2009JD013628, 2010.
Schumann, U., Weinzierl, B., Reitebuch, O., Schlager, H., Minikin, A., Forster, C., Baumann, R., Sailer, T., Graf, K., Mannstein, H., Voigt, C., Rahm, S., Simmet, R., Scheibe, M., Lichtenstern, M., Stock, P., Ruba, H., Schauble, D., Tafferner, A., Rautenhaus, M., Gerz, T., Ziereis, H., Krautstrunk, M., Mallaun, C., Gayet, J. F., Lieke, K., Kandler, K., Ebert, M., Weinbruch, S., Stohl, A., Gasteiger, J., Gross, S., Freudenthaler, V., Wiegner, M., Ansmann, A., Tesche, M., Olafsson, H., and Sturm, K.: Airborne observations of the Eyjafjalla volcano ash cloud over Europe during air space closure in April and May 2010, Atmos. Chem. Phys, 11, 2245–2279, doi:10.5194/acp-11-2245-2011, 2011.
Seinfeld, J. H. and Pandis, S. N.: Atmospheric chemistry and physics: from air pollution to climate change, 2nd edn., Book, John Wiley&Sons, Inc., Hoboken, N.J, 2006.
Sigmundsson, F., Hreinsdóttir, S., Hooper, A., Árnadóttir, T., Pedersen, R., Roberts, M. J., Óskarsson, N., Auriac, A., and Decriem, J.: Intrusion triggering of the 2010 Eyjafjallajökull explosive eruption, Nature 468, 426–430, doi:10.1038/nature09558, 2010.
Solomon, S., Daniel, J. S., Neely III, R. R., Vernier, J. P., Dutton, E. G., and Thomason, L. W.: The persistently variable "background" stratospheric aerosol layer and global climate change, Science, 333, 866–870, doi:10.1126/science.1206027, 2011.
Spracklen, D. V., Arnold, S. R., Sciare, J., Carslaw, K. S., and Pio, C.: Globally significant oceanic source of organic carbon aerosol, Geophys. Res.Lett., 35, L12811, doi:10.1029/2008GL033359, 2008.
Stramska, M.: Particulate organic carbon in the global ocean derived from SeaWiFS ocean color, Deep-Sea Research Part I, 56, 1459–1470, doi:10.1016/j.dsr.2009.04.009, 2009.
Suzuki, Y. J. and Koyaguchi, T.: Numerical determination of the efficiency of entrainment in volcanic eruption columns, Geophys. Res. Lett., 37, L05302, doi:10.1029/2009GL042159, 2010.
Thomas, H. E. and Prata, A. J.: Sulphur dioxide as a volcanic ash proxy during the April–May 2010 eruption of Eyjafjallajökull Volcano, Iceland, Atmos. Chem. Phys, 11, 6871–6880, doi:10.5194/acp-11-6871-2011, 2011.
Vernier, J.-P., Thomason, L. W., Pommereau, J.-P., Bourassa, A., Pelon, J., Garnier, A., Hauchecorne, A., Blanot, L., Trepte, C., Degenstein, D., and Vargas, F.: Major influence of tropical volcanic eruptions on the stratospheric aerosol layer during the last decade, Geophys. Res. Lett., 38, L12807, doi:10.1029/2011GL047563, 2011.
von Glasow, R., Bobrowski, N., and Kern, C.: The effects of volcanic eruptions on atmospheric chemistry, Chem. Geol., 263, 131–142, doi:10.1016/j.chemgeo.2008.08.020, 2009.
Waythomas, C. F., Scott, W. E., Prejean, S. G., Schneider, D. J., Izbekov, P., and Nye, C. J.: The 7–8 August 2008 eruption of

Kasatochi Volcano, central Aleutian Islands, Alaska, J. Geophys. Res., 115, B00B06, doi:10.1029/2010jb007437, 2010.

Weisenstein, D. K., Yue, G. K., Ko, M. K. W., Sze, N.-D., Rodriguez, J. M., and Scott, C. J.: A two-dimensional model of sulfur species and aerosols, J. Geophys. Res., 102, 13019–13035, doi:10.1029/97JD00901 1997.

Winker, D. M., Vaughan, M. A., Omar, A., Hu, Y. X., Powell, K. A., Liu, Z. Y., Hunt, W. H., and Young, S. A.: Overview of the CALIPSO Mission and CALIOP Data Processing Algorithms, J. Atmos. Ocean. Tech., 26, 2310–2323, doi:10.1175/2009jtecha1281.1, 2009.

Witham, C. S., Oppenheimer, C., and Horwell, C. J.: Volcanic ash-leachates: a review and recommendations for sampling methods, J. Volcanol. Geoth. Res., 141, 299–326, doi:10.1016/j.jvolgeores.2004.11.010, 2005.

Yang, K., Liu, X. O., Bhartia, P. K., Krotkov, N. A., Carn, S. A., Hughes, E. J., Krueger, A. J., Spurr, R. J. D., and Trahan, S. G.: Direct retrieval of sulfur dioxide amount and altitude from spaceborne hyperspectral UV measurements: Theory and application, J. Geophys. Res., 115, D00L09, doi:10.1029/2010jd013982, 2010.

Yoon, Y. J., Jennings, S. G., Dowd, C. D. O., Ceburnis, D., Cavalli, F., Jourdan, O., Putaud, J. P., Facchini, M. C., Decesari, S., Fuzzi, S., and Sellegri, K.: Seasonal characteristics of the physicochemical properties of North Atlantic marine atmospheric aerosols, J. Geophys. Res., 112, D04206, doi:10.1029/2005JD007044, 2007.

Yue, G. K., Poole, L. R., Wang, P. H., and Chiou, E. W.: Stratospheric aerosol acidity, density, and refractive index deduced from SAGE II and NMC temperature data J. Geophys. Res., 99, 3727–3738, doi:10.1029/93jd02989, 1994.

Zahn, A., Weppner, J., Widmann, H., Schlote-Holubek, K., Burger, B., Kuhner, T., and Franke, H.: A fast and precise chemiluminescence ozone detector for eddy flux and airborne application, Atmos. Meas. Tech., 5, 363–375, doi:10.5194/amt-5-363-2012, 2012.

Paper II

Tellus SERIES B CHEMICAL AND PHYSICAL METEOROLOGY
PUBLISHED BY THE INTERNATIONAL METEOROLOGICAL INSTITUTE IN STOCKHOLM

Sources of increase in lowermost stratospheric sulphurous and carbonaceous aerosol background concentrations during 1999–2008 derived from CARIBIC flights

By JOHAN FRIBERG[1]*, BENGT G. MARTINSSON[1], SANDRA M. ANDERSSON[1], CARL A. M. BRENNINKMEIJER[2], MARKUS HERMANN[3], PETER F. J. VAN VELTHOVEN[4] and ANDREAS ZAHN[5], [1]*Department of Physics, Lund University, Lund, Sweden;* [2]*Max Planck Institute for Chemistry, Mainz, Germany;* [3]*Leibniz Institute for Tropospheric Research, Leipzig, Germany;* [4]*Royal Netherlands Meteorological Institute, de Bilt, The Netherlands;* [5]*Institute for Meteorology and Climate Research, Karlsruhe Institute of Technology (KIT), Karlsruhe, Germany*

(Manuscript received 25 November 2013; in final form 19 February 2014)

ABSTRACT

This study focuses on sulphurous and carbonaceous aerosol, the major constituents of particulate matter in the lowermost stratosphere (LMS), based on in situ measurements from 1999 to 2008. Aerosol particles in the size range of 0.08–2 μm were collected monthly during intercontinental flights with the CARIBIC passenger aircraft, presenting the first long-term study on carbonaceous aerosol in the LMS. Elemental concentrations were derived via subsequent laboratory-based ion beam analysis. The stoichiometry indicates that the sulphurous fraction is sulphate, while an O/C ratio of 0.2 indicates that the carbonaceous aerosol is organic. The concentration of the carbonaceous component corresponded on average to approximately 25% of that of the sulphurous, and could not be explained by forest fires or biomass burning, since the average mass ratio of Fe to K was 16 times higher than typical ratios in effluents from biomass burning. The data reveal increasing concentrations of particulate sulphur and carbon with a doubling of particulate sulphur from 1999 to 2008 in the northern hemisphere LMS. Periods of elevated concentrations of particulate sulphur in the LMS are linked to downward transport of aerosol from higher altitudes, using ozone as a tracer for stratospheric air. Tropical volcanic eruptions penetrating the tropical tropopause are identified as the likely cause of the particulate sulphur and carbon increase in the LMS, where entrainment of lower tropospheric air into volcanic jets and plumes could be the cause of the carbon increase.

Keywords: lowermost stratosphere, elemental composition, volcanic aerosol, sulphurous aerosol, carbonaceous aerosol

1. Introduction

Aerosol particles play an important role in the radiation balance of the earth, with cooling and warming effects depending on particle composition. The combined aerosol effects are complex and estimated to provide a net negative radiative forcing (IPCC, 2007), which implies cooling of the earth surface. Because of the complexity and the scarcity of measurement data, the associated uncertainties are still large. Hence, it is important to learn more about particle chemical and elemental composition, not only for assessing the direct radiative effects, but also with regard to aerosol microphysical properties and, ultimately, cloud formation.

The major part of the particulate mass in the stratosphere is carried by submicrometer diameter particles (Deshler, 2008). Sedimentation velocities for such particles at these altitudes are low compared to the residence times of the air masses (Martinsson et al., 2005). Also for the upper troposphere (UT) and lowermost stratosphere (LMS), transport of air masses is of particular relevance for particles and precursor gases. We first briefly summarise some of the main

*Corresponding author.
email: johan.friberg@nuclear.lu.se

Citation: Tellus B 2014, **66**, 23428, http://dx.doi.org/10.3402/tellusb.v66.23428

aspects of the dynamics affecting this region of the atmosphere. The lower bound of the LMS is the tropopause and the upper one the 380 K isentropic surface (Hoskins, 1991; Holton et al., 1995). Large-scale transport in the stratosphere occurs via the Brewer–Dobson (BD) circulation (Brewer, 1949; Dobson, 1956), in which tropical tropospheric air is first transported upwards to the tropical stratosphere and subsequently polewards, to descend finally through the LMS into the extratropical troposphere. Air reaching the tropical stratosphere can undergo fast transport (month) to mid-latitudes in a transitional branch or be moved diabatically upwards in deeper branches of the BD circulation (years) (Gettelman et al., 2011). The downward mass flux across the 380 K isentrope varies with season. In the northern hemisphere, a maximum is found in January and a minimum in July (Appenzeller et al., 1996). The subsidence through the LMS takes months, resulting in a seasonal maximum of stratospheric influence at the tropopause in May (Tang et al., 2011). In addition, direct two-way mass exchange between the UT and LMS, through the extratropical tropopause, occurs along isentropic surfaces (Dessler et al., 1995; Sprenger and Wernli, 2003). The LMS can thus be regarded as a mixture of air from the troposphere and the stratosphere. Mixing of air in the LMS creates concentration gradients of trace gases (Lelieveld et al., 1997; Zahn and Brenninkmeijer, 2003) and particulate matter (Martinsson et al., 2005).

Studies on stratospheric aerosol composition started with Junge et al. (1961). They found a water-soluble sulphurous component, subsequently identified as sulphuric acid and water (Rosen, 1971), formed via gas to particle conversion of mainly OCS and SO_2 (Crutzen, 1976; Weisenstein et al., 1997). OCS photo-oxidises at high altitudes, within the deep BD branch, while SO_2 oxidises at all altitudes in the stratosphere. A recent study by Brühl et al. (2012) argues that OCS is the major source of non-volcanic particulate sulphur in the stratosphere, while Chin and Davis (1995) advocated that the emission rate of OCS alone is insufficient to explain the large amounts of particulate sulphur in the stratosphere. It remains unclear to what degree SO_2 from fossil fuel combustion penetrates the tropical troposphere because of difficulties to distinguish its contribution to the stratospheric aerosol from that of OCS and volcanism (Solomon et al., 2011).

Large volcanic eruptions represent the strongest source of variability in stratospheric aerosol as they can inject substantial amounts of particulate matter and SO_2 into the stratosphere (Robock, 2000). The eruption of Mount Pinatubo in 1991 was observed in the tropics (Dutton and Bodhaine, 2001) and delayed by more than half a year in the stratospheric column at mid-latitudes (Trickl et al., 2013). It perturbed the stratosphere for several years, with an estimated global surface cooling in the order of 0.5°C (McCormick et al., 1995) the year after eruption. A large decline in the aerosol load of the stratosphere was then observed in the following years (Deshler et al., 2006), until reaching a period of near-background conditions in the late 1990s.

LIDAR measurements (Hofmann et al., 2009) indicated increasing amounts of particulate matter in the stratosphere at mid-latitudes in the northern hemisphere after the year 2000. Vernier et al. (2011b) used satellite observations to address this increase and found that the trend increased after year 2005 in connection with volcanic eruptions, reaching the tropical stratosphere. The volcanic aerosol was eventually transported to mid-latitudes (Vernier et al., 2009), increasing the aerosol abundance in both the northern (Hofmann et al., 2009; Bazhenov et al., 2012) and southern hemisphere (Nagai et al., 2010). Solomon et al. (2011) estimated the effect of the stratospheric volcanic aerosol for the time period 2000–2010, to have had a mean radiative forcing of -0.1 W m^{-2}. In addition to the direct injection via explosive volcanic eruptions, Bourassa et al. (2012) found evidence that the eruption of the tropical volcano Nabro in 2011 reached the UT and was lifted to the lower stratosphere, by the South Asian monsoon, where the effluents were transported to the extratropical stratosphere within 4 weeks of the eruption. Neely et al. (2013) later found that the contribution to the stratospheric aerosol load in this period from anthropogenic emissions and that of transport within the South Asian monsoon to be small, further validating volcanic eruptions in the tropics as the main cause of perturbation.

In addition to sulphate, a carbonaceous component in stratospheric particles was observed more recently (Murphy et al., 1998) and was found to be a large fraction of the UT/LMS aerosol (Nguyen and Martinsson, 2007; Schmale et al., 2010). Using electron microscopy, PIXE (particle-induced X-ray emission) and PESA (particle elastic scattering analysis), Nguyen et al. (2008) found a mixture of sulphurous and carbonaceous components in UT and LMS particles, with LMS particles containing a framework of carbonaceous material. Martinsson et al. (2009) and Schmale et al. (2010) found a large carbonaceous component in the aerosol from the Kasatochi eruption. In a recent study, based on model results and satellite measurements of extinction ratios from SAGE, Brühl et al. (2012) suggest that organic particulate matter contributes a significant fraction to the light extinction in the LMS, as particulate sulphur concentrations from the model are insufficient to fully explain the observed light extinction in the stratosphere.

In situ measurements for elemental characterisation of particulate matter in the tropopause region are scarce. CARIBIC (Civil Aircraft for the Regular Investigation of the atmosphere Based on an Instrument Container,

www.caribic-atmospheric.com) is the first project providing in situ elemental characterisation of particulate matter in the UT and LMS on a regular basis.

In this study, the LMS background or close-to-background aerosol is investigated using the CARIBIC platform. For this purpose, datasets from the period 1999–2002 and 2005–2008 are used, spanning almost a decade (data after 2008 are omitted from this study as the LMS became perturbed by a direct injection of volcanic aerosol in Aug 2008). These data for sulphurous and carbonaceous fractions of LMS particles provide, as far as we know, the longest time series on particulate sulphur and the first long-term quantitative measurements of the particulate carbon content in the tropopause region. Aerosol concentrations are presented relative to the position of the tropopause, as temporal trends, seasonal differences and inter-annual variations. In addition, the chemical composition of the carbonaceous component is presented as stoichiometric ratios of oxygen to carbon, and aerosol sources are discussed and identified.

2. Methods

The first generation CARIBIC measurements (CARIBIC phase #1) (Brenninkmeijer et al., 1999) using intercontinental flights were performed in 1997–2002 on board a Boeing 767–300 ER from LTU International Airways providing the first long-term in situ observations of the chemical composition of aerosol particles, combined with particle number and trace gas concentrations. The present CARIBIC system (CARIBIC phase #2) is the second generation consisting of a 1.6-ton container with an extended scientific payload, sampling at cruise altitudes of 9–12 km (Brenninkmeijer et al., 2007). This new CARIBIC container is installed in a Lufthansa Airbus 340–600 on a monthly basis for four consecutive flights, since May 2005 (no aerosol samples were collected in the period May 2002–April 2005). This aircraft is equipped with a sophisticated inlet system for gases and particles. In situ measurements of aerosol particles and of trace gases (e.g. O_3, CO, NO/NO_y, VOCs, gaseous and condensed water) are carried out. Collected air samples are analysed for greenhouse gases, hydro- and halo carbons (Brenninkmeijer et al., 2007; Schuck et al., 2009; Baker et al., 2010; Oram et al., 2012). Monthly measurement flights depart from Frankfurt for destinations in South East Asia, East Asia, Southern Africa and North and South America, thus covering a large geographical area, mainly in the northern hemisphere.

2.1. Aerosol sampling

The aerosol data presented in this work from CARIBIC phase #1 and #2 have been obtained using two different inlet systems. Based on experimental studies and modelling, the CARIBIC phase #1 inlet efficiency for particle sizes of 0.1–1 μm was estimated to be 90% (Hermann et al., 2001). The present CARIBIC inlet system is described by Brenninkmeijer et al. (2007). Its sampling efficiency is estimated to be 60% at 5 μm particle diameter (Rauthe-Schöch et al., 2012), and based on modelling and experience with other aerosol inlets, its efficiency is estimated be at least 90% for particles of 0.01–1 μm diameter.

Collection of aerosol particles was undertaken by automated impactors (Nguyen et al., 2006), implemented in the CARIBIC instrument containers, collecting particles of 0.08–2 μm aerodynamic diameters. The CARIBIC phase #1 (phase #2) impactors have 14 (16) channels for sequential and integral samples. Each sequential sample is collected during typically 150 (100) minutes corresponding to flight distances of approximately 2200 (1500) km at cruise speed. The integral samples [1 (2) out of 14 (16) samples] are collected for the purpose of checking for sample contamination. The air sampling volume for a sequential sample is approximately 0.09 (0.25) m^3 STP [standard temperature (273.15 K) and pressure (1013.25 hPa)]. Sampling is suspended during take-off and landing, whenever pressure exceeds 350 hPa, to prevent mixed samples of lower tropospheric (or even boundary layer) and UT/LMS aerosol particles. Particles accelerated in 0.5 mm diameter impactor orifices are deposited in four spots (phase #2), forming a square pattern with centre distances between spots of 1.3 mm, whereas the CARIBIC phase #1 sampler collected aerosol from a single orifice (Martinsson et al., 2001). The sampling substrate consists of a 0.2 μm thin AP1™ polyimide film, a material well suited for ion beam analysis (IBA) (Papaspiropoulos et al., 1999; Nguyen and Martinsson, 2007).

2.2. Analyses of aerosol particles

Analyses were undertaken with a 2.55 MeV proton beam at the Lund IBA accelerator. The IBA measurement techniques used are PIXE and PESA. PIXE (Johansson and Campbell, 1988) was used for elements with an atomic number larger than 13 and PESA for measurements of lighter elements (hydrogen, carbon, nitrogen and oxygen). Analyses were run in two steps, using the technique described by Nguyen and Martinsson (2007). Typical elemental minimum detection limits (MDL) in units of ng m^{-3} STP are 1 (hydrogen), 15 (carbon), 7 (oxygen), 2 (sulphur) and 0.1 (iron). The accuracy of PIXE and PESA is estimated to be 10% (Nguyen and Martinsson, 2007). Concentrations below MDL were set to MDL/2. The detection frequencies, that is, the fraction of the samples with elemental concentrations above the MDL are: 100% (hydrogen),

83% (carbon), 100% (oxygen), 100% (sulphur) and 50% (iron).

Films with low deposited aerosol mass occasionally lead to significantly higher MDLs compared to the majority of the samples in the PESA analysis as a result of problems in identifying the aerosol deposit spot, which prevents analysis. This MDL problem is primarily associated with short sampling times. MDLs, in ng m^{-3}, were derived from sampled mass density, in μg cm^{-2}, on the exposed films and are thus highly dependent on sampling time. Samples with sampling times shorter than 60 minutes (caused for instance by aircraft landings) were therefore excluded to prevent these effects of high MDLs on the data set.

The analytical system used for detection of carbon was developed after 2002. Hence, no analysis of carbon was possible for samples collected with the first generation collection system. The carbon data in the present study is thus obtained from measurements with the second-generation collection system running since 2005.

2.3. Ozone measurements

We use the concurrent CARIBIC in situ ozone measurements to assist the interpretation of the variations in particulate carbon and sulphur concentrations in the UT/LMS. Two ozone analysers are currently installed in the CARIBIC container; an accurate, dual-beam UV-photometer serving as a calibrated standard instrument and a fast solid state chemiluminescence detector. The accuracy was estimated to be 2% for 10 Hz measurements (Brenninkmeijer et al., 2007; Zahn et al., 2012), while the uncertainty for the first generation CARIBIC system was 4% or 4 ppbv, whichever was larger (Zahn et al., 2002).

2.4. The tropopause definition

The dynamical tropopause, based on potential vorticity (PV) with a typical threshold value of 1.5–3.5 PVU (Potential Vorticity Units; 1 PVU = 10^{-6} K m^2 kg^{-1} s^{-1}) (Hoerling et al., 1991; Hoinka, 1997), is used for identifying samples collected in the LMS. PV values were derived from archived ECMWF (European Centre for Medium-range Weather Forecast) analyses with a resolution of 1×1 degree in the horizontal at 91 vertical hybrid sigma-pressure model levels and calculated by the Royal Netherlands Meteorological Institute, de Bilt, the Netherlands (KNMI). PV values were interpolated linearly in latitude, longitude, log pressure and time to the location of the aircraft and for each sample averaged over the duration of sampling. Samples at an average PV of over 2 PVU are accordingly regarded as stratospheric.

2.5. Exclusion of periods affected by direct injection into the LMS by extratropical, strong volcanic eruptions

Previous studies have shown a large impact on the LMS aerosol mass concentrations from volcanoes injecting directly into the LMS (Martinsson et al., 2009; Schmale et al., 2010; Andersson et al., 2013). The largest such eruptions in the period studied here (1999–2008) were Okmok (July 12, 2008) and Kasatochi (August 7–8, 2008), of which the latter strongly affected the LMS aerosol load (Martinsson et al., 2009). The first samples containing volcanic aerosol from Okmok and Kasatochi were collected by CARIBIC on August 15, 2008. Samples containing aerosol from these eruptions are excluded in our study. This refers to all LMS samples collected after August 15, 2008. After excluding samples affected by fresh volcanic clouds, this study on the background aerosol is based on 181 LMS samples, whereof 38 were from the period 1999–2002.

3. Results

3.1. Particulate sulphur and carbon concentrations in the LMS

Figure 1 shows the temporal evolution of particulate sulphur and carbon concentrations in the LMS for the period considered. The strong effect on the aerosol concentrations via a direct injection of volcanic aerosol into the extratropical LMS by the Kasatochi eruptions in August 2008, as reported by Martinsson et al. (2009) is evident, while the rest of the period represents an episode of low volcanic activity at mid-latitudes. Comparing the early sulphur data (1999–2002) with later data (2005–2008), a clear increase in concentration and variation is observed. Moreover, the concentrations increase substantially in the period 2005–2008, for both sulphur and carbon, with on average higher concentrations in 2008 than in any previous year investigated.

3.2. Vertical gradients and seasonal variations in the LMS

Ozone is formed deep in the stratosphere and is transported down to the LMS within the large-scale DB circulation. In the LMS, ozone has a chemical lifetime of >1 yr (Solomon et al., 1997; Smith et al., 2001); that is, it is basically an inert transport tracer and is solely diluted with inflowing ozone-poor tropospheric air, locally or via the lower BD branch. Thus, in the LMS ozone constitutes a reliable tracer for the degree of mixing with tropospheric air and an accurate measure for the distance above the tropopause (Sprung and Zahn, 2010). In Fig. 2, we use LMS

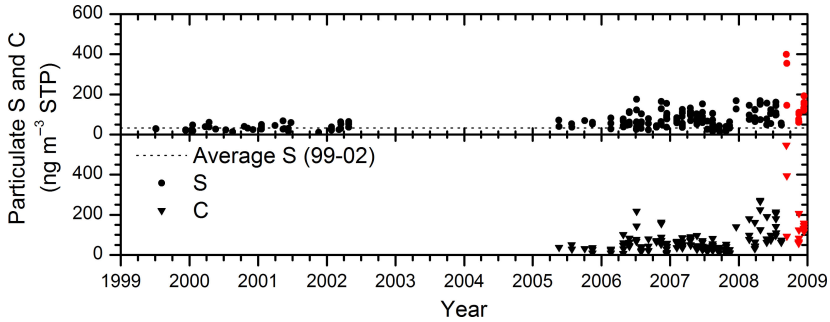

Fig. 1. Temporal variations of concentrations of particulate sulphur and carbon (ng m^{-3} STP) in the northern hemisphere LMS. Red dots illustrate observations after the eruption of Kasatochi. The dashed line shows the geometric average particulate sulphur concentrations during 1999–2002.

ozone concentrations, thus expressing distance to the tropopause, for the four different seasons. Increase in aerosol concentrations is investigated via a scatter plot of particulate sulphur vs. ozone to illustrate the vertical gradient of sulphur from the tropopause into the LMS. A linear fit is applied to the 1999–2002 data for comparison to the 2005–2008 data. This fit is based on data for all four seasons to obtain a significant number of results. Figure 2 shows the difference between the two periods much more clearly. For all seasons, over 90% of the observed concentrations in the period 05–08 is found to be higher than during 99–02, whereas measurements at lowest ozone concentrations, that is, close to the tropopause, show similar concentrations in the two periods. The difference between the periods is less pronounced during fall. In the period 05–08, the observed gradient is strongest during winter and decreases in strength

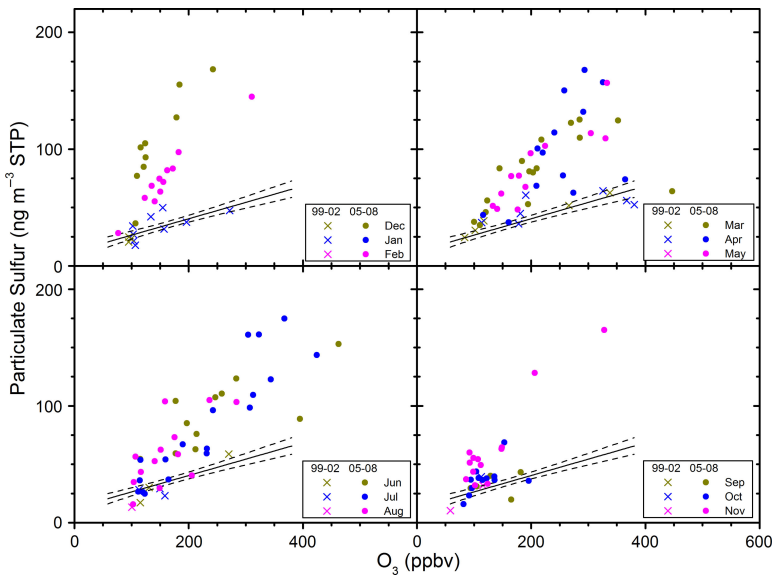

Fig. 2. Concentration of particulate sulphur vs. ozone for stratospheric samples (potential vorticity > 2 PVU) collected in the northern hemisphere. Upper left: winter (December, January, February). Upper right: spring (March, April, May). Lower left: summer (June, July, August). Lower right: fall (September, October, November). A regression model (full line), with 95% confidence interval (dashed lines) based on the 1999–2002 data is used to facilitate the comparison to the 2005–2008 data.

during spring and summer, to reach significantly lower levels in fall.

3.3. Inter-annual variations

To further explore seasonality of particulate sulphur in the LMS, the distance from the tropopause needs to be considered. We consider this using PV, a meteorological parameter with a strong gradient from the tropopause into the LMS. Hence, the sulphur to PV ratio is used in Fig. 3b and is subsequently compared to the corresponding ozone and particulate carbon ratios. The O_3/PV ratio in the LMS is primarily determined by the seasonally varying subsidence of stratospheric air in the BD circulation and thus maximises in mid-latitudes in late spring (Tang et al., 2011), at the seasonal maximum influence from the stratosphere. We observe no difference in the average O_3/PV for the periods 99–02 and 05–08, indicating that no major changes occurred in the transport from the stratosphere during this time. A sine curve fitting is applied with the relative amplitude of 0.31, as shown in Fig. 3a, which holds throughout the period 1999–2008, corroborating the absence of major changes in transport.

The contribution by downward transport of sulphurous aerosol formed in the stratosphere is evaluated in Fig. 3b, using S/PV. To account for the increase in sulphur concentrations from 99–02 to 05–08, two sine functions are used with the same relative amplitude and phase as for the O_3/PV model. In the period 05–08, the S/PV shows considerable agreement with the seasonal variation of O_3/PV with two large deviations (end of 2006 and 2007), and a tendency of higher values during 2008 compared to the two preceding years. Whereas the contribution from the deep branch is expected to follow the phase of the model, transport of SO_2 and particles in the shallow BD branch can cause deviation from this seasonal pattern. The data show that this may have been the case. Interestingly, for carbon the picture seems more complicated, as the C/PV ratio (Fig. 3c) lacks any clear resemblance to that of O_3/PV (Fig. 3a). Some larger deviations are found at the end of 2006 and 2007 and during 2008. These deviations will be further investigated in the Discussion section.

3.4. Composition of carbonaceous aerosol

Besides the very presence of carbonaceous aerosol in conjunction with sulphur and its variability, any information on its actual chemical moiety is valuable. Optical measurements of black carbon in the LMS (Schwarz et al., 2010) showed concentrations in the range of 0.1–4 ng m^{-3} STP. We are however dealing with concentrations that are up to two orders of magnitudes higher (Fig. 1), indicating that soot is only a minor constituent of the carbonaceous fraction in the LMS. The major part of the carbonaceous fraction is therefore likely to be organic.

By means of stoichiometric calculations we can use the PIXE and PESA elemental analyses to infer main properties of the chemical compounds in the samples. Previous CARIBIC measurements have shown that LMS particles have two major components, namely a sulphurous and a carbonaceous one (Nguyen and Martinsson, 2007). In addition several minor constituents can be found, with mineral particles from the earth's crust being the most frequently observed. Figure 4 illustrates the stoichiometric ratios of

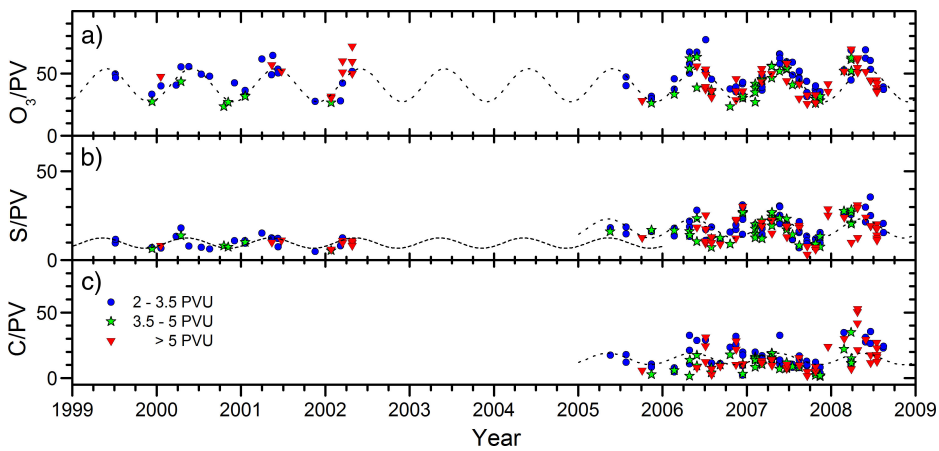

Fig. 3. Temporal trends of ratios to potential vorticity (PV) for a) ozone (ppbv PVU^{-1}), b) particulate sulphur (ng m^{-3} STP PVU^{-1}) and c) particulate carbon (ng m^{-3} STP PVU^{-1}). Sine functions, based on ozone to PV ratios in a) are used in b) and c) to guide the eye.

oxygen to sulphur against carbon to sulphur, for all LMS samples with concentrations above the MDLs of these elements (C, O and S). Oxygen is present in the sulphurous fraction and also in the crustal fraction. A crustal component was identified in 19 samples based on elemental concentration ratios between potassium, calcium, titanium and iron. The crustal contribution to the oxygen content was subtracted from the total stoichiometric amounts of oxygen shown in Fig. 4. The correction was based on the average mineral composition of the earth crust estimated by Rudnick and Fountain (1995). The contribution from the sulphurous fraction can be identified at an oxygen to sulphur ratio of 4 (O/S = 4), based on the assumption that all sulphur is present in the form of sulphate. Figure 4 indeed supports this, as most of the O/S ratios scatter at values exceeding 4. A positive trend from the line of O/S = 4 with increasing C/S ratio is present, which reflects the fraction of oxygen in the carbonaceous component. A relationship for the O/S ratios in relation to C/S ratios can be derived using a linear regression. Thus, the oxygen content in the carbonaceous fraction is obtained at an average O/C ratio of 0.2. Combined with the low concentrations of black carbon (Schwarz et al., 2010), this corroborates that the main part of carbonaceous LMS aerosol is organic.

4. Discussion

An upward trend of 5–6% per year in the background aerosol at 20–25 km altitude for the period 2000–2009 was observed using LIDAR measurements. Increasing coal combustion associated with sulphur emissions, primarily in China, was hypothesised as an explanation (Hofmann et al., 2009). However, Vernier et al. (2011b) used satellite observations to study the trend of increasing amounts of particulate matter in the stratosphere and found that several moderate volcanic eruptions with explosions reaching the tropical stratosphere had affected the aerosol load. In addition to volcanism, Vernier et al. (2011a) identified the South Asian summer monsoon as a likely transport path for aerosol and precursor gases to the tropical tropopause layer (TTL). The aerosol load in the TTL in that study was found to be fairly constant in the period 2006–2008, with a minor increase in 2008, discussed to be an effect of volcanic aerosol.

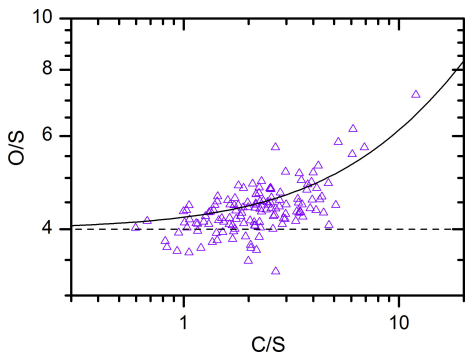

Fig. 4. Oxygen to sulphur vs. carbon to sulphur molar ratios. The dashed line represents O/S = 4, and the full line shows the best fit, i.e. O/S = 4 + 0.2 C/S.

The particulate sulphur concentration increases from the tropopause into the LMS and is significantly higher at the 380 K isentrope than at the tropopause or the UT (Martinsson et al., 2005). The same pattern but magnified appears in the period 2005–2008 (Fig. 2). The increase in aerosol concentration in the LMS in the period 2000–2009 thus indicates transport from the stratosphere, rather than from local mixing of air from the UT.

The difference in sulphur concentrations between the periods 99–02 and 05–08 is smallest in fall (Fig. 2), when ozone and particulate sulphur concentrations minimises, indicating the lowest contribution from the deep BD branch. Air mass budget analyses based on aircraft data demonstrated a strongly varying seasonal partitioning of stratospheric and tropospheric air in the LMS with a minimum influence from the deep BD branch in fall (Hoor et al., 2005). In summer and fall, the LMS is flushed with ozone-poor air from the TTL (Bönisch et al., 2009), additionally reducing the impact from the deep BD branch. This further emphasises our finding that the particulate sulphur is of stratospheric origin and varies in phase with the downward flux within the BD circulation. Bönisch et al. (2009) found the LMS above the extratropical transition layer (ExTL) to be more connected to the stratosphere than to the extratropical UT. Hence, the composition of the LMS air is essentially dependent on transport that occurs above the 380 K isentrope, that is, mixing of the deep and shallow BD branches. The shallow BD branch transports air from the tropical stratosphere to northern mid-latitudes within about 1–2 months (Bourassa et al., 2012; Flury et al., 2013), whereas transport in the deep branch takes a year or more (Holton et al., 1995).

Air transported polewards from the tropical stratosphere, experiences different exposure to photo-chemistry depending on altitude and speed along the transport paths. Whereas sulphuric acid is produced from SO_2 at all altitudes, ozone production and particulate sulphur production from OCS occur predominantly within the deep BD branch. Trace gas concentration distributions bare evidence of meridional mixing of air at high and low altitudes in the stratosphere (Gettelman et al., 1997). The ozone concentration at the 380 K isentrope varies by a factor of 2 (Fortuin and Kelder, 1998; Martinsson et al., 2005), with its maximum in March and minimum in September. That varia-

tion compares well to the corresponding O_3/PV variation in Fig. 3a, with a phase shift of 2 months (relative to the 380 K isentrope) and a peak-to-peak ratio of 1.9, indicating a strong coupling between the LMS and the stratosphere. Hence, the low ozone and sulphur concentrations in fall are results of less ozone and particulate sulphur in the air that is down-welling to the LMS as an effect of less transport via the deep BD branch, and an increasing importance of the shallow branch, during summer (Lin and Fu, 2013).

Regarding the sulphurous aerosol component we note that the approach used in Fig. 3b, based on the O_3/PV variability, does capture the overall pattern of the S/PV values. Nonetheless, several deviations from the general pattern indicate that not only OCS contributed to the observed sulphur concentrations. Regarding the C/PV values in Fig. 3c, larger deviations are seen and only a weak seasonal cycle exists. This suggests that oxidation of precursor gases in the deep BD branch in relative terms is less important for formation of particulate carbon, compared to particulate sulphur. It also indicates that other processes cause the variability in the carbon concentration. The O_3 concentration at the 380 K isentrope shows its seasonal minimum in September and maximum in March (Fortuin and Kelder, 1998; Martinsson et al., 2005). This seasonal variation is expected also in the concentration of sulphate aerosol formed from OCS, as it follows the deep BD branch, while transport of sulphate aerosol to the 380 K isentrope via the shallow BD branch can cause high S/O_3 ratios also during fall. Low ozone concentration in the LMS in winter concurrent with elevated particulate sulphur concentration is thus an indication of formation of particulate matter in SO_2-rich air that was transported in the stratosphere to mid-latitudes by the shallow BD branch. Hence to study the importance of particulate matter formation and transport in the shallow branch we use the seasonal variations of S/O_3 (Fig. 5). For the period 05–08 we have enough data to produce monthly averages. The S/O_3 is once again shown to be significantly higher in the period 05–08 than in the 99–02 ratios with a strong seasonal cycle. In the period 99–02, the S/O_3 remained fairly constant with a small increase at the turn of the year. For 05–08, the S/O_3 shows a clear saw-tooth pattern with a rapid rise from September to December. This increase in the S/O_3 indicates production and transport of sulphurous aerosol within the shallow BD branch. Revisiting the strong particulate-sulphur-to-ozone gradient in Fig. 2 during winter, we conclude that this is the consequence of down-welling of air that was transported in the shallow branch, from the overlying stratosphere, while the gradient in spring and in summer corresponds to mixing also via the deep branch.

Using Fig. 6, we can inspect deviations of particulate sulphur and carbon from seasonality in down-welling of O_3 from the stratosphere over a longer time span. During

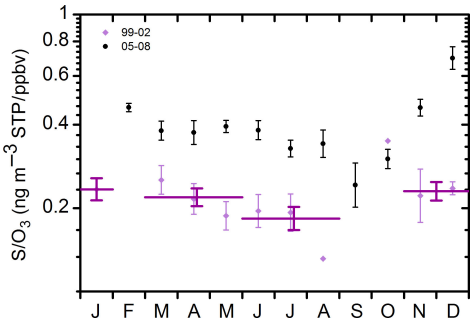

Fig. 5. Ratios of particulate sulphur to ozone mixing ratio (Unit: ng m^{-3} STP $ppbv^{-1}$) for the periods 1999–2002 and 2005–2008, expressed as monthly geometric averages (black and light purple). Purple lines denote averages in the period 1999–2002 for the months; January, March–May, June–August and November–December. Error bars represents standard errors.

05–08, there are periods (Fig. 6a) when S/O_3 values are similar to those of the period 99–02, in particular during July–October 2007. There are also large positive deviations from the geometric average of May 2005–August 2008 in the end of 2006 and in December 2007, while 2008 shows higher S/O_3 ratios compared to 2006 and 2007. A similar pattern is evident for the C/O_3 ratios in Fig. 6b. Deviations from the geometric average of the C/O_3 are essentially found in the end of 2006 and in December 2007, and during most of 2008. In fall 05–08 (Fig. 2), two of the observations have ozone and sulphur concentrations well above the average of the season. These were sampled on November 14–15, close to the end of the defined season and look more connected to the observations in the winter season.

While sulphuric acid is generally considered the main component in stratospheric and LMS aerosol much less is known of the other large component; the carbonaceous aerosol. The following two sections will address the cause of high concentrations of particulate carbon, and of the temporal trends of particulate sulphur and carbon in the LMS aerosol.

4.1. *Forest fires and biomass burning*

Combustion of biomass emits large amounts of soot and organic trace gases that lead to secondary aerosol formation (Andreae and Merlet, 2001). Episodes of increased scattering ratios coupled to pyroconvection from forest fires have been observed at altitudes above the tropopause, remaining for a month or more. A number of authors (Jost et al., 2004; Fromm et al., 2005, 2010; Damoah et al., 2006) discuss the possibility and magnitude of forest fire injection of

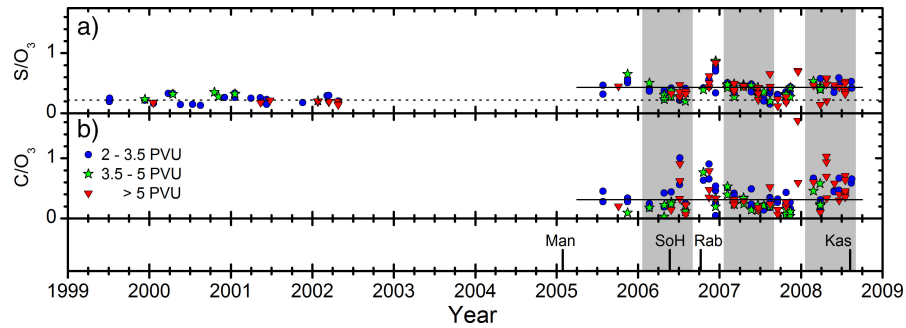

Fig. 6. Ratios of particulate sulphur and carbon concentration to ozone mixing ratio (Unit: ng m^{-3} STP $ppbv^{-1}$), for a) particulate sulphur and b) particulate carbon for stratospheric samples. Full and dashed horizontal lines represent geometric averages for the periods 2005–2008 and 1999–2002, respectively. The February–August period is indicated by a grey background. The four discussed volcanic eruptions (Manam, Soufriere Hills, Rabaul and Kasatochi) are indicated by vertical lines.

smoke particles into the LMS via pyroconvective transport. Based on optical measurements Fromm et al. (2008) estimate that a massive fire storm in Canada in the end of May 2001 injected a mass of smoke, corresponding to more than 5% of the background aerosol in the northern hemisphere lower stratosphere, that persisted until the end of summer. Such events are sporadic with uncertain occurrence frequency. Guan et al. (2010) estimate that approximately 140 plumes reached altitudes above 5 km, in the northern hemisphere, in the period 1979–2009, that is, on average less than 5 per year. Potassium (K) is one of the elements, besides carbon that is generally found in aerosol from biomass burning (Andreae and Merlet, 2001). Importantly, there is no correlation between C and K in the stratospheric CARIBIC samples ($R^2 = 0.004$), indicating that biomass burning had a negligible contribution to the LMS aerosol during the period considered here. The other large potential source of K in the LMS is crustal material. Besides K crustal particles also contain silicon, iron, titanium and calcium. Out of these elements, iron (Fe) is the element with the highest detection frequency in our samples. In Fig. 7, a scatter plot of Fe vs. K in stratospheric samples is used to study the possible impact of biomass burning and crust particles on the LMS aerosol. Aerosol from biomass burning would result in ratios <0.1 ng Fe/ng K (Andreae et al., 1998), while crustal material would be found at ratios >1 (Rudnick and Fountain, 1995). Only a few observations lie close to the 0.1 line (dashed), indicating that biomass burning has a minor impact on the LMS aerosol. A linear regression model shows a strong correlation between Fe and K, with an average ratio of 1.58 ng Fe/ng K. These observations give evidence that biomass burning is insufficient to explain the high carbon concentrations observed.

4.2. *Impact of mid-latitude volcanism*

Volcanic plumes bring high concentrations of particulate matter, SO_2 and other gases to the stratosphere. Gas to particle conversion of SO_2 in the stratosphere is fast compared to the residence times of the air mass and the entrained submicron particles. Volcanic injections of aerosol to the LMS from mid-latitude eruptions are expected to perturb the LMS for a few months or less depending on the altitude of the volcanic injection. Kasatochi's eruption in August 2008 increased the sulphurous aerosol concentrations by a factor of two in the following months. The SO_2 emissions from Okmok were estimated to be 5% (0.1 Tg) of that of Kasatochi's (2 Tg) (Yang et al., 2010; Thomas et al., 2011). In addition some minor eruptions on mid-latitudes

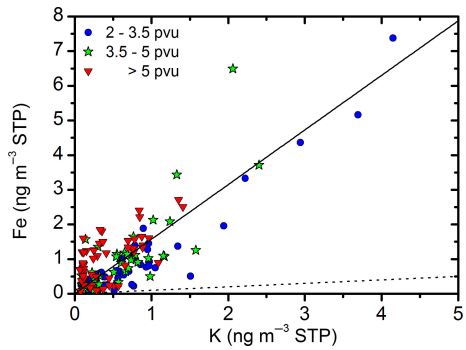

Fig. 7. Mass concentrations of Fe vs. K (ng m^{-3} STP) for stratospheric samples. Regression model shown by full line illustrating a ratio of 1.58 ng Fe/ng K. Dotted line shows Fe/K mass ratio of 0.1, a typical ratio for effluents from biomass burning.

were reported to have reached the tropopause region (Massie, 2014) in the period January 2005–August 2008. Satellite images (from OMI, GOME-2 and AIRS) tell that the SO_2 emissions from any of these eruptions were at least a factor of five lower than that from the eruption of Okmok, implying a maximum perturbation of the LMS aerosol of less than 2% in the months following one of these eruptions. Hence, it is most unlikely that the increases in aerosol concentrations from the periods 99–02 to 05–08 (Fig. 3) are caused by mid-latitude eruptions.

4.3. Impact of tropical volcanism

Mixing in the extratropical stratosphere occurs as air from high altitudes descends and mixes with air at lower altitudes. As a result, aerosol and trace gases injected into the tropical stratosphere can reach mid-latitudes in a time scale of months by stratospheric low altitude meridional mixing, via the shallow branch of the BD circulation, and in 1–2 yr via the deep BD branch. The time of the year of a tropical volcano's eruption is expected to affect the period of time for the effects to be observable in the LMS. Main effects from volcanic aerosol transported via the high-altitude branch may appear 2 yr after the eruption. Three tropical volcanoes had eruptions that reached the stratosphere in the time period 2003–2008, namely Manam, Soufriere Hills and Rabaul (Table 1). Based on the transport characteristics of the stratosphere the Manam eruption in January 2005 could affect the mid-latitude stratosphere primarily in 2005–2006, whereas the effects of the two eruptions in 2006 (Table 1) might be observable during late 2006, with the major effects in the downward transport in 2008. These patterns are essentially observed in measurements from the NASA satellite CALIPSO (Vernier et al., 2009, 2011b).

Volcanic aerosol is commonly considered to be composed of sulphate from the conversion of SO_2, combined with a minor fraction of ash constituents (e.g. potassium, calcium, titanium and iron) even though large amounts of carbonaceous aerosol have been observed in volcanic clouds on several occasions. Martinsson et al. (2009) found particulate carbon-to-sulphur-ratios (C/S, in terms of mass) of 2.6 in fresh plumes in the LMS, decreasing to 1 when most of the SO_2, from the eruption of Kasatochi had been converted, corresponding to an organic content of 25–50% (assuming all particulate carbon to have been organic). Measurements with mass spectrometric methods indicated organic fractions of 20–40% (Carn et al., 2011) and 20% (Schmale et al., 2010) in fresh and aged volcanic clouds, respectively. Hence, these studies indicate that particulate carbon is a major constituent of the aerosol in volcanic clouds, with a substantial effect on the stratosphere given the observations of a volcanically perturbed stratosphere in 2006–2008, as reported by Vernier et al. (2011b).

Despite a number of observations of elevated concentrations of particulate carbon in the LMS connected to volcanic clouds, little is known about the origin of this particulate carbon. In a recent study on volcanic aerosol, Andersson et al. (2013) argue, based on the global distribution of organic aerosol in the lower troposphere, that volcanic jets and plumes could bring large amounts of particulate carbon and organic trace gases to the tropopause region via entrainment of air from low altitudes. Entrainment of low altitude air to the tropical stratosphere, via jets from the three tropical volcanoes could be the cause of the observations of high particulate carbon concentrations in the present study, whereas particulate sulphur is expected from transformation of SO_2 emitted from the volcanoes. The term 'volcanic aerosol' will therefore be used for attributing, not only sulphurous, but also carbonaceous aerosol in the following sections.

It is not possible to attribute every deviation in Fig. 6 to a specific event of volcanic activity, but the main patterns will be discussed. The elevated ratios of S/O_3 and C/O_3 during the end of 2006 and December 2007, suggest down-

Table 1. Explosive volcanic eruptions most relevant for this study in the period 2005–August 2008

Eruption date[a]	Volcano	SO_2 (Tg)	VEI[a]	Longitude[a]	Latitude[a]	Altitude (km)
2005-01-27	Manam	0.09[b]	4	145	−4.1	18[b]
2006-05-20	Soufriere Hills	0.2[c]	3	−62	16.7	20[c]
2006-10-07	Rabaul	0.2[d]	4	152	−4.3	18[d]
2008-07-12	Okmok	0.1[e]	4	−168	55.3	15[f]
2008-08-07	Kasatochi	2[g]	4	−176	52.2	14[e]

[a]Volcanic Explosivity Index, from Global Volcanism Program (2011).
[b]Prata and Bernardo (2007).
[c]Carn and Prata (2010).
[d]Carn et al. (2009).
[e]Thomas et al. (2011).
[f]Massie et al. (2014).
[g]Yang et al. (2010).

ward transport of volcanic aerosol from the low altitude branch of the BD circulation, carrying aerosol from the Soufriere Hills eruption. Towards the end of 2006, in the build-up to the maximum downward transport to the LMS in December, Rabaul could also have contributed via the shallow branch of the BD. When downward transport increased during the end of 2007, the volcanic aerosol was located at higher altitudes (Vernier et al., 2009) compared to the end of 2006, and it therefore took longer for the volcanic aerosol to be transported to the LMS, resulting in deviations occurring later in the annual cycle than in 2006. The February–August periods for 2008 S/O_3 ratios are clearly elevated, and even more so for C/O_3 ratios compared to 2006 and 2007, in connection with the down-welling of aerosol from the 2006 eruptions of Soufriere Hills and Rabaul.

4.4. *Inter-annual trends*

The trend of increasing concentrations of particulate matter above the LMS, as reported by Hofmann et al. (2009) and Vernier et al. (2011b), should be expected to be visible in the particulate sulphur and/or carbon concentrations also in the LMS. The strong influence on the LMS aerosol from the Kasatochi eruption effectively eliminated the possibility to study background stratospheric aerosol after August 2008 (Martinsson et al., 2009), shown in Fig. 1. Our data have 3 yr of good coverage for the months February to the beginning of August for both sulphur and carbon, in the period 05–08, and for sulphur 2 yr in the period 99–02. This part of the year, which is also the part of the year when the LMS is strongly influenced by air from higher stratospheric altitudes, is used to study the evolution with time of particulate sulphur and carbon concentrations in the LMS. The time dependence of the 'background aerosol' concentration is investigated using Fig. 8a and b, where the averaged concentration ratios of particulate sulphur and carbon to ozone are plotted, for the February–August periods. The years 1999, 2002 and 2005 are excluded as they lack observations for several months, while the data in the February to August periods of the years 2000 and 2001 are combined in one average, because of the small number of data for these years. The observed ratios of S/O_3 and C/O_3 for the February–August periods are increasing from 2006 to 2008. This coincides with the influence from volcanic eruptions on the LMS as discussed above, and also found by Vernier et al. (2011b) in studies of the stratosphere.

The optical measurements on aerosol in the stratosphere used by Hofmann et al. (2009) and Vernier et al. (2011b) do not reveal the chemical composition of particulate matter, but rather capture the average optical effects of the particulate matter in the studied region. The trend revealed from the optical measurements might therefore be more connected to the sum of the concentrations of the major constituents

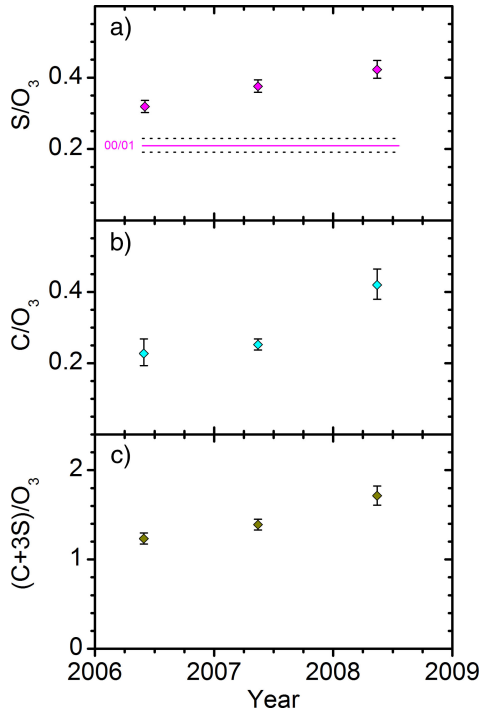

Fig. 8. Geometric average of ratios (a) particulate sulphur (b) carbon and (c) carbon + 3 sulphur concentration to ozone mixing ratio (ng m^{-3} STP $ppbv^{-1}$) for the February–August periods of 2000/2001, 2006, 2007 and 2008.

rather than with individual constituents. Hence, the trend for the sum of the two major components of the LMS aerosol, the carbonaceous and sulphurous fractions, is investigated in Fig. 8c. The sulphurous fraction is assumed to be composed of sulphate, with a mass three times that of sulphur, while the mass of the carbonaceous fraction is represented by the mass of carbon. The ratio of the sum of carbonaceous and sulphurous mass concentrations to ozone $[(C + 3S)/O_3]$ is shown in Fig. 8c for the February–August periods. A significant increase from 2006 to 2008 can be identified. This increase was 30%, with a stronger relative increase for carbon (70%; Fig. 8b) than for sulphur (23%; Fig. 8a).

Overall, a doubling is shown in the S/O_3 from the 2000/2001 to the year 2008 (Fig. 8a). Hofmann et al. (2009) found an increase at 20–25 km altitude of 6.3% $year^{-1}$ in the mid-latitudes (Boulder, 40°N) over the years 2000–2009, corresponding to a total increase of 73%. The differences to our data can be caused by difference in altitude, time period studied or measurement method. The particulate mass

concentrations presented here are particle volume oriented, whereas optical methods are basically particle surface oriented with a complicated response to particle size, shape and chemical composition. Another reason is that the data presented here pertain to the time of the year when the influence from the deep BD branch is strong.

The steady increase in S/O_3 in the LMS (Fig. 8a) combined with the sudden rise in C/O_3 from 2007 to 2008 (Fig. 8b) indicates different compositions for stratospheric aerosol in 2007 than in 2008. A comparison of particulate carbon-to-sulphur-ratios (C/S) for these years, shows a significant difference in the geometric average of 0.66–0.99, with geometric standard deviations of 1.06 and 1.08, respectively (i.e. a 1-sigma-range of 0.62–0.70 and 0.92–1.08). Could this increase in the C/S be an effect of different aerosol compositions from the different volcanic clouds?

The time span for the tropical volcanoes impact on the stratosphere is expected to depend on their penetration depth into the stratosphere. Volcanic clouds reaching high altitudes are expected to affect aerosol via the deep BD branch, while aerosol injected to lower altitudes would follow the shallow branch. Based on CALIPSO observations Vernier et al. (2009) illustrated that aerosol from the Soufriere Hills eruption reached higher altitude (>20 km) compared to that from the Rabaul eruption (≤ 18 km), by the end of 2006. Hence, a larger fraction of the Soufriere Hills aerosol is expected to be transported via the deep branch, whilst the Rabaul aerosol would to a larger extent have been transported to mid-latitudes via the shallow BD branch. As the shallow branch transports air from the tropics to mid-latitudes within months, the deep branch affects the mid-latitude stratosphere after a year or more. The composition of the mid-latitude stratospheric aerosol, down-welling to the LMS in 2007, would thus be more connected to aerosol from the eruption of Rabaul, whereas the main effects of the Soufriere Hills aerosol would be visible during 2008. Studies based on satellite measurements (Stramska, 2009) and models (Spracklen et al., 2008) indicate higher regional organic aerosol concentrations in lower tropospheric air at the time of the Soufriere Hills eruption than for that of Rabaul. The eruption of Rabaul thus had a lower potential to entrain particulate carbon in the volcanic jet and plume. As these two eruptions emitted similar amounts of SO_2 (Table 1) a higher C/S concentration ratio could be expected for the Soufriere Hills eruption in agreement with our observations.

5. Conclusions

The present work is based on measurements of LMS aerosol particle composition sampled by CARIBIC (Civil Aircraft for the Regular Investigation of the atmosphere Based on an Instrument Container, www.caribic-atmospheric.com) in the periods 1999–2002 and 2005–2008. IBA was used to derive detailed elemental concentrations, finding a sulphurous and a carbonaceous component to be dominant. The concentration of the carbonaceous component corresponded on average to approximately 25% of that of the sulphurous, in terms of mass, and could not be explained by forest fires or other types of biomass burning. Stoichiometric O/C ratios of 0.2 and the fact that the measured particulate carbon concentrations greatly exceed literature data on black carbon concentrations indicate that the carbonaceous aerosol is organic in nature.

Particulate sulphur showed a distinct concentration gradient from the tropopause into the mid-latitude LMS. The gradient was strongest during winter and weakest during fall, indicating transport from the stratosphere as the cause of high concentration of particulate sulphur in the LMS. The gradient was also significantly stronger in the period 2005–2008 than in the earlier (1999–2002) period. Variations in the particulate sulphur and carbon concentrations were compared to that of O_3 to track the effect of transport from high altitudes of the stratosphere via the deep Brewer-Dobson branch. That comparison indicated an increased importance for transport of sulphurous aerosol via the shallow BD branch in the period 2005–2008 compared to that of the earlier period, suggesting oxidation of SO_2 as a likely cause for the strengthening of the concentration gradient.

The elevation and the variations in aerosol concentrations in the period 2005–2008 are associated with varying concentrations of particulate matter above the LMS, depending on mainly three volcanic eruptions in the tropics, with plumes reaching the tropical stratosphere. Subsequent transport by the BD circulation then carried the volcanic aerosol to the LMS, resulting in the elevated concentrations of particulate matter observed by CARIBIC in the following years. Entrainment of air from low altitudes, with high concentrations of particulate carbon and organic trace gases, in volcanic jets and plumes is proposed as the cause of high concentrations of particulate carbon in the stratosphere, while sulphur is expected from the volcanic effluents. The eruption in 2006 by Soufriere Hills reached deeper into the stratosphere than Rabaul later the same year, causing a longer duration of the influence from Soufriere Hills. The higher C/S ratios during 2008 could thus be connected with higher concentrations of carbonaceous aerosol at low altitude around the Soufriere Hills volcano.

Comparison of aerosol concentrations in the LMS during the February–August periods of 2006, 2007 and 2008 reveals an increase of 30% from 2006 to 2008. The rate of increase over that period was stronger for carbon (70%) than for the other major constituent sulphur (23%), hence indicating that volcanism had a stronger relative impact on the concentration of carbonaceous than on sulphu-

rous aerosol in the stratosphere, although the increase in the absolute amount of sulphurous aerosol in the form of sulphate was larger than that of the carbonaceous aerosol.

Mass concentrations of sulphurous and carbonaceous aerosol, the two main components in the northern hemisphere mid-latitude LMS aerosol, increased in the period studied here. The former approximately doubled from the period 2000–2001 to the year 2008. This could to a large degree be attributed to intermediate volcanic eruptions in the tropics. Previous studies found an increasing stratospheric aerosol burden above 15 km altitude in the period 2000–2009, which potentially cooled the climate. This study extends these findings to the LMS.

6. Acknowledgements

We especially acknowledge C. Koeppel, D. S. Scharffe, S. Weber and all other members of the CARIBIC project. Lufthansa and Lufthansa Technik are gratefully acknowledged for enabling this scientific experiment. Financial support from the Swedish Research Council and the Swedish Research Council for Environments, Agricultural Sciences and Spatial Planning under grants 621-2007-4639 and 214-2009-613 is gratefully acknowledged.

References

Andersson, S. M., Martinsson, B. G., Friberg, J., Brenninkmeijer, C. A. M., Rauthe-Schöch, A. and co-authors. 2013. Composition and evolution of volcanic aerosol from eruptions of Kasatochi, Sarychev and Eyjafjallajökull in 2008–2010 based on CARIBIC observations. *Atmos. Chem. Phys.* **13**, 1781–1796. DOI: 10.5194/acp-13-1781–2013.

Andreae, M. O., Andreae, T. W., Annegarn, H., Beer, J., Cachier, H. and co-authors. 1998. Airborne studies of emissions from savanna fires in southern Africa. 2. Aerosol chemical composition. *J. Geophys. Res.* **103**, 32119–32128.

Andreae, M. O. and Merlet, P. 2001. Emission of trace gases and aerosols from biomass burning. *Global Biogeocheml. Cycles.* **15**, 955–966.

Appenzeller, C., Holton, J. R. and Rosenlof, K. H. 1996. Seasonal variation of mass transport across the tropopause. *J. Geophys. Res.* **101**, 15071–15078.

Baker, A. K., Slemr, F. and Brenninkmeijer, C. A. M. 2010. Analysis of non-methane hydrocarbons in air samples collected aboard the CARIBIC passenger aircraft. *Atmos. Meas. Tech.* **3**, 311–321.

Bazhenov, O. E., Burlakov, V. D., Dolgii, S. I. and Nevzorov, A. V. 2012. Lidar observations of aerosol disturbances of the stratosphere over Tomsk (56.5 N; 85.0 E) in volcanic activity period 2006–2011. *Int. J. Opt.* **2012**. DOI: 10.1155/2012/786295.

Bourassa, A. E., Robock, A., Randel, W. J., Deshler, T., Rieger, L. A. and co-authors. 2012. Large volcanic aerosol load in the stratosphere linked to Asian monsoon transport. *Science.* **337**, 78–81. DOI: 10.1126/science.1219371.

Brenninkmeijer, C. A. M., Crutzen, P. J., Fischer, H., Güsten, H., Hans, W. and co-authors. 1999. CARIBIC—Civil aircraft for global measurement of trace gases and aerosols in the tropopause region. *J. Atmos. Oceanic Technol.* **16**, 1373–1383.

Brenninkmeijer, C. A. M., Crutzen, P., Boumard, F., Dauer, T., Dix, B. and co-authors. 2007. Civil Aircraft for the regular investigation of the atmosphere based on an instrumented container: the new CARIBIC system. *Atmos. Chem. Phys.* **7**, 4953–4976.

Brewer, A. W. 1949. Evidence for a world circulation provided by the measurements of helium and water vapour distribution in the stratosphere. *Q. J. Roy. Meteorol. Soc.* **75**, 351–363.

Brühl, C., Lelieveld, J., Crutzen, P. J. and Tost, H. 2012. The role of carbonyl sulphide as a source of stratospheric sulphate aerosol and its impact on climate. *Atmos. Chem. Phys.* **12**, 1239–1253. DOI: 10.5194/acp-12-1239-2012.

Bönisch, H., Engel, A., Curtius, J., Birner, T. and Hoor, P. 2009. Quantifying transport into the lowermost stratosphere using simultaneous in-situ measurements of SF6 and CO2. *Atmos. Chem. Phys.* **9**, 5905–5919.

Carn, S. A., Froyd, K. D., Anderson, B. E., Wennberg, P., Crounse, J. and co-authors. 2011. In situ measurements of tropospheric volcanic plumes in Ecuador and Colombia during TC4. *J. Geophys. Res.* **116**, D00J24. DOI: 10.1029/2010JD014718.

Carn, S. A., Krueger, A. J., Krotkov, N. A., Yang, K. and Evans, K. 2009. Tracking volcanic sulfur dioxide clouds for aviation hazard mitigation. *Nat. Hazards.* **51**, 325–343. DOI: 10.1007/s11069-008-92284.

Carn, S. A. and Prata, F. J. 2010. Satellite-based constraints on explosive SO_2 release from Soufrière Hills Volcano, Montserrat. *Geophys. Res. Lett.* **37**, L00E22. DOI: 10.1029/2010GL044971.

Chin, M. and Davis, D. D. 1995. A reanalysis of carbonyl sulfide as a source of stratospheric background sulfur aerosol. *J. Geophys. Res.* **100**, 8993–9005.

Crutzen, P. J. 1976. The possible importance of CSO for the sulfate layer of the stratosphere. *Geophys. Res. Lett.* **3**, 73–76.

Damoah, R., Spichtinger, N., Servranckx, R., Fromm, M., Eloranta, E. W. and co-authors. 2006. A case study of pyro-convection using transport model and remote sensing data. *Atmos. Chem. Phys.* **6**, 173–185.

Deshler, T. 2008. A review of global stratospheric aerosol: measurements, importance, life cycle, and local stratospheric aerosol. *Atmos. Res.* **90**, 223–232.

Deshler, T., Anderson-Sprecher, R., Jäger, H., Barnes, J., Hofmann, D. J. and co-authors. 2006. Trends in the nonvolcanic component of stratospheric aerosol over the period 1971–2004. *J. Geophys. Res.* **111**, D01201. DOI: 10.1029/2005jd006089.

Dessler, A. E., Hintsa, E. J., Weinstock, E. M., Anderson, J. G. and Chan, K. R. 1995. Mechanisms controlling water vapor in the lower stratosphere: "a tale of two stratospheres." *J. Geophys. Res.* **100**, 23167–23172.

Dobson, G. M. B. 1956. Origin and distribution of the polyatomic molecules in the atmosphere. *Proc. R. Soc. London, Ser. A.* **236**, 187–193.

Dutton, E. G. and Bodhaine, B. A. 2001. Solar irradiance anomalies caused by clear-sky transmission variations above Mauna Loa: 1958–99. *J. Clim.* **14**, 3255–3262.

Flury, T., Wu, D. L. and Read, W. G. 2013. Variability in the speed of the Brewer–Dobson circulation as observed by Aura/MLS. *Atmos. Chem. Phys.* **13**, 4563–4575. DOI: 10.5194/acp-13-4563-2013.

Fortuin, J. P. F. and Kelder, H. 1998. An ozone climatology based on ozonesonde and satellite measurements. *J. Geophys. Res.* **103**, 31709–31734.

Fromm, M., Bevilacqua, R., Servranckx, R., Rosen, J., Thayer, J. P. and co-authors. 2005. Pyro-cumulonimbus injection of smoke to the stratosphere: observations and impact of a super blowup in northwestern Canada on 3–4 August 1998. *J. Geophys. Res.* **110**, D08205. DOI: 10.1029/2004JD005350.

Fromm, M., Lindsey, D. T., Servranckx, R., Yue, G., Trickl, T. and co-authors. 2010. The untold story of pyrocumulonimbus. *Bull. Am. Meteorol. Soc.* **91**, 1193–1209. DOI: 10.1175/2010BAMS3004.1.

Fromm, M., Torres, O., Diner, D., Lindsey, D., Vant Hull, B. and co-authors. 2008. Stratospheric impact of the Chisholm pyrocumulonimbus eruption: 1. Earth-viewing satellite perspective. *J. Geophys. Res.* **113**, D08202. DOI: 10.1029/2007JD009153.

Gettelman, A., Holton, J. R. and Rosenlof, K. H. 1997. Mass fluxes of O_3, CH_4, N_2O and CF_2Cl_2 in the lower stratosphere calculated from observational data. *J. Geophys. Res.* **102**, 19149–19159.

Gettelman, A., Hoor, P., Pan, L. L., Randel, W. J., Hegglin, M. I. and co-authors. 2011. The extratropical upper troposphere and lower stratosphere. *Rev. Geophys.* **49**, RG3003. DOI: 10.1029/2011RG000355.

Guan, H., Esswein, R., Lopez, J., Bergstrom, R., Warnock, A. and co-authors. 2010. A multi-decadal history of biomass burning plume heights identified using aerosol index measurements. *Atmos. Chem. Phys.* **10**, 6461–6469. DOI: 10.5194/acp-10-6461-2010.

GVP 2011. Global Volcanism Program. Online at: http://www.volcano.si.edu/index.cfm

Hermann, M., Stratmann, F., Wilck, M. and Wiedensohler, A. 2001. Sampling characteristics of an aircraft-borne aerosol inlet system. *J. Atmos. Ocean. Technol.* **18**, 7–19.

Hoerling, M. P., Schaack, T. K. and Lenzen, A. J. 1991. Global objective tropopause analysis. *Mon. Weather Rev.* **119**, 1816–1831.

Hofmann, D., Barnes, J., O'Neill, M., Trudeau, M. and Neely, R. 2009. Increase in background stratospheric aerosol observed with lidar at Mauna Loa Observatory and Boulder, Colorado. *Geophys. Res. Lett.* **36**, L15808. DOI: 10.1029/2009GL039008.

Hoinka, K. P. 1997. The tropopause: discovery, definition and demarcation. *Meteorol. Z.* **6**, 281–303.

Holton, J. R., Haynes, P. H., McIntyre, M. E., Douglas, A. R., Rood, R. B. and co-authors. 1995. Stratosphere–troposphere exchange. *Rev. Geophys.* **33**, 403–439.

Hoor, P., Fischer, H. and Lelieveld, J. 2005. Tropical and extratropical tropospheric air in the lowermost stratosphere over Europe: a CO-based budget. *Geophys. Res. Lett.* **32**. DOI: 10.1029/2004GL022018.

Hoskins, B. J. 1991. Towards a PV-θ view of the general circulation. *Tellus, Ser AB.* **43**, 27–35.

Intergovernmental Panel on Climate Change. 2007. *Contribution of Working Group I to the Fourth Assessment Report of the Intergovernmental Panel on Climate Change, 2007*. (eds. S. Solomon, et al.). Cambridge University Press, Cambridge, United Kingdom and New York, NY, USA.

Johansson, S. A. E. and Campbell, J. L. 1988. *PIXE: A Novel Technique for Elemental Analysis*. John Wiley, Hoboken, NJ.

Jost, H. J., Drdla, K., Stohl, A., Pfister, L., Loewenstein, M. and co-authors. 2004. In-situ observations of mid-latitude forest fire plumes deep in the stratosphere. *Geophys. Res. Lett.* **31**, L11101. DOI: 10.1029/2003GL019253.

Junge, C. E., Chagnon, C. W. and Manson, J. E. 1961. A world-wide stratospheric aerosol layer. *Science.* **133**, 1478–1479.

Lelieveld, J., Bregman, B., Arnold, F., Bürger, V., Crutzen, P. J. and co-authors. 1997. Chemical perturbation of the lowermost stratosphere through exchange with the troposphere. *Geophys. Res. Lett.* **24**, 603–606.

Lin, P. and Fu, Q. 2013. Changes in various branches of the Brewer–Dobson circulation from an ensemble of chemistry climate models. *J. Geophys. Res.* **118**, 73–84. DOI: 10.1029/2012JD018813.

Martinsson, B. G., Brenninkmeijer, C. A. M., Carn, S. A., Hermann, M., Heue, K. P. and co-authors. 2009. Influence of the 2008 Kasatochi volcanic eruption on sulfurous and carbonaceous aerosol constituents in the lower stratosphere. *Geophys. Res. Lett.* **36**, L12813. DOI: 10.1029/2009GL038735.

Martinsson, B. G., Nguyen, H. N., Brenninkmeijer, C. A. M., Zahn, A., Heintzenberg, J. and co-authors. 2005. Characteristics and origin of lowermost stratospheric aerosol at northern midlatitudes under volcanically quiescent conditions based on CARIBIC observations. *J. Geophys. Res.* **110**, D12201. DOI: 10.1029/2004JD005644.

Martinsson, B. G., Papaspiropoulos, G., Heintzenberg, J. and Hermann, M. 2001. Fine mode particulate sulphur in the tropopause region measured from intercontinental flights (CARIBIC). *Geophys. Res. Lett.* **28**, 1175–1178.

Massie, S. T. 2014. *AURA Cloud/Aerosol/SO2Working Group*. Online at: http://avdc.gsfc.nasa.gov/PDF/volcano.pdf

McCormick, M. P., Thomason, L. W. and Trepte, C. R. 1995. Atmospheric effects of the Mt Pinatubo eruption. *Nature.* **373**, 399–404.

Murphy, D. M., Thomson, D. S. and Mahoney, M. J. 1998. In situ measurements of organics, meteoritic material, mercury, and other elements in aerosols at 5 to 19 kilometers. *Science.* **282**, 1664–1669. DOI: 10.1126/science.282.5394.1664.

Nagai, T., Liley, B., Sakai, T., Shibata, T. and Uchino, O. 2010. Post-Pinatubo evolution and subsequent trend of the stratospheric aerosol layer observed by mid-latitude lidars in both hemispheres. *Sola.* **6**, 69–72. DOI: 10.2151/sola.2010-018.

Neely III, R. R., Toon, O. B., Solomon, S., Vernier, J. P., Alvarez, C. and co-authors. 2013. Recent anthropogenic increases in SO_2 from Asia have minimal impact on stratospheric aerosol. *Geophys. Res. Lett.* **40**, 999–1004. DOI: 10.1002/grl.50263.

Nguyen, H. N., Gudmundsson, A. and Martinsson, B. G. 2006. Design and calibration of a multi-channel aerosol sampler for tropopause region studies from the CARIBIC platform. *Aerosol Sci. Technol.* **40**, 649–655. DOI: 10.1080/02786820600767807.

Nguyen, H. N. and Martinsson, B. G. 2007. Analysis of C, N and O in aerosol collected on an organic backing using internal

blankmeasurements and variable beam size. *Nucl. Instrum. Methods Phys. Res. Sect. B.* **264**, 96–102. DOI: 10.1016/j.nimb.2007.08.001.

Nguyen, H. N., Martinsson, B. G., Wagner, J. B., Carlemalm, E., Ebert, M. and co-authors. 2008. Chemical composition and morphology of individual aerosol particles from a CARIBIC flight at 10 km altitude between 50 N and 30 S. *J. Geophys. Res.* **113**, D23209. DOI: 10.1029/2008JD009956.

Oram, D. E., Mani, F. S., Laube, J. C., Newland, M. J., Reeves, C. E. and co-authors. 2012. Long-term tropospheric trend of octafluorocyclobutane (c-C4F8 or PFC-318). *Atmos. Chem. Phys.* **12**, 261–269. DOI: 10.5194/acp-12-261-2012.

Papaspiropoulos, G., Mentes, B., Kristiansson, P. and Martinsson, B. G. 1999. A high sensitivity elemental analysis methodology for upper tropospheric aerosol. *Nucl. Instrum. Methods Phys. Res. Sect. B.* **150**, 356–362.

Prata, A. J. and Bernardo, C. 2007. Retrieval of volcanic SO_2 column abundance from atmospheric infrared sounder data. *J. Geophys. Res.* **112**, D20204. DOI: 10.1029/2006JD007955.

Rauthe-Schöch, A., Weigelt, A., Hermann, M., Martinsson, B. G., Baker, A. K. and co-authors. 2012. CARIBIC aircraft measurements of Eyjafjallajökull volcanic clouds in April/May 2010. *Atmos. Chem. Phys.* **12**, 879–902. DOI: 10.5194/acp-12-879-2012.

Robock, A. 2000. Volcanic eruptions and climate. *Rev. Geophys.* **38**, 191–219.

Rosen, J. M. 1971. The boiling point of stratospheric aerosols. *J. Appl. Meteorol.* **10**, 1044–1046.

Rudnick, R. L. and Fountain, D. M. 1995. Nature and composition of the continental crust: a lower crustal perspective. *Rev. Geophys.* **33**, 267–309.

Schmale, J., Schneider, J., Jurkat, T., Voigt, C., Kalesse, H. and co-authors. 2010. Aerosol layers from the 2008 eruptions of Mount Okmok and Mount Kasatochi: in situ upper troposphere and lower stratosphere measurements of sulfate and organics over Europe. *J. Geophys. Res.* **115**, D00L07. DOI: 10.1029/2009JD013628.

Schuck, T. J., Brenninkmeijer, C. A. M., Slemr, F., Xueref-Remy, I. and Zahn, A. 2009. Greenhouse gas analysis of air samples collected onboard the CARIBIC passenger aircraft. *Atmos. Meas. Tech.* **2**, 449–464.

Schwarz, J. P., Spackman, J. R., Gao, R. S., Watts, L. A., Stier, P. and co-authors. 2010. Global-scale black carbon profiles observed in the remote atmosphere and compared to models. *Geophys. Res. Lett.* **37**, L18812. DOI: 10.1029/2010GL044372.

Smith, J. B., Hintsa, E. J., Allen, N. T., Stimpfle, R. M. and Anderson, J. G. 2001. Mechanisms for midlatitude ozone loss: heterogeneous chemistry in the lowermost stratosphere? *J. Geophys. Res.* **106**, 1297–1309.

Solomon, S., Borrmann, S., Garcia, R. R., Portmann, R., Thomason, L. and co-authors. 1997. Heterogeneous chlorine chemistry in the tropopause region. *J. Geophys. Res.* **102**, 21411–21429.

Solomon, S., Daniel, J. S., Neely, R. R., Vernier, J. P., Dutton, E. G. and co-authors. 2011. The persistently variable "background" stratospheric aerosol layer and global climate change. *Science*. **333**, 866–870. DOI: 10.1126/science.1206027.

Spracklen, D. V., Arnold, S. R., Sciare, J., Carslaw, K. S. and Pio, C. 2008. Globally significant oceanic source of organic carbon aerosol. *Geophys. Res. Lett.* **35**, L12811.

Sprenger, M. and Wernli, H. 2003. A northern hemispheric climatology of cross-tropopause exchange for the ERA15 time period (1979–1993). *J. Geophys. Res.* **108**(D12), 8521. DOI: 10.1029/2002JD002636.

Sprung, D. and Zahn, A. 2010. Acetone in the upper troposphere/lowermost stratosphere measured by the CARIBIC passenger aircraft: distribution, seasonal cycle, and variability. *J. Geophys. Res.* **115**, D16301. DOI: 10.1029/2009JD012099.

Stramska, M. 2009. Particulate organic carbon in the global ocean derived from SeaWiFS ocean color. *Deep Sea Res. Part I.* **56**, 1459–1470.

Tang, Q., Prather, M. J. and Hsu, J. 2011. Stratosphere–troposphere exchange ozone flux related to deep convection. *Geophys. Res. Lett.* **38**, L03806. DOI: 10.1029/2010GL046039.

Thomas, H. E., Watson, I. M., Carn, S. A., Prata, A. J. and Realmuto, V. J. 2011. A comparison of AIRS, MODIS and OMI sulphur dioxide retrievals in volcanic clouds. *Geomatics Nat. Hazards Risk*. **2**(3), 217–232. DOI: 10.1080/19475705.2011.564212.

Trickl, T., Giehl, H., Jäger, H. and Vogelmann, H. 2013. 35 yr of stratospheric aerosol measurements at Garmisch-Partenkirchen: from Fuego to Eyjafjallajökull, and beyond. *Atmos. Chem. Phys.* **13**, 5205–5225. DOI: 10.5194/acp-13-5205-2013.

Vernier, J. P., Pommereau, J. P., Garnier, A., Pelon, J., Larsen, N. and co-authors. 2009. Tropical stratospheric aerosol layer from CALIPSO lidar observations. *J. Geophys. Res.* **114**, D00H10. DOI: 10.1029/2009JD011946.

Vernier, J. P., Thomason, L. W. and Kar, J. 2011a. CALIPSO detection of an Asian tropopause aerosol layer. *Geophys. Res. Lett.* **38**, L07804. DOI: 10.1029/2010GL046614.

Vernier, J. P., Thomason, L. W., Pommereau, J. P., Bourassa, A., Pelon, J. and co-authors. 2011b. Major influence of tropical volcanic eruptions on the stratospheric aerosol layer during the last decade. *Geophys. Res. Lett.* **38**, L12807. DOI: 10.1029/2011GL047563.

Weisenstein, D. K., Yue, G. K., Ko, M. K. W., Sze, N. D., Rodriguez, J. M. and co-authors. 1997. A two-dimensional model of sulfur species and aerosols. *J. Geophys. Res.* **102**, 13019–13035.

Yang, K., Liu, X., Bhartia, P. K., Krotkov, N. A., Carn, S. A. and co-authors. 2010. Direct retrieval of sulfur dioxide amount and altitude from spaceborne hyperspectral UV measurements: theory and application. *J. Geophys. Res.* **115**, D00L09.

Zahn, A. and Brenninkmeijer, C. A. M. 2003. New directions: a chemical tropopause defined. *Atmos. Environ.* **37**, 439–440.

Zahn, A., Brenninkmeijer, C. A. M., Asman, W. A. H., Crutzen, P. J., Heinrich, G. and co-authors. 2002. Budgets of O_3 and CO in the upper troposphere: CARIBIC passenger aircraft results 1997–2001. *J. Geophys. Res.* **107**(D17), 4337. DOI: 10.1029/2001JD001529.

Zahn, A., Weppner, J., Widmann, H., Schlote-Holubek, K., Burger, B. and co-authors. 2012. A fast and precise chemiluminescence ozone detector for eddy flux and airborne application. *Atmos. Meas. Tech.* **5**. DOI: 10.5194/amt-5-363-2012.

Paper III

Atmos. Meas. Tech., 7, 2581–2596, 2014
www.atmos-meas-tech.net/7/2581/2014/
doi:10.5194/amt-7-2581-2014

Atmospheric Measurement Techniques
Open Access

Comparison between CARIBIC Aerosol Samples Analysed by Accelerator-Based Methods and Optical Particle Counter Measurements

B. G. Martinsson[1], J. Friberg[1], S. M. Andersson[1], A. Weigelt[2,*], M. Hermann[2], D. Assmann[2], J. Voigtländer[2], C. A. M. Brenninkmeijer[3], P. J. F. van Velthoven[4], and A. Zahn[5]

[1]Division of Nuclear Physics, Lund University, Lund, Sweden
[2]Leibniz Institute for Tropospheric Research, Leipzig, Germany
[3]Division of Atmospheric Chemistry, Max Planck Institute for Chemistry, Mainz, Germany
[4]Royal Netherlands Meteorological Institute (KNMI), De Bilt, The Netherlands
[5]Institute of Meteorology and Climate Research, Forschungszentrum Karlsruhe, Karlsruhe, Germany
[*]now at: Institute for Coastal Research, Helmholtz-Zentrum Geesthacht, Geesthacht, Germany

Correspondence to: B. G. Martinsson (bengt.martinsson@nuclear.lu.se)

Received: 5 February 2014 – Published in Atmos. Meas. Tech. Discuss.: 1 April 2014
Revised: 4 July 2014 – Accepted: 10 July 2014 – Published: 19 August 2014

Abstract. Inter-comparison of results from two kinds of aerosol systems in the CARIBIC (Civil Aircraft for the Regular Investigation of the atmosphere Based on a Instrument Container) passenger aircraft based observatory, operating during intercontinental flights at 9–12 km altitude, is presented. Aerosol from the lowermost stratosphere (LMS), the extra-tropical upper troposphere (UT) and the tropical mid troposphere (MT) were investigated. Aerosol particle volume concentration measured with an optical particle counter (OPC) is compared with analytical results of the sum of masses of all major and several minor constituents from aerosol samples collected with an impactor. Analyses were undertaken with the following accelerator-based methods: particle-induced X-ray emission (PIXE) and particle elastic scattering analysis (PESA). Data from 48 flights during 1 year are used, leading to a total of 106 individual comparisons. The ratios of the particle volume from the OPC and the total mass from the analyses were in 84 % within a relatively narrow interval. Data points outside this interval are connected with inlet-related effects in clouds, large variability in aerosol composition, particle size distribution effects and some cases of non-ideal sampling. Overall, the comparison of these two CARIBIC measurements based on vastly different methods show good agreement, implying that the chemical and size information can be combined in studies of the MT/UT/LMS aerosol.

1 Introduction

The particles of the atmospheric aerosol have a broad spectrum of sources, where the anthropogenic contribution often can be difficult to quantify due to influences from natural sources at background conditions (Andreae and Rosenfeld, 2008). Despite being trace constituents of the atmosphere, particles are of considerable concern, such as adverse health effects and premature deaths (Pope III and Dockery, 2006) and climate change (IPCC, 2013), where in the latter case the direct and indirect effects of atmospheric particles can act as to mask the climate impact of greenhouse gases (Schwartz et al., 2010).

In this study the aerosol at 9–12 km altitude is investigated, thus dealing with the upper troposphere (UT) and the lowermost stratosphere (LMS) in the extratropics and the middle troposphere (MT) in the tropics. The vast majority of all studies of atmospheric aerosol concerns surface conditions. Aircraft measurements and remote sensing from the surface (Mattis et al., 2010) or from satellites, such as the NASA satellite CALIPSO (Vernier et al., 2011), are used to study the aerosol at higher altitudes. Besides information on scattered intensity for a given wavelength, multi-wavelength measurements combined with assumptions on particle composition and shape has been used to estimate particle size distribution in the 0.1 to above 1 µm diameter range (Bauman et

al., 2003). Smaller particles cannot be detected by remote sensing, and therefore also most of the aerosol dynamics cannot be studied. In addition, aerosol chemical information is normally not available by remote sensing except in very special circumstances (Rinsland et al., 1994). Remote sensing thus needs to be complemented by in situ observations of particle size distributions and composition in order to study sources and processes forming the aerosol. Research aircraft and balloons have been used for in situ studies of particle formation (de Reus et al., 1998), particle size distributions (Deshler et al., 2003) and particle chemical composition (Huebert et al., 2004). Based on the use of in-service passenger aircraft, long-term aerosol observations have been undertaken from the CARIBIC (Civil Aircraft for the Regular Investigation of the atmosphere Based on a Instrument Container) platform for the years 1997–2002 and 2005 to present (Brenninkmeijer et al., 1999, 2007) concerning particle chemical composition (Martinsson et al., 2001) and particle number concentrations (Hermann et al., 2003).

Aerosol particles in the 9–12 km altitude region contain a significant fraction of sulfurous aerosol (Dibb et al., 2000; Xu et al., 2001; Martinsson et al., 2001, 2005; Kojima et al., 2004). The carbonaceous fraction is another major component of the aerosol in this region (Murphy et al., 1998, 2006; Nguyen et al., 2008, Friberg et al., 2014). Black carbon constitutes a small fraction of the total carbon (Schwarz et al., 2010; Friberg et al., 2014). Occasionally chemical elements connected with crustal matter and fires are observed (Papaspiropoulos et al., 2002), which on rare occasions can have a strong influence on aerosol particle concentration (Eguchi et al., 2009; Dirksen et al., 2009; Fromm et al., 2010). Particles from explosive volcanism have strong effects on the studied region at times, affecting the climate (Ammann et al., 2003; Solomon et al., 2011), stratospheric ozone (McCormick et al., 1995) and aviation (Gislason et al., 2011). The aerosol particles in volcanic clouds contain besides the ash component (Schumann et al., 2011; Andersson et al., 2013) large sulphurous and carbonaceous components (Martinsson et al., 2009; Schmale et al., 2010; Carn et al., 2011).

The size distribution of the aerosol in the lowermost stratosphere is also strongly influenced by volcanism (Bauman et al., 2003). Hervig and Deshler (2002) compared balloon-borne optical particle counter (OPC) measurements with satellite-based measurements of extinction for several wavelengths from SAGE II and HALOE and found good agreement during periods of strong volcanic influence, whereas the OPC registered considerably higher particle surface area than the satellites during periods with little volcanic influence.

The study presented here deals with two very different CARIBIC aerosol measurements. Particle volume is obtained by integrating the size distributions obtained from an OPC. Subsequently these results are compared with the aerosol mass from samples that were analysed with PIXE (particle-induced X-ray emission) and PESA (particle elastic scattering analysis) for concentrations of all major and several minor chemical elements. Together these different measurements can deepen our understanding of the atmospheric aerosol by this combination of chemical and physical information. However, to reach that goal an assessment of the degree of agreement between the two measurements is needed. Therefore this paper is devoted to the comparison of the total particle volume concentration obtained from the CARIBIC OPC and the total mass concentration obtained from the analyses of the CARIBIC aerosol samples.

2 Methods

The measurements presented here were undertaken from the CARIBIC observatory (Brenninkmeijer et al., 2007; www.caribic-atmospheric.com/) where a large number of trace gases are measured and aerosol particles are characterized with respect to size distribution and composition during monthly sets of usually four intercontinental flights at 9–12 km altitude. The CARIBIC system comprises an instrumented container that is connected to a multiple probe inlet system for trace gases and aerosol that is permanently mounted on the belly of a Lufthansa Airbus A340-600. Concentrations of CO, O_3, NO/NO_y, VOCs, gaseous and condensed water are determined, and air samples collected are analysed for greenhouse gases, hydro and halo carbons (Brenninkmeijer et al., 2007; Schuck et al., 2009; Baker et al., 2010; Oram et al., 2012). Aerosol particle number concentration measurements down to a diameter of 4 nm are undertaken with three condensation particle counters (CPC, TSI model 7610; Hermann et al., 2003), and for the particle size distribution in the diameter range $\sim$130–$\sim$1000 nm a 16-channel OPC (RION, KS-93) is used (Rauthe-Schöch et al., 2012). Furthermore, aerosol samples are collected for subsequent analysis with respect to all major and several minor constituents (Martinsson et al., 2001; Nguyen et al., 2006; Nguyen and Martinsson, 2007). Details of the inlet system are described by Brenninkmeijer et al. (2007). The efficiency of the aerosol inlet is estimated to be 60 % for 5 µm diameter particles (Rauthe-Schöch et al., 2012). Based on modelling and previous experience the efficiency of the inlet is estimated to exceed 90 % for particles in the size range 0.01–1 µm diameter.

This comparison of the CARIBIC OPC and the analytical results obtained from the aerosol sampler span 1 year from April 2011 to March 2012. The measurements were undertaken during flights from Frankfurt in Germany to northern South America (24 flights), western North America (14), the Indian subcontinent (8) and eastern Asia (2), thus spanning a large region from 120° W to 120° E and 10 to 75° N. The average flight altitude was 10 900 m with a span of 9500 to 11 900 m. For those samples collected in clouds the average air temperature was below 230 K, implying that the

clouds were dominated of ice particles (Koop et al., 2000; Rosenfeld and Woodley, 2000). The meteorological modelling along the CARIBIC flight paths indicates that each sample affected by clouds encountered hydrometeors that in most cases consisted to 100 % of ice, the lowest fraction of ice being 99 % (http://www.knmi.nl/samenw/campaign_support/CARIBIC/). This is consistent with measured temperatures.

The aerosol sampling requires the longest sampling time of the two methods, thereby determining the amount of data available. For the investigated period of 1 year, 153 aerosol samples are available. This number available for comparison is lower by constraints that, of course, OPC data should be available and that uncertainties in total mass due to detection limit should be within ±5 % (described below). In addition, clouds were found to seriously affect the comparison. Therefore also measurements of gaseous and total water concentrations should be available for identification of samples collected in cloudy conditions. These requirements together reduce the number of samples available for the comparison to 106. The OPC – aerosol sampler intercomparison primarily deals with the integrated particle volume concentration obtained from the OPC (C_V) and the total aerosol mass concentration obtained as the sum of all major and several minor constituents of the aerosol samples (C_m).

2.1 Aerosol sampling and analysis

CARIBIC aerosol samples are collected by impaction on a 0.2 µm polyimide film, Proline-10, from Moxtek Inc., Orem, Utah, USA. The sampling unit contains three kinds of nozzles. Here nozzles connected the 14 channels that were sequentially activated for sampling and subsequent PIXE/PESA (Particle-Induced X-ray Emission/Particle Elastic Scattering Analysis) analysis were used. The typical sampling time for each sequential sample is 100 min. The collection efficiency of the sampler is 97 % ± 4 % for particles with aerodynamic diameter larger than 0.2 µm, and the 50 % cut-off diameter is 0.08 µm (Nguyen et al., 2006).

A cyclone separator placed up-stream of the sampler limits the upper particle size to 2 µm aerodynamic diameter. The penetration of the cyclone by particles smaller than 1 µm diameter has been measured to be 100 % ± 3 % (Nguyen et al., 2006). This cyclone is used exclusively for the aerosol sampler, implying that the OPC, to be described below, does not have the same definition of the upper size limit.

The collected samples were analysed for elemental composition by ion beam analysis (IBA). For sulphur (S) and elements with larger atomic number PIXE is used (Johansson and Campbell, 1988). The lower limit of the PIXE analysis of this study with respect to atomic number is connected with spectral interference, see Andersson et al. (2013) for further details. Hydrogen (H), carbon (C), nitrogen (N) and oxygen (O) are analysed by PESA. The analytical setup has been optimised with respect to sampling substrate and analytical parameters for PIXE (Papaspiropoulos et al., 1999) and PESA (Nguyen and Martinsson, 2007). During the time period of this study the detection efficiencies (i.e. the fraction of the samples where the element was detected) for H, C, N, O and S were 100, 96, 82, 95 and 100 %. Minor constituents were detected less frequently, like for instance potassium (K) 41 %, iron (Fe) 44 % and nickel (Ni) 30 %. The accuracy of the analyses is estimated to 10 % (Papaspiropoulos et al., 2002; Nguyen and Martinsson, 2007).

The total aerosol mass concentration (in ng m^{-3} STP; standard temperature and pressure) was obtained as the sum of all elemental mass concentrations. An element that was not detected in a sample was represented by the half of its minimum detection limit (MDL) which was added to the sum of the elements. When more than 5 % of that sum was from undetected elements (represented by half the MDL) the measurement was discarded, implying that the total mass concentration given has a ±5 % uncertainty due to elemental concentrations below the MDL. This requirement implied that only samples with detection of all the five major elements, H, C, N, O and S, were selected for this analysis. Uncertainties slightly larger than 5 % could appear for samples with a significant crustal component because some of the crustal elements, most notable silicon, are not analysed with adequate detection limits. This could lead to an underestimation of the crustal component by approximately 41 % according to average crust composition (Weaver and Tarney, 1984). For the two samples with the largest mass fractions of crust, containing 22 and 13 %, respectively, the total mass concentration could thus be underestimated by 9 and 5 %, respectively.

Combining the uncertainties of the sampling efficiency (4 and 3 %), elemental analysis (10 %) and effects from the minimum detection limit (5 %) the combined uncertainty of the mass concentration obtained from sampling and analysis becomes 12 %.

The aerosol sampler has demonstrated excellent properties in calibration procedures (Nguyen et al., 2006). Calibration results were obtained using liquid aerosol consisting of dioctyl serbacate (DOS) with traces of uranine. The performance of impactors is, however, sensitive to particle material as well as the amount of mass deposited. Solid particles can bounce off the sampling substrate, and in that way be lost. Bounce-off can be counteracted by the use of a coating of the impaction surface. Pak et al. (1992) showed that a coating of Apiezon-L grease needs to be more than 9 µm thick to obtain close to 100 % impactor collection efficiency for solid particles, whereas silicon oil shows more promising properties with rather high efficiency at 0.3 µm thickness. However, applying such a thickness would result in a factor of 2.5 thicker sampling substrate causing typically a factor 1.6 worse PIXE detection limits (if contamination in the coating process can be avoided). The effect on carbon detection can be expected to be much stronger, because the coating thickness variance will be added to that of the polyimide film which is low (Nguyen and Martinsson, 2007). Given the usually low

UT/LMS aerosol concentrations and the short sampling time, minimum detections limits are very important. Therefore no coating of the impaction surface was used. This should not be seen as a general recommendation, but rather as an adaption to a special measurement situation with respect to required detection limits and properties of MT/UT/LMS particles. Overloaded impactor substrates could suffer blow-off, where a sizable fraction of a solid or semi-solid deposit is blown away from the impaction zone. Impactors overloaded with liquid particles may wet the surface of the sampling substrate, causing a drift of deposited material away from the impaction region. Mass deposited away from this region might be outside the area where the analytical beam impinges on the sample. That mass will not interact with the beam thus causing too low measured concentrations.

In order to study the influence from the distorting effects on the aerosol samples of this study, all the 106 samples were photographed using a Canon EOS 550D with an EFS 15–85 mm lens. A photodiode placed behind the sample was used for illumination. The images were systematically evaluated based on the appearance of the deposit. Evidence of bounce-off could be found for one group of samples. Liquid samples wetting the surface outside the impaction region could also be observed, whereas no signs of large features at the outer part of the sample indicative of blow-off were obtained from any of the samples. Each of the four orifices of the impactor nozzle should produce a deposit, thus causing a square pattern of four deposits with a distance of 0.9 mm to the centre of the sampling substrate. The samples were classified in four basic groups. The first group, type 1, contains samples with no deviation from the ideal appearance, see Fig. 1a. Some samples contain low amounts of deposited mass, making identification of secondary deposition pattern more difficult. Type 1 samples are subdivided in normal (type 1.1) and low-loaded (1.2) samples. Frequently thin filaments of deposit stretching outside the regular impaction area were found (type 2, Fig. 1b). The type 2 samples are subdivided according to (2.1) wetting only inside the analytical beam area, (2.2) minor wetting outside the beam area and (2.3) considerable wetting outside the beam area. When the impactor jet meets the sampling surface the air flows out over the surface in all directions. Because of the fact that the present impactor contains four jets this outflow causes an interaction between the jets, causing secondary deposition of bounce-off-particles in between the ordinary deposition area. This is manifested by a deposition spot in the centre (Fig. 1c). In some cases a cross can be discerned, marking the outflow path of air from the central area. These type 3 samples were subdivided into three categories: (3.1) central spot discerned, (3.2) cross discerned and (3.3) cross clearly visible, in expected order of increasing severity of the bounce-off problem observed. Several images reveal tiny spots outside the central deposition area. This could be caused by imperfection of the polyimide film or it could be single particles that have bounced. A few samples have a large number of tiny spots outside the regular deposition area. When the number of spots over the 16 mm diameter polyimide film exceeded 15, the samples were classified as type 4. Otherwise they were classified according to the appearance of central deposit. An example of these type 4 samples is shown in Fig. 1d.

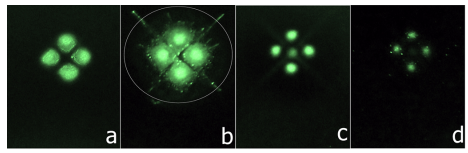

Figure 1. Photographic images of aerosol deposits from the CARIBIC aerosol sampler, where particles are collected from four impactor orifices. **(a)** Type 1: four spots of deposit (detected mass 100 ng). **(b)** Type 2: thin filaments of liquid aerosol out from the main deposit (670 ng). **(c)** Type 3: four spots and a secondary deposition pattern (92 ng). **(d)** Type 4: several small spots outside the deposition area (32 ng). The ellipse in **(b)** illustrates the beam size which is 5.5 mm vertically and 5.5/cos(23°) horizontally.

The different deposition types were summarized by a qualitative indicator (QI) expressing qualitatively the problem with losses for each sample based on the deposition pattern. QI = 0 are the samples where no significant losses are expected. The deposit types with QI = 0 are 1.1, 1.2, 2.1 and 2.2. Samples indicating discernible losses (QI = 1) comprise only type 3.1 samples. Sample deposits indicating more serious losses (QI = 2) include deposit types 2.3, 3.2, 3.3 and 4. Classification in these main and sub categories will be used in the evaluation of the comparison between the sampler and OPC.

To further substantiate the findings from images of the samples, use will be made of results from the elemental analysis itself. All samples are analysed in two steps, the first with a large ion beam area (5.5 mm diameter with beam current 150 nA and duration of 200 s per sample) used only for quantitative PIXE analysis. The second method, used for relative PIXE and PESA analyses, is based on a small beam (1 mm diameter). This small-beam analysis is based on three irradiations (beam current 15 nA with duration 3×200 s per sample), one over the aerosol deposit and two blank irradiations outside the main deposit area of the impactor at 4 mm distance from the deposit centre at opposite sides (Nguyen and Martinsson, 2007). These two internal blank measurements can be utilized to obtain an estimate of aerosol deposit outside the 5.5 mm diameter beam of the quantitative PIXE analysis. They should represent an area from the outer bound of the large beam to an outer bound where half of this doughnut area is inside a 4 mm radius. A circle with 4 mm radius has approximately twice the area of the beam in the slightly tilted sample plane (23°). Adding the same surface area outside the 4 mm radius, the blank spots can be

seen as to represent an area twice the size of the large beam, between diameters 5.5 and 9.5 mm. The estimated mass deposited is the areal density of an element (in ng cm^{-2}) multiplied with the surface area. To estimate non-ideal deposition outside the primary impactor deposition area the ratio between the mass deposited between 5.5 and 9.5 mm diameter (m_{udet}) and the mass detected in the quantitative analysis within 5.5 mm diameter (m_{det}) is formed. This ratio can only be formed for elements detected with PIXE because of the strong signal of H, C, N and O from the polyimide sampling substrate. The major aerosol constituent sulphur is detected with PIXE, and will therefore serve as the element used for estimation of deposition outside the main deposition area of the impactor. From Fig. 1c it is clear that secondary deposition is inhomogeneous in the vicinity of the impactor jets. It is not clear to what degree the secondary deposition pattern reaches outside the irradiated area of the sample. Therefore the m_{udet} / m_{det} ratios should be treated with some caution, especially for sample types 3.2 and 3.3. Additionally, this ratio only describes the aerosol components internally mixed with the sulphate aerosol. Components of other size modes, like crustal particles, may behave differently, as will be shown in Sect. 3.1. Samples with QI = 0, i.e. samples showing no visible imperfections in the deposition pattern, have m_{udet} / m_{det} ratios narrowly distributed around 0.03 indicating that 3 % of the aerosol deposit was outside the 5.5 mm ion beam used in the quantitative PIXE analysis. All samples were therefore corrected by that percentage to account for regular deposition outside the analysed area.

The analyses of the aerosol samples are undertaken in high vacuum of approximately 10^{-5} hPa. The samples remain at this pressure for 6 h, the duration of both analytical steps for a batch of 21 samples. This will cause losses of chemical compounds with a vapour pressure larger than the order of 10^{-7} Pa at room temperature (Martinsson, 1987; Deiters and Randzio, 2007). The main aerosol components observed in the analysed UT/LMS samples over the years are sulphurous and carbonaceous components, but sometimes also a significant crustal component can be observed. The sulphate compounds common in the atmosphere are not lost during analysis when particles, like in this study, are deposited onto a thin substrate, unless an external heating source is used (Martinsson and Hansson, 1988; Mentes et al., 2000). Among other common inorganic salts of the atmospheric aerosol, sodium chloride is stable during analysis, whereas ammonium nitrate will evaporate, if present. The occasional crustal component is expected to remain in the sample during analysis. The atmospheric carbonaceous aerosol component contains a broad range of vapour pressures. Therefore a definition of what is analysed is of need (Martinsson, 1987). In this case the IBA analytical definition most likely deviates from that during the OPC measurements, implying that the amount of carbonaceous aerosol determined by IBA could be smaller than the amount present during the OPC measurements.

2.2 Optical particle counter

For CARIBIC, a KS-93 OPC (RION CO., Ltd., Japan) was modified and applied for the first time onboard aircraft. The KS-93 has a diode laser with 830 nm wavelength, a lower detection limit of about 120 nm particle diameter, a robust synthetic quartz optical cell and is relatively small in size ($135 \times 280 \times 150$ mm), which makes it all well suited for airborne atmospheric research. The modified OPC is mounted together with the flow control system and the data acquisition in a 19″ rack unit. For data analysis the signals of the three OPC internal amplifiers are recorded with a real-time data acquisition system (PXI, National Instruments, USA) with 3 µs resolution. As the signal of one particle has an average duration of about 60 to 90 µs, each pulse is resolved with 20 to 30 data points. This data acquisition allows a free choice of the sampling time and number of channels. For the present analysis particle pulse heights were sorted into 16 channels and averaged over 300 s. For CARIBIC, the KS-93 signal output is improved by applying particle free sheath air (0.135 L min^{-1}) around the aerosol sampling air (0.015 L min^{-1}). In this configuration the CARIBIC OPC yields reliable data for particles larger than about 130 nm (optical diameter). The largest particle diameter which can be size-resolved is between 1.0 and 1.3 µm and depends on the particle refractive index and the respective calibration curve. However, as can be seen in Fig. 8, most of the volume distributions in the UT/LMS have their maximum in the particle size range between 300 and 600 nm. Hence the analysis in this study does not strongly depend on the OPC upper particle diameter limit. For the present analysis a theoretical response function based on spherical particles and the Mie theory was used (van de Hulst, 1981; Bohren and Huffman, 1983). This curve was related to the signal output by calibrating the OPC with latex and ammonium sulfate particles in the laboratory. Note that the OPC also counts particles larger than the upper size limit, but cannot determine their exact size. These particles are assigned to the largest particle size channel, which is therefore biased and not used in the analysis here. Uncertainties of the OPC data evaluation originate mainly from the "unknown", hence to be estimated particle refractive index, and the accuracy of the sampling air flow. They amount to ~ 10 % in particle size and ~ 19 % for the particle number concentration. Due to the cubed dependence of the particle volume on diameter the combined uncertainty of C_{V} becomes 50 %. For CARIBIC, the refractive index was calculated using literature values of the UT particle chemical composition (44 % H_2SO_4, 44 %, $(NH_4)_2SO_4$, 10 % organic carbon and 2 % soot) and a mixing rule to $1.479–0.0143i$. This refractive index was applied for the whole OPC size range. Additional information of the OPC unit is given in Rauthe-Schöch et al. (2012).

2.3 Additional methods

Besides the data from the OPC and the aerosol sampler, measurements of water are used to identify measurements that were influenced by clouds. The CARIBIC inlet system houses a forward-facing inlet tube for total water (H_2O_{tot}; being the sum of cloud water/ice and gaseous water) and one sideways-facing inlet tube for gaseous water (H_2O_{gas}) only. These two inlet lines are connected with two water vapour sensors, a chilled mirror frost point hygrometer (FPH) measuring total water (time resolution 10–180 s) and a two-channel photoacoustic laser spectrometer (PAS) detecting H_2O_{tot} and H_2O_{gas} (time resolution: $\sim$ 5 s). The PAS data are calibrated post-flight using the FPH data showing a total uncertainty of approximately 0.5 K (verified by regular laboratory-based cross-checks to high precision FHP instrument MWB LX-373). The calibrated PAS data have a precision of 2 % or 0.5 ppmv (whichever is higher).

We use the dynamical tropopause to differentiate between tropospheric and stratospheric air. This tropopause is based on the strong gradient in potential vorticity (PV) in the tropopause region (Hoerling et al., 1991; Hoinka, 1997). The PV along the flight track was obtained from archived European Centre for Medium-Range Weather Forecasts (ECMWF) analyses with a resolution of 1×1 degree in the horizontal and at 91 vertical hybrid sigma-pressure model levels. The PV was interpolated linearly in longitude, latitude, log pressure and time to the position of the aircraft. Based on PV, air masses were classified as tropospheric for average PV < 1.5 PVU (potential vorticity units; 1 PVU = 10^{-6} K m^2 kg^{-1} s^{-1}), and as belonging to the tropopause region for 1.5 < PV < 3 PVU. The samples taken in the LMS are subdivided in three groups of varying depth into the LMS, 3–5 PVU, 5–7 PVU and measurements taken in air masses with PV > 7 PVU.

3 Results and discussion

The primary measure used in the comparison between the OPC and the aerosol samples is the ratio of the OPC particle volume concentration (C_V) to the total mass concentration (C_m) obtained as the sum of the elemental concentrations from PIXE and PESA analysis of the aerosol samples. Figure 2 shows the 1 year data used to evaluate the relative performance of the two methods that are based on completely different physical principles. From the distribution it is clear that a large fraction of the measurements (85 %) have C_V / C_m ratios from 0.55 to 1.55 cm^3 g^{-1}. Out of the 106 samples 14 were found to have C_V / C_m ratios larger than the 1.55 cm^3 g^{-1} upper limit of this range and three were below the lower limit. The causes contributing to these 17 outliers will be investigated next.

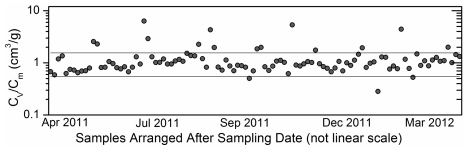

Figure 2. One year time series from CARIBIC measurements of the ratio of aerosol elemental concentrations from samples analysed with PIXE and PESA (C_m) and particle volume concentrations obtained from the OPC (C_V).

3.1 Examination of outlying data points

To shed light on the causes of outlying C_V / C_m ratios, the measurement situation, elemental composition features, size distribution and aerosol sample deposit patterns will be scrutinized. First the special case of sampling in clouds will be studied. Based on the CARIBIC measurements of gaseous and total water mixing ratios, intercepted clouds are detected (Brenninkmeijer et al., 2007). Figure 3a shows the C_V / C_m ratio related to the cloud ice concentration. Approximately half of the samples were obtained without any contact with clouds. The degree of cloud contact of the other samples varies strongly (note the logarithmic scale). When the cloud ice concentration is high, several measurements show high C_V / C_m ratio. The aerosol inlet is designed to collect particles of a few micrometre in diameter or smaller. When the inlet approaches particles at a cruise speed of 230 m s^{-1}, large particles that hit the leading edge of the shroud or, less likely the inlet cone itself, can disintegrate adding artifactual particles to the sampling airstream (Korolev et al., 2011). Because the leading edges and rim of the CARIBIC inlet have a surface-coating of nickel, we evaluated the connection between nickel elemental concentration and cloud ice concentrations. Figure 3b demonstrates a strong correlation for cloud ice concentration above 5 ppmv with aerosol sample nickel mass fractions larger than 0.05 %, indeed showing that, besides break-up of ice particles, the inlet contributes nickel when measuring inside clouds. This group of 10 samples will be further investigated, starting with photographic images of the aerosol samples to inspect the deposition patterns of the samples.

Out of this group of 10 instances four occurred in the tropics, five in the extra-tropical UT and one in the tropopause region. Figure 4a contains indeed a very incoherent message on the connection between deposition pattern and cloud influence or C_V / C_m ratio. Four of the samples show clear signs of losses based on a non-ideal deposition pattern (QI = 2; one type 3.2 and three type 4), four show traces of secondary deposition and the remaining two samples are classified as QI = 0 samples. The two samples most affected by clouds, sample No. 1 and 2, have deposition pattern type 4. They also have the two highest C_V / C_m ratios. The type 4 samples

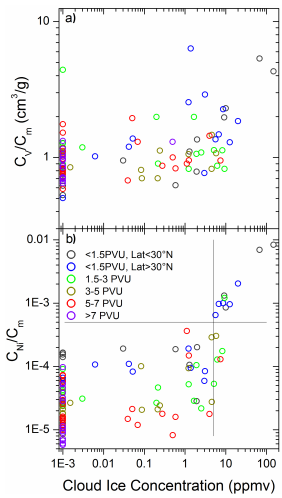

Figure 3. (a) Dependence of the ratio of particle volume to mass concentrations from OPC and IBA measurements (C_V / C_m), respectively, on average cloud ice concentration during each sampling period. **(b)** The latter related to the mass fraction of nickel in the samples. Note, in order to display zero cloud ice concentration in the logarithmic scale, 10^{-3} ppmv was added to each data point.

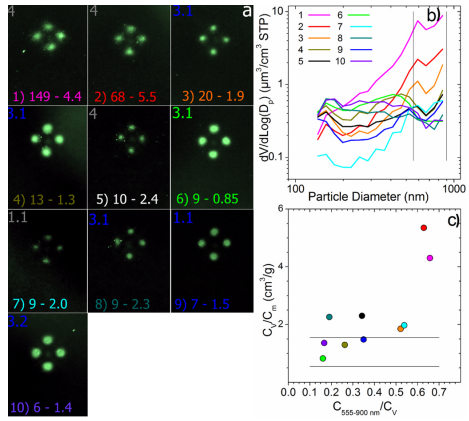

Figure 4. (a) Aerosol deposition pattern for samples affected by ice clouds. Numbers on bottom of pictures are measurement number, cloud ice concentration (ppmv) and OPC volume to IBA mass concentration ratio (C_V / C_m; cm^3 g^{-1}). The numbers in the top left corners show the aerosol deposit classification and their colour indicates air mass type according to the legend of Fig. 3. **(b)** Particle volume size distribution for measurements affected by clouds. Numbers in legends are measurement numbers in **(a)**. **(c)** C_V / C_m related to particle volume fraction in the four OPC channels of the largest sizes (555–900 nm). The colour of distributions in **(b)** and markers in **(c)** corresponds to bottom text colours in **(a)**.

are, as will be shown later, rather unusual, suggesting that the artefact particles generated at the inlet have a high probability for bounce-off and become spread over the surface. The volume size distributions of Fig. 4b are typical of artefactual particles due to particle break-up in clouds and do not appear in the absence of clouds. High values of the C_V / C_m ratio (Fig. 4c) are connected with high concentrations of large particles. It is also clear that there is a strong correlation between nickel in the aerosol samples and cloud ice concentration (Fig. 3b) likely originating in collisions between ice particles and materials of the walls of the inlet (Murphy et al., 2004). However, the amount of nickel collected in the sampler is much less than the signal registered in the OPC channels for large particles. Bounce-off could cause reduced collection efficiency of these newly formed, solid particles in the aerosol sampler. Another difficulty arises from the fact that the OPC measurements are based on the assumption of a sulphate-dominated aerosol, thus causing large sizing uncertainties for nickel particles due to the use of inadequate refractive index in the data evaluation. Additionally, nickel has a large density (8.9 g cm^{-3}) implying that the cyclone in front of the sampler catches particles approximately a factor of 3 smaller in terms of geometrical diameter compared to 2 µm aerodynamic diameter cut-off. Hence it is likely that a large fraction of the particles registered by the OPC is outside the range of the sampler, thus further adding to the uncertainties. It is clear that the large diameter channels of the CARIBIC OPC are severely affected by clouds, as are the CARIBIC nickel concentration measurements from the aerosol samples.

Measurements where the crustal component is significant were identified from the iron concentration and its relative concentration to potassium, calcium and titanium. Six samples have a relative iron concentration (C_{Fe} / C_m) larger than 0.3 %, corresponding to a crustal fraction (C_{crust} / C_m) of approximately 6 % according to average crust composition (Weaver and Tarney, 1984). The deposition patterns of crust-containing samples (Fig. 5a and, for sample No. 1, Fig. 4a) all show signs of losses. Five of the samples have QI = 2 and the remaining sample QI = 1. The C_V / C_m ratio is connected with the deposition pattern to a higher degree than the cloud-influenced samples. The size distributions of measurements with a strong crustal component are shown in Fig. 5b. The size distribution of the cloud-affected measurement (No. 1) differs markedly from the other crust-influenced measurements with high concentrations of the largest particles artificially produced in the inlet. Yet, all but sample No. 12 show high concentration in the OPC channel for the largest particles. Crustal particles usually are larger than

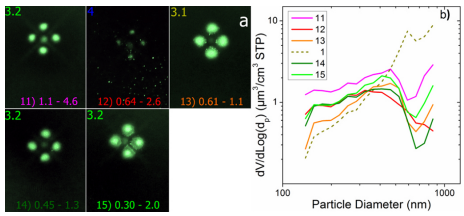

Figure 5. (a) Particle deposition patterns on the aerosol samples with a strong crustal component. Sample No., C_{Fe} / C_m mass ratio (%) and C_V / C_m ($cm^3\,g^{-1}$) are shown in the bottom of the images. Numbers in top left corners show deposition pattern and the colour indicates air mass type according to the legend of Fig. 3. **(b)** Volume size distributions from the OPC for samples with an Fe fraction larger than 0.3 % of the particle mass. Sample 1 (dashed) is also affected by clouds.

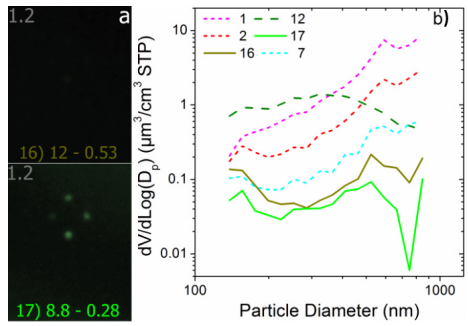

Figure 6. (a) Particle deposition patterns on the aerosol samples with a strong carbonaceous component. Sample No., C / S mass ratio and C_V / C_m ($cm^3\,g^{-1}$) are shown in the bottom of the images. Numbers in top left corners show deposition pattern and the colour indicates air mass type according to the legend of Fig. 3. **(b)** Volume size distributions from the OPC for samples with C / S mass ratio larger than 5. Samples also affected by clouds (short dashed in **b**) [No. 1 (C / S = 32), 2 (12) and 7 (6.2)], as well as those affected by crust (dashed) [No. 12 (9.5)], are shown only in **(b)**. Images of deposition patterns for these samples are displayed in Figs. 4 and 5, respectively.

sulphurous/carbonaceous particles indicating that the crustal particles mainly appear in the OPC channels for the largest particle sizes. Crustal particles differ significantly from the sulphate OPC calibration substance in refractive index as well as in particle shape, implying that the uncertainty of the OPC sizing of the crustal particles is large. The density of crustal particles is comparatively high, usually around $2.7\,g\,cm^{-3}$. This increases the probability that particles in the upper channels of the OPC are outside the upper aerodynamic limit of the aerosol sampler. The balance of these circumstances indicates that a mismatch in particle size range of the OPC and the aerosol sampler contributes to the high C_V / C_m ratios as well as non-ideal collection of crustal particles demonstrated by the deposition patterns.

The ratio of carbon (C) to sulphur (S) mass concentration varies by a factor of more than 100 between the samples in this study. Such variability in composition will of course affect the refractive index of the particles. Here samples with mass concentration ratio C / S > 5 will be examined. The mass of sulphate aerosol composed H_2SO_4 – $(NH_4)_2SO_4$ can be estimated to be 4 times the mass of S, implying that the carbonaceous component in these samples most likely is larger than the sulphurous fraction. Six of the 106 samples in this study had C / S mass concentration ratios larger than 5. Three of these samples were affected by clouds and one contained crust, which strongly affect the results of the comparison between the OPC and the sampler. The remaining two samples (Fig. 6a) show rather faint deposition patterns, the deposit of sample No. 16 being barely visible. Both of them are classified as type 1.2. These two measurements differ markedly from the cloud-affected and crust-containing samples with respect to size distribution (Fig. 6b) by showing a mode of small particles (most clear for sample 16). This indicates that a fraction of the particles escapes detection in the OPC while collected by the sampler having a much lower cut-off. This could be the cause of low C_V / C_m ratios. Also deviations of the actual optical properties from the refractive index assumed in the size attribution could be significant for these carbon-rich particles, e.g. underestimation of the soot fraction would lead to underestimation of C_V.

After the examination of the influence from clouds, crust and C / S composition 11 of the 17 outliers with respect to C_V / C_m ratio have been identified. The remaining six outliers are shown in Fig. 7. It is clear that the sampling failed to produce quantitative collection for samples 18–20 (Fig. 7a). The remaining measurements (No. 21, 22 and 23) show good sampling characteristics. The size distribution of sample 23, (Fig. 7b) indicates that a significant fraction of the particle volume can be found on particles smaller than the lowest size channel of the OPC, thus causing a low C_V / C_m ratio. The other two measurements (21 and 22) were taken in the LMS and display unusually large particles. This point will be discussed further in the next section.

3.2 Problems connected with the size distributions

To further evaluate the relation between the measurements with the OPC and the aerosol sampler, the size distributions will be examined. Difference in size range between the OPC (measuring 130–900 nm optical diameter) and the sampler (80–2000 nm aerodynamical diameter) could cause mismatch between the measurements, as discussed above. Assuming that the OPC measurements approximately resemble

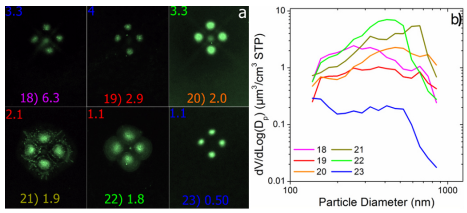

Figure 7. Samples outside the C_V / C_m range of 0.55–1.55 cm^3 g^{-1} marked in Fig. 2 that cannot be connected with cloud, crust or large carbonaceous fraction. **(a)** Particle deposition patterns on the aerosol samples with measurement No. and C_V / C_m (cm^3 g^{-1}) at bottom of the images. Numbers in top left corners show deposition pattern and the colour indicates air mass type according to the legend of Fig. 3. **(b)** Volume size distributions from the OPC.

the geometrical diameter the measurements would have the same upper size limit for particles of density of 5 g cm^{-3}. A lower density, usually true for atmospheric aerosol particles, would move the upper OPC limit downwards in aerodynamical size. In Fig. 8 particle volume size distributions are shown for all measurements not shown in Sect. 3.1 arranged according to the measurement region, i.e. UT, MT and LMS. It is clear that almost all measurements indicate that the particle volume outside the upper size limit of the OPC is small, implying that problems with mismatching upper size limits usually are small outside clouds (Fig. 4a) and in measurements with a strong crustal component (Fig. 5b).

The lower limits in particle size of the OPC and the impactor coincide at a particle density of approximately 0.4 g cm^{-3}. This low value implies that size distributions with large volume in the channel for the smallest particles might be underrepresented in terms of total particle volume from the OPC. Some size distributions show high concentrations in the two smallest particle channels without having a dominant mode of larger particles. These distributions could be expected to be most affected in the C_V / C_m ratio by particle volume outside the lower OPC measurement limit. In the tropics three measurements were taken in the fresh volcanic cloud from the eruption of Nyamurgira (DR Congo) in November 2011 with particle volume (and mass) concentrations similar to those deep into the LMS, see measurements 26, 27 and 28 in Fig. 8a (red vertical scale). These measurements together with 29 and 32 have C_V / C_m ratios of 0.69, 0.79, 0.80, 0.90 and 1.3 cm^3 g^{-1}. The low C_V / C_m ratios together with the size distributions of the measurements in the fresh volcanic cloud thus indicate some particle volume outside the OPC measurement range. All the measurements from the extratropical UT (Fig. 8b) have size distributions that indicate particle volume outside the lower size limit. However, the size distributions alone cannot explain variability in the C_V / C_m ratio of 0.77–1.4 cm^3 g^{-1}, for example

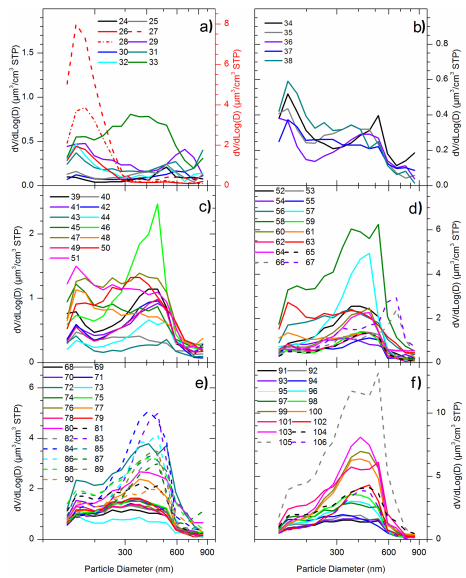

Figure 8. Particle volume distributions from the OPC for measurements without influence from clouds, high crustal or carbonaceous fractions. The legends show measurement number. **(a)** Tropics middle troposphere. Measurements 26–28 are shown on the axis to the right. **(b)** Extratropical UT (PV < 1.5 PVU). **(c)** Tropopause region (1.5 < PV < 3 PVU). **(d)** LMS 3 < PV < 5 PVU. **(e)** LMS 5 < PV < 7 PVU. **(f)** LMS PV > 7 PVU.

distributions 34 and 38 (the smallest and largest C_V / C_m ratio in this group) are similar both in terms of the distribution of small particles and relative particle volume for large particles. Measurements from the tropopause region (Fig. 8c) in some cases, in particular measurements 40, 43, 45 and 51, show significant concentration in the two lowest OPC channels without a dominant mode of larger particles. The respective C_V / C_m ratios are 0.83, 0.89, 1.0 and 1.2 cm^3 g^{-1}. All the measurement numbers are arranged in order of increasing C_V / C_m ratio in each of Fig. 8a–f. Presence of particles outside the lower size limit thus cannot explain the variability in the C_V / C_m ratio for measurements in the tropopause region. Finally, in Fig. 8d–f it can be seen that problems with particle volume outside the lower particle size limit are minor for the LMS aerosol. In conclusion it is clear that most size distributions from the MT tropics and the UT extratropics, and some of those from the tropopause region, indicate particle volume outside the lower size limit of the OPC, although it is not a major factor behind the variability of the C_V / C_m ratio. Measurements taken in the LMS do not indicate this problem.

In addition to investigating the conditions at the lower and upper size limit of the OPC, patterns associated with the volume mean diameter (VMD) will be examined. Figure 9 shows the C_V / C_m ratio related to the VMD. There is no clear correlation between these parameters for the tropospheric and tropopause region measurements. For measurements taken in the LMS weak correlation is found in the PV range 3–5 PVU, whereas the 5–7 PVU and PV > 7 PVU ranges show a clear correlation, i.e. when VMD increases from 270 to 360 nm (where most of these measurements are found) the C_V / C_m ratio in the LMS increases from 0.7 to 1.2 $cm^3\,g^{-1}$. Two of the measurements (red stars) in Fig. 9 are the two outliers (measurements 21 and 22 in Fig. 7) where no reason for the deviation could be found. Figure 9 indicates that the VMD is important for the observed deviation. As already pointed out, LMS size distributions show no sign of problems with the lower or upper size limits of the OPC measurements. However, the OPC response to particle size needs to be considered. Besides dependence on composition (refractive index) and particle shape, the calibration curve for a given composition is complicated. The range 0.7–1.2 $cm^3\,g^{-1}$ in C_V / C_m ratio corresponds to approximately ±25 % around the central value. If for the present, we disregard problems with the aerosol sampling and analysis this would indicate 25 % particle volume measurement uncertainty, corresponding to a range of a modest 8 % in terms of particle diameter for particles deep into the LMS.

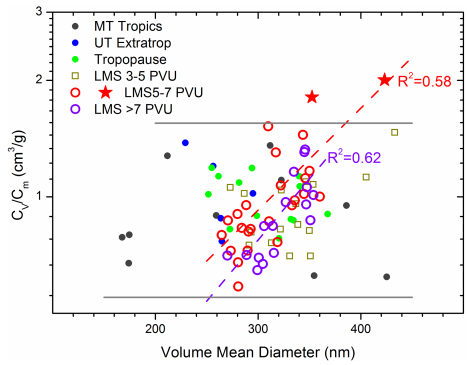

Figure 9. Dependence on volume mean diameter of the ratio of particle volume concentration (C_V, from the OPC) to mass concentration (C_m, from the aerosol samples). Purple and red lines are exponential fits to PV > 7 PVU and 5 < PV < 7 PVU data, respectively. Red stars are measurements classified as outliers where no explanation could be found in Sect. 3.1.

3.3 Problems in aerosol sampling and analysis

It is clear that problems in the aerosol sampling were responsible for some of the outliers with respect to the C_V / C_m ratio. The aerosol sampler collection efficiency shows excellent characteristics for liquid particles (Nguyen et al., 2006) and the errors from the PIXE and PESA analyses are small. However, solid particles could affect the sampling efficiency. Therefore all sample images not already dealt with in the previous sections (i.e. Figs. 4–7) will be investigated with respect to deposition pattern to find out to what degree the sampling suffered from losses.

Figure 10 shows the aerosol deposits of the samples taken in the tropical middle troposphere, the extratropical upper troposphere and the tropopause region. Ten tropical samples do not belong to the categories of outliers that were presented in Sect. 3.1. The aerosol sampling in the tropics usually worked well with seven QI = 0 (i.e. deposit types 1.1, 1.2, 2.1 and 2.2) samples and three samples with QI = 1 (deposit type 3.1), whereas none of the samples showed indications of severe losses (QI = 2; deposit types 2.3, 3.2, 3.3 and 4). Only five samples in Fig. 10 were taken in the extratropical UT. Three showed no signs of losses, one indicated minor losses and one major losses. Out of the 13 samples taken in the tropopause region, six showed no signs of losses, six minor losses and one sample indicated major losses. Overall, of the 28 samples from these three sampling regions 57, 36 and 7 % had QIs 0, 1 and 2, respectively.

The stratospheric samples are displayed in Fig. 11. Deposits with filaments wetting the surface of the polyimide film become more common in the stratosphere. Out of the 16 samples from the lowest stratospheric level, 3 < PV < 5 PVU (Fig. 11), 12 show no signs of losses (QI = 0), three show minor losses and one indicates significant losses (QI = 2). Deeper into the stratosphere, the PV range 5–7 PVU, 23 samples are available. Seventeen are of QI = 0, three of QI = 1 and three of QI = 2. Further up in the stratosphere, PV > 7 PVU, 15 out of 16 have QI = 0 and the only sample with QI = 2 shows wetting of the sampling substrate that is deemed to cause significant losses (type 2.3). Together the samples from the three stratospheric sampling levels have QI values of 0, 1 and 2 in 80, 11 and 9 % of the cases. Thus the fraction of the samples with major sampling problems is similar in the troposphere/tropopause and stratosphere, whereas a larger fraction of the stratospheric samples showed no signs of reduced collection efficiency.

Table 1 provides further overview of the classification with respect to aerosol deposit of the samples. Out of the total of 106 samples, 67 have deposit types that do not indicate losses in the sampling (QI = 0), 21 indicates minor losses (QI = 1) and 18 more severe losses (QI = 2). Eighty-three samples do not belong to the outlier categories clouds, crust, large carbonaceous fraction or the outlier samples presented in Fig. 7. Out of these 83 samples 72 % show no signs of losses (QI = 0) and 8 % have deposition patterns indicating major losses (QI = 2). It is clear that C_V / C_m shows a dependence on QI which is stronger when all samples are considered in comparison with when the four outlier

Table 1. Classification based on photographic images of all samples.

Category	Explanation	No. Samples Excl. outliers (All)[a]	C_V / C_m^b Excl. outliers (All)[a]	QI[c]
Type 1 – the expected pattern				
1.1	medium–high-loaded samples	26 (30)	0.86 (0.91)	0
1.2	low-loaded samples	1 (3)	[0.63] (0.45)	0
Type 2 – wetting of sampling substrate by liquid				
2.1	wetting only within beam area	28 (29)	0.89 (0.92)	0
2.2	minor wetting outside beam area	5 (5)	0.89 (0.89)	0
2.3	considerable wetting outside beam area	1 (1)	[1.3 (1.3)]	2
Type 3 – secondary deposition pattern				
3.1	central spot visible	16 (21)	1.0 (1.1)	1
3.2	cross visible	3 (7)	1.1 (1.5)	2
3.3	cross clearly visible	1 (3)	[1.1] (2.4)	2
Type 4 – large number of particles outside main deposit				
4		2 (7)	1.4 (2.6)	2
Qualitative Indicator (QI[c])				
0	types 1.1, 1.2, 2.1, 2.2	60 (67)	0.87 (0.88)	0
1	type 3.1	16 (21)	1.0 (1.1)	1
2	types 2.3, 3.2, 3.3, 4	7 (18)	1.2 (2.0)	2
All QI	all types	83(106)	0.93 (1.1)	All

[a] Referring to all samples except samples in the categories cloud, crust, C / S composition and "outliers" presented in Sect. 3.1 and to all samples in the study, respectively. [b] Geometrical average ($cm^3\,g^{-1}$) for each category. [ ] marks C_V / C_m of categories containing only one sample. [c] Qualitative indicator on the degree that the relation between measured to actual concentrations for the aerosol samples could be affected.

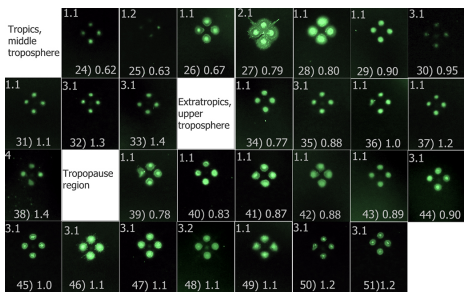

Figure 10. Photographic images of particle deposition patterns for middle troposphere tropics, extratropical upper troposphere and tropopause region samples not presented in Figs. 4–7. The upper left corner of each image shows the classification code of the deposit according to Table 1, and in the lower part sample number and C_V / C_m ($cm^3\,g^{-1}$) are shown. The bright lines in the image of sample 43 are caused by reflection in wrinkles present in this polyimide film.

categories are excluded see Table 1. The average C_V / C_m of the latter samples belonging with QI = 0 is $0.87\,cm^3\,g^{-1}$. The average of all the 83 samples is $0.93\,cm^3\,g^{-1}$, implying that the 23 samples with QI = 1 and QI = 2 increase the average C_V / C_m by 6 %.

It is clear that the deposition pattern based on qualitative classification of the samples in part can explain variability in the C_V / C_m ratio. Thereto we will briefly compare these results with measurements outside the regular 5.5 mm diameter proton beam used for quantitative analysis as explained in Sect. 2.1. Figure 12a shows the ratio of estimated, undetected sulfur mass outside the beam area of 5.5 mm diameter and the mass detected within the beam area, m_{udet} / m_{det}, in relation to particulate S concentration. Small, filled symbols indicate that particulate S was not detected in the two blank spots. These samples are represented by half the detection limit. It can be seen that particulate S could not be detected in the blank spots for samples with QI = 0 when the concentration was less than $100\,ng\,m^{-3}$ STP. This is also true for most of the QI = 1 samples (type 3.1), whereas most of the QI = 2 samples show detection with high m_{udet} / m_{det} ratio in that concentration range. For samples with particulate S concentration higher than $100\,ng\,m^{-3}$ STP the m_{udet} / m_{det} is low with a few exceptions. When relating m_{udet} / m_{det} to the C_V / C_m ratio for the samples where particulate S was detected in the blank spots a high degree of consistency can be found (Fig. 12b). m_{udet} / m_{det} is in all but one case low when the C_V / C_m ratio is low, and the deposit types are to a high degree of QI = 0 and 1. In the other end both the parameters usually are high and almost all samples have QI = 2. The agreement between the different measures further supports the consistency of the two different CARIBIC aerosol

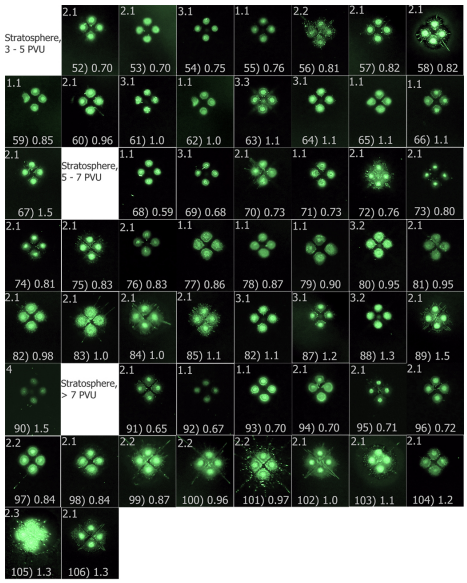

Figure 11. Photographic images of particle deposition patterns for stratospheric samples not presented in Figs. 4–7. Upper left corner of each image shows the classification code of the deposit according to Table 1, and in the lower part are sample number and C_V / C_m ($cm^3\,g^{-1}$).

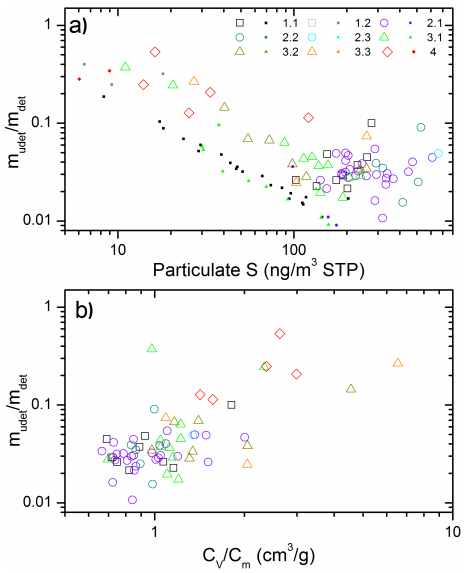

Figure 12. Ratio of estimated particulate sulphur mass outside the analytical beam (m_{udet}) to detected mass (m_{det}) related to **(a)** atmospheric particulate sulphur concentration and **(b)** the ratio total particle volume from the OPC (C_V) and total mass from the analyses of the aerosol samples (C_m). Particulate sulphur was detected in the analytical area of all samples. Open samples show analyses where sulphur was detected also outside the analytical area, whereas the small, closed symbols show samples where sulphur was not detected.

measurement methods. The m_{udet} / m_{det} ratio also provides an internal measure on the quality of a sample with respect to non-ideal effects in sampling with impactors.

3.4 Apparent particle density

To avoid bias from the outlier categories they are not retained in the data set used to further investigate the relation between the particle volume from the OPC and the mass from the sampling and analysis. The 83 measurements that did not belong to the outlier categories were all in the C_V / C_m range of 0.55–1.55 $cm^3\,g^{-1}$. Figure 13 shows C_V related to C_m. It is obvious that these measurements correlate well over approximately a factor of 50 in C_m and C_V ranges. The relative spread in the data (logarithmic scale) is essentially independent of the concentration, implying causes other than statistical for the variability within the 0.55–1.55 $cm^3\,g$ C_V / C_m range. By computing the geometric average (for consistency not the arithmetic average) of the ratio between C_m and C_V an estimate of the density of the aerosol particles is obtained. This apparent particle density becomes 1.08 $g\,cm^{-3}$. It is clear that non-ideal sampling affected some of the measurements. Removing these measurements result in the density 1.15 $g\,cm^{-3}$. The main components of the UT/LMS aerosol are sulphurous and carbonaceous aerosol. Occasionally the aerosol also contains a significant crustal fraction. The density of pure sulphuric acid is 1.84 $g\,cm^{-3}$, which could be somewhat lowered by mixing with water. Other possible forms of sulphate are ammonium bisulphate and ammonium sulphate with densities of 1.78 and 1.77 $g\,cm^{-3}$, respectively. The C / S elemental concentration ratio varies between 0.3 and 30 in the samples of this study. The carbonaceous fraction is to a large degree organic (Friberg et al., 2014). Probably the organic component acts as to lower the density of the particles, but likely not down to 1.15 $g\,cm^{-3}$. Previous measurements at remote location (Saarikoski et al., 2005; Kannosto et al., 2008) and an urban location (Hu et al., 2012) estimate the density of sub-micrometer atmospheric particles to approximately 1.5 $g\,cm^{-3}$. The apparent density of 1.15 $g\,cm^{-3}$ from this study is 30 % lower, thus calling for a discussion of the patterns behind this apparent density.

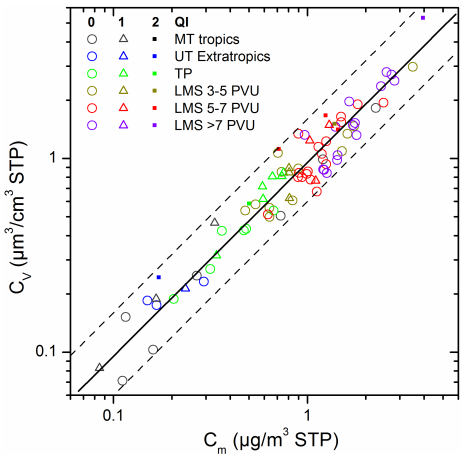

Figure 13. Particle volume concentration obtained from the OPC as a function of mass concentration from the aerosol samples taken at three PV levels in the stratosphere, the tropopause, the extratropical UT and the middle troposphere of the tropics. The colour of the symbols shows sampling location and the shape shows the quality indicator (QI) of the samples.

The measurements with the OPC and the elemental analyses of the samples are undertaken at approximately the same temperature. However, the analyses are undertaken in high vacuum, which can induce losses of organic material from the samples (Sect. 2.1). The composition and therefore the volatility of the organic fraction of the aerosol are not known. Therefore the losses during analysis cannot be estimated directly. The average carbon-to-sulphate mass ratio in samples of this study is 0.37, the ratio being higher in the troposphere (0.75) than in the stratosphere (0.26). To increase the apparent density to a value of 1.5 g cm^{-3} by increasing the carbon concentration in an attempt to reach more plausible value, the carbon concentrations need to be multiplied by approximately 2. This would increase the carbon-to-sulphate mass ratio average over all samples to 0.8, and for stratospheric samples carbon to sulphate mass ratio would become larger than 0.5, which is not in line with studies based on another analytical method (Murphy et al., 2006, 2007). In addition, studies of volcanic aerosol based on CARIBIC aerosol samples (Martinsson et al., 2009) agree well with studies based on other methods (Schmale et al., 2010; Carn et al., 2011) in the relation between the carbonaceous and sulphurous fractions of the aerosol. The increase of the carbonaceous fraction to reach 1.5 g cm^{-3} density would bring our volcanic measurements into disagreement with the mentioned other studies.

Losses of organic material would thus only explain part of the difference to previous observations at other locations. The uncertainties of the mass from the aerosol samples disregarding evaporative losses, is estimated to 12 %. The combined uncertainty in the number concentration and particle size combine to 50 % uncertainty in the particle volume determinations from the OPC. Taking the combined uncertainties of the two measurements into account, the observed apparent density is not deviating from previous observations.

4 Conclusions

Two aerosol measurement methods aboard the CARIBIC platform for studies of the upper troposphere (UT) and the lowermost stratosphere (LMS) were compared. The particle volume concentration (C_V) obtained from the CARIBIC optical particle counter (OPC) and total mass concentrations (C_m) obtained from aerosol samples analysed for all major and several minor constituents by ion beam analysis were compared by forming the ratio of the two measurements (C_V / C_m). 89 of the 106 measurements investigated have a C_V / C_m ratio confined to a rather narrow interval of 0.55–1.55 cm^3 g^{-1}. Problems in the aerosol sampling were identified by photographic images of the deposition pattern, where secondary deposits indicate non-ideal sampling characteristics. Out of the 17 measurements outside the usual C_V / C_m range of 0.55–1.55 cm^3 g^{-1}, six were connected with ice particles forming artificial particles in the inlet severely affecting total particle volume collected by the OPC and, in most cases, the aerosol deposition pattern of the samples. Three of the outliers were caused by non-ideal sampling of crustal particles and to some degree by problems with refractive index of the OPC and mismatch of the size ranges of the two measurements. Two of the measurements that were dominated by carbonaceous aerosol were below the usual C_V / C_m range because part of the size distribution was below the lower size limit of the OPC, and, probably due to a mismatch of the refractive index of the actual particles and that used in the OPC calibration. Of the remaining six measurements three showed poor sampling efficiency and the fourth mismatch in size range. The remaining two samples could be associated with the complicated relation between particle size and OPC signal, which was manifested by a correlation between particle volume mean diameter and the C_V / C_m ratio.

84 % of the measurements have C_V / C_m ratios within the range of 0.55–1.55 cm^3 g^{-1}. The volume and mass concentrations span approximately a factor of 50 without significant change in relative residuals, thus indicating causes other than statistical for the variability. From this correlation the apparent average density of the particles was estimated to 1.15 g cm^{-3} after removal of 6 % bias from non-ideal sampling effects of the impactor. This apparent particle density is lower than previous estimates by 30 %. The combined

uncertainties of the two methods, however, accommodate this difference.

Visual inspection and classification of the samples aerosol deposits was found to be an efficient means to identify samples where non-ideal sampling appeared, which was corroborated by the C_V / C_m ratio. The analytical methodology utilizing blank spots of the sample provided further insights to the problem of non-ideal impactor sampling. This method can be applied routinely with minimal effort, thus providing the means to significantly reduce problems, however moderate in this study, from impactor sampling imperfections.

In conclusion, two methods based on widely different principles were inter-compared over a range of a factor of 50 in atmospheric aerosol concentration. The composition expressed as the ratio between the two main aerosol components in the aerosol particles, carbon and sulphur, varied over a range of a factor 100 thus further illustrating the variable condition in the UT/LMS. Except for a few outliers that could be connected with ice clouds, crust, size range mismatch or non-ideal sampling, a strong correlation between the two methods indicates that in most cases the CARIBIC aerosol sampling/analysis and OPC produce consistent and reliable results. This implies that the CARIBIC measurements with the OPC and the aerosol sampler can be combined to further understand the physical and chemical nature of the upper tropospheric and lowermost stratospheric aerosol.

Acknowledgements. We especially acknowledge C. Koeppel, D. S. Scharffe, S. Weber and all other members of the CARIBIC project. Lufthansa and Lufthansa Technik are gratefully acknowledged for enabling this scientific experiment. Financial support from the Swedish Research Council for Environments, Agricultural Sciences and Spatial Planning under grant 214-2009-613 is gratefully acknowledged.

Edited by: W. Maenhaut

References

Ammann, C. M., Meehl, G. A., Washington, W. M., and Zender, C. S.: A monthly and latitudinally varying volcanic forcing dataset in simulations of 20th century climate, Geophys. Res. Lett., 30, 1657, doi:10.1029/2003GL016875, 2003.

Andersson, S. M., Martinsson, B. G., Friberg, J., Brenninkmeijer, C. A. M., Rauthe-Schöch, A., Hermann, M., van Velthoven, P. F. J., and Zahn, A.: Composition and evolution of volcanic aerosol from eruptions of Kasatochi, Sarychev and Eyjafjallajökull in 2008–2010 based on CARIBIC observations, Atmos. Chem. Phys., 13, 1781–1796, doi:10.5194/acp-13-1781-2013, 2013.

Andreae, M. O. and Rosenfeld, D.: Aerosol-cloud-precipitation interactions, Part 1. The nature and sources of cloud-active aerosols, Earth-Sci. Rev., 89, 13–41, 2008.

Baker, A. K., Slemr, F., and Brenninkmeijer, C. A. M.: Analysis of non-methane hydrocarbons in air samples collected aboard the CARIBIC passenger aircraft, Atmos. Meas. Tech., 3, 311–321, doi:10.5194/amt-3-311-2010, 2010.

Bauman, J. J., Russell, P. B., Geller, M. A., and Patrick, H.: A stratospheric aerosol climatology from SAGE II and CLAES measurements: 2. Results and comparisons, 1984–1999, J. Geophys. Res., 108, 4383, doi:10.1029/2002JD002993, 2003

Bohren, C. F. and Huffman, D. R.: Absorption and Scattering of Light by Small Particles, 1st Edn., p. 530, New York: John Wiley & Sons, 1983.

Brenninkmeijer, C. A. M., Crutzen, P. J., Fischer, H., Güsten, H., Hans, W., Heinrich, G., Heintzenberg, J., Hermann, M., Immelmann, T., Kersting, D., Maiss, M., Nolle, M., Pitscheider, A., Pohlkamp, H., Scharffe, D., Specht, K., and Wiedensohler, A.: CARIBIC civil aircraft for global measurement of trace gases and aerosols in the tropopause region, J. Atmos. Ocean. Tech., 16, 1373–1383, 1999.

Brenninkmeijer, C. A. M., Crutzen, P., Boumard, F., Dauer, T., Dix, B., Ebinghaus, R., Filippi, D., Fischer, H., Franke, H., Frieß, U., Heintzenberg, J., Helleis, F., Hermann, M., Kock, H. H., Koeppel, C., Lelieveld, J., Leuenberger, M., Martinsson, B. G., Miemczyk, S., Moret, H. P., Nguyen, H. N., Nyfeler, P., Oram, D., O'Sullivan, D., Penkett, S., Platt, U., Pupek, M., Ramonet, M., Randa, B., Reichelt, M., Rhee, T. S., Rohwer, J., Rosenfeld, K., Scharffe, D., Schlager, H., Schumann, U., Slemr, F., Sprung, D., Stock, P., Thaler, R., Valentino, F., van Velthoven, P., Waibel, A., Wandel, A., Waschitschek, K., Wiedensohler, A., Xueref-Remy, I., Zahn, A., Zech, U., and Ziereis, H.: Civil Aircraft for the regular investigation of the atmosphere based on an instrumented container: The new CARIBIC system, Atmos. Chem. Phys., 7, 4953–4976, doi:10.5194/acp-7-4953-2007, 2007.

Carn, S. A., Froyd, K. D., Anderson, B. E., Wennberg, P., Crounse, J., Spencer, K., Dibb, J. E., Krotkov, N. A., Browell, E. V., Hair, J. W., Diskin, G., Sachse, G., and Vay, S. A.: In situ measurements of tropospheric volcanic plumes in Equador and Colombia during TC^4, J. Geophys. Res., 116, D00J24, doi:10.1029/2010JD014718, 2011.

Deiters, U. K. and Randzio, S. L.: A combined determination of phase diagrams of assymetric binary mixtures by equations of state and transitiometry, Fluid Phase Equilibr., 260, 87–97, 2007

de Reus, M., Ström, J., Kulmala, M., Pirjola, L., Lelieveld, J., Schiller, C., and Zöger, M.: Airborne aerosol measurements in the tropopause region and the dependence of new particle formation on preexisting particle number concentration, J. Geophys. Res., 103, 31255–31263, 1998.

Deshler, T., Hervig, M. E., Hofmann, D. J., Rosen, J. M., and Liley, J. B.: Thirty years of in situ stratospheric aerosol size distribution measurements from Laramie, Wyoming (41° N), using balloon-borne instruments, J. Geophys. Res., 108, 4167, doi:10.1029/2002JD002514, 2003.

Dibb, J. E., Talbot, R. W., and Scheuer, E. M.: Composition and distribution of aerosols over the North Atlantic during the subsonic assessment ozone and nitrogen oxide experiment (SONEX), J. Geophys. Res., 105, 3709–3717, doi:10.1029/1999JD900424, 2000.

Dirksen, R. J., Boersma, K. F., de Laat, J., Stammes, P., van det Werf, G. R., Martin, M. V., and Kelder, H. M.: An aerosol boomerang: Rapid around-the-world transport of smoke from the December 2006 Australian forest fires observed from space, J. Geophys. Res., 114, D21201, doi:10.1029/2009JD012360, 2009.

Eguchi, K., Uno, I., Yumimoto, K., Takemura, T., Shimizu, A., Sugimoto, N., and Liu, Z.: Trans-pacific dust transport: integrated analysis of NASA/CALIPSO and a global aerosol transport model, Atmos. Chem. Phys., 9, 3137–3145, doi:10.5194/acp-9-3137-2009, 2009.

Friberg, J., Martinsson, B. G., Andersson, S. M., Brenninkmeijer, C. A. M., Hermann, M., van Velthoven, P. J. F., and Zahn, A.: Sources of increase in LMS sulfurous and carbonaceous aerosol background concentrations during 1999–2008 from CARIBIC flights, Tellus B, 66, 23428, doi:10.3402/tellusb.v66.23428, 2014.

Fromm, M., Lindsey, D. T., Servranckx, R., Yue, G., Trickl, T., Sica, R., Douchet, P., and Godin-Beekmann, S.: The untold story of pyrocumulonimbus, B. Am. Meteorol. Soc., 91, 1193–1209, doi:10.1175/2010BAMS3004.1, 2010.

Gislason, S. R., Hassenkam, T., Nedel, S., Bovet, N., Eiriksdottir, E. S., Alfredsson, H. A., Hem, C. P., Balogh, Z. I., Dideriksen, K., Oskarsson, N., Sigfusson, B., Larsen, G., and Stripp, L. S.: Characterization of Eyjafjallajökull volcanic ash particles and protocol for rapid risk assessment, P. Natl. Acad. Sci. USA, 108, 7307–7312, 2011.

Hermann, M., Heintzenberg, J., Wiedensohler, A., Zahn, A., Heinrich, G., and Brenninkmeijer, C. A. M.: Meridional distributions of aerosol particle number concentrations in the upper troposphere and lower stratosphere obtained by Civil Aircraft for Regular Investigation of the Atmosphere Based on an Instrument Container (CARIBIC) flights, J. Geophys. Res., 108, 4114, doi:10.1029/2001JD001077, 2003.

Hervig, M. and Deshler, T.: Evaluation of aerosol measurements from SAGE II, HALOE, and balloon-borne optical particle counters, J. Geophys. Res., 107, 4031, doi:10.1029/2001JD000703, 2002.

Hoerling, M. P., Schaak, T. K., and Lenzen, A. J.: Global objective tropopause analysis, Mon. Weahter Rev., 119, 1816–1831, 1991.

Hoinka, K. P.: The tropopause discovery, definition and demarcation, Meteorol. Z., 6, 281–303, 1997.

Hu, M., Peng, J., Sun, K., Yue, D., Guo, S., Wiedensohler, A., and Wu, Z.: Estimation of size-resolved ambient particle density based on the measurement of aerosol number, mass and chemical size distributions in the winter in Beijing, Environ. Sci. Technol., 46, 9941–9947, doi:10.1021/es204073t, 2012.

Huebert, B., Bertram, T., Kline, J., Howell, S., Eatough D., and Blomquist, B.: Measurements of organic and elemental carbon in Asian outflow during ACE-Asia from the NSF/NCAR C-130, J. Geophys. Res., 109, D19S11, doi:10.1029/2004JD004700, 2004.

IPCC: Climate Change 2013: The Physical Science Basis. Contribution of working group I to the fifth assessment report of the Intergovernmental Panel on Climate Change, edited by: Stocker, T. F., Qin, D., Plattner, G.-K., Tignor, M. M. B., Allen, S. K., Boschung, J., Nauels, A., Xia, Y., Bex, V., and Midgley, P. M., Cambridge University Press, United Kingdom and New York, NY, USA, 1535 pp., 2013.

Johansson, S. A. E. and Campbell, J. L.: PIXE: A novel technique for elemental analysis, 347 pp., John Wiley, Hoboken, N. J., 1988.

Kannosto, J., Virtanen, A., Lemmetty, M., Mäkelä, J. M., Keskinen, J., Junninen, H., Hussein, T., Aalto, P., and Kulmala, M.: Mode resolved density of atmospheric aerosol particles, Atmos. Chem. Phys., 8, 5327–5337, doi:10.5194/acp-8-5327-2008, 2008.

Kojima, T., Buseck, P. R., Wilson, J. C., Reeves, J. M., and Mahoney, M. J.: Aerosol particles from tropical convective systems: Cloud tops and cirrus anvils, J. Geophys. Res., 109, D12201, doi:10.1029/2003JD004504, 2004.

Koop, T., Luo, B., Tsias, A., and Peter, T.: Water activity as the determinant for homogeneous ice nucleation in aqueous solutions, Nature, 406, 611–614, 2000

Korolev, A. V., Emery, E. F., Strapp, J. W., Cober, S. G., Isaac, G. A., Wasey, M., and Marcotte, D.: Small ice particles in tropospheric clouds: Fact or artifact?, B. Am. Meteorol. Soc., 92, 967–973, doi:10.1175/2010BAMS2935.1, 2011.

Martinsson, B. G.: An external beam PIXE/PESA setup for characterization of fine aerosols, Nucl. Instr. Meth. B, 22, 356–363, 1987.

Martinsson, B. G. and Hansson, H.-C.: Ion beam thermography – analysis of chemical compounds using ion beam techniques, Nucl. Instr. and Meth. B, 34, 203–208, 1988.

Martinsson, B. G., Papaspiropoulos, G., Heintzenberg, J., and Hermann, M.: Fine mode particulate sulphur in the tropopause region from intercontinental commercial flights, Geophys. Res. Lett., 28, 1175–1178, 2001.

Martinsson, B. G., Nguyen, H. N., Brenninkmeijer, C. A. M., Zahn, A., Heintzenberg, J., Hermann, M., and van Velthoven, P. F. J.: Characteristics and origin of lowermost stratospheric aerosol at northern midlatitudes under volcanically quiescent conditions based on CARIBIC observations, J. Geophys. Res., 110, D12201, doi:10.1029/2004JD005644, 2005.

Martinsson, B. G., Brenninkmeijer, C. A. M., Carn, S. A., Hermann, M., Heue, K.-P., van Velthoven, P. F. J., and Zahn, A.: Influence of the 2008 Kasatochi volcanic eruption on sulfurous and carbonaceous aerosol constituents in the lower stratosphere, Geophys. Res. Lett., 36, L12813, doi:10.1029/2009GL038735, 2009.

Mattis, I., Siefert, P., Müller, D., Tesche, M., Hiebesch, A., Kanitz, T., Schmidt, J., Finger, F., Wandinger, U., and Ansmann, A.: Volcanic aerosol layers observed with multiwavelength Raman lidar over central Europe in 2008–2009, J. Geophys Res., 115, D00L04, doi:10.1029/2009JD013472, 2010.

McCormick, M. P., Thomason, L. W., and Trepte, C. R.: Atmospheric effects of the Mt Pinatubo eruption, Nature, 373, 399–404, 1995.

Mentes, B., Papaspiropoulos, G., and Martinsson, B. G.: Ion-beam thermography analysis of the H_2SO_4 – $(NH_4)_2SO_4$ system in aerosol samples, Nucl. Instr. Meth. B, 168, 533–542, 2000.

Murphy, D. M., Thomson, D. S., and Mahoney, M. J.: In situ measurements of organics, meteoritic material, mercury, and other elements in aerosols at 5 to 19 kilometers, Science, 282, 5394, doi:10.1126/science.282.5394.1664, 1998.

Murphy, D. M., Cziczo, D. J., Hudson, P. K., Thomson, D. S., Wilson, J. C., Kojima, T., and Buseck, P. R.: Particle generation and resuspension in aircraft inlets when flying in clouds, Aerosol Sci. Technol., 38, 401–409, 2004.

Murphy, D. M., Cziczo, D. J., Froyd, K. D., Hudson, P. K., Matthew, B. M., Middlebrook, A. M., Peltier, R. E., Sullivan, A., Thomson, D. S., and Weber, R. J.: Single-particle mass spectrometry of tropospheric aerosol particles, J. Geophys. Res., 111, D23S32, doi:10.1029/2006JD007340, 2006.

Murphy, D. M., Cziczo, D. J., Hudson, P. K., and Thomson, D. S.: Carbonaceous material in aerosol particles in the lower strato-

sphere and tropopause region, J. Geophys. Res., 112, D04203, doi:10.1029/2006JD007297, 2007.

Nguyen H. N. and Martinsson B. G.: Analysis of C, N and O in aerosol collected on an organic backing using internal blank measurements and variable beam size, Nucl. Instr. Meth. B, 264, 96–102, 2007.

Nguyen, H. N., Gudmundsson, A., and Martinsson, B. G.: Design and calibration of a multi-channel aerosol sampler for studies of the tropopause region from the CARIBIC platform, Aerosol Sci. Technol., 40, 649–655, 2006.

Nguyen, H. N., Martinsson, B. G., Wagner, J. B., Carlemalm, E., Ebert, M., Weinbruch, S., Brenninkmeijer, C. A. M., Heintzenberg, J., Hermann, M., Schuck, T., van Velthoven, P. F. J., and Zahn, A.: Chemical composition and morphology of individual aerosol particles from a CARIBIC fight at 10 km altitude between 50° N and 30° S, J. Geophys. Res., 113, D23209, doi:10.1029/2008JD009956, 2008.

Oram, D. E., Mani, F. S., Laube, J. C., Newland, M. J., Reeves, C. E., Sturges, W. T., Penkett, S. A., Brenninkmeijer, C. A. M., Röckmann, T., and Fraser, P. J.: Long-term tropospheric trend of octafluorocyclobutane (c-C_4F_8 or PFC-318), Atmos. Chem. Phys., 12, 261–269, doi:10.5194/acp-12-261-2012, 2012.

Pak, S. S., Liu, B. Y. H., and Rubow, K. L.: Effects of coating thickness on particle bounce in inertial impactors, Aerosol Sci. Technol., 16, 141–150, 1992

Papaspiropoulos, G., Mentes, B., Kristiansson, P., and Martinsson, B. G.: A high sensitivity elemental analysis methodology for upper tropospheric aerosol, Nucl. Instr. Meth. B, 150, 356–362, 1999.

Papaspiropoulos, G., Martinsson, B. G., Zahn, A., Brenninkmeijer, C. A. M., Hermann, M., Heintzenberg, J., Fischer, H., and van Velthoven, P. F. J.: Aerosol elemental concentrations in the tropopause region from intercontinental flights with the CARIBIC platform, J. Geophys. Res., 107, 4671, doi:10.1029/2002JD002344, 2002.

Pope III, C. A. and Dockery, D. W.: Health effects of fine particulate air pollution: Lines that connect, J. Air Waste Manage., 56, 709–742, 2006.

Rauthe-Schöch, A., Weigelt, A., Hermann, M., Martinsson, B. G., Baker, A. K., Heue, K.-P., Brenninkmeijer, C. A. M., Zahn, A., Scharffe, D., Eckhardt, S., Stohl, A., and van Velthoven, P. F. J.: CARIBIC aircraft measurements of Eyjafjallajökull volcanic clouds in April/May 2010, Atmos. Chem. Phys., 12, 879–902, doi:10.5194/acp-12-879-2012, 2012.

Rinsland, C. P., Yue, G. K., Gunson, M. R., Zander, R. and Abrams, M. C.: Mid-infrared extinction by sulphate aerosols from the Mt Pinatubo eruption, J. Quart. Radiat. Transfer, 52, 241–252, 1994.

Rosenfeld, D. and Woodley, W. L.: Deep convective clouds with sustained supercooled liquid water down to −37.5 °C, Nature, 405, 440–442, 2000.

Saarikoski, S., Mäkälä, T., Hillamo, R., Aalto, P. P., Kerminen, V.-M., and Kulmala, M.: Physico-chemical characterization and mass closure of size-segregated atmospheric aerosols in Hyytiälä, Finland, Boreal Environ. Res., 10, 385–400, 2005.

Schmale, J., Schneider, J., Jurkat, T., Voight, C., Kalesse, H., Rautenhaus, M., Lichtenstern, M., Schlager, H., Ancellet, G., Arnold, F., Gerding, M., Mattis, I., Wendisch, M., and Borrmann, S.: Aerosol layers from the 2008 eruptions of Mount Okmok and Mount Kasatochi: In situ upper troposphere and lower stratosphere measurements of sulfate and organics over Europe, J. Geophys. Res., 115, D00L07, doi:10.1029/2009JD013628, 2010.

Schuck, T. J., Brenninkmeijer, C. A. M., Slemr, F., Xueref-Remy, I., and Zahn, A.: Greenhouse gas analysis of air samples collected onboard the CARIBIC passenger aircraft, Atmos. Meas. Tech., 2, 449–464, doi:10.5194/amt-2-449-2009, 2009.

Schumann, U., Weinzierl, B., Reitebuch, O., Schlager, H., Minikin, A., Forster, C., Baumann, R., Sailer, T., Graf, K., Mannstein, H., Voigt, C., Rahm, S., Simmet, R., Scheibe, M., Lichtenstern, M., Stock, P., Rüba, H., Schäuble, D., Tafferner, A., Rautenhaus, M., Gerz, T., Ziereis, H., Krautstrunk, M., Mallaun, C., Gayet, J.-F., Lieke, K., Kandler, K., Ebert, M., Weinbruch, S., Stohl, A., Gasteiger, J., Groß, S., Freudenthaler, V., Wiegner, M., Ansmann, A., Tesche, M., Olafsson, H., and Sturm, K.: Airborne observations of the Eyjafjalla volcano ash cloud over Europe during air space closure in April and May 2010, Atmos. Chem. Phys., 11, 2245–2279, doi:10.5194/acp-11-2245-2011, 2011.

Schwartz, S. E., Charlson, R. J., Kahn, R. A., Ogren, J. A., and Rodhe, H.: Why hasn't earth warmed as much as expected?, J. Climate, 23, 2453–246, 2010.

Schwarz, J. P., Spackman, J. R., Gao, R. S., Watts, L. A., Stier, P., Schulz, M., Davis, S. M., Wofsy, S. C., and Fahey, D. W.: Global-scale black carbon profiles observed in the remote atmosphere and compared to models, Geophys. Res. Lett., 37, L18812, doi:10.1029/2010GL044372, 2010.

Solomon, S., Daniel, J. S., Neely III, R. R., Vernier, J.-P., Dutton, E. G., and Thomason, L. W.: The persistently variable "background" stratospheric aerosol layer and global climate change, Science, 333, 866–870, 2011.

Van de Hulst, H. C.: Light Scattering by Small Particles, 2nd Edn., 23 pp., 124–126, New York: Dover Publications, ISBN: 0-486-64228-3, 1981.

Vernier, J.-P., Thomason, L. W., Pommereau, J.-P., Bourassa, A., Pelon, J., Garnier, A., Hauchecorne, A., Blanot, L., Trepte, C., Degenstein, D., and Vargas, F.: Major influence of tropical volcanic eruptions on the stratospheric aerosol layer during the last decade, Geophys. Res. Lett., 38, L12807, doi:10.1029/2011GL047563, 2011.

Weaver, B. L. and Tarney, J.: Empirical approach to estimating the composition of the continental crust, Nature, 310, 575–577, 1984.

Xu, L., Okada, K., Iwasaka, Y., Hara, K., Okuhara, Y., Tsutsumi, Y., and Shi, G.: The composition of individual aerosol particle in the troposphereand stratosphere over Xianghe (39.45° N, 117.0° E), China, Atmos. Environ., 35, 3145–3153, doi:10.1016/S1352-2310(00)00532-X, 2001.

Paper IV

Significant radiative impact of volcanic aerosol in the lowermost stratosphere

Sandra M. Andersson[1]*, Bengt G. Martinsson[1], Jean-Paul Vernier[2,3], Johan Friberg[1], Carl A. M. Brenninkmeijer[4], Markus Hermann[5], Peter F. J. van Velthoven[6] & Andreas Zahn[7]

[1] Department of Physics, Lund University, Lund, Sweden;
[2] Science Systems and Applications, Inc., Hampton, Virginia
[3] NASA Langley Research Center, Hampton, Virginia
[4] Max Planck Institute for Chemistry, Mainz, Germany;
[5] Leibniz Institute for Tropospheric Research, Leipzig, Germany;
[6] Royal Netherlands Meteorological Institute, de Bilt, the Netherlands;
[7] Institute for Meteorology and Climate Research, Karlsruhe Institute of Technology (KIT), Germany

Global warming over the last 20 years is overestimated by practically all CMIP5 (coupled model intercomparison project) models[1,2]. This is a concern both in terms of sensitivity to human climate influence[3] and natural variability of climate[4,5]. Here we investigate large volcanic eruptions inducing "persistent variability" in the stratospheric aerosol layer[6-8]. Volcanic sulfur dioxide forms sulfate particles that reflect sunlight back to space, exerting a cooling effect[9]. Because the CMIP5 model runs did not account for volcanism actually occurring after the year 2000 this can in part explain why predicted warming was overestimated[5,8]. Importantly, currently used stratospheric aerosol optical depth (AOD) is based on observations made above 380 K in potential temperature (on average 15 km altitude)[10,11]. The same lower limit has been used for experimental data in radiative forcing estimates[5,8,12-14]. Recently it has been suggested that the stratosphere below 380K, the lowermost stratosphere (LMS), contributes to stratospheric AOD[15], and a first estimate has been presented[16]. Here we present the first high resolution study that connects AOD changes in the LMS to specific volcanic eruptions. Using aircraft and satellite measurements we show that the LMS was clearly affected by volcanism from 2005 to 2012. Analyzing the effects of the eruptions of extra-tropical Kasatochi (2008), Sarychev (2009) and tropical Nabro (2011), we find that inclusion of the LMS in the computations increases global AOD by more than a factor of 2 and radiative forcing by a factor of 1.7.

The LMS is sandwiched between the 380 K potential temperature level and the underlying tropopause, constituting over 40% of the stratospheric mass[17]. The stratosphere above 380 K potential temperature is connected to the troposphere only by an upward flow across the tropical tropopause in the Brewer-Dobson (BD) circulation. The underlying LMS at mid and high latitudes is supplied by seasonally varying fractions of subsiding stratospheric air from higher altitudes and tropospheric air crossing the extra-tropical tropopause. These flow patterns cause characteristic concentration gradients of trace gases[18,19] and aerosols[20].

Volcanic aerosol reaches the LMS either by direct injection in the extra-tropics or by transport from above via the lower and upper branch of the Brewer-Dobson circulation[19]. Global estimates of the contribution from volcanism to stratospheric aerosol have historically been performed by limb viewing satellite instruments, such as SAGE II, GOMOS, and presently OSIRIS. Their long line of sight is obscured by the occurrence of clouds close to the tropopause, which makes observations below 380 K potential temperature difficult[21]. Since 2006 a nadir viewing Lidar on the satellite CALIPSO is able to measure through the aerosol column from the stratosphere down to the ground with high vertical resolution, thus we have the possibility to also make observations in the UT/LMS.

Here we use CALIPSO observations combined with the analyses of aerosol collected by the IAGOS-CARIBIC passenger aircraft based observatory (cruise altitude 10-12 km, 40 to 50 % within the LMS) to quantify the radiative forcing of volcanic aerosol in the LMS. Special emphasis is placed on the period 2008 to early 2012, covering several important eruptions. The aerosol cloud from the Kasatochi eruption in August 7 – 8 in 2008 will be used to illustrate volcanic aerosol distributions in the stratosphere.

To identify volcanic influence on aerosol sampled in the LMS, the ratio of particulate sulfur to in situ ozone, S/O_3, is a powerful tracer[22] as the (non-volcanic) background S/O_3 ratio is set deep in the stratosphere before being transported downwards into the LMS. S/O_3 time series in the LMS (Fig. 1) obtained from near monthly intercontinental IAGOS-CARIBIC flights show solid evidence of influence from volcanic eruptions. After a period of little volcanic influence 1999-2002, large S/O_3 ratios (increases of up to a factor of 16) were measured following three extra-tropical eruptions between 2008 and 2011. Also a number of tropical eruptions can be attributed to elevated S/O_3 ratios between 2005 and 2012[23]. Their effects in the LMS are delayed due to the time required for transport from the tropics. In 2013 the LMS aerosol concentrations approached once again the "background" levels of 1999-2002.

Focusing on the eruption of Kasatochi in August 2008 (insert in Fig. 1), its volcanic aerosol was encountered by the CARIBIC observatory for the first time one week after eruption[22]. Elevated S/O_3 ratios indicate that the LMS was influenced by Kasatochi at least until March 2009, seven months after eruption. The S/O_3 ratios then increased again following eruptions of the Redoubt volcano in March/April 2009.

Whereas the majority of CARIBIC measurements take place at cruise altitude, i.e. 10 – 12 km, CALIPSO scans the entire stratospheric aerosol column (Fig. 2). The Kasatochi eruption placed its effluents in two layers, one above 15 km that eventually spread over the entire northern hemisphere (NH), and one below 15 km in the NH LMS and extra-tropical UT. During the first weeks after the eruption, the amount of aerosol increased due to the conversion of SO_2 into

sulfate particles[24,25]. The volcanic particles produced in the LMS had almost vanished by November 2008 through export to the troposphere, from where they are removed efficiently. The LMS particle concentrations were however re-elevated by the subsidence of the upper cloud, explaining the recurring increase in S/O_3 ratios observed by CARIBIC in December (inset in Fig. 1).

The LMS received the largest impact from the Kasatochi eruption. This is clear from looking at the extra tropically averaged aerosol scattering (Fig. 3, being the total scattering minus molecular scattering), which is optical equivalent to the aerosol concentration (in contrast to the scattering ratios in Fig. 2). The lower volcanic cloud had a relatively short but very large effect on the aerosol concentrations in the LMS lasting approximately 2.5 months. The subsequent effect from the upper branch prolonged the influence on the LMS.

Besides the Kasatochi (2008, 52.2^{o}N) eruption, the Sarychev (2009, 48.1^{o}N) and Nabro (2011, 13.4^{o}N) eruptions clearly increased the global stratospheric AOD in 2008-mid 2012 (Fig. 4a). In addition at least four other volcanic eruptions had minor influence on the stratospheric aerosol load. The eruption of Grimsvötn in May 2011 had little global impact despite a strong signal in the S/O_3 ratio (Fig. 1), because the effluents were injected in the UT and the tropopause region explaining the rapid decline in S/O_3. The contribution of the LMS to total stratospheric aerosol is evident from comparing the global AOD calculated for only 15 to 35 km altitude (the range used in almost all previous studies) to the total reaching from the tropopause to 35 km (Fig. 4a). The relevance of the LMS for climate is investigated in the same way from calculations of the radiative forcing (Fig 4b), dependent on season and latitude (Extended Data Fig.1).

To estimate the impact from the three main eruptions between 2008 and mid-2012, the background AOD and radiative forcing of the time period was set to the values in between the Kasatochi, Sarychev and Nabro eruptions. Time integration over the elevated AOD during volcanic influence (Fig 4a) provides then the total impact of an eruption in "AOD days". For the stratospheric layer at 15 – 35 km the Kasatochi, Sarychev and Nabro eruptions produced 0.22, 0.40 and 0.36 AOD days, respectively, whereas these numbers with the LMS included increase to 0.69, 0.87 and 0.60 AOD days. This means that on average only 45% (32%, 46% and 59%) of the AOD from the three eruptions is accounted for when limiting the observations to altitudes above 15 km. Making a similar integration of the radiative forcing ("RF days", Fig 4b) the 15 – 35 km results are -8.9, -17 and -15 W/m^2 days whereas the total values are -20, -31 and -19 W/m^2 days. Thus on average only 58% (44%, 56% and 77%) of the total radiative forcing originated from above 15 km altitude.

The extra tropical location of the LMS implies a stronger cloud cover and a seasonal dependence in sunlight hours, which affects the relation between AOD and radiative forcing. A clear elevation of the LMS AOD (defined as the time period when the LMS AOD exceeded 50% of its peak value for each eruption) lasted from mid-August to the end of October after the Kasatochi eruption. The influence from Sarychev lasted much longer, from the middle of 2009 until the turn of the year. This implies that both these eruptions had their main impacts approximately symmetrically around the autumn equinox. The dominant part of the aerosol from the eruption of the tropical volcano Nabro was carried to the north with the main impact on the LMS AOD from the end of August to mid-February. The seasonal-dependence of the number of day-light hours thus significantly reduced the LMS radiative impact from the Nabro eruption.

The eruptions studied here have clear geographical signatures (Fig 4c). Most affected by the three largest eruptions, including the tropical Nabro, were the NH extra-tropics, both in terms of radiative forcing and AOD (not shown). A complete description of the forcing from the stratosphere, including the LMS and the pronounced geographical signatures (which likely can be further refined) will improve our understanding of the effects of volcanism. This helps identification of climate responses[5] and to clarify the role of volcanism in, for example, the present global temperature hiatus[2].

The average contribution of the stratosphere below 15 km to the global stratospheric AOD post 2000 has been estimated to 30 – 70%, based on ground and balloon-borne measurements[16]. Our results for the years 2008 – 2011 shows an average LMS contribution of 30% to the total global AOD. This result obtained in the most volcanically influenced period after the turn of the millennium is at the lower limit of the previous estimate. The global stratospheric AOD presented by the IPCC[11] is based only on the stratosphere above 380 K in potential temperature[10], resulting in an aerosol radiative forcing of 0.11 (-0.15 to -0.08) W/m^2 in 2008-2011. Our results indicate that inclusion of the LMS increases global radiative forcing in this period by 30%.

Our detailed eruption-specific analysis is important for the understanding of volcanic contributions to the stratospheric background aerosol. For the three largest eruptions in the time period 2008 - 2011 the LMS increased the average global stratospheric AOD and radiative forcing by factors 2.2 and 1.7. The warming hiatus over past 15 years cannot presently be explained by CMIP5 models[2]. Volcanism has contributed cooling not accounted for in these models[5,8]. The present study substantially increases the estimated radiative forcing from volcanism, contributing further cooling.

Method

CARIBIC observatory, sampling and analysis

We used data from the CARIBIC observatory (www.caribic-atmospheric.com) which is based on a 1.5 ton measurement container transported onboard a long range passenger aircraft during mostly monthly sets of four consecutive measurement flights[26]. Aerosol sampling in CARIBIC is based on impaction of particles of 0.08-2.0 μm diameter on 0.2 μm thick polyimide films[27,28], at a time resolution of 100 minutes (150 minutes before 2002). Collected particles were analyzed for elemental composition by two accelerator-based methods; Particle Induced X-ray Emission and Particle Elastic Scattering Analysis[29] at the Lund ion beam accelerator facility. The accuracy is estimated to be 10%[29]. We also use O_3 mixing ratios obtained from CARIBIC which have an accuracy of 0.3 – 1%[30]. Particle size distributions were measured in 16 size channels in the diameter range of 0.13-0.9 μm with an optical particle counter[27]. The dynamical tropopause was used for classification of samples, where those taken in air masses with average potential vorticity (PV) larger than 2 PVU (1 PVU = 10^{-6} K m^2 kg^{-1} s^{-1}) were classified as stratospheric. PV was obtained from ECMWF reanalysis data at a 1 x 1 degree horizontal resolution and 91 vertical hybrid sigma-pressure levels.

CALIPSO data processing

Lidar data from the CALIPSO Level 1 nighttime output of the 532 nm parallel and perpendicular polarized channels were processed based on the method developed by Vernier, et al.[31], including a shift of aerosol free reference altitude from 30 – 34 km to 36 – 39 km. Each satellite swath was averaged horizontally to 1° latitudinal resolution and 180 m vertical resolution. Cloud pixels were identified and removed using a 5% threshold on the depolarization ratio to create a cloud mask[31]. The cloud mask was expanded vertically, 180 m upwards to reduce the probability of missing faint upper edges of the clouds, and downwards towards the surface to remove attenuated signals from below the cloud. The final products used in this study are scattering ratios (measured total backscatter/ calculated molecular backscatter) and aerosol scattering (measured total backscatter - calculated molecular backscatter). The molecular scattering was modelled based on air and ozone molecule number concentrations[32,33], using ozone number density and pressure from the Global Modeling and Assimilation Office (GMAO,http://gmao.gsfc.nasa.gov/) and temperature from the European Centre for Medium-Range Weather Forecasts (ECMWF, http://www.ecmwf.int/).

Aerosol optical depth

The conversion of aerosol scattering to AOD is dependent on particle size distribution. CARIBIC OPC size distributions of Nabro volcanic aerosol, measured 4 months after the eruption in 2011 after transport to the extra-tropical LMS[27], is similar to that of the stratospheric background aerosol in 1999 [34]. For these conditions CALIPSO aerosol scattering is transformed into extinction using a conversion factor of 50[35].

AOD is obtained by integration over the atmospheric depth. In this, we used two lower limits, 15 km altitude (as done in previous studies) and the tropopause level. For Aug – Nov 2008 the lower limit was set to 2 km below the tropopause to include the total influence from the Kasatochi volcanic cloud, which partly resided in the UT. The tropopause altitude varies in time and space. This variable altitude implies that zonal averaging has to be performed over different amounts of pixels, which have been corrected for by weighting towards the fraction of available pixels. Winter time data at latitudes above 60°S were removed because of frequent occurrence of polar stratospheric clouds (PSCs) that could not be handled by the cloud mask. PSCs at NH occurred much less frequent and could be identified and removed manually. Further restrictions on data availability at high latitudes arise from that CALIPSO nighttime data do not reach all the way to the poles in the summer season (maximum latitude ranging from 55 to 80° over the year). The scattering of these regions were estimated based on extrapolation of neighboring data. Due to the relatively small surface area contribution from high latitudes, approximately 7 % beyond 60°, uncertainties of actual aerosol concentrations in these regions are expected to have a small effect on the calculated global AOD.

Radiative forcing

Short wave Radiative Forcing was calculated for AODs derived from CALIPSO data, using a box-model[36]. Stratospheric aerosol was approximated as thin layers at 12.5 and 17.5 km altitude to represent average aerosol altitudes in the LMS and above 15 km, where the latter resided between 15 and 20 km.

$\Delta F = F_0 T^2 (1 - f_c) (1 - A_s)^2 \beta\delta$
Eq. 1

In this equation F_0 = 1370 W/m^2 is the solar constant, T^2 the two way transmission of incident light above the aerosol layer, A_s the surface albedo, f_c the cloud fraction, β the upscatter fraction, and δ the aerosol optical depth. The net radiative forcing (including the long wave component) is estimated to 70% of the shortwave forcing[37]. The global average over the time period studied of the resulting net radiative forcing for AOD =1 is -23 W/m^2, which is consistent with data from literature[38].

The surface albedo and cloud fraction was obtained from monthly ERA interim reanalysis data[39]. The two way transmission was calculated at 532 nm as a function of solar zenith angle. Upscatter fraction as a function of particle size and solar zenith angle was obtained from Nemesure, et al.[40], in combination with Schwartz[41] to deduce the upscatter fraction for sulfuric acid particles with different particle radii. Extinction coefficients of solar radiation on sulfuric acid aerosol were calculated, again using the size distribution of background aerosol in 1999[34]. The extinction coefficients were used to integrate over the upscatter fraction in the aerosol radii range 0.029-0.679 μm.

The resulting radiative forcing is thus sensitive to variation in latitude and season through the dependence on day-light hours, solar zenith angle, and the variation in cloud cover and surface albedo (Fig. S1), however the effect of the zenith angle on solar insolation and aerosol optical depth cancel each other out[36].

References

1 Fyfe, J. C., Gillett, N. P. & Zwiers, F. W. Overestimated global warming over the past 20 years. *Nature Clim. Change* **3**, 767-769 (2013).

2 Flato, G. *et al.* Evaluation of Climate Models. In: Climate Change 2013: The Physical Science Basis. Contribution of Working Group I to the Fifth Assessment Report of the Intergovernmental Panel on Climate Change (Cambridge University Press, Cambridge, United Kingdom and New York, NY, USA, 2013).

3 Ramanathan, V. & Feng, Y. On avoiding dangerous anthropogenic interference with the climate system: Formidable challenges ahead. *Proc Natl Acad Sci USA* **105**, 14245-14250 (2008).

4 Carslaw, K. S. *et al.* Large contribution of natural aerosols to uncertainty in indirect forcing. *Nature* **503**, 67-71 (2013).

5 Santer, B. D. *et al.* Volcanic contribution to decadal changes in tropospheric temperature. *Nat. Geosci.* **7**, 185-189 (2014).

6 Vernier, J.-P. *et al.* Major influence of tropical volcanic eruptions on the stratospheric aerosol layer during the last decade. *Geophys. Res. Lett.* **38**, L12807, (2011).

7 Bourassa, A. E. *et al.* Large volcanic aerosol load in the stratosphere linked to Asian monsoon transport. *Science* **337**, 78-81 (2012).

8 Solomon, S. *et al.* The persistently variable "background" stratospheric aerosol layer and global climate change. *Science* **333**, 866-870 (2011).

9 Robock, A. Volcanic eruptions and climate. *Rev. Geophys.* **38**, 191-219 (2000).

10 Sato, M., Hansen, J. E., McCormick, M. P. & Pollack, J. B. Stratospheric aerosol optical depths, 1850–1990. *J. Geophys Res.* **98**, 22987-22994 (1993).

11 Myhre, G. *et al.* Anthropogenic and Natural Radiative Forcing. In: Climate Change 2013: The Physical Science Basis. Contribution of Working Group I to the Fifth Assessment Report of the Intergovernmental Panel on Climate Change. (Cambridge University Press, Cambridge, United Kingdom and New York, NY, USA, 2013).

12 Kravitz, B., Robock, A. & Bourassa, A. Negligible climatic effects from the 2008 Okmok and Kasatochi volcanic eruptions. *J. Geophys Res.* **115**, D00L05 (2010).

13 Haywood, J. M. *et al.* Observations of the eruption of the Sarychev volcano and simulations using the HadGEM2 climate model. *J. Geophys. Res.* **115**, D21212 (2010).

14 Haywood, J. M., Jones, A. & Jones, G. S. The impact of volcanic eruptions in the period 2000–2013 on global mean temperature trends evaluated in the HadGEM2-ES climate model. *Atmos. Sci. Lett.* **15**, 92-96 (2014).

15 Fromm, M. *et al.* Correcting the record of volcanic stratospheric aerosol impact: Nabro and Sarychev Peak. *J. Geophys Res.* **119**, 10,343-310,364 (2014).

16 Ridley, D. *et al.* Total volcanic stratospheric aerosol optical depths and implications for global climate change. *Geophys. Res. Lett.* (2014).

17 Appenzeller, C., Holton, J. R. & Rosenlof, K. H. Seasonal variation of mass transport across the tropopause. *J. Geophys. Res.* **101**, 15071-15078 (1996).

18 Hoor, P., Fischer, H., Lange, L., Lelieveld, J. & Brunner, D. Seasonal variations of a mixing layer in the lowermost stratosphere as identified by the CO-O3 correlation from in situ measurements. *J. Geophys. Res* **107**, ACL 1-1-ACL 1-11 (2002).

19 Bönisch, H., Engel, A., Curtius, J., Birner, T. & Hoor, P. Quantifying transport into the lowermost stratosphere using simultaneous in-situ measurements of SF 6 and CO2. *Atm. Chem. Phys.* **9**, 5905-5919 (2009).

20 Martinsson, B. G. *et al.* Characteristics and origin of lowermost stratospheric aerosol at northern midlatitudes under volcanically quiescent conditions based on CARIBIC observations. *J. Geophys Res.* **110**, D12201 (2005).

21 Bourassa, A. E., Degenstein, D. A., Elash, B. J. & Llewellyn, E. J. Evolution of the stratospheric aerosol enhancement following the eruptions of Okmok and Kasatochi: Odin-OSIRIS measurements. *J. Geophys Res.* **115**, D00L03 (2010).

22 Martinsson, B. G. *et al.* Influence of the 2008 Kasatochi volcanic eruption on sulfurous and carbonaceous aerosol constituents in the lower stratosphere. *Geophys. Res. Lett.* **36**, L12813, (2009).

23 Friberg, J. *et al.* Sources of increase in lowermost stratospheric sulphurous and carbonaceous aerosol background concentrations during 1999-2008 derived from CARIBIC flights. *Tellus B* **66**, 23428 (2014).

24 Bluth, G. J. S., Doiron, S. D., Schnetzler, C. C., Krueger, A. J. & Walter, L. S. Global tracking of the SO2 clouds from the june, 1991 Mount-Pinatubo eruptions. *Geophys. Res. Lett.* **19**, 151-154 (1992).

25 Andersson, S. M. *et al.* Composition and evolution of volcanic aerosol from eruptions of Kasatochi, Sarychev and Eyjafjallajökull in 2008–2010 based on CARIBIC observations. *Atm. Chem. Phys.* **13**, 1781-1796 (2013).

26 Brenninkmeijer, C. A. M. *et al.* Civil Aircraft for the regular investigation of the atmosphere based on an instrumented container: The new CARIBIC system. *Atmos. Chem. Phys* **7**, 4953-4976, (2007).

27 Martinsson, B. G. *et al.* Comparison between CARIBIC aerosol samples analysed by accelerator-based methods and optical particle counter measurements. *Atmos. Meas. Tech.* **7**, 2581-2596, (2014).

28 Nguyen, N. H., Gudmundsson, A. & Martinsson, B. Design and calibration of a multi-channel aerosol sampler for tropopause region studies from the CARIBIC platform. *Aerosol Sci. Tech.* **40**, 649-655, (2006).

29 Nguyen, H. N. & Martinsson, B. G. Analysis of C, N and O in aerosol collected on an organic backing using internal blank measurements and variable beam size. *Nucl. Instrum. Methods* **264**, 96–102, (2007).

30 Zahn, A. *et al.* A fast and precise chemiluminescence ozone detector for eddy flux and airborne application. *Atmospheric Measurement Techniques* **5**, 363-375 (2012).

31 Vernier, J. P. *et al.* Tropical stratospheric aerosol layer from CALIPSO lidar observations. *J. Geophys Res.* **114**, D00H10 (2009).

32 Vernier, J.-P. *et al.* Overshooting of clean tropospheric air in the tropical lower stratosphere as seen by the CALIPSO lidar. *Atmos. Chem. Phys*, 9683–9696 (2011).

33 Hostetler, C. A. *et al.* CALIOP AlgorithmTheoretical Basis Document (ATBD): Calibration and level 1 data pro-ducts. *Doc. PC-SCI-201* (2006).

34 Jäger, H. & Deshler, T. Lidar backscatter to extinction, mass and area conversions for stratospheric aerosols based on midlatitude balloonborne size distribution measurements. *Geophys. Res. Lett.* **29**, 35-31-35-34 (2002).

35 Jäger, H. & Deshler, T. Correction to “Lidar backscatter to extinction, mass and area conversions for stratospheric aerosols based on midlatitude balloonborne size distribution measurements”. *Geophys. Res. Lett.* **30**, 1382 (2003).

36 Charlson, R. J., Langner, J., Rodhe, H., Leovy, C. & Warren, S. Perturbation of the northern hemisphere radiative balance by backscattering from anthropogenic sulfate aerosols. *Tellus A* **43**, 152-163 (1991).

37 Lacis, A., Hansen, J. & Sato, M. Climate forcing by stratospheric aerosols. *Geophys. Res. Lett.* **19**, 1607-1610 (1992).

38 Hansen, J. *et al.* Efficacy of climate forcings. *J. Geophys Res.* **110**, D18104 (2005).

39 Dee, D. *et al.* The ERA-Interim reanalysis: Configuration and performance of the data assimilation system. *Q. J. Roy. Meteor. Soc.* **137**, 553-597 (2011).

40 Nemesure, S., Wagener, R. & Schwartz, S. E. Direct shortwave forcing of climate by the anthropogenic sulfate aerosol: Sensitivity to particle size, composition, and relative humidity. *JGR* **100**, 26105-26116 (1995).

41 Schwartz, S. E. in *Aerosol Metrology for Climate Workshop,Gaithersburg, MD* (http://www.ecd.bnl.gov/steve/pres/NIST_aerosol_pptiesW.pdf, 2011).

Acknowledgements

We acknowledge all members of the CARIBIC project and Lufthansa and Lufthansa Technik for enabling the CARIBIC observatory. Aerosol measurements from CALIPSO were produced by NASA Langley Research Center. We also thank André Ahlgren for support with programming.

Author Contributions

S.M.A. and B.G.M. performed data processing, analysis, computations and wrote the paper. They contributed to measurements of CARIBIC aerosol elemental concentrations. J.-P. V. supervised CALIPSO data processing and provided recalibration data. J.F. contributed to the analysis and to measurements of CARIBIC aerosol elemental concentrations. C.A.M. was responsible for the operation of the CARIBIC container with the help of A.Z and M.H. and M.H., P.F.J.V. and A.Z. provided CARIBIC aerosol size distribution, meteorology and ozone data, respectively, and contributed equally to the project.

Figures

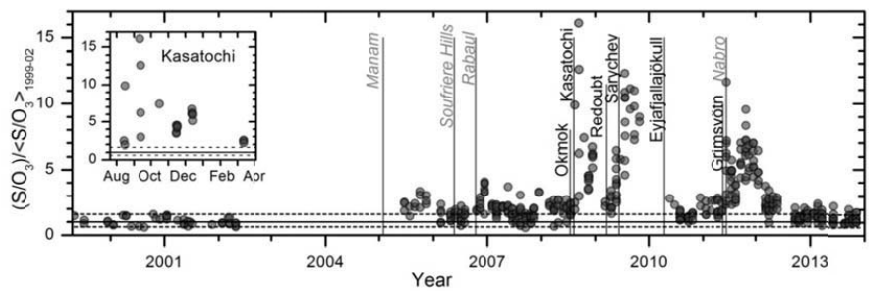

Figure 1. Identification of volcanic aerosol in the LMS. CARIBIC time series of S/O_3 in the LMS normalized by average S/O_3 during the 1999 - 2002 period of low volcanic influence. The full line indicates ratio 1 (geometrical average 1999 – 2002), and the broken lines the minimum and maximum of the 1999 – 2002 period. The time of tropical (grey italic text) and extra tropical (black text) eruptions are displayed by vertical lines. The inset gives details for the Kasatochi eruption.

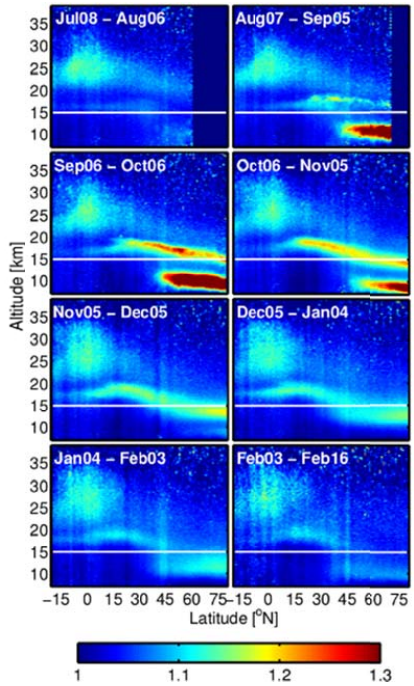

Figure 2. Latitude and altitude distributions of Kasatochi volcanic aerosol. Distribution of the Kasatochi volcanic aerosol shown by monthly (2 weeks in Feb.) and zonally averaged scattering ratios (total backscatter from CALIPSO /molecular backscatter) from July2008 - Feb 2009. The feature in the tropics at 25 km is not related to the Kasatochi eruption. The white line indicates 15 km altitude.

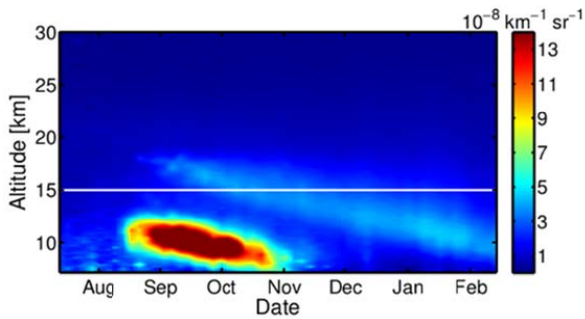

Figure 3. Downward transport of Kasatochi volcanic aerosol. Time series of aerosol scattering (total backscatter from CALIPSO minus molecular backscatter) for 40-80°N showing the descent of the Kasatochi volcanic aerosol. The white line indicates 15 km altitude.

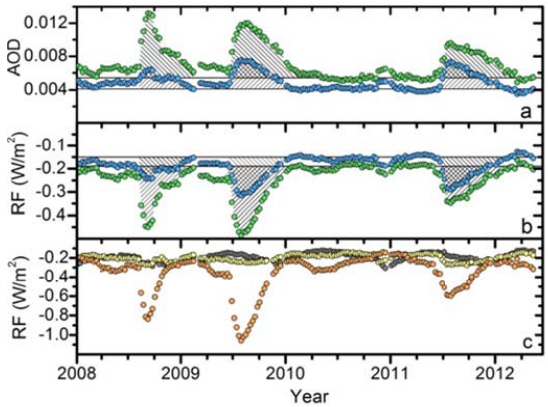

Figure 4. Global volcanic influence. a) Global aerosol optical depth and b) aerosol radiative forcing calculated from integrated CALIPSO aerosol scattering from 35 km to 15 km altitude (blue) and from 35 km to the tropopause (-2 km in Aug-Nov 2008) (green)The solid lines indicate the estimated background concentrations of the time period, and the filling the total integrated volcanic AOD and aerosol radiative forcing from the Kasatochi (2008, 52.2°N), Sarychev (2009, 48.1°N) and Nabro (2011, 13.4°N) eruptions. c) Stratospheric radiative forcing in three regions equal in surface area; -90 to -20°N (gray), -20 to 20 °N (yellow) and 20 to 90 °N (orange).

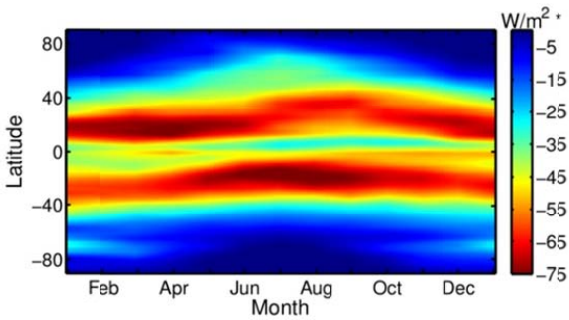

Extended Data Figure 1. **Latitudinal and seasonal dependence of shortwave radiative forcing**. Geographical and seasonal dependences of the average net radiative forcing in 2008-2011 for AOD=1, normalized by relative latitude area (*). The structures results from variability in day-length, upscatter fraction, surface albedo, cloudiness and transmission down to the aerosol layer.

Paper V

Variability in LMS volcanic sulfurous aerosol and consequences for UT aerosol and cirrus clouds

Johan Friberg[1], Bengt G. Martinsson[1], Moa K. Sporre[1], Sandra M. Andersson[1], Carl A. M. Brenninkmeijer[2], Markus Hermann[3], Peter F.J. van Velthoven[4] and Andreas Zahn[5]

[1]Department of Physics, Lund University, Lund, Sweden;
[2]Max Planck Institute for Chemistry, Mainz, Germany;
[3]Leibniz Institute for Tropospheric Research, Leipzig, Germany;
[4]Royal Netherlands Meteorological Institute, de Bilt, the Netherlands;
[5]Institute for Meteorology and Climate Research, Karlsruhe Institute of Technology (KIT), Germany

Abstract

We investigate the influence of the concentration of sulfurous aerosol in the lowermost stratosphere (LMS) on that in the upper troposphere (UT) and on cirrus clouds, based on CARIBIC observations between 1999-2002 and 2005-2013. First, we show that the loading of sulfurous aerosol in the LMS (S_{LMS}) was largely controlled by volcanic eruptions. The initial period, 1999-2002, was volcanically quiescent after which S_{LMS} became affected by several volcanic eruptions starting 2005. In fall 2008 and during 2009, volcanic eruptions at mid-latitudes had induced up to approximately tenfold increase in S_{LMS}. Perturbations of the same magnitude were observed in fall 2011 to spring 2012 after the eruption of the tropical volcano Nabro. From 2005 to 2008 and in 2013, volcanic aerosol from several tropical eruptions increased S_{LMS} and due to consequent subsidence the sulfur loading of the upper troposphere S_{UT}, too. Comparisons of S_{LMS} and S_{UT} during the seasons March-July and August-November showed a close coupling of the LMS and UT. Finally, the relationship between the LMS sulfur loading S_{LMS} and the cirrus cloud reflectance (CR) retrieved from MODIS spectrometer (onboard the satellites Terra and Aqua) was studied. S_{LMS} and CR showed a strong anti-correlation, with a factor of 3.5 increase in S_{LMS} and decrease of CR by 8±2% over the period 2001 to 2011. We suggest that the cirrus CR decrease depends on the coinciding increase of S_{LMS} due to volcanism which led to a negative radiative forcing in the order of -2 Wm^{-2} in the Northern Hemisphere midlatitudes.

Keywords: volcanic aerosol, cirrus reflectance, sulfurous aerosol

1. Introduction

The present study focuses on particulate matter collected in the lowermost stratosphere (LMS) and upper troposphere (UT) by the passenger aircraft based CARIBIC observatory (Brenninkmeijer et al., 2007). The transport of air enriched in ozone and particulate sulfur from the stratosphere into the troposphere can be optimally monitored by CARIBIC throughout the seasons and years. Although the cruise altitude is nearly constant, the variable altitude of the extra-tropical tropopause allows the retrieval of vertical profiles across the tropopause and a sampling both in the LMS and in the UT. By this CARIBIC can follow the fate of stratospheric aerosol. Recent findings have highlighted the importance of volcanisms direct effects on cooling of the Earth's surface ((Solomon et al., 2011; Ridley et al., 2014); Andersson et al., 2014). In the present study volcanism's indirect effects on cirrus clouds will be investigated.

The sulfurous fraction is the major component of the stratospheric aerosol (Rosen, 1971; Deshler, 2008). Recent studies (Murphy et al., 1998; Martinsson et al., 2009; Schmale et al., 2010) find that the aerosol also contains carbonaceous species. In addition small crustal (Andersson et al., 2013) and meteoric (Murphy et al., 2014) components are found in stratospheric aerosol particles.

The two largest sources of sulfuric acid particles in the stratosphere are the photolysis and oxidation of OCS and SO_2 (Crutzen, 1976; Weisenstein et al., 1997), with a minor contributions from direct injection of sulfurous particles from the tropical troposphere. SO_2 forms sulfuric acid at all altitudes in the stratosphere, via oxidation by radicals, while OCS is photo-oxidized chiefly at high altitudes in the stratosphere. Injections of particulate matter via volcanism is by far the source inducing most variability in the stratospheric aerosol (Robock, 2000). Remote sensing at lidar stations (in Boulder, Colorado and in Mauna Loa, Hawaii) revealed a trend of increasing aerosol burden in the stratosphere (20-25 km altitude) in the period 2000-2009 (Hofmann et al., 2009), that was later shown to be caused by volcanism in the tropics (Vernier et al., 2011). The stratosphere's increasing aerosol concentration has been found to cause a negative radiative forcing of -0.1 Wm^{-2} (Solomon et al., 2011). Latest studies (Andersson et al., 2014; (Ridley et al., 2014) find that volcanic aerosol, not only typically being in the stratospheric aerosol layer, but also the LMS contributes significantly to the climate forcing in that period, pointing at volcanism being a major cause for the deviations between actual and predicted global warming (Flato et al., 2013).

The Brewer-Dobson circulation transports air from the tropical tropopause via the middle and high stratosphere (deep branch) and quasi-horizontally (shallow branch) to mid- and high-latitudes (Holton et al., 1995). The deep branch brings air with high concentrations of O_3 and sulfuric acid particles from the Junge-layer to lower altitudes where it mixes with air from the lower branch. Whereas the deep branch transports air to midlatitudes within years, the shortcut via the lower branch requires only a few months.

The LMS is restricted downwards by the tropopause, while its upper boarder is defined as the 380 K isentrope (Holton et al., 1995). Stratospheric air with high concentrations of O_3 and particulate sulfur that reaches the LMS undergoes here a mixing with air from the troposphere. On a local scale, mixing through the tropopause results in a 2-3 km thick layer with strong vertical gradients of trace gases (Hoor et al., 2004; Pan et al., 2004), called the extratropical

tropopause transition layer (ExTL). Seasonality in the strength of the transport paths results in seasonally varying proportions of and tropospheric air in the LMS, for example leading to varying ozone concentrations during the year, with highest concentrations in spring and lowest during fall (Zahn and Brenninkmeijer, 2003). Via observations of trace gas concentrations Bönisch et al. (2009) revealed a seasonal cycle in the mean age of air in the LMS, decreasing from spring to fall.

Further down in the atmosphere, UT aerosol particles are involved in the formation of cirrus clouds. Cirrus ice crystals form either homogeneously via freezing of super-cooled solution droplets or heterogeneously when water crystallizes directly on ice nuclei (IN) (Pruppacher and Klett, 1997). Mineral dust and metallic particles have been found to be the main suppliers of IN in the UT (DeMott et al., 2003; Cziczo et al., 2013) and laboratory experiments revealed that coating of such particles affect how well they perform as IN (Hoose and Möhler, 2012).

There is still some debate as to the mechanisms of most importance for cirrus formation. Recent studies (Cziczo et al., 2013) indicate that heterogeneous freezing is the dominant mechanism for cirrus clouds over Central America and parts of North America. However, Barahona et al. (2014) find homogeneous freezing to be the dominant mechanism globally except over Central Asia, the Arctic and the west coast of North America. Campbell et al. (2012) found cirrus clouds below a stratospheric layer of volcanic aerosol from the Kasatochi eruption in 2008, likely formed when the volcanic sulfate and ash were transported into the more humid UT near a tropopause fold.

Cirrus clouds are estimated to have an overall larger impact on the long-wave than on the short-wave radiation, resulting in a net warming of the surface (Chen et al., 2000; Boucher et al., 2013). Estimations of radiative forcing from cirrus clouds hold considerable uncertainties (Boucher et al., 2013) depending on a range of factors (Baran, 2009) including; ice crystal shape, size, number concentration, cloud coverage, cloud thickness and temperature (Fusina et al., 2007).

Here we present a study on the influence of the LMS on midlatitude UT aerosol concentration, based on elemental analyses of aerosol samples collected by CARIBIC (Civil aircraft for regular investigation of the atmosphere based on an instrument container) between 1999 and 2013. Perturbation of LMS aerosol by volcanism during these 15 years ranged from low to moderate With the direct impact of volcanic aerosol in the UT/LMS having been addressed by Andersson et al. (2014), we also present a comparison between measured UT/LMS aerosol concentrations and MODIS (Moderate Resolution Imaging Spectroradiometer) retrieved cirrus reflectance (CR), in the light of the indirect climate impact of volcanism.

2. Methods

The period 1999-2013 was covered by CARIBIC in a near monthly rhythm for flight destinations that can basically be gleaned from Figure 1, except for the 2.5 year period mid-2002 to 2005 (c.f. Figure 2) which was used for a transition from CARIBIC 1 (Boeing 767 ER aircraft, leaving Düsseldorf and Munich airports) (Brenninkmeijer et al., 1999) to CARIBIC 2 (Airbus A340-600 aircraft based in Frankfurt) (Brenninkmeijer et al., 2007). The CARIBIC system is currently

based on a 1.5 ton automated measurement container constituting a compact laboratory. The container is installed monthly for 2-6 consecutive flights in a Lufthansa passenger Airbus A340-600, which has been retrofitted for this task with a permanent inlet system having inlet probes for water vapor, cloud water, aerosol and trace gases. So far about 100 publications deal with methods and results (www.caribic-atmospheric.com). The CARIBIC system is part of IAGOS (In situ Aircraft for a Global Observing System, www.iagos.org)

2.1. Air-inlet for aerosol sampling

Different inlet-systems were used for the CARIBIC phase #1 and #2. The inlet used in phase #1 had an estimated sampling efficiency of 90% for 0.1-1 µm particles (Hermann et al., 2001). The presently used (phase #2) system has a sampling efficiency of 60% for 5 µm particles and a high transmission (>90%) for sub-micron particles (Rauthe-Schöch et al., 2012; Martinsson et al., 2014). A cyclone with close to 100% transmission for sub-micron particles (Nguyen et al., 2006) with a cut-off size of 2 µm is installed to reduce the influence from larger particles.

2.2. The aerosol sampler

Aerosol particles with aerodynamic diameters of 0.08-2 µm were collected using an automated aerosol sampler with close 100% collection efficiency (Nguyen et al., 2006) based on the use of impactors. Particles were deposited on 0.2 µm thin AP1™ polyimide films (Papaspiropoulos et al., 1999). Similar impactors were used during phase #1 and #2. The phase #2 (phase #1) device consists of 14 (12) channels for sequential samples. In addition, 2 channels were used to collect integral samples, to check for contaminations. Typical air volumes of 0.25 (0.09) m^3 STP were sampled during 100 (150) minutes, or 1500 (2200) km flight distance. Sampling during flights is suspended when the pressure exceeds 350 hPa (landing and take-off cycles), to avoid sampling of aerosol from lower altitudes.

2.3. Aerosol composition analysis

Chemical characterization of aerosol particles is obtained using PIXE (particle induced x-ray emission) (Johansson and Campbell, 1988). Samples were irradiated by a proton beam of 2.55 MeV at the Lund ion beam analysis facility. Elemental concentrations were derived for elements with atomic numbers larger than 15, with an estimated accuracy of 10% (Papaspiropoulos et al., 1999; Martinsson et al., 2014). The present study focuses on the sulfur data, which have a typical minimum detection limit (MDL; detection of an element with a confidence of 99%) of 2 ng m^{-3} STP. Sulfur concentrations below MDL were set to MDL/2. Detection frequencies for sulfur were 99% (UT) and 100% (LMS).

2.4. Sampling in the midlatitude UT/LMS

The present study deals with the northern hemisphere extratropics. Because the aircraft collects samples in a narrow altitude interval (9-12 km a.s.l.), either the extratropical UT/LMS or the tropical middle troposphere is investigated. However, due to the relative movement of the

tropopause to the aircraft flight track, air masses with vertical distances relative to the tropopause from 5 km below the tropopause to 5 km above the tropopause are probed. At mid and higher latitudes the tropopause is frequently crossed. In the present study, samples collected on latitudes south of 30°N are excluded to keep the influence from tropical air low.

2.4.1. The dynamical tropopause

We will use potential vorticity (PV) to define the tropopause. PV-values were derived from archived ECMWF (European Centre for Medium-range Weather Forecast) analyses with a resolution of 1×1 degree in the horizontal at 91 vertical hybrid sigma-pressure model levels. PV-values were interpolated linearly in latitude, longitude, log pressure and time to the location of the aircraft and for each sample averaged over the duration of sampling. Typically, PV-values of 1.5 – 3.5 PVU (Hoerling et al., 1991; Hoinka, 1997) are employed defining the dynamical tropopause. In the present study the tropopause is set to 2 PVU.

2.4.2. Classification of UT and LMS samples

Samples with an average PV > 2 PVU are classified to be stratospheric, while UT samples are those below 1.5 PVU. The sampling time for the impactor is relatively long, sometimes resulting in samples representing air from both the UT and the LMS. To eliminate a bias in the UT aerosol concentration from samples partially taken in the LMS, samples collected at average PV lower than 1.5 PVU were nonetheless excluded from this investigation if the aircraft had crossed the tropopause (2 PVU) during the sampling interval.

2.5. Exclusion of samples affected by fresh volcanic aerosol

Volcanic clouds reaching the UT/LMS can enhance the background aerosol concentrations tremendously. We identified several such occasions. In the weeks following an eruption the emitted SO_2 is converted to sulfate and the resulting volcanic aerosol mixes at various degrees with the background. Moreover fresh volcanic aerosol injected in the UT is susceptible to scavenging by precipitation formation. Therefore, samples collected within 30 days after volcanic eruptions that reached the extra-tropical UT/LMS (listed in Table 1) were excluded. An extremely high particulate sulfur concentration was observed for one additional sample (August 2001). Trajectory analysis shows direct transport from the area of an eruption of Bezymianny, at the Kamchatka peninsula, Russia. Hence, this sample taken in a fresh volcanic cloud is also excluded from our study.

2.6. Contour graphs

The geographical distribution of particulate sulfur concentration is illustrated by using contour graphs, based on a matrix of concentrations. For that, the flight track for each sample was split into 10 equidistant steps and the average position of the aircraft (in longitude×latitude coordinates) was calculated for each step, yielding 10 steps, of typically 150 km along the flight route. The ten sample steps were assigned aerosol concentrations according to the analytical

results, i.e. the same concentration for each sample step. Concentrations were then sorted into and averaged on a longitude×latitude grid of 5×5 degrees and a center-weighted 2D-smoothing was performed. Grid cells with fewer than 10 samples in their surrounding grid cells were excluded, to reduce the risk of bias in regions with few samples. The final matrix was created by interpolation to 1×1 degrees (longitude×latitude). A similar contour graph was created illustrating the geographical variation of potential vorticity.

2.7. Satellite measurements

Satellite data of cirrus clouds from the Moderate Resolution Imaging Spectroradiometer (MODIS) instruments were used in the study. One MODIS instrument is placed on the satellite Terra, launched in December 1999, and the other on Aqua, launched in May 2003. Terra has a descending orbit while Aqua has an ascending orbit and their equatorial crossing times are 10:30 and 13:30 local solar time (Platnick et al., 2003). MODIS is a whiskbroom scanning radiometer with 36 wavelength channels spread between 0.620 and 14.4 μm. One of these channels, centered at 1.38 μm, was selected specifically for the study of cirrus clouds (Gao and Kaufman, 1995). The incoming solar radiation at 1.38 μm is either reflected and scattered by the cirrus clouds or completely absorbed by the underlying atmosphere, due to high water vapor absorption at this wavelength (Gao et al., 2002; Meyer and Platnick, 2010). Hence, this channel can together with a channel in the visible spectrum (0.66 μm) be used to retrieve the cirrus cloud reflectance (Gao et al., 2002). Our analysis is based on the Level 3 monthly averaged cirrus reflectance with a resolution of 1×1 degrees.

During dry atmospheric conditions not all the solar radiation at 1.38 μm will be absorbed by the underlying atmosphere. Hence, reflection from the surface or lower lying clouds can contaminate the cirrus reflectance product (Meyer and Platnick, 2010). The atmospheric water vapor product from MODIS has therefore been used to screen out dry atmospheric conditions. Similar results were obtained when using the total column water vapor from the ECMWF. The limit was set to 0.4 cm after recommendation from B.-C. Gao (personal communication, 2014) and investigation of the cirrus reflectance and atmospheric water vapor data. Since the same area is to be used for all monthly averages, pixels that have atmospheric water vapor exceeding 0.4 cm during the investigated years are removed from the entire dataset. This was done for Terra and Aqua separately but the areas included are very similar. It is mainly continental areas over central North America and Asia that are excluded but also some small ocean areas east of these continents. Since the satellite data will be compared to the CARIBIC data, only data from 30°N to 60°N are used to create average monthly cirrus products. Due to the latitude dependence of temperature and therefore atmospheric water concentration, the fraction of pixels that are too dry increases with latitude. To avoid bias from this phenomenon, first zonal averages were computed using 1x1 degree pixels. These averages were then weighed according to area in order to form the average cirrus reflectance for 30 - 55°N. For Terra, no data is used from spring or summer of the year 2000 since internal checkups of the MODIS instrument were still ongoing then. The Aqua and CARIBIC are not available simultaneously until May 2005 only Aqua data from this year and onwards will be used. The averaged Aqua cirrus reflectance values are somewhat higher (13-19%) than the Terra values. This could be caused by the later overpass time for the Aqua satellite which enables more convective activity and thereby cirrus anvils to affect the reflectance products.

3. Results

3.1. Geographical distributions of sulfur and PV

CARIBIC measurements over the years cover latitudes 30°S to 70°N and longitudes 120°W to 120°E. Figure 1a provides a geographical view of the particulate sulfur concentrations at 9-12 km altitude for all samples, tropospheric and stratospheric. Large variations are shown with the geographical location of sampling. A strong latitudinal gradient of the concentration of particulate sulfur is observed, with higher concentration in the northern hemispheric midlatitudes, than in the subtropics. Martinsson et al. (2005) found a correlation of sulfur and PV in the LMS, due to downwelling of particulate sulfur from the higher altitudes. A comparison of the geographical distribution of particulate sulfur concentrations (Figure 1a) and that of the average PV during sampling (Figure 1b) clearly demonstrates the stratospheric origin of high sulfur concentrations. Hence, particle formation in the stratosphere is a major particulate sulfur source in northern midlatitudes. The samples in the subtropics are somewhat influenced by stratospheric air, while the tropical samples are purely tropospheric. The gradient to the tropics could also be caused by other differences in source patterns as well as by more efficient wet scavenging of the hygroscopic sulfur particles in the tropics by deep convective clouds. The following sections deal with the coupling of the LMS and midlatitude UT.

3.2. Volcanic influence on particulate sulfur in the midlatitude UT and LMS

Over the 15 year time span considered, particulate sulfur concentrations in the UT and LMS vary by a factor of about 100. To investigate this large variability we look at the time series (Figure 2). In the LMS, the sulfur concentrations need to be normalized by PV in order to eliminate the strong gradient of sulfur in the LMS and to highlight deviations from the non-volcanically influenced particulate sulfur distribution. UT data are scarce as most of the midlatitude samples were collected in the LMS. Thus, details in the variability in sulfur concentrations do not show as clearly in the UT as in the LMS. The following sections will therefore focus on the variability in the sulfur concentrations in the LMS.

3.2.1. The period April 1999 – March 2002

The average S/PV ratio for the period 1999 - 2002 is low indicating a time of low volcanic impact on the stratosphere (Martinsson et al., 2005). However, particulate sulfur was affected by volcanic aerosol to various degrees after year 2005 (Figure 2). The 2.5 year period mid 2002 to 2005 was not monitored, but is known to have had little volcanic activity (Myhre et al., 2013).

3.2.2. The period May 2005 – July 2008

In the period May 2005 - July 2008 the LMS aerosol was influenced by three volcanic eruptions in the tropics (Manam, Soufriere Hills and Redoubt). They injected large amounts of SO_2

(Table 1) into the tropical stratosphere (Vernier et al., 2011), that was subsequently, while being oxidized, transported to midlatitudes within the BD-circulation. Subsequent downwelling (Friberg et al., 2014) explains the observed increase in the LMS sulfur concentrations from the 99-02 base-line. Concomitant increase in UT sulfur concentrations is evident.

3.2.3. The period August 2008 – 2013

Figure 2 shows several large peaks, starting with the Kasatochi explosion in August 2008 which produced a direct injection to the LMS that increased sulfur concentrations by an order of magnitude compared to the background level. Thereafter S/PV decreased with the particulate sulfur formed in the stratosphere being transported across the tropopause into the UT. This decrease in S/PV was terminated in March 2009 when Redoubt exploded, after which the Sarychev eruption in June 2009 restored the S/PV to similar level as after the Kasatochi eruption. After that, the LMS concentrations decreased again until the Grimsvötn eruption in May 2011. Three weeks later, the tropical volcano Nabro exploded. Nabro was estimated to have emitted about the same amount of SO_2 (1.5 Tg) as Kasatochi and Sarychev did. After a delay due to transport from the tropics, downwelling through the LMS explains the observed rise in S/PV from late summer 2011. Volcanic clouds reaching the tropical stratosphere can affect the extratropical LMS for years via transport in the deep BD-branch. However, the long-lasting perturbations after Nabro were limited to the first half of the year 2012, because most of the aerosol from Nabro was found in the tropical transition layer or in the lower BD-branch (Bourassa et al., 2012). Finally, remaining aerosol particles from the Nabro explosion transported in the deep BD-branch slightly elevated the concentration level in spring/summer 2013.

3.2.4. Grouping LMS data depending on volcanic influence on the LMS

Based on the volcanic impact in the LMS, we divide the data into three groups; 1) background conditions, 2) samples affected by direct injections into the LMS, 3) samples influenced by volcanic aerosol downwelling from the stratosphere from above the 380 K isentrope. Thus we derive:

1) 1999-2002 as the period that represents background levels.

2) Midlatitude eruptions penetrating the extratropical tropopause can cause a large impact on the LMS that lasts for months depending on their penetration depths. The combined injections from Kasatochi, Redoubt and Sarychev caused such perturbations in the period August 2008 - 2009. Hence, this group will be represented by the period Aug 2008-2009.

3) When volcanic clouds have reached the tropical stratosphere the aerosol is transported through the LMS in the following years. Over the 15 years studied here, such perturbations occurred during several periods, with largely varying magnitudes. These periods will be grouped based on the volcanic eruptions effect on the sulfur concentrations in the LMS, because averaging large concentration differences will affect the forthcoming analyses negatively. Category a) will represent periods strongly affected by volcanism (i.e. the period after Nabro's eruption, late

summer 2011 – summer 2012, while category b) represents an intermediately affected LMS (i.e. the periods May 2005-July 2008 (until the Kasatochi eruption) and the year 2013.

In spite of the scarcity of UT data there are similarities in its variability in sulfur concentrations to that of the S/PV in the LMS. Peaks and periods of high S/PV in the LMS are reflected to a degree in the UT (Figure 2), for example the peaks after the eruptions of Kasatochi and Sarychev, the decreasing concentrations from spring/summer to fall in 2006 and 2007, and the increased sulfur concentrations after the eruption of Nabro. These similarities call for scrutinizing the influence of the LMS on the aerosol concentrations in the UT.

3.3. Impact on UT/LMS aerosol from tropical volcanism

To explore the influence of indirect volcanic injections to the LMS on the aerosol concentrations in the midlatitude UT we compare sulfur concentrations from the periods May 2005-July 2008 and 2013 to that of the period 1999-2002 (hereinafter termed periods 05-08/13 and 99-02, respectively). The LMS contains a larger proportion of high-stratospheric air in spring and summer, compared to fall when a large fraction of the LMS' air is of recent tropospheric origin (Bönisch et al., 2009). Hence, in the periods 05-08/13 elevated aerosol concentrations are expected in the LMS and midlatitude UT during spring when volcanic aerosol is brought down from higher altitudes, while concentrations in fall are expected to be more connected to the aerosol concentrations in the troposphere. We explore seasonal differences by combining data from the two periods into one season of large stratospheric influence (March – July) and one season with large tropospheric influence (September – November).

3.3.1. Latitude dependence of particulate sulfur UT concentration

The latitudinal distribution of sulfur in the UT is displayed in Figure 3, revealing a clear tendency of increasing concentrations from the tropics to higher latitudes. For Mar-Jul, this gradient is more pronounced in the periods 05-08/13 than during 99-02 (Figures 3a and b). A direct comparison of the Mar-Jul moving averages (Figure 3c), shows similar concentration levels in the tropics and part of the subtropics. While the 05-08/13 periods shows a steep increase with latitude, north of 30°N, the increase observed for the period 99-02 is not significant. This difference is largest at 45°N, which is the northernmost latitude for the average of the 99-02, where the sulfur concentrations of the 05-08/13 are twice that of the 99-02. Hence, aerosol from tropical volcanic eruptions is detectable not only in the stratosphere, but also in the midlatitude UT.

3.3.2. Seasonal variation in the midlatitude UT and LMS

The 05-08/13 data will now be further investigated in order to address the origin of the particulate sulfur in the midlatitude UT and the cause of its seasonally varying concentrations. In Figure 4 the seasonally varying concentrations in the midlatitude UT are compared to the S/PV of different depths (PV-levels) into the LMS.

In the LMS, high S/PV is observed in spring with a reduction during summer that reaches a minimum around August-October. The maximum coincides with the downwelling of high-stratospheric air (within the deep BD branch) carrying particulate sulfur to the LMS. The minimum in August-October (Figure 4a) again illustrates the small contribution from high-stratospheric air in the LMS during late summer and fall.

We observe large similarities in the variation of sulfur in the UT to that in the LMS with the maximum concentrations found in May. In Figure 4c, a comparison of the moving averages for the sulfur concentrations in the UT and that of the S/PV in the LMS shows that the seasonal variations span approximately a factor of two. In fall, the S/PV values close to the tropopause are higher than at higher PV values. However, this is not caused by higher sulfur concentration at the lower PV values. Instead, it is an effect of fairly constant sulfur concentrations in the LMS during fall (Friberg et al., 2014), resulting in high S/PV for low PV values.

4. Discussion

The large similarities in the seasonally varying sulfur concentrations in the LMS and in the UT (Figure 4) indicate a strong coupling of the aerosol concentrations between these altitudes. Combined with previous findings of perturbations of the LMS from tropical volcanic injections transported to the LMS, these findings point to a strong influence from volcanism on the UT particulate sulfur concentration during the periods 05-08/13. To investigate the impact of volcanism and the coupling of the UT and LMS further we will extend the study by a direct comparison of the sulfur concentrations in the UT with the S/PV in the LMS.

4.1. Transport of volcanic aerosol from the LMS to the UT

4.1.1. Volcanic impact in spring/summer

To compare LMS and UT concentrations directly one needs to account for the variability in the transport across the extratropical tropopause. We therefore use the March to July data for a comparison in the season of large stratospheric influence. To deal with the scarcity of observations in the UT we group the years together, based on each year's average S/PV in the LMS, thus improving statistics. The years 2009 and 2011 are excluded in this comparison as midlatitude eruptions (Redoubt, Sarychev and Grimsvötn) occurred during the spring/summer. The year 2012 is excluded since only one UT observation is available. This results in four groups of years for comparison of the LMS and UT (00-02, 10/13, 05/06 and 07/08). Finally, average sulfur concentrations in the UT and the S/PV in the LMS are compared using a scatter plot (Figure 5, yellowish data points). Samples taken in air masses with PV less than 5 PVU are used here as they are expected to be more connected to the sulfur concentrations in the UT than those taken further away from the tropopause (Bönisch et al., 2009). A positive correlation emerges with the 00-02 data at the lowest UT concentrations (13 ng m^{-3} STP) up to highest concentration in 07/08 (32 ng m^{-3} STP). The correlation turns out to be high ($R^2 = 0.73$), with a significance level of 85%.

4.1.2. Volcanic impact in fall

For data taken in fall, we have the possibility to extend the UT/LMS-comparison to include the years that were affected by direct injections to the LMS. To gain better statistics we extend the fall season to include August. Aerosol samples collected in the August to November months after Kasatochi (Aug 2008), Sarychev (June 2009) and Nabro (June 2011) were all largely affected by volcanism. As Kasatochi exploded in August, samples from August and September 2008 are excluded.

The coupling between the LMS and UT is further explored (Figure 5) via a comparison of the fall data (Figure 5, magenta data points) for the years when the LMS were strongly affected by volcanism (2008, 2009 and 2011) to that of the less affected years (2006, 2007 and 2012). Unfortunately, comparison to the period 99-02 is not possible, as only two observations of the sulfur concentrations in the LMS in fall are available. A linear regression of the fall data, results in a strong correlation (R^2 = 0.95) of high significance (>99%). The 2008 (Kasatochi) data is omitted in this calculation as only one observation from the UT is available. Interestingly, the slope in spring/summer is a factor 4 larger than in fall. The lower slope in fall is attributed to reduced stratosphere-to-troposphere transport in fall (Sprenger and Wernli, 2003), resulting in a lower fraction of stratospheric aerosol in the UT.

4.2. Implications of volcanic impact on the UT

Whereas aerosol particles in the stratosphere affects Earth's radiation budget directly, tropospheric aerosols can also affect the budget indirectly by altering the occurrence and properties of clouds. In the previous sections the variability of sulfur in the northern midlatitude UT was found to be caused (i) by the seasonally varying subsidence of high-stratospheric air and (ii) by the varying contribution of volcanic aerosol mixed-in from the LMS. The logic question arises, if volcanism influences the radiation budget via interaction with cirrus clouds.

4.2.1. Comparison to the MODIS retrieved cirrus reflectance

To explore a possible impact of downwelling particulate sulfur on cirrus clouds, the particulate sulfur concentration measured during CARIBIC is compared to the cirrus reflectance (CR) retrieved by MODIS (see section 2.7) (Gao et al., 2002). Because of the scarcity of UT data we use the S/PV in the LMS as a reasonable proxy for the UT particulate sulfur, which was validated above (using samples collected below 5 PVU as in Figure 5). Only the season with largest stratospheric impact on the UT/LMS (March-July) is investigated here. The comparison is then illustrated as time-series (Figure 6a) of each year's average S/PV from CARIBIC and CR from the Terra and Aqua satellites. While no CARIBIC measurements were performed in the years 2003 and 2004, also the years 2002 and 2009 need to be excluded since too few months of CARIBIC data are available for these years.

The year-to-year changes of the cirrus cloud reflectance of both satellites agree very well, in which the AQUA values are by ~20% higher, see explanation in section 2.7. The year-to-year variability and the general trend in S/PV is anti-correlated to CR; note the inverted scale of S/PV.

S/PV increases gradually from 2001 until 2011/2012 as a result of volcanism, whereas CR decreases. A slightly weaker decrease for Aqua's CR is observed, which could be caused by stronger influence of convection on that satellites CR. Since the CR obtained by Terra is less influenced by convective activity, it is expected to be more sensitive to changes in the UT/LMS conditions which in this case concerns changes in the sulfur concentrations. We therefore use the CR of Terra to illustrate the close coupling of S/PV and CR as a scatter plot (Figure 6b). A linear regression reveals a good anti-correlation between CR and S/PV (R^2 = 0.63, p = 0.01), even though the two parameters compared were obtained using fundamentally different measurement methods (the corresponding results for Aqua are R^2 = 0.74, p = 0.006). The relative decrease in CR between 2001 and 2011 is 8±2%, while the particulate sulfur concentration in LMS has increased by 3-4 during this time. In the following section possible causes for the anti-correlation will be discussed.

4.2.2. Cloud microphysics and climate

Recent geoengineering (GE) studies suggest that increased stratospheric sulfur aerosol concentration can affect cirrus cloud reflectance either by providing large homogeneous nucleation sites (Cirisan et al., 2013) or by affecting the temperature and that way updraft conditions in the cloud formation (Kuebbeler et al., 2012). Sulfurous aerosol could also affect heterogeneous freezing. When the sulfuric acid is neutralized by ammonia, the downwelling LMS aerosol could increase the IN concentration, as the formed ammonium sulfate or –bisulfate acts as IN (Abbatt et al., 2006; Hoose and Möhler, 2012). Increases in IN concentrations has been found to seed cirrus clouds and make them optically thinner, except in pure heterogeneous freezing regimes (Storelvmo and Herger, 2014).

One of the discussed mechanisms, or a combination of them, may have caused the decrease in cirrus reflectance seen in Figure 6. A decrease in cirrus reflectance implies that the clouds are optically thinner and both reflects less shortwave radiation, and absorbs less longwave radiation. Because the latter effect dominates, a decrease in cirrus reflectance therefore corresponds to a smaller greenhouse effect from cirrus clouds (Storelvmo et al., 2013). The strong response of 8% decrease in CR to a 3.5 fold increase of S/PV in the LMS indicates a substantial radiative forcing. Making use of the fact that CR and cloud optical thickness (COT) are linearly dependent for thin clouds (Meyer et al., 2007), and the sensitivity of net radiative forcing to changes in COT according to Cirisan et al. (2013; their Figure 8) the maximum decrease of 8% of CR in the time period studied corresponds to approximately -2 Wm^{-2} in net radiative forcing at NH midlatitudes. This regional result pertains to the season March to July.

5. Conclusions

This study focuses on particulate sulfur in the Northern Hemisphere's upper troposphere (UT) and lowermost stratosphere (LMS) in the period 1999-2013 measured by the CARIBIC observatory. Particulate sulfur concentrations varied by a factor of about 100 in this period, mainly as a result of volcanic injections. The sulfurous aerosol concentration in the UT had a

strong connection to that in the LMS, as downwelling aerosol constituted the major fraction of the UT particulate sulfur.

During the 15 year time span the UT/LMS was perturbed by volcanism to various degrees. The lowest sulfur concentrations were observed in 1999-2002, a volcanically quiescent period. The largest perturbations in the LMS were found after extratropical volcanic eruptions, specifically in 2008 (Kasatochi) and 2009 (Sarychev), but also in fall 2011-spring 2012 after an eruption of the tropical volcano Nabro.

In the periods 2005-2008 and 2013, the sulfur concentration's variability was dominated by downwelling of volcanic aerosol from tropical volcanism that was transported through the stratosphere. In that period, the LMS' sulfur concentration peaked in May as a result of downwelling of air transported in the deep Brewer-Dobson branch. The same seasonal variation was found in the UT, illustrating a strong coupling of the LMS and the UT. Downwelling of volcanic aerosol was found to double the spring and summer UT particulate sulfur concentrations compared to the background levels.

A comparison of sulfur concentrations to satellite observations of the MODIS retrieved cirrus reflectance (CR) from the satellites Terra and Aqua, for the season of largest stratospheric impact on the UT and LMS (March-July), resulted in strong anti-correlations (R^2 = 0.63 (Terra), R^2 = 0.72 (Aqua). The CR and thereby the cloud optical thickness (COT) decreased by 8% in the period 2001-2011. During this time the particulate sulfur concentration increase by a factor of 3.5 in the LMS. This indicates that volcanism has a large impact on the radiative forcing from midlatitude cirrus clouds and ultimately Earth's surface temperatures.

Previous studies have shown that volcanism induced a significant radiative forcing after the turn of the millennium (Solomon et al., 2011; Santer et al., 2014) by the direct effect from stratospheric aerosol. New findings of the importance of LMS aerosol in this respect further increase this estimated forcing (Ridley et al., 2014; Andersson et al, 2014). Here we introduce the indirect effect by volcanism caused by changes to the reflectance of cirrus clouds in response to volcanically-induced increases in the concentration of particulate sulfur in the upper troposphere. The CMIP5 (coupled model intercomparison project) models used by United Nations climate panel (IPCC) do not account for volcanism occurring after year 2000. The models overestimate the global warming over the last 15 years (Flato et al., 2013; Fyfe et al., 2013). Evidence is growing that volcanism is an important reason behind the mismatch of model results and observations.

6. Acknowledgements

We especially acknowledge C. Koeppel, D. S. Scharffe, S. Weber and all other members of the CARIBIC project. Lufthansa and Lufthansa Technik are gratefully acknowledged for enabling this scientific experiment. Frankfurt Airport is gratefully acknowledged for financial support. Contact the authors for CARIBIC data. The satellite data from the MODIS instruments were supplied by the United States national aeronautics and space agency (http://ladsweb.nascom.nasa.gov/index.html).

References

Abbatt, J. P. D., Benz, S., Cziczo, D. J., Kanji, Z., Lohmann, U. and co-authors 2006. Solid ammonium sulfate aerosols as ice nuclei: A pathway for cirrus cloud formation. *Science* **313**, 1770-1773.

Andersson, S. M., Martinsson, B. G., Friberg, J., Brenninkmeijer, C. A. M., Rauthe-Schöch, A. and co-authors 2013. Composition and evolution of volcanic aerosol from eruptions of Kasatochi, Sarychev and Eyjafjallajökull in 2008–2010 based on CARIBIC observations. *Atmos. Chem. Phys.* **13**, doi: 10.5194/acp-13-1781-2013.

Barahona, D., Molod, A., Bacmeister, J., Nenes, A., Gettelman, A. and co-authors 2014. Development of two-moment cloud microphysics for liquid and ice within the NASA Goddard Earth Observing System Model (GEOS-5). *Geosci. Model Dev.* **7**, doi: 10.5194/gmd-7-1733-2014.

Baran, A. J. 2009. A review of the light scattering properties of cirrus. *J. Quant. Spectrosc. Radiat. Transf.* **110**, doi: 10.1016/j.jqsrt.2009.02.026.

Boucher, O., Randall, D., Artaxo, P., Bretherton, C., Feingold, G. and co-authors 2013. *Clouds and Aerosols. In: Climate Change 2013: The Physical Science Basis. Contribution of Working Group I to the Fifth Assessment Report of the Intergovernmental Panel on Climate Change* Cambridge University Presss, Cambridge, United Kingdom and New York, NY, USA.

Bourassa, A. E., Robock, A., Randel, W. J., Deshler, T., Rieger, L. A. and co-authors 2012. Large volcanic aerosol load in the stratosphere linked to Asian monsoon transport. *Science* **337**, doi: 10.1126/science.1219371.

Brenninkmeijer, C. A. M., Crutzen, P. J., Fischer, H., Güsten, H., Hans, W. and co-authors 1999. CARIBIC-Civil aircraft for global measurement of trace gases and aerosols in the tropopause region. *Journal of Atmospheric and Oceanic Technology* **16**, 1373-1383.

Brenninkmeijer, C. A. M., Crutzen, P., Boumard, F., Dauer, T., Dix, B. and co-authors 2007. Civil Aircraft for the regular investigation of the atmosphere based on an instrumented container: The new CARIBIC system. *Atmos. Chem. Phys.* **7**, 4953-4976.

Bönisch, H., Engel, A., Curtius, J., Birner, T. and Hoor, P. 2009. Quantifying transport into the lowermost stratosphere using simultaneous in-situ measurements of SF6 and CO2. *Atmos. Chem. Phys.* **9**, 5905–5919.

Campbell, J. R., Welton, E. J., Krotkov, N. A., Yang, K., Stewart, S. A. and co-authors 2012. Likely seeding of cirrus clouds by stratospheric Kasatochi volcanic aerosol particles near a mid-latitude tropopause fold. *Atmos. Environ.* **46**, doi: 10.1016/j.atmosenv.2011.09.027.

Carn, S. A., Krueger, A. J., Krotkov, N. A., Yang, K. and Evans, K. 2009. Tracking volcanic sulfur dioxide clouds for aviation hazard mitigation. *Natural hazards* **51**, doi: 10.1007/s11069-008-9228-4.

Carn, S. A. and Prata, F. J. 2010. Satellite-based constraints on explosive SO2 release from Soufrière Hills Volcano, Montserrat. *Geophys. Res. Lett.* **37**, doi: 10.1029/2010GL044971.

Chen, T., Rossow, W. B. and Zhang, Y. 2000. Radiative effects of cloud-type variations. *J. Climate* **13**, 264-286.

Cirisan, A., Spichtinger, P., Luo, B. P., Weisenstein, D. K., Wernli, H. and co-authors 2013. Microphysical and radiative changes in cirrus clouds by geoengineering the stratosphere. *J. Geophys. Res.* **118**, doi: 10.1002/jgrd.50388.

Clarisse, L., Hurtmans, D., Clerbaux, C., Hadji-Lazaro, J., Ngadi, Y. and co-authors 2012. Retrieval of sulphur dioxide from the infrared atmospheric sounding interferometer (IASI). *Atmos. Meas. Tech.* **5**, doi: 10.5194/amt-5-581-2012.

Crutzen, P. J. 1976. The possible importance of CSO for the sulfate layer of the stratosphere. *Geophys. Res. Lett.* **3**, 73-76.

Cziczo, D. J., Froyd, K. D., Hoose, C., Jensen, E. J., Diao, M. and co-authors 2013. Clarifying the dominant sources and mechanisms of cirrus cloud formation. *Science* **340**, doi: 10.1126/science.1234145.

DeMott, P. J., Cziczo, D. J., Prenni, A. J., Murphy, D. M., Kreidenweis, S. M. and co-authors 2003. Measurements of the concentration and composition of nuclei for cirrus formation. *P Natl Acad Sci USA* **100**, 14655-14660.

Deshler, T. 2008. A review of global stratospheric aerosol: Measurements, importance, life cycle, and local stratospheric aerosol. *Atmos. Res.* **90**, 223-232.

Flato, G., Marotzke, J., Abiodun, B., Braconnot, P., Chou, S. C. and co-authors 2013. Evaluation of Climate Models. In: Climate Change 2013: The Physical Science Basis. Contribution of Working Group I to the Fifth Assessment Report of the Intergovernmental Panel on Climate Change (ed. Stocker, T. F., D. Qin, G.-K. Plattner, M. Tignor, S.K. Allen, J. Boschung, A. Nauels, Y. Xia, V. Bex and P.M. Midgley), Cambridge University Press, Cambridge, United Kingdom and New York, NY, USA.

Friberg, J., Martinsson, B. G., Andersson, S. M., Brenninkmeijer, C. A. M., Hermann, M. and co-authors 2014. Sources of increase in lowermost stratospheric sulphurous and carbonaceous aerosol background concentrations during 1999-2008 derived from CARIBIC flights. *Tellus B* **66**.

Fusina, F., Spichtinger, P. and Lohmann, U. 2007. Impact of ice supersaturated regions and thin cirrus on radiation in the midlatitudes. *J Geophys Res-Atmos* **112**.

Fyfe, J. C., Gillett, N. P. and Zwiers, F. W. 2013. Overestimated global warming over the past 20 years. *Nature Clim. Change* **3**, 767-769.

Gao, B.-C. and Kaufman, Y. J. 1995. Selection of the 1.375-um MODIS channel for remote sensing of cirrus clouds and stratospheric aerosols from space. *J Atmos Sci* **52**, 4231-4237.

Gao, B.-C., Yang, P., Han, W., Li, R.-R. and Wiscombe, W. J. 2002. An algorithm using visible and 1.38-μm channels to retrieve cirrus cloud reflectances from aircraft and satellite data. *Geoscience and Remote Sensing, IEEE Transactions on* **40**, 1659-1668.

GVP 2011. Global Volcanism Program, http://www.volcano.si.edu/index.cfm.

Haywood, J. M., Jones, A., Clarisse, L., Bourassa, A., Barnes, J. and co-authors 2010. Observations of the eruption of the Sarychev volcano and simulations using the HadGEM2 climate model. *J. Geophys. Res.* **115**, doi: 10.1029/2010JD014447.

Hermann, M., Stratmann, F., Wilck, M. and Wiedensohler, A. 2001. Sampling characteristics of an aircraft-borne aerosol inlet system. *Journal of Atmospheric and Oceanic Technology* **18**, 7-19.

Hoerling, M. P., Schaack, T. K. and Lenzen, A. J. 1991. Global objective tropopause analysis. *Mon. Weather Rev.* **119**, 1816-1831.

Hofmann, D., Barnes, J., O'Neill, M., Trudeau, M. and Neely, R. 2009. Increase in background stratospheric aerosol observed with lidar at Mauna Loa Observatory and Boulder, Colorado. *Geophys. Res. Lett.* **36**, doi: 10.1029/2009GL039008.

Hoinka, K. P. 1997. The tropopause: Discovery, definition and demarcation. *Meteorol. z* **6**, 281–303.

Holton, J. R., Haynes, P. H., McIntyre, M. E., Douglas, A. R., Rood, R. B. and co-authors 1995. Stratosphere-troposphere exchange. *Rev. Geophys.* **33**, 403-439.

Hoor, P., Gurk, C., Brunner, D., Hegglin, M. I., Wernli, H. and co-authors 2004. Seasonality and extent of extratropical TST derived from in-situ CO measurements during SPURT. *Atmos. Chem. Phys.* **4**, 1427-1442.

Hoose, C. and Möhler, O. 2012. Heterogeneous ice nucleation on atmospheric aerosols: a review of results from laboratory experiments. *Atmos. Chem. Phys.* **12**, doi: 10.5194/acp-12-9817-2012.

Johansson, S. A. E. and Campbell, J. L. 1988. *PIXE: A novel technique for elemental analysis*. Hoboken, N. J., John Wiley.

Kuebbeler, M., Lohmann, U. and Feichter, J. 2012. Effects of stratospheric sulfate aerosol geo-engineering on cirrus clouds. *Geophys. Res. Lett.* **39**, doi: 10.1029/2012GL053797.

Lopez, T. M., Carn, S. A., Webley, P., Pfeffer, M. A., Doukas, M. P. and co-authors 2009. Evaluation of satellite derived sulfur dioxide measurements for volcano monitoring during the 2009 Redoubt eruption. *American Geophysical Union, Fall Meeting 2009*, abstract #V51F-03.

Martinsson, B. G., Nguyen, H. N., Brenninkmeijer, C. A. M., Zahn, A., Heintzenberg, J. and co-authors 2005. Characteristics and origin of lowermost stratospheric aerosol at northern midlatitudes under volcanically quiescent conditions based on CARIBIC observations. *J. Geophys. Res.* **110**, doi: 10.1029/2004JD005644.

Martinsson, B. G., Brenninkmeijer, C. A. M., Carn, S. A., Hermann, M., Heue, K. P. and co-authors 2009. Influence of the 2008 Kasatochi volcanic eruption on sulfurous and carbonaceous aerosol constituents in the lower stratosphere. *Geophys. Res. Lett.* **36**, doi: 10.1029/2009GL038735.

Martinsson, B. G., Friberg, J., Andersson, S. M., Weigelt, A., Hermann, M. and co-authors 2014. Comparison between CARIBIC aerosol samples analysed by accelerator-based methods and optical particle counter measurements. *Atmos. Meas. Tech.* **7**, doi: 10.5194/amt-7-2581-2014.

Meyer, K., Yang, P. and Gao, B.-C. 2007. Ice Cloud Optical Depth From MODIS Cirrus Reflectance. **4**, 471-474.

Meyer, K. and Platnick, S. 2010. Utilizing the MODIS 1.38 μm channel for cirrus cloud optical thickness retrievals: Algorithm and retrieval uncertainties. *Journal of Geophysical Research: Atmospheres* **115**, D24209.

Murphy, D. M., Thomson, D. S. and Mahoney, M. J. 1998. In situ measurements of organics, meteoritic material, mercury, and other elements in aerosols at 5 to 19 kilometers. *Science* **282**, doi: 10.1126/science.282.5394.1664.

Murphy, D. M., Froyd, K. D., Schwarz, J. P. and Wilson, J. C. 2014. Observations of the chemical composition of stratospheric aerosol particles. *Q. J. R. Meteorol. Soc.* **140**, 1269–1278.

Myhre, G., Shindell, D., Bréon, F., Collins, W., Fuglestvedt, J. and co-authors 2013. Anthropogenic and natural radiative forcing Climate Change 2013: The Physical Science Basis. Contribution of Working Group I to the Fifth Assessment Report of the Intergovernmental Panel on Climate Change [Stocker, T.F., D. Qin, G.-K. Plattner, M. Tignor, S.K. Allen, J. Boschung, A. Nauels, Y. Xia, V. Bex and P.M. Midgley (eds.)]. Cambridge University Press, Cambridge, United Kingdom and New York, NY, USA.

Nguyen, H. N., Gudmundsson, A. and Martinsson, B. G. 2006. Design and Calibration of a Multi-Channel Aerosol Sampler for Tropopause Region Studies from the CARIBIC Platform. *Aerosol Sci. Technol.* **40**, doi: 10.1080/02786820600767807.

Pan, L. L., Randel, W. J., Gary, B. L., Mahoney, M. J. and Hintsa, E. J. 2004. Definitions and sharpness of the extratropical tropopause: A trace gas perspective. *J. Geophys. Res.* **109**, doi: 10.1029/2004JD004982.

Papaspiropoulos, G., Mentes, B., Kristiansson, P. and Martinsson, B. G. 1999. A high sensitivity elemental analysis methodology for upper tropospheric aerosol. *Nucl. Instrum. Methods Phys. Res., Sect. B* **150**, 356-362.

Platnick, S., King, M. D., Ackerman, S. A., Menzel, W. P., Baum, B. A. and co-authors 2003. The MODIS cloud products: Algorithms and examples from Terra. *Ieee T Geosci Remote* **41**, 459-473.

Prata, A. J. and Bernardo, C. 2007. Retrieval of volcanic SO_2 column abundance from atmospheric infrared sounder data. *J. Geophys. Res.* **112**, doi: 10.1029/2006JD007955.

Pruppacher, H. R. and Klett, J. D. 1997. *Microphysics of Clouds and Precipitation*. Dordrecht, The Netherlands, Kluwer Academic Publishers.

Rauthe-Schöch, A., Weigelt, A., Hermann, M., Martinsson, B. G., Baker, A. K. and co-authors 2012. CARIBIC aircraft measurements of Eyjafjallajökull volcanic clouds in April/May 2010. *Atmos. Chem. Phys.* **12**, doi: 10.5194/acp-12-879-2012.

Ridley, D. A., Solomon, S., Barnes, J. E., Burlakov, V. D., Deshler, T. and co-authors 2014. Total volcanic stratospheric aerosol optical depths and implications for global climate change. *Geophys. Res. Lett.*, doi: 10.1002/2014GL061541.

Robock, A. 2000. Volcanic eruptions and climate. *Rev. Geophys.* **38**, 191-219.

Rosen, J. M. 1971. The boiling point of stratospheric aerosols. *Journal of applied meteorology* **10**, 1044-1046.

Santer, B. D., Bonfils, C., Painter, J. F., Zelinka, M. D., Mears, C. and co-authors 2014. Volcanic contribution to decadal changes in tropospheric temperature. *Nature Geoscience* **7**, 185-189.

Schmale, J., Schneider, J., Jurkat, T., Voigt, C., Kalesse, H. and co-authors 2010. Aerosol layers from the 2008 eruptions of Mount Okmok and Mount Kasatochi: In situ upper troposphere and lower stratosphere measurements of sulfate and organics over Europe. *J. Geophys. Res.* **115**, doi: 10.1029/2009JD013628.

Solomon, S., Daniel, J. S., Neely, R. R., Vernier, J. P., Dutton, E. G. and co-authors 2011. The persistently variable "background" stratospheric aerosol layer and global climate change. *Science* **333**, doi: 10.1126/science.1206027.

Sprenger, M. and Wernli, H. 2003. A northern hemispheric climatology of cross-tropopause exchange for the ERA15 time period (1979–1993). *J. Geophys. Res.* **108**, doi: 10.1029/2002JD002636.

Storelvmo, T., Kristjansson, J. E., Muri, H., Pfeffer, M., Barahona, D. and co-authors 2013. Cirrus cloud seeding has potential to cool climate. *Geophys Res Lett* **40**, 178-182.

Storelvmo, T. and Herger, N. 2014. Cirrus cloud susceptibility to the injection of ice nuclei in the upper troposphere. *Journal of Geophysical Research: Atmospheres* **119**, 2375-2389.

Thomas, H. E., Watson, I. M., Carn, S. A., Prata, A. J. and Realmuto, V. J. 2011. A comparison of AIRS, MODIS and OMI sulphur dioxide retrievals in volcanic clouds. *Geomatics, Natural Hazards and Risk* **2**, doi: 10.1080/19475705.2011.564212.

Weisenstein, D. K., Yue, G. K., Ko, M. K. W., Sze, N. D., Rodriguez, J. M. and co-authors 1997. A two-dimensional model of sulfur species and aerosols. *J. Geophys. Res.* **102**, 13019-13035.

Vernier, J. P., Thomason, L. W., Pommereau, J. P., Bourassa, A., Pelon, J. and co-authors 2011. Major influence of tropical volcanic eruptions on the stratospheric aerosol layer during the last decade. *Geophys. Res. Lett.* **38**, doi: 10.1029/2011GL047563.

Yang, K., Liu, X., Bhartia, P. K., Krotkov, N. A., Carn, S. A. and co-authors 2010. Direct retrieval of sulfur dioxide amount and altitude from spaceborne hyperspectral UV measurements: Theory and application. *J. Geophys. Res.* **115**, D00L09.

Zahn, A. and Brenninkmeijer, C. A. M. 2003. New directions: a chemical tropopause defined. *Atmos. Environ.* **37**, 439-440.

Zahn, A., Christner, E., Velthoven, P. F. J., Rauthe-Schöch, A. and Brenninkmeijer, C. A. M. 2014. Processes controlling water vapor in the upper troposphere/lowermost stratosphere: An analysis of 8 years of monthly measurements by the IAGOS-CARIBIC observatory. *J. Geophys. Res.* **119**, doi: 10.1002/2014JD021687.

Tables

Table 1. Large volcanic eruptions in the tropics and in the northern extratropics, identified to have influenced the particulate sulfur concentrations in the LMS (also marked in Figure 1) in the period 1999-2013.

Eruption Date[ǂ]	Volcano	SO_2 (Tg)	VEI[ǂ]	Longitude[ǂ]	Latitude[ǂ]
2005-01-27	Manam	0.09[§]	4	145	-4.1
2006-05-20	Soufriere Hills	0.2[ʃ]	3	-62	16.7
2006-10-07	Rabaul	0.2[‡]	4	152	-4.3
2008-07-12	Okmok	0.1[†]	4	-168	55.3
2008-08-07	Kasatochi	2[≠]	4	-176	52.2
2009-03-20	Redoubt	0.08[ƹ]	3	-153	60.5
2009-06-12	Sarychev	1.2[Þ]	4	153	48.1
2011-05-21	Grimsvötn	0.4[ð]	4	-17.3	64.4
2011-06-12	Nabro	1.5[ð]	4	41.7	13.4

[ǂ] Volcanic Explosivity Index, from Global Volcanism Program (2011)
[§] Prata and Bernardo (2007)
[ʃ] Carn and Prata (2010)
[‡] Carn et al. (2009)
[†] Thomas et al. (2011)
[≠] Yang et al. (2010)
[ƹ] Lopez et al. (2009)
[Þ] Haywood et al. (2010)
[ð] Clarisse et al. (2012)

Figures

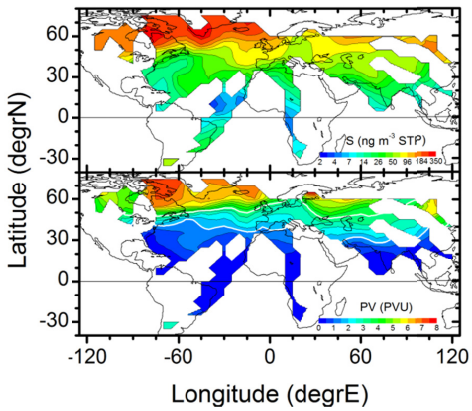

Figure 1. Contour graphs illustrating the geographical distribution of a) particulate sulfur concentrations and b) PV, based on all aerosol samples collected by CARIBIC in the period 1999-2013. White lines in b) marks the PV isopleths of 1.5 and 3.5 PVU, explicitly the typical range of PV that are used to represent the dynamical tropopause**.**

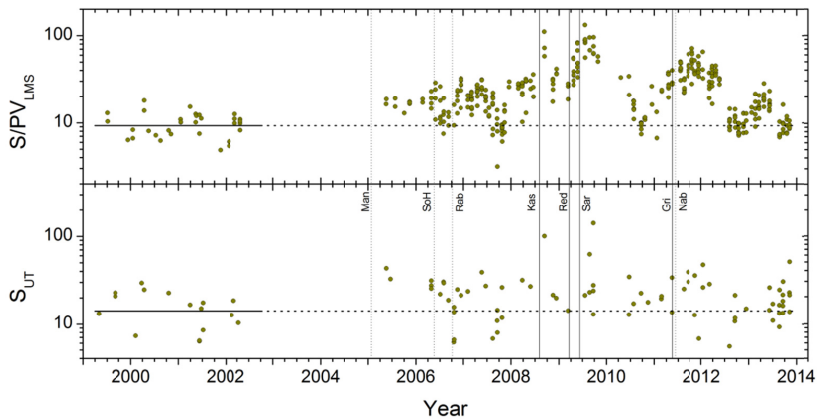

Figure 2. Temporal variations in the northern midlatitude of a) S/PV values in the LMS (S/PV_{LMS}) and b) sulfur concentrations in the UT (S_{UT}). The horizontal lines show geometric averages for the period 99-02. Vertical lines marks large volcanic eruptions identified to have influenced the particulate sulfur concentrations in the LMS. Vertical dashed and full lines represent eruptions in the tropics and northern midlatitudes, respectively. Data for the 30 days following these eruptions are excluded.

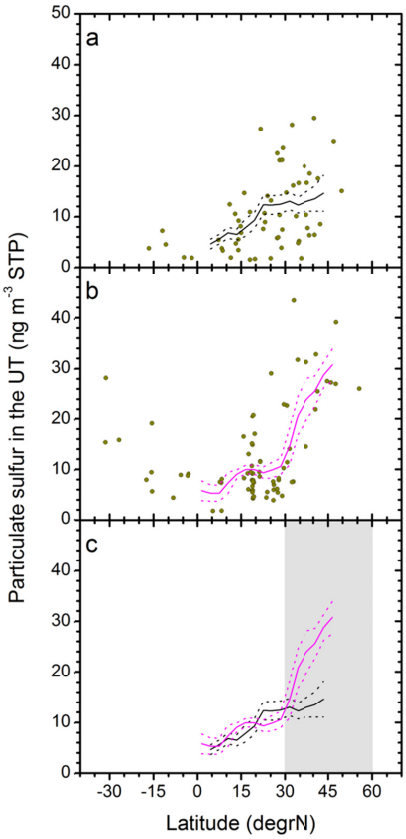

Figure 3 (left). The latitudinal variation of particulate sulfur in the UT during a) March-July 99-02, b) March-July 05-08/13, c) a direct comparison of the averaged profiles shown as lines in a) and b). Dashed lines illustrate the 95% prediction interval. The grey shaded area in c) marks the northern midlatitudes, the latitude band of interest in the following figures and discussions.

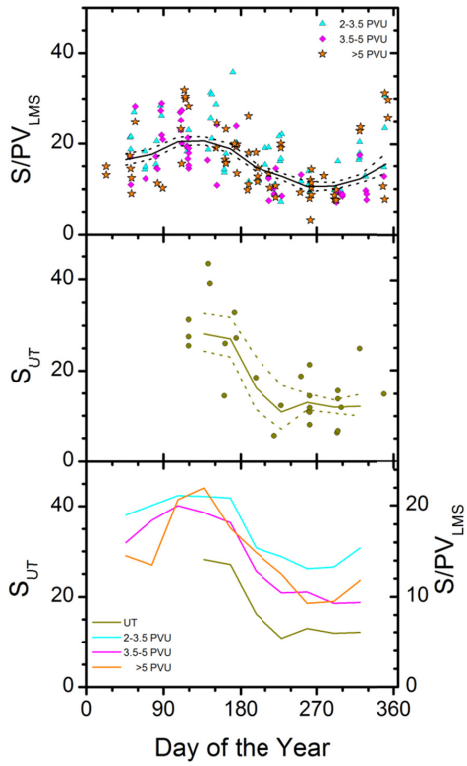

Figure 4 (right). Illustration of the seasonal variation of a) S/PV at different PV-intervals in the LMS (S/PV_{LMS}), b) the particulate sulfur concentration in the UT (S_{UT}) and c) a direct comparison of the S/PV_{LMS} to the S_{UT}. Full and dashed lines illustrates moving geometric averages with 95% prediction interval.

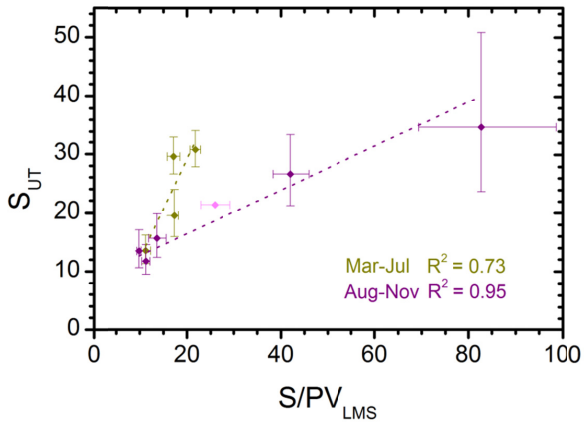

Figure 5. Comparison of the geometric averages of the particulate sulfur concentrations in the UT (S_{UT}) to the S/PV in the LMS (S/PV_{LMS}), for the seasons March – July (dark yellow diamonds) and Aug – Nov (magenta diamonds), for samples taken below 5 PVU. Dashed lines represents linear regressions for the respective season. Error bars represents the geometric standard errors. The years that have been averaged for the season March – July, in order of their S/PV_{LMS}, are; 00-02, 10/13, 05/06 and 07/08, while the Aug-Nov are; 07, 10/12, 06, 11 (Nabro) and 09 (Sarychev). The 2008 (Kasatochi) data (light magenta, diamond) were excluded in the regression due to its poor statistics.

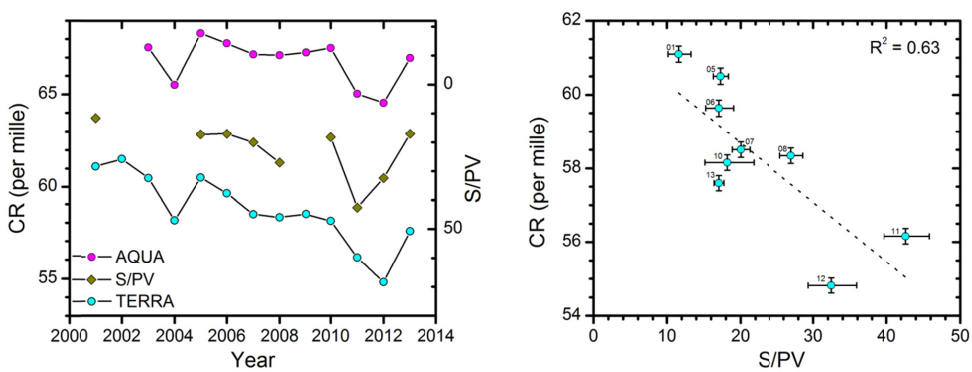

Figure 6. a) Time series of the geometric average S/PV in the LMS (S/PV_{LMS}) (note the reversed scale) and the arithmetic average of the MODIS retrieved parameter, cirrus reflectance (CR) from AQUA and TERRA, for samples taken below 5 PVU in the season March-July. b) A comparison of S/PV and Terra's CR as in a). A linear regression fit is shown as a dotted line. In 2011, the S/PV was elevated mainly by aerosol from Grimsvötn's eruption.